UNIVERSITA' VITA-SALUTE SAN RAFFAELE

CORSO DI DOTTORATO DI RICERCA INTERNAZIONALE IN MEDICINA MOLECOLARE

CURRICULUM IN GENE AND CELL THERAPY

IL-1β^{+} MACROPHAGES FUEL PATHOGENIC INFLAMMATION IN PANCREATIC CANCER

DoS: Prof, Renato Ostuni

Second Supervisor: Prof, Ivan Zanoni

Tesi di DOTTORATO di RICERCA di Francesco Maria Vittoria

Matr. 017115

Ciclo di dottorato XXXVI

SSD BIO/11

Anno Accademico 2020/2021

CONSULTAZIONE TESI DI DOTTORATO DI RICERCA

Il sottoscritto/*I* Francesco Maria Vittoria
Matricola/ *registration number* 017115
nato a/ *born at*: Napoli/ *Naples*
il/ *on* 06/12/1994
autore della tesi di Dottorato di Ricerca dal titolo /*author of the PhD thesis entitled*: IL-1β^{+} macrophages fuel pathogenic inflammation in pancreatic cancer

AUTORIZZA la Consultazione della tesi/ **AUTHORIZES** the public release of the thesis

Data ..... Firma.....

DECLARATION

This thesis has been:

- composed by myself and has not been used in any previous application for a degree. Throughout the text I use both 'I' and 'We' interchangeably.
- has been written according to the editing guidelines approved by the University.

Permission to use images and other material covered by copyright has been sought and obtained.

All the results presented here were obtained by myself. I performed all the *in vivo* and *in vitro* functional experiments and, additionally, I interacted and discussed with the bioinformaticians in the lab, contributing to the decision-making process.

Here I listed the experiments performed by other people in the lab or by internal/external collaborators:

1. *In vitro* experiments with KPC-derived organoids and spheroids, which were performed by Dr. Marta Pellegatta and Paolo Canevazzi from the laboratory of Dr. Carla Taveggia (IRCCS San Raffaele Scientific Institute, Milan).
2. Generation of scRNAseq libraries which were performed by Dr. Nicoletta Caronni in the laboratory of Prof. Renato Ostuni (SR-Tiget, IRCCS San Raffaele Scientific Institute, Milan).
3. Spatial transcriptomic experiments of human PDAC samples, which were performed by Dr. Nicoletta Caronni together with Dr. Marco Genua in the laboratory of Prof. Renato Ostuni (SR-Tiget, IRCCS San Raffaele Scientific Institute, Milan).
4. Computational analyses which were performed by Federica La Terza and Dr. Giulia Barbiera from the laboratory of Prof. Renato Ostuni (SR-Tiget, IRCCS San Raffaele Scientific Institute, Milan).
5. Lineage tracing experiments which were performed by Dr. Garett Dunsmore from the laboratory of Prof. Florent Ginhoux (Gustave Roussy Cancer Campus, Villejuif, France)

6. Mass spectrometry analyses which were performed by Dr. Denise Drago and Dr. Annapaola Andolfo (Center for Omics Sciences (COSR), IRCCS San Raffaele Scientific Institute, Milan, Italy).

Most of the results present in this PhD thesis have been published in a research article (on peer-reviewed scientific journal) where I am listed as a co-first author (Caronni et al., 2023) and which I contributed to write and edit. Thus, part of the text, mainly in the Results, Figures and Material and Methods are shared with the cognate publication.
Additionally, during my PhD degree, I have been listed as co-author in two publications from my laboratory, as partial fulfilment of the PhD degree (Cilenti et al., 2021; Montaldo et al., 2022). Thus, there might be a partial overlap in the Material and Methods sections because of shared technologies and experiments.

All sources of information are acknowledged by means of reference.

ACKNOLEDGMENTS

I would like to acknowledge:
My DoS, Prof. Renato Ostuni, for giving me the opportunity to join his lab and work on this challenging and fascinating project. Additionally, I would like to thank him for sustaining my scientific career during these last three years and for the critical correction of my PhD thesis.

Dr. Nicoletta Caronni for her every-day supervision, the critical scientific discussions and the practical and theoretical teaching in designing, performing and critically analyzing the experiments. I would like also to thank her for the correction of my PhD thesis.

I would like to thank all the members of my laboratory. In particular:
Luca Mezzanzanica for the help with *in vitro* and *in vivo* experiments.
Simona Barresi for the daily technical support.
Dr. Marco Genua, who together with Dr. Nicoletta Caronni, performed the spatial transcriptomic experiments in human PDAC patients.
Dr. Giulia Barbiera and Federica La Terza for performing all the computational analyses present in this work.
All the other members of the lab for the daily help: Vincenzo Cuzzola, Luca Frosio, Roza Maria Barouni.

Additionally, I would like to thank my second supervisor, Prof. Ivan Zanoni, for the scientific support and advices.

Finally, we would like to acknowledge:
Dr. Marta Pellegatta and Paolo Canevazzi, from the laboratory of Dr. Carla Taveggia (IRCCS San Raffaele Scientific Institute, Milan), for the *in vitro* experiments with KPC-derived organoids and spheroids.
Dr. Denise Drago and Dr. Annapaola Andolfo (Center for Omics Sciences (COSR), IRCCS San Raffaele Scientific Institute, Milan, Italy) for mass spectrometry analyses.

Dr. Garett Dunsmore from the laboratory of Prof. Florent Ginhoux (Gustave Roussy Cancer Campus, Villejuif, France) for the fate mapping experiments.

Dr. Alessandra Mortellaro (SR-TIGET, IRCCS San Raffaele Scientific Institute, Milan, Italy) for providing NLRP3 KO mice, Prof. Cecilia Garlanda (IRCCS, Humanitas Research Hospital, Milan, Italy) for providing IL1R1 KO animals and Prof. Matteo Iannacone (IRCCS San Raffaele Scientific Institute, Milan) for providing CCR2 KO and IFNAR KO mouse models.

Prof. Lorenzo Piemonti (IRCCS San Raffaele Scientific Institute, Milan) for providing DT6606 and K8484 cell lines and Dr. Anna Mondino (IRCCS San Raffaele Scientific Institute, Milan) for providing 5M7101 and K4651 cell lines.

ABSTRACT

Pancreatic ductal adenocarcinoma (PDAC) is a lethal disease with high resistance to therapies. The immunologically cold tumor microenvironment (TME), characterized by high infiltration of suppressive immune cells and devoid of $CD8^+$ T cells, allows immune evasion of PDAC. Tumor-associated macrophages (TAMs) control immune dynamics in the TME, but their heterogeneity and plasticity have hampered our understanding of the underlying mechanisms.

Here, we combined single-cell and spatial genomics with functional experiments to elucidate macrophage functions in PDAC.

We uncovered an inflammatory cross-talk between tumor cells and TAMs that fuels disease progression. In particular, scRNAseq analysis of human PDAC and of mouse models of pancreatic cancer uncovered IL-$1\beta^+$ TAMs, a subset co-expressing inflammatory and reparative genes. Virtually undetectable in the healthy pancreas, IL-$1\beta^+$ TAMs accumulated during PDAC progression in discrete inflamed area of the tumor stroma and were elicited by a local synergy between prostaglandin E_2 (PGE_2) and tumor necrosis factor (TNF)-α. Physical proximity with IL-$1\beta^+$ TAMs was associated with inflammatory reprogramming and acquisition of pathogenic properties by a subset of PDAC cells. This occurrence was an early event in pancreatic tumorigenesis and led to persistent transcriptional changes associated with disease progression and poor patient outcome.

Interfering with the PGE_2-IL-1β axis elicited TAMs reprogramming and antagonized tumor cell-intrinsic and -extrinsic inflammation, leading to PDAC control *in vivo*.

In conclusion, our data highlight a key role of the PGE_2-IL-1β axis in driving pathogenic inflammation and fueling cancer progression. Thus, targeting the PGE_2-IL-1β axis may enable preventive or therapeutic strategy to reprogram the immune dynamics in pancreatic cancer.

TABLE OF CONTENTS

ACRONYMS AND ABBREVIATIONS 5

LIST OF FIGURES 8

1. INTRODUCTION 10

1.1. Macrophages 10

1.1.1. Heterogeneity of macrophages: a genomic perspective 11

1.1.2. Determinants of macrophage heterogeneity 13

1.1.3. Prostaglandin E_2 controls inflammatory activation of macrophages 15

1.2. Tumor-associated macrophages 17

1.2.1. Co-option of macrophage functions during tumor progression 17

1.2.2. Heterogeneity of TAMs 19

1.2.3. Therapeutic targeting of TAMs 20

1.3. Pancreatic Ductal Adenocarcinoma 21

1.3.1. Heterogeneity of PDAC 22

1.3.2. Genomic drivers of PDAC 23

1.3.3. Models of pancreatic tumorigenesis 26

1.3.4. Cooperation of injury and oncogenic mutations 27

1.3.5. Inflammation in pancreatic tumorigenesis 28

1.4. PDAC microenvironment 29

1.4.1. T cells 31

1.4.2. Dendritic cells 32

1.4.3. Cancer-associated fibroblasts 32

1.4.4. Tumor-associated macrophages 34

1.5. Role of PGE_2 in the TME 37

2. AIM OF THE WORK 40

3. RESULTS 41

3.1. *IL1B*$^+$ TAMs correlate with poor prognosis in human PDAC 41

3.2. Characterization of *Il1b*$^+$ TAMs in mouse models of pancreatic cancer 47

3.3. Monocytes differentiate into IL-1β$^+$ TAMs upon exposure to TME factors .. 52

3.4. PGE_2 and TNF-α cooperatively elicit the IL-1β$^+$ TAM state 54

3.5. PDAC-derived PGE_2 elicits IL-1β$^+$ TAMs and promotes tumor growth 61

3.6. IL-1β signaling in PDAC cells promotes tumor growth 67

3.7. IL-1β signaling in PDAC cells sustains TAM recruitment and conditioning 70

3.8. Inflammatory reprogramming occurs early during pancreatic tumorigenesis 72

3.9. IL-1β$^+$ TAMs spatially colocalize with T1RS$^+$ PDAC cells in patients 76

4. DISCUSSION 80

5. MATERIAL AND METHODS 87

5.1. Patient samples 87

5.2. Mouse PDAC 88

5.3. CRISPR-Cas9-mediated gene targeting 89

5.4. *In vivo* animal studies 90

5.5. Orthotopic tumors 91

5.6. Heterotopic tumors 91

5.7. *In vivo* treatments 91

5.8. Bone Marrow (BM) chimeras. 92

5.9. Tissue processing 92

5.10. Culture of mouse monocytes and macrophages 93

5.11. *Ex vivo* stimulation of mouse cells 94

5.12. Generation and culture of mouse PDAC spheroids 94

5.13. Generation and culture of mouse PDAC organoids 95

5.14. *In vitro* stimulation of murine PDAC organoids 95

5.15. Analysis of organoid-forming efficiency 96

5.16. *In vitro* stimulation of tumor cells and organoids with IL-1β for gene expression analysis 96

5.17. Lentiviral transduction of KPC cells 97

5.18. Flow cytometry 97

5.19. Cell proliferation assay 101

5.20. RT-qPCR 101

5.21. Analyses of cell culture supernatant 101

5.22. Extraction of prostaglandins (PGs) by SPE (C-18) purification 102

5.23. Chromatographic separation of PGE_2 and PGD_2 and their LC-MS/MS detection 103

5.24. Western Blot analyses 103

5.25. Generation of and processing of single-cell RNA-Seq data 104

5.25.1. Data generation 104

5.25.2. Data processing 105

5.25.3. Batch correction 105

5.25.4. Graph-based clustering and differential gene expression analyses. 106

5.25.5. Inference of copy-number variants (CNV) 106

5.25.6. Human-mouse comparison of TAM clusters 106

5.25.7. RNA Velocity and single-cell trajectories 106

5.25.8. Gene set enrichment analysis (GSEA) 107

5.25.9. IL1B gene expression in human cell types. 107

5.25.10. Reanalysis of human PDAC cells in Naïve samples. 107

5.25.11. scRNA-Seq datasets collected in this study 108

5.25.12. scRNA-Seq dataset from pancreatitis patients 108

5.25.13. scRNA-Seq datasets from other mouse models 108

5.26. Generation and processing of spatial transcriptomic (ST) data 109

Molecular Cartography™ data 109

5.26.1. Data generation 109

5.26.2. Cell Segmentation 111

5.26.3. Cell filtering and annotation 111

5.26.4. Spatial neighborhood analysis 111

5.26.5. ST datasets collected in this study. 111

5.27. Generation and processing of bulk RNA-Seq data 112

5.27.1. Data generation 112

5.27.2. Data processing 112

5.27.3. Definition of TNF-α+PGE_2 synergized genes. 112

5.27.4. Definition of tumor-intrinsic IL-1β response signature (T1RS) gene signature. 113

5.27.5. RNA-Seq datasets collected in this study. 113

5.27.6. TCGA data analyses. 113

5.27.7. Survival analysis of TAM markers and T1RS genes in PAAD cohort. 113
5.27.8. Survival analysis on *IL1B*$^{+}$ TAMs gene signature. 114
5.27.9. Association of T1RS and *IL1B*$^{+}$ TAMs signatures 114
5.27.10. Cell type deconvolution of TCGA PDAC samples 114
5.28. Quantification and statistical analyses 114
6. BIBLIOGRAPHY 116

ACRONYMS AND ABBREVIATIONS

AA	Arachidonic Acid
ADEX	Aberrantly Differentiated Endocrine Exocrine
ApCAF	Antigen Presenting Cancer Associated Fibroblast
ARG1	Arginase 1
BAM	Border Assocated Macrophage
BM	Bone Marrow
BMDM	Bone Marrow derived Macrophage
BP	Biological Processes
CAFs	Cancer Associated Fibroblasts
cAMP	Cyclic Adenosine Monophosphate
CAR	Chimeric Antigen Receptor
CCL	Chemokine (C-C motif) Ligand
CCR	Chemokine (C-C motif) Receptor
CD	Cluster of Differentiation
cDC	Convetional Dendritic Cell
C/EBP	Ccaat Enhancer Binding Proteins
COX	Cycloxygenase
CRC	Colorectal Carcinoma
CREB	cAMP Response Element Binding Protein
CSF	Colony Stimulating Factor
CTLA4	Cytotoxic T-Lymphocyte Antigen 4
CXCL	Chemokine (C-X-C motif) Ligand
DAMP	Danger Associated Molecular Pattern
db-cAMP	dibutyryl-cAMP
DEG	Differentially Expressed Gene
ECM	Extracellular Matrix
EMT	Epithelialo-to-Mesenchymal Transition
FAP	Fibroblasts Acivation Protein
FC	Fold Change
FDA	Food and Drug Administration
FLICA	Fluorochrome Labeled Inhibitors of Caspase
FOLR2	Folate Receptor 2
GEMM	Genetically Engineered Mouse Model
GM-CSF	Granulocyte Monocyte Colony Stimulating Factor
GMP	Granulocyte Monocyte Precursor
GO	Gene Ontology
GSEA	Gene Set Enrichment Analysis
GZMB	Granzyme B
H3K27Ac	Histone 3 Lysine 27 Acetylation
hHCC	Human HepatoCellular Carcinoma

HSC	Hematopoietic Stem Cell
IAV	Influenza A Virus
iCAF	Inflammatory Cancer Associated Fibroblast
ICB	Immune Checkpoint Blockade
IDO	Indoleamine-pyrrole 2,3-Dioxygenase
IFN	Interferon
IFNAR	Interferon alpha/beta Receptor 1
IL	Interleukin
IL1R1	Interleukin 1 Receptor 1
iNOS	Inducible Nitric Oxide Synthase
IPMN	Intraductal Papillary Mucinous Neoplasia
IRF	Interferon Regulatory Factor
JAK	Janus Tyrosine Kinase
KC	Kupffer Cell
KO	Knock Out
LIF	Leukemia Inhibitory Factor
LPS	Lipopolysaccharide
M-CSF	Macrophage Colony Stimulating Factor
MAPK	Mitogen-activated Protein Kinase
MDSC	Myeloid Derived Suppressor Cell
MEF	Myocyte Enhancer Factor
MHC	Major Histocompatibility Complex
MNP	Mononuclear Phagocyte
mPGES	Microsomal Prostaglandin E Synthase
mregDC	Mature Regulatory DC
myCAF	Myofibroblast Cancer Associated Fibroblast
NES	Normlized Enrichment Score
NF-kB	Nuclear Factor Kappa B
NGS	Next Generation Sequencing
NK	Natural Killer
NLRP	Nucleotide-binding oligomerization domain, Leucine rich Repeat and Pyrin domain containing
NSCLC	Non Small Cell Lung Cancer
PanIN	Pancreatic Intraepithelia Neoplasia
PD	Programmed Death
PDAC	Pancreatic Ductal AdenoCarcinoma
PDGFR	Platelet-Derived Growth Factor Receptor
PDL	Programmed Death Ligand
PDPN	Podoplanin
PF1	Perforin 1
PG	Prostaglandin
PGES	Prostaglandin E Synthase

PKA	Protein Kinase A
PPAR	Peroxisome Proliferator Activated Receptor
PRR	Pattern Recognition Receptor
ROS	Reactive Oxygen Species
ScRNAseq	Single Cell RNA Sequencing
SIRP	Signal Regulatory Protein
SMA	Smooth Muscle Chain
SMAD	Small Mothers Against Decapentaplegic
SNV	Single Nucleotide Variant
SPP	Signal Peptide Peptidase
STING	Stimulator of Interferon Response CGAMP Interactor 1
STAT	Signal Transducer and Activator of Transcription
T1RS	Tumor-intrinsic IL-1b Response Signature
TAM	Tumor Associated Macrophage
TCGA	The Cancer Genome Atlas
TCM	Tumor Conditioned Media
TEI	Tumor Eliciting Inflammation
TF	Transcription Factor
TGFb	Tumor Growth Factor Beta
Th	T Helper
TIM3	T cell Immunogobulin Mucin-3
TME	Tumor MicroEnvironemnt
TNF	Tumor Necrosis Factor
Treg	T Regulatory
TRM	Tissue Resident Macrophage
VEGF	Vascular Endothelial Growth Factor
WT	Wild Type

LIST OF FIGURES

Figure 1. scRNAseq analysis of human PDAC patients……..42

Figure 2. scRNAseq analysis of human PDAC patients uncovers IL1B$^+$ TAMs……44

Figure 3. IL1B+ TAMs showed an inflammatory profile while being depleted of antigen presentation and IFN-related signature……45

Figure 4. IL1B$^+$ TAMs correlate with poor prognosis in human PDAC…….46

Figure 5. scRNAseq analysis of KPC-derived mouse PDAC model……..47

Figure 6. IL-1β$^+$ TAMs are conserved in mouse models of pancreatic cancer…….48

Figure 7. IL-1β$^+$ macrophages accumulate early during tumor progression and are conserved in multiple murine PDAC models……..50

Figure 8. Immunophenotypic analysis of IL-1β$^+$ TAMs……52

Figure 9. CellRank analysis identify tumor-infiltrating monocytes as bona fide precursors of IL-1β$^+$ TAMs……...53

Figure 10. Monocytes differentiate into IL-1β$^+$ TAMs upon exposure to TME factors...54

Figure 11. Investigation of local factors eliciting the Il1b$^+$ TAM phenotype……..55

Figure 12. PGE_2 is highly expressed in human and mouse PDAC……...56

Figure 13. PGE_2 and TNF-α synergistically induce Il1b expression in mouse macrophages and monocytes……...57

Figure 14. PGE_2 and TNF-α cooperatively elicit the IL-1β$^+$ TAM state……59

Figure 15. cAMP is able to phenocopy PGE_2-dependent synergistic activity with inflammatory stimuli……...61

Figure 16. Inhibition of COX-2 reduces PDAC progression…….62

Figure 17. Disruption of Ptgs2 in tumor cells impairs PGE_2 production without affecting their vitality and proliferation in vitro……..63

Figure 18. COX2 KO tumors show impaired tumor growth in immunocompetent mice.64

Figure 19. PDAC-derived PGE_2 elicits the IL-1β$^+$ TAM phenotype……..66

Figure 20. Neutralization of IL-1β impairs PDAC growth…….67

Figure 21. Inhibition of Il-1β signaling in stromal or hematopoietic cells does not alter PDAC growth……..68

Figure 22. IL-1β signaling in PDAC cells is critical for tumor growth……..69

Figure 23. IL-1β intrinsic signaling affects organoid-forming efficiency of tumor cells.70

Figure 24. IL-1β signaling induces an inflammatory reprogramming of tumor cells….72
Figure 25. T1RS is associated with IL-1β^{+} TAMs abundance and poor prognosis in PDAC patients……. 73
Figure 26. Inflammatory reprogramming occurs early during pancreatic tumorigenesis …….74
Figure 27. Tissue damage and oncogene activation cooperatively promotes inflammatory reprogramming of pancreatic cells…… . 76
Figure 28. Identification of T1RS^{+} PDAC cells in human PDAC patients…….77
Figure 29. IL-1β^{+} TAMs spatially colocalize with T1RS^{+} PDAC cells in patients…….78

1. INTRODUCTION

1.1. Macrophages

Macrophages are myeloid cells of the innate immune system that colonize virtually all tissues throughout our body. First identified by Metchnikoff in the 19th century, they were initially described as immune cells capable of phagocytosing solid substances like foreign bodies and dead cells (Metschnikoff, 1891). Indeed, macrophages serve as the initial line of defense for the organs, particularly the skin and internal mucosa, which are continually exposed to external insults (Park et al., 2022). Macrophages continually patrol tissues to eliminate foreign threats, such as bacteria or infected cells, recognized through the expression of pattern recognition receptors (PRR) on their surface. Upon infection, macrophages adopt an inflammatory profile, releasing mediators like tumor necrosis factor-α (TNF-α) and interleukin (IL)-1, thereby amplifying the downstream inflammatory cascade (Murray & Wynn, 2011). However, macrophages are equally crucial in clearing dying cells from the surrounding tissue. In particular, their phagocytosis of apoptotic cells, known as efferocytosis, promotes the production of anti-inflammatory mediators, like IL-10 and transforming growth factor-β (TGF-β). This mechanism helps dampen the inflammatory response to prevent excessive tissue damage (Kourtzelis et al., 2020; Ortega-Gómez et al., 2013). Furthermore, macrophages transition into a tissue repair phenotype, characterized by the secretion of growth factors, such as vascular endothelial growth factor α (VEGFα), that support cell proliferation and formation of new blood vessels (Wynn & Vannella, 2016). Simultaneously, macrophages promote the activation and differentiation of tissue fibroblasts, facilitating the deposition of new extracellular matrix (ECM) (Murray & Wynn, 2011). Nonetheless, the traditional view of macrophages as mere sentinels and scavengers has evolved. Specific subsets of macrophages, originating from embryonic precursors, colonize organs during development and persist into adulthood, establishing long-lasting relationships with their tissue of residence. Here, tissue resident macrophages (TRMs) exert a spectrum of organ-specific functions, critical for maintenance of homeostasis (Amit et al., 2016; Blériot et al., 2020; Ginhoux & Guilliams, 2016). For example, brain microglia actively eliminate defective or immature synapses through synaptic pruning (Amit et al., 2016; Paolicelli et al., 2011). Lung alveolar macrophages clear surfactant and eosinophilic materials in the

alveolar space (Whitsett et al., 2010; Wright, 1990). Kupffer cells (KC) in the liver and red pulp splenic macrophages phagocyte senescent and damaged erythrocytes and recycle iron (Haldar et al., 2014; Kohyama et al., 2009; Theurl et al., 2016). Finally, cardiac macrophages contribute to heart fitness by supporting angiogenesis and cardiomyocyte proliferation (Park et al., 2022). These are just a few examples of the diverse activities performed by TRMs. This shift in perspective has transformed our understanding of macrophages. No longer seen as mere sentinels and scavengers, they are now recognized as fully integrated components of the tissue, contributing to non-immune functions that are critical for maintaining tissue homeostasis.

1.1.1. Heterogeneity of macrophages: a genomic perspective

When exposed to various instructive signals, such as metabolic, homeostatic, and modulatory cues, macrophages adapt to perform tissue-specific functions. The differentiation and tissue-specificity of resident macrophages rely on the activation and regulation of specific transcriptional programs, which depend on available *cis*-regulatory repertoire (Amit et al., 2016; Glass & Natoli, 2016; Natoli & Ostuni, 2019).

Mechanistically, transcription factors (TFs) that determine myeloid lineage, prompted by various signals like macrophage colony stimulating factor (M-CSF), collaborate to establish and maintain a basal and inducible core transcriptional and genomic program (Garber et al., 2012; Ghisletti et al., 2010; Heinz et al., 2010; Mossadegh-Keller et al., 2013). These TFs, often called pioneer TFs, have the remarkable ability to open up tightly packed chromatin regions for access. Key pioneer TFs for macrophage differentiation include PU.1, IRF8, C/EBPα, and C/EBPβ (Heinz & Glass, 2012; Natoli & Ostuni, 2019; Ostuni & Natoli, 2013). These TFs establish a prototype macrophage state, which is further refined by the local environment (Amit et al., 2016). Upon homing to a specific tissue, macrophages respond to local signals that activate polarizing TFs. These polarizing TFs shape the macrophages to have characteristics suited to that particular organ (Glass & Natoli, 2016; Lavin et al., 2014; Natoli & Ostuni, 2019; Ostuni & Natoli, 2013; Varol et al., 2015). For instance, alveolar macrophages depend on the expression of PPARγ, induced by granulocyte-macrophage colony-stimulating factor (GM-CSF) in the alveolar space, to clear surfactants and maintain homeostasis (Schneider et al., 2014). Similarly, retinoic acid triggers the expression of GATA-6, which, together with other

factors, initiates a specific transcriptional program for peritoneal macrophages (Gautier et al., 2014; Rosas et al., 2014). Heme, released during erythrocyte clearance, drives the expression of SPI-C, crucial for the differentiation of red pulp splenic macrophages and Kupffer cells (Haldar et al., 2014).

However, tissues are dynamic environments exposed to constant changes that disrupt homeostasis. This introduces another layer of diversity, as condition-specific signals activate effector TFs, further influencing macrophage states and phenotypes (Natoli & Ostuni, 2019; Ostuni & Natoli, 2013). For instance, exposure to external stimuli like lipopolysaccharide (LPS) or inflammatory and immune-modulatory cytokines activates stimulus-dependent TFs that target predefined genomic regions and latent enhancers (Garber et al., 2012; Ostuni et al., 2013). Latent enhancers, not marked in steady-state macrophages, become active upon stimulation, leaving an epigenetic signature of encountered stimuli. This memory leads to a quicker response when macrophages are re-stimulated with the same or unrelated stimuli, highlighting their ability to adapt to the instructive signals of the surrounding environment (Natoli & Ostuni, 2019; Ostuni et al., 2013).

In 2000, Mills and colleagues attempted to categorize macrophage polarization states when exposed to inflammatory or anti-inflammatory stimuli. They described two programs, M1 and M2, induced by Interferon (IFN)-γ and IL-4, respectively (Mills et al., 2000). While M1 macrophages have pro-inflammatory characteristics and increased microbicidal activity, M2 macrophages exhibit anti-inflammatory traits and tissue repair abilities (Mills et al., 2000; Piccolo et al., 2017). However, *in vivo*, macrophages are exposed to a multitude of stimuli, some with opposing effects. Co-stimulation with IFN-γ and IL-4 results in a mixed transcriptional profile, where M1 and M2 characteristics coexist. Some genes are repressed, indicating a selective antagonism between the two stimuli (Natoli & Ostuni, 2019; Piccolo et al., 2017).

In summary, macrophages encounter multiple, sometimes conflicting signals, including lineage-determining, tissue-specific, and environmental cues. Thanks to their adaptability, macrophages can integrate and respond to these stimuli by acquiring context-dependent genetic and functional programs (Natoli & Ostuni, 2019).

1.1.2. Determinants of macrophage heterogeneity

Numerous factors contribute to and shape the diversity of macrophage phenotypes and functions, as outlined below.

Ontogeny: The traditional notion that tissue-resident macrophages in a steady state are solely replenished by blood monocytes originating from hematopoietic stem cells (HSCs) in adult bone marrow has been challenged. Seminal studies have revealed that mature macrophages appear during murine embryogenesis before HSCs (Alliot et al., 1999; Blériot et al., 2020; L. Morris et al., 1991). Tissue-resident macrophages can have various origins, including yolk-sac progenitors, fetal liver monocytes, or bone marrow hematopoietic stem cells (Blériot et al., 2020; Ginhoux et al., 2010; Gomez Perdiguero et al., 2015; Hoeffel et al., 2015). Lineage tracing experiments showed that adult tissues contain varying proportions of these three ontogenically distinct macrophages (Blériot et al., 2020). Brain microglia originate from yolk sac precursors and persist in adulthood by self-renewal and local proliferation, with minimal contribution from blood circulating monocytes (Ginhoux et al., 2010; Hoeffel et al., 2015). In contrast, fetal-derived gut macrophages are gradually replaced by circulating monocytes after birth (Bain et al., 2014). Finally, in some tissues, macrophages exhibit a mixed profile: for instance, alveolar macrophages are able to self-renew although a proportion, increasing with aging, is of blood monocytic origin (Park et al., 2022). However, disruption of homeostasis can greatly affect the relative proportions of embryo- and monocyte-derived macrophages. For example, in cases where TRMs succumb to infections, like KCs during *Listeria* infection, this can trigger the recruitment of circulating monocytes to fill empty niches, replenish TRMs, and initiate tissue-repair pathways (Blériot et al., 2015; Park et al., 2022).

Niche: Local microenvironmental factors in tissue niches where macrophages reside influence their specific phenotypes and functions (Amit et al., 2016; Gautiar et al., 2012). For example, type II alveolar pneumocytes release GM-CSF, a critical factor for alveolar macrophage differentiation (Gschwend et al., 2021). Likewise, erythrocyte-associated heme induces the expression of SPI-C, a transcription factor controlling iron recycling by red pulp splenic macrophages and Kupffer cells (Haldar et al., 2014). While the influence of ontogeny versus local environment on macrophage phenotype remains unclear, recent research suggests that niche factors may prevail over origin. Yolk sac progenitors, fetal

monocytes, and adult monocytes can all efficiently differentiate into alveolar macrophages when transplanted into newborn *Csf2rb*$^{-/-}$ mice, with alveolar macrophage deficiencies (van de Laar et al., 2016). Furthermore, even peritoneal macrophages intratracheally transplanted in adult *Csf2rb*$^{-/-}$ mice could acquire an alveolar-macrophage-like transcriptional program (Lavin et al., 2014). Nonetheless, the duration of residence within a specific environment is crucial for a full acquisition of a particular phenotype (Blériot et al., 2020).

Time of residence: The time a macrophage spends in a particular environment is crucial for its full differentiation. For instance, in the liver, upon the deletion of Kupffer cells, monocytes can infiltrate the liver and acquire a Kupffer cell-like transcriptional program within days. However, they lack key markers of Kupffer cells, such as *Timd4* or *Clec4f* , which are acquired only after several weeks, underscoring the time needed for complete differentiation (Guilliams & Scott, 2017; Scott et al., 2016). Consequently, embryonic-derived macrophages, established before birth, coexist with monocyte-derived macrophages recently infiltrated in the same organ (Blériot et al., 2020).

Considering these factors, along with advancements in single-cell technologies, macrophage heterogeneity within organs has become more evident in recent years. Various tissue subpopulations have been identified. For instance, in the brain, apart from microglia, multiple populations of border-associated macrophages (BAMs) have been described (Van Hove et al., 2019). Similarly, the lungs house not only alveolar macrophages but also interstitial macrophages, with two distinct subpopulations identified (Chakarov et al., 2019; Schyns et al., 2019). These subpopulations exhibit different transcriptional programs and are often spatially segregated within sub-tissue niches, exposed to distinct environmental factors (Blériot et al., 2020).

However, despite these organ-specific differences, certain core functions are shared across different tissues, including the clearance of cell-related materials, defense against pathogens, and maintenance of vascular tone and integrity (Park et al., 2022). Recent studies have identified recurring macrophage subsets with conserved origins and a common core gene signature across various murine tissues (Dick et al., 2022). In summary, while tissue resident macrophages exhibit high heterogeneity and specialization, they also share essential common elements across different organs.

1.1.3. Prostaglandin E2 controls inflammatory activation of macrophages

Among the numerous signals influencing polarization of macrophages, here we focused on prostaglandin E2 (PGE_2), a lipid mediator with pleiotropic functions in tissue homeostasis, repair and inflammation. Produced by various cell types, including epithelial, stromal, and immune cells, PGE_2 is derived from arachidonic acid (AA), which is released from the cell membrane by the action of phospholipase A2. Subsequently, it is converted into prostaglandin H2 (PGH_2) by cyclooxygenase-1 and -2 (COX-1 and COX-2) enzymes (H. Cheng et al., 2021; Ricciotti & Fitzgerald, 2011; D. Wang & Dubois, 2010). While COX-1 is constitutively expressed, COX-2 is mainly induced during inflammatory responses (DuBois et al., 1998). PGH_2 can then be transformed into different prostaglandins or thromboxane A_2. Specifically, three enzymes can convert PGH_2 into PGE_2: cytosolic prostaglandin E synthase (cPGES) and microsomal prostaglandin E synthases 1/2 (mPGES-1/2). While cPGES and mPGES-2 are constitutively expressed, mPGES1 is primarily associated with COX-2 during inflammation (H. Cheng et al., 2021; D. Wang & Dubois, 2010). Once synthesized, PGE_2 is released into the extracellular environment, where it carries out its functions by binding to four receptors: EP1, EP2, EP3, and EP4. These receptors are all transmembrane G-protein-coupled receptors, but they activate different downstream signaling pathways (H. Cheng et al., 2021; D. Wang & Dubois, 2010). EP2 and EP4, the primary receptors on leukocytes, are coupled to G stimulatory proteins, leading to intracellular cAMP accumulation and PKA activation (Markovič et al., 2017). EP4 can also activate other players like β-arrestin or β-catenin (Yokoyama et al., 2013). In contrast, EP3 is coupled to a G inhibitory protein, reducing intracellular cAMP levels, while EP1 is coupled to a Gq protein, increasing intracellular calcium levels (Narumiya, 2009; Tang et al., 2005). The widespread distribution of these receptors and their varying presence in different tissues account for the diverse roles PGE_2 plays in both normal and pathological conditions. PGE_2 is crucial for tissue homeostasis and regeneration (Caronni et al., 2021; H. Cheng et al., 2021). For example, it can expand HSCs and multipotent progenitors in species like zebrafish and mice (North et al., 2007). Additionally, PGE_2 has been associated with improved homing and regeneration of HSCs, as well as maintenance of stemness during *ex vivo* manipulation (Hoggatt et al., 2009; Zonari et al., 2017). During intestinal homeostasis, it promotes the formation of structures with increased stemness

and organoid-forming ability but can also lead to the expansion of stem cells with tumorigenic potential when aberrantly produced by a peri-cryptal population of fibroblasts (Roulis et al., 2020).

PGE_2 also plays critical roles during inflammation, contributing to vasodilation, leukocyte recruitment, pain, and fever (Ricciotti & Fitzgerald, 2011). It increases arterial dilation and vascular permeability, leading to swelling and edema in inflamed tissues. Moreover, PGE_2 directly stimulates pain sensation through its effects on sensory neurons and central sites in the nervous system (Funk, 2001). Targeting PGE_2 production by inhibiting mPGES1 has shown promise in reducing the inflammatory response in various mouse models, such as in rheumatoid arthritis (Brenneis et al., 2011; Kamei et al., 2004; Trebino et al., 2003; M. Wang et al., 2006).

In recent years, PGE_2 has emerged as a crucial regulator of macrophage inflammatory activation. Specifically, PGE_2, through a cAMP/CREB-dependent mechanism, drove an alternative polarization of macrophages. This process enhanced the induction of canonical M2 markers, such as *Arg1*, *Mrc1*, and *Fizz1*, particularly in response to IL-4 (Luan et al., 2015). Furthermore, PGE_2 has been found to downregulate the production of type I IFN in various scenarios. For instance, when peritoneal macrophages were exposed to LPS and an EP4 selective antagonist, they released higher levels of IFN-β compared to macrophages treated with LPS alone (Perkins et al., 2018). Similarly, in a Salmonella Typhimurium infection model, mice treated with an EP4 antagonist showed increased *Ifnb* expression in the spleen (Perkins et al., 2018). Likewise, following an Influenza A virus (IAV) infection, *Ptges*$^{-/-}$ alveolar macrophages produced higher levels of IFN-β compared to WT macrophages (Coulombe et al., 2014). Mechanistically, macrophages exhibit a remarkable ability to integrate opposing signals, as discussed above. For example, co-exposure of macrophages to LPS and PGE_2 resulted in impaired expression of several LPS-induced genes encoding for inflammatory cytokines (*Ifnb*, *Il12b*, *Tnf*), chemokines (*Cxcl9*, *Cxcl10*) and transcription factors (*Irf1*). Simultaneously, this correlated with an increased expression of anti-inflammatory molecules like *Il10* (Cilenti et al., 2021). Defective induction of LPS-induced genes is associated with impaired chromatin remodeling and reduced deposition of acetylation on histone H3 lysine 27 (H3K27Ac) (Cilenti et al., 2021). However, while suppressing type I IFN production, PGE_2 plays a critical role in the expression of IL-1β, a prototypical

inflammatory cytokine. Exogenous PGE_2, for instance, enhanced IL-1β production in macrophages treated with LPS. Furthermore, blocking COX activity in LPS-treated macrophages led to a reduction in IL-1β accumulation, indicating the pivotal role of endogenous PGE_2 in LPS-induced *Il1b* expression (Zasłona et al., 2017).

In conclusion, PGE_2 has a profound impact on macrophage inflammatory activation, exerting opposing functions. It promotes alternative macrophage activation and inhibits type I IFN production, while simultaneously being critical for the expression of key inflammatory mediators such as IL-1β.

1.2. Tumor-associated macrophages

Tumor-associated macrophages (TAMs) are an abundant leukocyte population in the tumor microenvironment (TME) (Christofides et al., 2022). Given their remarkable plasticity, TAMs can exert opposing functions in the TME, either restraining or promoting tumor progression, as further discussed below. Nevertheless, the presence of TAMs is generally associated with a poor prognosis in most human tumors, making them an appealing target for therapeutic interventions (Q. wen Zhang et al., 2012). Traditionally, TAMs were classified as anti-tumorigenic when they displayed an M1-like phenotype, characterized by high expression of inflammatory factors like inducible nitric oxide synthase (iNOS) and major histocompatibility complex (MHC) II molecules. Conversely, TAMs that expressed anti-inflammatory and immunomodulatory molecules, such as IL-10, Arginase1 (ARG1), and CD206, resembled an M2-like activation state and were considered pro-tumorigenic (Mantovani et al., 2002). However, this model resulted to be over simplistic as TAMs with pro-tumor activities don't always express the typical M2-like markers and M1 and M2 signatures are often co-expressed (Bill et al., 2023; S. Cheng et al., 2021; Pittet et al., 2022). This complexity highlights the need for a more nuanced understanding of heterogeneity and roles of TAMs within the TME, which could lead to more effective therapeutic strategies in the future.

1.2.1. Co-option of macrophage functions during tumor progression

Macrophages play a crucial role in the TME, where their natural tissue-supportive functions are hijacked by tumors, fueling their growth and malignancy. As growing tumors disrupt tissue homeostasis, they trigger the activation of macrophages that attempt

to repair the tumor tissue, often defined as a "wound that never heals" (Caronni et al., 2021; Christofides et al., 2022; Dvorak, 1986; Kloosterman & Akkari, 2023). As cancer advances, accumulation of danger-associated molecules (DAMPs) in the TME is sensed by TAMs. This sensing sets off an inflammatory cascade, leading to the recruitment and activation of stromal and immune cells (Hernandez et al., 2016). However, while trying to restore tissue homeostasis and healing the tumor, macrophages also activates tissue-reparative functions and aim to prevent excessive immune activation, which can result in the suppression of cytotoxic responses (Kloosterman & Akkari, 2023; Kourtzelis et al., 2020). Furthermore, as part of the healing process, macrophages are instrumental in reorganizing the extracellular matrix and promoting neo-angiogenesis, as discussed above. This, in turn, provides the tumor tissue with more oxygen, nutrients, and growth factors (Egeblad et al., 2010; Riabov et al., 2014). Lastly, macrophages promote an epithelial-to-mesenchymal transition (EMT) as a final step in closing the wound. EMT is a hallmark of malignancy and is associated with metastatic dissemination and the colonization of distant organs (Hanahan, 2022).

While the abundance of TAMs typically correlates with a poor prognosis, and tumors co-opt their functions, macrophages can also exert anti-tumor activities. As professional phagocytic cells, TAMs can directly engulf dying cancer cells and opsonized cells by recognizing specific eat-me signals. However, tumor cells often downregulate these signals or increase don't-eat-me molecules to avoid being killed by TAMs (Kloosterman & Akkari, 2023; Molgora & Colonna, 2021). TAMs also contribute to anti-tumor activities by producing factors with tumoricidal effects, such as nitric oxide, and by supporting T cell responses through antigen presentation or the release of chemokines and cytokines (Majety et al., 2018; Molgora & Colonna, 2021). Recent single-cell analysis of human breast tumors identified a subset of TAMs located in healthy adjacent tissue that resemble TRMs (Nalio Ramos et al., 2022). Interestingly, the presence of these TAMs was associated with improved prognosis in breast cancer patients and a higher presence of immune cells typically involved in anti-tumor responses. Spatial analysis revealed that these TAMs specifically reside in the tumor stroma, near CD8 T cells, in this way establishing prolonged interactions. *In vitro* co-culture experiments confirmed the superior ability of these TAMs in promoting CD8 T cell activation (Nalio Ramos et al., 2022).

In summary, considering the pivotal roles that macrophages play in promoting tumor progression, they present promising targets in the field of immunoncology. However, any therapeutic strategy should acknowledge their significant heterogeneity.

1.2.2. Heterogeneity of TAMs

The advent of single cells technologies has shed light on the remarkable heterogeneity and functional versatility of TAMs. Depending on the tumor types, stage of the disease and treatment methods, different populations of TAMs have been reported in different tumors (Caronni et al., 2021; Ma et al., 2022). Nevertheless, recurrent TAM states sharing similar transcriptional programs have been identified. For instance, TAMs resembling tissue-resident populations have been observed in various contexts, often with contrasting functions (Ma et al., 2022). In non-small cell lung cancer (NSCLC), a population of TRMs plays a pivotal role in establishing an immunosuppressive and pro-tumorigenic microenvironment during the initial stages of tumor progression (Casanova-Acebes et al., 2021). Mechanistically, these TRMs promote tumor cell invasiveness, the acquisition of an EMT program, and the differentiation of regulatory T cells (Tregs). Spatial analysis has shown close proximity among tumor cells, TRMs, and Tregs in the early phases of tumor development, with TRMs relocating to the tumor periphery in later disease stages. Interestingly, specific depletion of TRMs results in reduced tumor progression and a shift in the TME toward an anti-tumor phenotype, marked by increased T-cell infiltration and activation (Casanova-Acebes et al., 2021). Similarly, recent findings in human hepatocellular carcinoma (hHCC) indicate an onco-fetal reprogramming of the TME with a subset of TAMs transcriptionally resembling fetal liver macrophages, largely absent in the healthy adult liver. These TAMs co-localize with endothelial cells exhibiting a fetal-like phenotype and Tregs, suggesting a potential role in immunosuppression and tumor growth (Sharma et al., 2020).

Another recurring TAM state is characterized by the expression of genes associated with lipid metabolism (Ma et al., 2022; Mulder et al., 2021). In human prostate cancer, a subset of TAMs expressing the scavenger receptor MARCO and genes related to lipid metabolism and accumulation correlates with poor survival. MARCO, induced by tumor-derived IL-1β, is directly involved in lipid uptake, promoting cancer cell migration through the production and release of chemokines like CCL6. Neutralizing antibodies

against MARCO reduce tumor progression and lipid accumulation in TAMs (Masetti et al., 2021).

Furthermore, as macrophages have been consistently linked to supporting tumor neo-angiogenesis, populations of TAMs expressing an angiogenic signature also have been recurrently described (Ma et al., 2022). In a comprehensive study analyzing the myeloid cell population in 15 human tumor types, *SPP1*$^{+}$ TAMs highly expressing angiogenesis-related genes were found in eight different tumors. Notably, subsets of macrophages expressing angiogenesis-related genes were also observed in tumors without *SPP1*$^{+}$ TAMs (S. Cheng et al., 2021).

In addition, TAMs play a crucial role in promoting inflammation and can exhibit different inflammatory profiles. Some TAMs express high levels of genes encoding for cytokines and chemokines like *IL1B* and *CXCL1/2*, contributing to cancer-promoting inflammation (Ma et al., 2022). In a recent study of renal cell carcinoma, a subset of *IL1B*$^{+}$ TAMs was found in close proximity to tumor cells expressing an EMT signature (Ruoyan Li et al., 2022). Conversely, another recurrent subset of TAMs expresses IFN-related genes. While this type I IFN signature might imply an anti-tumor role, these TAMs can also exert immunosuppressive functions by highly expressing immune checkpoint molecules, including IDO, an enzyme involved in tryptophan degradation and T-cell suppression (Sadik et al., 2020).

These are just few examples of recurring TAM states that play crucial roles in the TME. It's worth noting that mixed populations of TAMs, which co-express characteristics of different TAM subsets, can also exist. In conclusion, TAMs play a critical role in the TME, exhibiting both pro-tumor and anti-tumor potential. An increasing number of studies are now focused on addressing TAM heterogeneity using single-cell technologies, particularly examining their spatial distribution. This spatial information not only adds another dimension to their diversity but also provides valuable insights into specific cell-to-cell interactions within the TME. Understanding the stability of these TAM subsets and their potential for manipulation and repolarization will be essential moving forward.

1.2.3. Therapeutic targeting of TAMs

In light of the pivotal roles that macrophages play in promoting tumor progression, they emerge as promising therapeutic targets in immunoncology. Current therapeutic

strategies being clinically investigated aim to hinder monocyte recruitment or the survival of TAMs by targeting the CCL2-CCR2 and CSF1-CSF1R signaling pathways, respectively (DeNardo & Ruffell, 2019; Kloosterman & Akkari, 2023; Molgora & Colonna, 2021). While these approaches have demonstrated efficacy in pre-clinical models, they have shown limited therapeutic potential as standalone treatments in clinical settings, suggesting that combining them with other therapies is worth exploring. However, there are concerns regarding their safety, as they indiscriminately deplete macrophages in normal tissues, and they can lead to resistance and rebound effects that worsen the disease outcome. Moreover, they fail to account for the diverse subtypes of TAMs, as they non-selectively deplete even TAM subsets with potential anti-tumor properties (Cassetta & Pollard, 2018; DeNardo & Ruffell, 2019; Mantovani et al., 2017). Consequently, novel selective strategies aimed at reprogramming TAMs towards a more immune-stimulatory phenotype are currently under investigation (Kloosterman & Akkari, 2023; Molgora & Colonna, 2021). These strategies involve targeting surface receptors directly involved in immunosuppressive activities, such as MARCO, or receptor-ligand pairs that inhibit phagocytosis, like CD47-SIRPα. In the latter case, blocking antibodies and other molecules targeting CD47 are currently undergoing clinical trials, showing promising preliminary results (Molgora & Colonna, 2021). Furthermore, targeting innate immune receptors may overcome immunosuppression, leading to TAM reprogramming and changes in the TME (Caronni et al., 2021). For instance, monoclonal antibodies directed against CD40, a co-stimulatory receptor, have effectively reshaped the TME, enabling T-cell responses in a mouse model of pancreatic cancer (Vonderheide, 2018). Finally, genetic engineering of macrophages has recently been explored to create chimeric antigen receptor (CAR)-macrophages, which could potentially address several limitations of CAR-T therapies for solid tumors (Klichinsky et al., 2020).

In conclusion, given their abundance and significant impact on tumor progression, TAMs remain attractive therapeutic targets, although the development of well-designed therapeutic approaches is imperative.

1.3. Pancreatic Ductal Adenocarcinoma

Pancreatic Ductal Adenocarcinoma (PDAC) is one of the most aggressive human tumors, with a survival rate of just 12% beyond five years after diagnosis. With a

persistently increasing incidence, in the United States PDAC has already become the third leading cause of cancer-related deaths and it is projected to surpass colorectal cancer before 2040 (Halbrook et al., 2023; Rahib et al., 2014, 2021). Multiple factors contribute to the high lethality of PDAC. To begin, reliable tumor biomarkers, detectable through blood or urine tests, are still lacking, which severely hinders early cancer detection (Singhi, Koay, et al., 2019). Additionally, unspecific clinical symptoms often associated with PDAC, such as back pain, loss of appetite, and weight loss, makes its diagnosis even more challenging. Furthermore, the anatomical characteristics of the pancreas - located centrally in the abdominal cavity, lacking a distinct organ capsule, and surrounded by numerous blood and lymphatic vessels - favor both local and distant tumor spread (Halbrook et al., 2023; Hessmann et al., 2020). As a result, over 80% of patients are ruled out as candidates for surgical resections, being diagnosed either with locally advanced primary tumors or distant metastases (Strobel et al., 2019). Among the remaining 15-20% of patients eligible for surgery, nearly three out of four will experience local or distant recurrence within two years following the surgical resection, hinting at the presence of micro-metastases (Groot et al., 2018). To date, the standard clinical approach for the majority of PDAC patients, regardless of surgical eligibility, is systemic chemotherapy (Halbrook et al., 2023). Gemcitabine monotherapy held the gold standard for several decades until the approval of two novel treatment regimens (Burris et al., 1997). The first is a combination of chemotherapeutic drugs known by the acronym FOLFIRINOX, which includes 5-fluorouracil, leucovorin, irinotecan, and oxaliplatin (Conroy et al., 2011). The second combines gemcitabine with nab-paclitaxel (Von Hoff et al., 2013). While a combination of surgery and chemotherapy has extended the overall survival for a small fraction of PDAC patients, the increasing incidence, high mortality rate, and resistance to most therapies underscore a significant, unmet medical need for PDAC.

1.3.1. Heterogeneity of PDAC

In recent years, several studies have aimed to categorize transcriptional subtypes in pancreatic cancer. These subtypes could potentially help with patient stratification, prognosis assessment, and treatment selection (Collisson et al., 2019). While there is no consensus on nomenclature, two main subtypes are consistently observed in most studies: classical and squamous (Bailey et al., 2016; Collisson et al., 2011, 2019; Moffitt et al.,

2015; Puleo et al., 2018). The classical subtype is marked by increased expression of adhesion-related and epithelial genes, while the squamous subtype expresses mesenchymal-related genes and often loses endodermal pancreatic identity genes, like *GATA6*, which are highly expressed in the classical subtype (Bailey et al., 2016; Collisson et al., 2011). Some studies have identified additional subgroups within these two main categories. For instance, in 2011, Collison and colleagues identified an exocrine-like subgroup with high expression of digestive enzymes (Collisson et al., 2011). In 2016, Bayley and coworkers found a subpopulation with characteristics of a more differentiated pancreas, termed aberrantly differentiated endocrine exocrine (ADEX) (Bailey et al., 2016). These populations could potentially represent more specific variations of the classical subtype (Collisson et al., 2019).

Survival analyses showed that the squamous subtype has a worse prognosis compared to the classical subtype (Collisson et al., 2019). Additionally, preliminary experiments suggested that different subtypes may respond differently to chemotherapeutic agents. For example, *in vitro* tests using gemcitabine on pancreatic cell lines resembling classical and squamous subtypes indicated that the latter is more sensitive to this treatment (Collisson et al., 2011). Similarly, recent clinical data indicates that patients with the classical subtype tend to respond better to 5-fluorouracil-based regimens (Aung et al., 2018).

In summary, although still in the early stages, molecular subtyping of pancreatic cancer holds significant therapeutic potential. It will be crucial to explore further variations within these primary subtypes and their associations with specific treatment responses. Key points to address include the stability of these subtypes and the ability of cancer cells to transition from one subtype to another, together with the impact of therapeutic interventions on subtype specifications (Collisson et al., 2019).

1.3.2. Genomic drivers of PDAC

Genetic changes in PDAC are extensively studied. Roughly 90% of PDAC patients carry mutations in the *KRAS* gene (The Cancer Genome Atlas Research Network & Raphael, 2017). Mutant *KRAS* plays a key role in initiating and advancing tumors through various mechanisms, including sustaining mitogen-activated protein kinase (MAPK) activation, promoting tumor cell growth, and altering tumor cell metabolism (Dey et al.,

2020; Sears et al., 2000; Ying et al., 2012). Oncogenic activation of *KRAS* also triggers the formation of a fibro-inflammatory environment characterized by high levels of immune cell infiltration and matrix deposition, promoting PDAC growth (Sherman & Beatty, 2023). In particular, *Kras* signaling by cancer cells induces the infiltration of $CD11b^+$ myeloid cells, crucial for creating a tumor-supportive microenvironment, as they acquire an immunosuppressive phenotype partly due to the production of GM-CSF (Bayne et al., 2012; Pylayeva-Gupta et al., 2012; Y. Zhang et al., 2017).

Given the significant tumor-promoting activities of *KRAS* mutations and their widespread occurrence in patients, PDAC was thought to be heavily reliant on mutant *KRAS*. Research using genetically engineered mouse models (GEMMs) with inducible and reversible oncogenic *Kras* expression has shown that shutting down *Kras* signaling in cancer cells can lead to regression of invasive PDAC and metastatic lesions, although some tumors can re-occur in a *Kras*-independent manner (Collins, Bednar, et al., 2012; Collins, Brisset, et al., 2012; Kapoor et al., 2014). This has sparked growing interest in therapeutically targeting *KRAS* signaling in cancer cells using small molecule inhibitors, either targeting broadly mutant *KRAS* (pan*KRAS* inhibitors) or specific *KRAS* mutations (Hallin et al., 2022; Hofmann et al., 2022; Kim et al., 2020). Initial clinical trials focused on $KRAS^{G12C}$ mutations, present in about 1-2% of PDAC patients, as these molecules were already approved for other *KRAS*-mutated cancers, such as NSCLC (Jänne et al., 2022; Waters & Der, 2018). While a small number of patients (about 20%) responded to the treatment, the benefits were only transient, possibly due to the development of resistance mechanisms (Strickler et al., 2023; Tanaka et al., 2021; Tsai et al., 2022). Nevertheless, recent pre-clinical studies in PDAC models have shown promising results by targeting the $Kras^{G12D}$ mutation, present in about 40-45% of PDAC patients (Kemp et al., 2023; Waters & Der, 2018). For example, Mahadevan and colleagues demonstrated that MRTX1133, a $Kras^{G12D}$ inhibitor, efficiently blocked *Kras* signaling and downstream MAPK activation in various pancreatic cell lines, resulting in reduced tumor cell proliferation. *In vivo*, MRTX1133 effectively delayed or regressed tumor growth in different PDAC models. Mechanistically, *Kras* inhibition upregulated FAS on cancer cells, making them susceptible to FASL-mediated $CD8^+$ T cell killing (Mahadevan et al., 2023). Despite these promising results, $KRAS^{G12D}$ inhibitors may encounter similar

limitations to *KRAS*^{G12C} inhibitors in clinical trials. Therefore, exploring potential therapeutic combinations represents an intriguing alternative for further investigation.

Beside *KRAS* mutations, other key genetic drivers in PDAC include loss of function mutations in *TP53*, *CDKN2A*, and *SMAD4*, which influence the disease phenotype differently (The Cancer Genome Atlas Research Network & Raphael, 2017; Waddell et al., 2015). *TP53* is the most commonly mutated tumor suppressor gene in PDAC, leading to increased genomic instability, metabolic changes, and a higher tendency for metastasis (Hingorani et al., 2005; J. P. Morris et al., 2019; Weissmueller et al., 2014). However, missense mutations may have different effects on cancer cell activity compared to truncated mutations or deletions that completely abolish *TP53* function, potentially adding an additional layer of heterogeneity (Escobar-Hoyos et al., 2020; Weissmueller et al., 2014). Chromosomal deletion of *CDKN2A* is often associated with the loss of a nearby region containing interferon-related genes, creating a cold and immunosuppressive tumor microenvironment (Barriga et al., 2022). On the other hand, the loss of *SMAD4* is generally linked to a poor prognosis and increased metastatic spread (Blackford et al., 2009; Lacobuzio-Donahue et al., 2009).

Recent advances in next generation sequencing (NGS) have helped identify rare mutations (Bailey et al., 2016; The Cancer Genome Atlas Research Network & Raphael, 2017; Waddell et al., 2015). For instance, approximately 5-7% of PDAC patients carry mutations in *BRCA* genes, which are involved in homologous recombination repair (Zhen et al., 2015). Additionally, chromatin-remodeling genes are frequently altered in PDAC (Bailey et al., 2016; The Cancer Genome Atlas Research Network & Raphael, 2017; Waddell et al., 2015). Moreover, in cases where patients have wild-type *KRAS*, they often have oncogenic mutations in other driver genes, such as *BRAF* or *EGFR*, which activate the MAPK pathway, similar to mutant *KRAS* (Aguirre et al., 2018; Singhi, George, et al., 2019).

In summary, the genetic drivers of PDAC are well-established, and there is a significant effort to target these key mutations therapeutically. Ongoing research aims to link specific genetic alterations to the distinctive features and characteristics of cancer cells. However, despite its aggressive nature, PDAC has a lower mutational burden compared to other cancers.

1.3.3. Models of pancreatic tumorigenesis

PDAC is the most common neoplasm of the pancreas, accounting for more than 90% of pancreatic malignancies (Halbrook et al., 2023). Molecular profiling coupled with histological analysis revealed that PDAC can emerge from distinct pre-malignant precursor lesions (Maitra et al., 2003). Approximately 10-15% of PDAC are estimated to originate from cystic precursor lesions, such as intraductal papillary mucinous neoplasms (IPMNs), within the main pancreatic duct or its branches (Matthaei et al., 2011; Singhi, Koay, et al., 2019). The vast majority of PDAC (about 85-90%) develop from pancreatic intraepithelial neoplasia (PanINs), microscopic lesions not easily detected by abdominal imaging (Overbeek et al., 2016; Singhi, Koay, et al., 2019). Mutations in the *KRAS* gene can be observed in low-grade PanINs and IPMNs, suggesting that *KRAS* mutations might be an early event in the development of exocrine neoplasia (Fujikura et al., 2021; Kanda et al., 2012; The Cancer Genome Atlas Research Network & Raphael, 2017). On the other hand, loss of function mutations in *CDKN2A* and chromatin remodeling genes typically occur during the transition from low-grade to high-grade lesions. Alterations in *TP53* and *SMAD4* are generally detected in high-grade lesions or fully established cancers (Halbrook et al., 2023; Maitra et al., 2003; Sohn et al., 2001). Interestingly, IPMNs are incidentally discovered in about 10% of individuals undergoing abdominal imaging for various reasons (Lévy & Rebours, 2019). Similarly, PanINs lesions have also been observed in healthy individuals, spanning different ages and races, with no indications of pancreatic pathology. These PanINs were multifocal, dispersed throughout the pancreas, and exhibited a high degree of transcriptional similarity to PanINs found in PDAC patients (Carpenter et al., 2023). However, considering the incidence of pancreatic cancer and the frequency of PanINs in the population, these preneoplastic lesions only rarely progress to invasive malignancy and several studies estimated that the multistep process from precursor lesions toward invasive PDAC likely spans multiple years (Carpenter et al., 2023; Yachida et al., 2010). This extended time frame offers an opportunity for early detection and treatment, which has generated a great interest in identifying early biomarkers. It also suggests that additional factors, potentially non-genetic insults, may play a critical role in promoting and accelerating pancreatic tumorigenesis.

1.3.4. Cooperation of injury and oncogenic mutations

There is growing evidence suggesting that certain factors, such as inflammation, may provide a competitive advantage to cells carrying oncogenic mutations at any stage of cancer development (Weeden et al., 2023). Seminal work by Berenblum and Shubik already defined this concept in 1949 in a model of skin carcinogenesis, where topical administration of a mutagen compound was not sufficient to induce tumor formation. Instead, tumor development occurred when an inflammatory agent was subsequently applied to animals exposed to mutagens (Berenblum & Shubik, 1949). Similarly, administering carcinogens to rats with spontaneous *Hras* mutations in their mammary glands increased tumor formation without increasing mutational burden (Cha et al., 1994). More recently, Hill and colleagues reported a positive correlation between air pollution levels and the incidence of *EGFR*-driven lung cancers in humans. Mouse models of lung adenocarcinoma confirmed that exposure to air pollution exacerbates lung tumorigenesis by reprogramming lung mutant epithelial cells towards a progenitor-like cell state (Hill et al., 2023). Mechanistically, IL-1β signaling played a critical role, as exposure to particulate matter led to the accumulation of IL-1β-producing macrophages and IL-1β neutralization was effective in reducing the formation of *EGFR*-driven lung adenocarcinoma (Hill et al., 2023). Indeed, several studies have demonstrated that IL-1β, a classic inflammatory cytokine, is a key driver of a cancer promoting inflammation (Garlanda & Mantovani, 2021). For instance, Dmitrieva-Posocco and colleagues showed that IL-1β plays a crucial role in promoting colorectal carcinogenesis, in part, by sustaining the production of IL-17A and IL-22, which fuel tumor-eliciting inflammation (TEI). Specifically, inhibiting IL-1β signaling in T cells reduced colorectal carcinoma (CRC) progression, concomitantly with decreased production of IL-17A and IL-22 (Dmitrieva-Posocco et al., 2019). Similarly, inhibition of IL-1β production by pancreatic tumor cells led to reduced PDAC growth, along with decreased production of inflammatory mediators by cancer-associated fibroblasts (CAFs) (Das et al., 2020). This was associated with a reprogramming of the TME characterized by reduced infiltration of immunosuppressive cells, including TAMs, myeloid-derived suppressor cells (MDSCs), and T helper 17 (Th17) cells, as well as increased activation of tumor-infiltrating cytotoxic T cells (Das et al., 2020). Notably, the recent phase 3 CANTOS trial, conducted in patients with a history of myocardial infarction, showed that administering

the anti-IL-1β antibody canakinumab significantly reduced the incidence of lung cancer. This was observed in a population at higher-than-average risk, as they exhibited a persistent inflammatory response, and many were current or former smokers (Ridker et al., 2017).

Collectively, these studies, together with others, highlight the crucial role of inflammation, with IL-1β as key driver, in cooperating with oncogenic mutations to drive cancer progression. Targeting tumor-promoting inflammation, even as a preventive measure, has the potential to significantly reduce the risk of developing cancer.

1.3.5. Inflammation in pancreatic tumorigenesis

The process of pancreatic tumor development has been extensively studied in GEMMs. Hingorani and colleagues generated a mouse model where they induced oncogenic *Kras* in the early stages of embryonic pancreatic development using a pancreas-specific promoter to control the expression of *Cre* recombinase ($Kras^{LSL\text{-}G12D/+};Pdx1^{Cre/WT}$; KC mice). This targeted oncogenic *Kras* expression led to the development of various stages of PanINs, which resembled the human disease. Occasionally, these mice spontaneously developed invasive adenocarcinoma and metastatic disease (Hingorani et al., 2003). Instead, pancreas-specific combination of *Kras* activation and *Trp53* loss-of-function strongly accelerated tumorigenesis, with most of the mice developing locally invasive and metastatic PDAC by 16 weeks of age ($Kras^{LSL\text{-}G12D/+};Tpr53^{LSL\text{-}R270H/+};Pdx1^{Cre/WT}$; KPC mice) (Hingorani et al., 2005). However, when oncogenic *Kras* was activated only in adult mice, it was insufficient to induce the formation of premalignant lesions and invasive cancer. This suggests that mutant *Kras* alone is weakly oncogenic in adult pancreatic acinar cells (Guerra et al., 2007; Sherman & Beatty, 2023). Nonetheless, adult mice effectively developed PanINs and invasive PDAC when mutant *Kras* expression was combined with low-grade chronic pancreatitis, highlighting the cooperation between genetic mutations and non-genetic factors in promoting pancreatic tumorigenesis (Guerra et al., 2007; Sherman & Beatty, 2023). Further studies demonstrated that acute inflammatory responses to tissue damage, induced by cerulein or IL-33 administration, can cooperate with oncogenic mutations and exacerbate pancreatic carcinogenesis (Alonso-Curbelo et al., 2021). In particular, the combination of oncogenic mutations and tissue injury leads to significant chromatin

remodeling in epithelial cells. This results in the acquisition of a specific epigenetic and transcriptional program that contributes to tumor initiation and is maintained throughout malignant progression and in established PDAC (Alonso-Curbelo et al., 2021; Burdziak et al., 2023). Moreover, research by Del Poggetto and colleagues demonstrated that cancer-promoting factors can act even before genetic alterations occur (Del Poggetto et al., 2021). Inflammation, even in the absence of an existing *Kras* mutation, can sensitize pancreatic epithelial cells to subsequent *Kras*-driven malignant transformation. In an inducible model of mutant *Kras*, mice that experienced a transient and resolved inflammatory event were more susceptible to and succumbed earlier to tumor development compared to mice only experiencing oncogenic *Kras* expression. Mechanistically, epithelial cells retain an adaptive memory of the inflammatory episode, which is critical in limiting the damage from subsequent inflammatory events. However, this epigenetic reprogramming can then cooperate with oncogene activation, promoting pancreatic tumorigenesis (Del Poggetto et al., 2021).

In summary, these studies underscore the crucial roles of the interaction between genetic mutations and environmental factors in the early stages of pancreatic neoplasia.

1.4. PDAC microenvironment

PDAC exhibits an immunologically cold TME, highly infiltrated by suppressive immune cells and devoid of activated $CD8^+$ T cells, suggesting a dysfunctional adaptive response (Bear et al., 2020; Binnewies et al., 2018). The highly suppressive TME, combined with a low mutational burden and the absence of potent immunogenic neoantigens, allows immune evasion of PDAC (Schumacher & Schreiber, 2015). Moreover, the excessive deposition of ECM alters tissue architecture, creating a physical barrier that results in elevated interstitial pressure, abnormal vasculature, limited exposure to chemotherapy drugs and impaired infiltration of cytotoxic cells (Henderson et al., 2020; Hessmann et al., 2020; Jacobetz et al., 2013). Additionally, PDAC has proven highly resistant to FDA-approved immunotherapies, which have been effective in other solid tumors, such as melanoma and lung cancer (Bear et al., 2020). Targeted immunotherapies, particularly monoclonal antibodies against cytotoxic T-lymphocyte antigen 4 (CTLA4) and programmed cell death ligand 1 (PD-L1), have shown no objective responses in clinical trials, and overall survival has not improved (Brahmer et

al., 2012; Royal et al., 2010). Even a recent phase II randomized trial comparing αPD-L1 alone with a combination of αPD-L1 and αCTLA4 revealed limited objective responses and no significant survival benefits (O'Reilly et al., 2019).

Nevertheless, a detailed examination of human PDAC samples through clinical histopathological analyses unveiled three distinct tumor regions based on leukocyte infiltration: hypo-inflamed, myeloid-enriched, and lymphoid-enriched (Liudahl et al., 2021). Myeloid-enriched regions had high levels of myeloid cells, while lymphoid-enriched regions exhibited a higher lymphoid-to-myeloid cell ratio. In contrast, hypo-inflamed regions showed the lowest leukocyte infiltrate. Notably, both treatment-naive and pre-surgically treated patients classified as lymphoid-enriched demonstrated increased survival. Specifically, pre-surgically treated patients with increased abundance of intratumor $CD8^+$ T cells showed a significant survival advantage. However, within individual tumor sections, the density of leukocyte subpopulations varies across different histopathological regions, underscoring intratumor variability (Liudahl et al., 2021). On the same line, Grunwald and colleagues identified spatially distinct tumor sub-regions, referred to as subTMEs, within the same lesion (Grünwald et al., 2021). They categorized these as reactive or deserted subTMEs, with the former characterized by high cellular infiltration and the latter marked by sparse cellular components and abundant collagen deposition. While neither of these subTMEs correlated with improved survival, the co-occurrence of both within the same patient was associated with a poor prognosis. Nonetheless, tumors dominated by a reactive landscape showed an increased number of single nucleotide variants (SNV) and neoantigens, indicating an immunologically hot, T cell-inflamed environment. In contrast, the deserted regions seemed to provide protection against chemotherapy, with their prevalence increasing after treatment (Grünwald et al., 2021).

In summary, the complexity of PDAC ecosystems underscores the need for a more in-depth investigation to inform rational drug combinations that enhance T cell function while transitioning the TME from a cold and immunosuppressive state to a hot and immune-stimulatory phenotype.

1.4.1. T cells

In recent years, various T cell subgroups have been identified, each with distinct pro-tumorigenic functions within the TME (Daley et al., 2016; McAllister et al., 2014; Perusina Lanfranca et al., 2020; Y. Zhang et al., 2014). Single-cell RNA sequencing (scRNAseq) analyses of the T cell landscape in human PDAC highlighted a significant presence of dysfunctional or exhausted T cell subsets. These subsets exhibited elevated expression of multiple inhibitory checkpoint molecules, including *CTLA4*, *PDCD1* (programmed cell death, PD-1), *HAVCR2* (T cell immunoglobulin mucin-3, TIM3), while showing low expression of T-cell activation markers (Schalck et al., 2022). These findings align with the generally low immunogenicity of PDAC, potentially contributing to its resistance to immunotherapies, such as immune checkpoint inhibitors. Nonetheless, cytotoxic $CD8^+$ T cells, identified by their expression of *GZMB* (Granzyme B) and *PRF1* (Perforin 1), were still present in human PDAC, and their abundance correlated with extended patient survival (Fukunaga et al., 2004; Schalck et al., 2022). Notably, the longest survival in PDAC patients is associated with a combination of abundant $CD8^+$ T cell infiltration and a high quantity of neoantigens, particularly within the *MUC16* gene locus (Balachandran et al., 2017), supporting the notion that the adaptive immune system and cytotoxic anti-tumor responses might be elicited in PDAC patients. Indeed, a recent study with personalized RNA neoantigen vaccines demonstrated that 50% of treated patients generated an effective neoantigen-specific T cell response against at least one vaccine neoantigen (Rojas et al., 2023). Single-cell analyses revealed these expanded T cell clones were $CD8^+$ T cells expressing activation markers, such as *GZMB* and *PF1*, along with cytokines like IFN-γ. Remarkably, these clones persisted for up to two years after surgery, and responder patients experienced delayed PDAC recurrence compared to non-responders (Rojas et al., 2023). In summary, these findings indicate that despite the low mutational burden and the immune-excluded, deserted phenotype of the PDAC TME, mRNA vaccines can elicit effective T cell activity, which is associated with a favorable clinical response. Nonetheless, several challenges remain, including the need for additional mechanistic studies on the roles of the immunosuppressive TME and strategies to optimize neoantigen selection and mRNA vaccine potency.

1.4.2. Dendritic cells

Conventional dendritic cells (cDCs) are specialized antigen presenting cells crucial for anti-tumor immunity. They can be classified as either cDC1 or cDC2 based on specific markers, like XCR1 for cDC1 or CLEC10A for cDC2 (Merad et al., 2013). Importantly, cDC1s can cross present antigens to both $CD8^+$ and $CD4^+$ T cells and are important for generating powerful anti-tumor responses (Ferris et al., 2020; Garris et al., 2018; Maier et al., 2020; Mattiuz et al., 2021) In contrast, cDC2s present soluble antigens to $CD4^+$ T cells and contribute to generating protective $CD4^+$ T cell immunity against tumors (Binnewies et al., 2019; Dudziak et al., 2007). Notably, several studies showed that pre-malignant and established pancreatic lesions harbored low amounts of cDCs, mirrored by a poor abundance of migratory DCs in the draining lymph nodes (Hegde et al., 2020; Lin et al., 2020). Furthermore, cDCs in PDAC exhibited low levels of co-stimulatory and maturation markers, tended to be located away from the tumor, and had reduced antigen presentation capabilities (Hegde et al., 2020; Lin et al., 2020). This deficiency was also observed in PDAC patients, who had almost undetectable circulating DCs compared to healthy individuals and displayed low expression of cDC1 gene signatures (Hegde et al., 2020; Lin et al., 2020). The paucity and dysfunctional features of DCs are associated to defective T cell priming and activation, thus underlying dysregulated immune surveillance in PDAC. However, combination treatments involving αCD40 and other immune-modulatory agents can effectively restore the recruitment and activation of DCs, promoting stronger anti-tumor T cell responses (Bear et al., 2020; Hegde et al., 2020; Lin et al., 2020).

In summary, given the crucial role of DCs in the anti-tumor response and their dysfunction in the PDAC TME, they represent promising therapeutic targets. Strategies focused on increasing their numbers, improving their infiltration, and restoring their functions could efficiently activate T cell responses, potentially leading to the eradication of PDAC.

1.4.3. Cancer-associated fibroblasts

Fibroblasts are the most abundant cell type in the PDAC TME, where they secrete soluble factors and engage in close interactions with immune and tumor cells (Lavie et al., 2022). Fibroblasts control the production and deposition of extracellular matrix,

which alters tissue structure and forms a physical barrier that isolated the tumor tissue, as previously discussed. Consequently, CAFs are considered relevant therapeutic targets. Adoptive transfer of engineered T cells to target and delete fibroblast activation protein $(FAP)^+$ CAFs, a marker of activated CAFs, succeeded in disrupting tumor desmoplasia and supporting anti-tumor immunity in mouse models of pancreatic cancer (Lo et al., 2015). However, genetic deletion of α-smooth muscle actin $(\alpha SMA)^+$ fibroblasts, another marker for CAFs, resulted in decreased survival of mice and expansion of immunosuppressive Tregs (Özdemir et al., 2014). The conflicting results of targeting CAFs likely reflect the heterogeneity of these cells. Recently, at least three major CAF subtypes have been identified in mouse and human PDAC. Myofibroblast CAFs (myCAFs) are characterized by the expression of genes encoding for collagen and ECM proteins, suggesting they might regulate matrix deposition and remodeling. Inflammatory CAFs (iCAFs) express high levels of genes encoding for inflammatory cytokines and chemokines, such as IL-6 and leukemia inhibitory factor (LIF), possibly contributing to immune dysfunction in the PDAC TME (Caligiuri & Tuveson, 2023; Öhlund et al., 2017). The identity of these two CAF subtypes correlates with a differential exposure to environmental signals and spatial localization in the PDAC TME: myCAFs were found to be induced by the TGFβ/SMAD-2/3 pathway and to be mainly localized in close contact with tumor cells, whereas iCAFs are driven by the IL1/JAK-STAT3 pathway and are more dispersed in the TME (Biffi et al., 2019; Öhlund et al., 2017). Recent studies by the Tuveson laboratory have also identified a population of antigen-presenting CAFs (apCAFs) expressing MHCII and genes of the antigen presentation machinery (Elyada et al., 2019). ApCAFs originated from mesothelial cells that, once exposed to factors in the TME, downregulated mesothelial marker genes and acquired a fibroblastic phenotype. *In vitro* co-culture experiments showed that apCAFs can present antigens to $CD4^+$ T cells but failed to provide co-stimulatory signals, ultimately promoting differentiation and expansion of Tregs. These data support immunosuppressive role of apCAFs in PDAC (Huang et al., 2022).

Recent efforts have aimed to classify CAFs based on the expression of specific factors. Mass cytometry analyses revealed that markers like podoplanin (PDPN) and CD90 are expressed on most CAFs, while markers like αSMA and platelet-derived growth factor receptor (PDGFR) α/β vary in different CAF clusters. Notably, CD105, the co-receptor

of the TGFβ receptor, could efficiently identify two distinct CAF populations. Co-injection experiments with tumor cells, highlighted a tumor-restraining role of the $CD105^-$ fraction, dependent on the adaptive immune system, although the exact mechanisms are still to be investigated. Interestingly, both the $CD105^+$ and the $CD105^-$ fraction expressed markers of the myCAFs and iCAFs subtypes *in vivo*, while marker of apCAFs were mainly enriched in the $CD105^-$ fraction, suggesting apCAFs subtypes with opposing functions might exist (Bärthel et al., 2023; Hutton et al., 2021).

The heterogeneity of CAFs is further complicated by their origin and plasticity. The normal pancreas contains various fibroblast populations – namely, pancreatic stellate cells, perivascular fibroblasts and additional parenchymal fibroblasts – that expand differently during carcinogenesis, possibly giving rise to different CAF subpopulations (Halbrook et al., 2023). However, it is still not clear whether these different CAF populations exist as stable and defined cellular states or whether they are plastic and able to adapt to the different cues from the TME. Preliminary *in vitro* experiments suggest potential plasticity, especially between myCAFs and iCAFs, but further investigation is needed (Biffi et al., 2019).

In conclusion, CAF biology in pancreatic cancer is an active area of research. Understanding the mechanisms driving CAF heterogeneity and the context-dependent roles of different subpopulations is essential for identifying vulnerabilities and developing successful therapeutic approaches for deleting or reprogramming CAFs (Bärthel et al., 2023).

1.4.4. Tumor-associated macrophages

The high infiltration of TAMs is a hallmark of the PDAC microenvironment, and their abundance is associated with worse survival in PDAC patients (Cassetta & Pollard, 2018; Ino et al., 2013; Kurahara et al., 2011). Fate mapping experiments in healthy and tumor-bearing animals revealed that pancreatic TRMs have heterogeneous origins, as they can derive from adult HSCs as well as from embryonic precursors (Baer et al., 2023; Zhu et al., 2017). Transcriptional analyses and functional experiments have shown that HSC-derived macrophages are enriched in antigen presentation and T-cell activation pathways. They exhibited an increased ability for antigen uptake and T-cell activation in co-culture experiments, indicating their pivotal role in shaping the immune response. In contrast,

embryonic-derived macrophages expressed genes related to ECM remodeling and growth factor signaling and they were specifically localized between the lobules of the pancreas (Baer et al., 2023; Zhu et al., 2017).

Interestingly, the depletion of TRMs has different outcomes depending on the type of injury. Mice experiencing pancreatic tissue damage due to cerulein administration failed to recover and reached an endpoint survival when TRMs were depleted by clodronate liposome and αCSF-1 treatment. Mice depleted of TRMs had reduced numbers of fibroblasts, which displayed a transcriptional rewiring, increasing the expression of inflammatory genes while downregulating the production of ECM components (Baer et al., 2023). These findings underscore the critical role of TRMs in restoring pancreatic homeostasis and driving a fibrotic response essential for recovery from acute tissue damage. In contrast, depletion of TRMs in KPC mice correlated with better outcomes as mice exhibited fewer high-grade PDAC lesions, lower accumulation of podoplanin^{+} fibroblasts, and reduced stromal desmoplasia, a hallmark of the PDAC microenvironment associated with a poor prognosis (Baer et al., 2023). These divergent outcomes upon depletion of TRMs demonstrate how tumors co-opt the tissue-supportive and protective functions of macrophages to fuel their progression. Further studies have shed light on the close interactions between macrophages and fibroblasts in the pancreatic environment. Fibroblasts are a primary source of CSF-1, which promotes macrophage proliferation and induces the expression of p21, a cell-cycle inhibitor that plays a crucial role in shaping the activation state of macrophages (Zuo et al., 2023). TAMs expressing high levels of p21 exhibited an inflammatory polarization characterized by the enrichment of hypoxia and TNF-α signaling pathways, as well as increased expression of canonical inflammatory mediators like IL-1α and IL-1β. Moreover, p21^{high} TAMs were associated with signatures of immune escape and T-cell exhaustion, indicating a shift towards a tumor-supportive inflammatory phenotype that drives immune dysfunction in the TME (Zuo et al., 2023). Inflammatory subsets of TAMs have also been identified through spatial analysis of human PDAC samples. In particular, TAMs expressing *IL1B*, resembling an M1-like inflammatory state, were enriched in the stroma and cancer regions, while M2-like TAMs were mainly localized in the ducts (Moncada et al., 2020).

Additionally, a subset of TNFα-producing inflammatory TAMs has been shown to promote the development of poorly-differentiated tumor subtypes which are generally associated to increased aggressiveness and reduced survival (Tu et al., 2021).

Given their abundance and tumor-supportive functions, several attempts have been made to target TAMs in PDAC. For instance, inhibiting CSF1R led to macrophage depletion and rewiring of the TME, reducing tumor progression in KPC mice (Candido et al., 2018). Bulk transcriptome analysis of the tumor microenvironment in treated mice showed downregulation of genes related to the cell cycle, DNA damage response, and hypoxia, along with upregulation of genes associated with immune activation. These changes correlated with increased T-cell infiltration and reduced expression of cytokines and chemokines typically associated with tumor progression, such as IL-6, IL-10, and CCL2 (Candido et al., 2018). Unfortunately, CSF1R inhibition, when combined with αPD-1 and chemotherapy, did not improve progression-free survival in advanced PDAC patients compared to chemotherapy alone (Bear et al., 2020).

More recently, as discussed above, novel approaches aimed at polarizing, rather than eliminating TAMs, have been tested. Administration of a CD11b agonist in PDAC murine models has shown promising results, reducing tumor progression and TAM infiltration while increasing T-cell numbers and proliferation (X. Liu et al., 2023). Single-cell RNA sequencing of TAMs in treated mice revealed a downregulation of inflammatory and NF-kB-related processes, along with upregulation of reactive oxygen species (ROS) and oxidative phosphorylation signatures. Mechanistically, the CD11b agonist promoted NF-kB proteasomal degradation, reducing the expression of inflammatory genes, such as *Il1a* and *Il1b*. Simultaneously, this agonist activated the STING pathway, promoting the expression of type I IFN, which is typically reduced in PDAC TAMs compared to TAMs from other tumors (X. Liu et al., 2023). These promising results have led to a first-in-human clinical trial of the CD11b agonist (named GB1275) as monotherapy or in combination with αPD-1 in advanced treatment-refractory solid tumors. Preliminary results have shown increased levels of $STING^+$ TAMs in most treated patients, although only a fraction of them displayed concomitant reduced NF-kB expression (X. Liu et al., 2023).

In conclusion, TAMs are key components of the PDAC TME, mainly exhibiting tumor-supportive functions. Therapeutic approaches aimed at either eliminating or

reprogramming TAMs have shown promising results in pre-clinical models and are now under clinical investigation. However, a more thorough investigation of the phenotypic and functional heterogeneity of TAMs in PDAC is still necessary, as it could provide novel insights into TAM-dependent tumor-supportive functions and potential therapeutic targets.

1.5. Role of PGE_2 in the TME

In the complex landscape of signals that govern cell interactions within the TME, our focus has been on PGE_2. While acting as a *bona fide* inflammatory mediator, PGE_2 exerts complex immune-regulatory activities as it is critical in shaping and polarizing the TME toward a tumor-promoting inflammatory phenotype (Bonavita et al., 2020; Böttcher et al., 2018; Zelenay et al., 2015; Zelenay & Reis e Sousa, 2016). In 2015, Zelenay and co-workers showed that, in a melanoma murine model, tumor-derived PGE_2 is essential for tumor growth. Tumor cell lines lacking *Ptgs1* and *Ptgs2* (the genes encoding COX-1 and COX-2) or *Ptges* (encoding mPGES) were entirely rejected when transplanted into immune-competent mice (Zelenay et al., 2015). However, PGE_2-deficient tumor cells progressively grew in mice lacking DCs or depleted of either natural killer (NK) or $CD8^+$ T cells, suggesting that tumor-derived PGE_2 actively promotes immune evasion (Bonavita et al., 2020; Böttcher et al., 2018; Zelenay et al., 2015). Bulk transcriptome analysis revealed a shift in the inflammatory profile of *Ptgs*$^{-/-}$ tumors, with increased expression of inflammatory players, including type I interferons, CXCL9/10, and IL-12, associated with the recruitment and activation of immune cells linked to anti-tumor responses. In contrast, WT tumors were dominated by the expression of inflammatory molecules, including CXCL1/2, IL-1β, and IL-6, promoting a pro-tumor phenotype (Bonavita et al., 2020; Coussens et al., 2013; Mantovani et al., 2008). Similarly, TAMs isolated from *Ptgs*$^{-/-}$ tumors exhibited this shift, downregulating prostaglandin and IL-1 signaling while upregulating type I and type II interferon pathways (Bonavita et al., 2020; Zelenay et al., 2015). Consistent with these results, *Ptgs*$^{-/-}$ tumors failed to be rejected when implanted in *Ifnar*$^{-/-}$ mice - unresponsive to type I interferons - or in *Ifng*$^{-/-}$ animals, highlighting the crucial role of both types of interferons in rejecting PGE_2-deficient tumors (Bonavita et al., 2020; Zelenay et al., 2015). Interestingly, further studies shed light on additional mechanisms exerted by PGE_2 in driving immune dysfunction. PGE_2

has been found to affect cDCs by inhibiting the expression of transcription factors and molecules involved in their activation, like IRF8, CXCL9, and IL-12. Specific ablation of EP2 and EP4 receptors in DCs restored their activation and ability to stimulate NK cytotoxicity as well as T cell activation and proliferation (Bayerl et al., 2023). PGE_2 can also hinder the recruitment of cDCs to the TME by downregulating critical chemokine receptors (*Ccr5* and *Xcr1*) on their surface and chemokine production by NK cells (Böttcher et al., 2018). Indeed, while WT tumors harbored few cDCs located mainly at the border of the tumor mass, $Ptgs^{-/-}$ tumors showed increased accumulation of cDCs, that tended to localize within the tumor mass, far from the border or blood vessel, and in close contact with NK and $CD8^+$ T cells (Bayerl et al., 2023; Böttcher et al., 2018). Notably, PGE_2 signaling on NK cells is necessary in driving immune evasion, as ablation of EP2 and EP4 receptors on NK cells resulted in the rejection of WT tumor cells as well. In line with this, $Ptgs^{-/-}$ tumors not only progressively grew in NK-cell depleted mice, but also failed to switch their inflammatory profile toward a cancer-inhibitory phenotype (Bonavita et al., 2020). All these findings underscore the critical role of PGE_2 in immune evasion by suppressing key cellular and molecular players involved in the anti-tumor immune response. However, PGE_2 can also promote cancer-associated inflammation by increasing the expression of inflammatory and angiogenic genes, such as *Ptgs2*, *Il1b*, and *Vegf*, in myeloid cells (Thumkeo et al., 2022). In particular, in a mouse model of lung carcinoma, PGE_2 supported the recruitment of Tregs by increasing the production of CCL17 and CCL22 by mature DCs enriched in immunoregulatory molecules (mregDCs) (Maier et al., 2020). Blocking PGE_2 signaling through EP2 and EP4 receptor antagonists led to a reduction in inflammatory and angiogenesis-associated genes, decreased infiltration of Tregs, upregulation of interferon-stimulated genes, and reduced tumor growth (Thumkeo et al., 2022). Furthermore, a recent study identified a population of lung adventitial fibroblasts with key roles in shaping the pre-metastatic niche. These fibroblasts expressed high levels of *Ptgs2* and other key inflammatory mediators, including *Cxcl1*, *Ccl2* and *Il6* (Gong et al., 2022). Co-culture experiments revealed their role in driving an immunosuppressive phenotype in DCs and monocytes, leading to impaired NK and T cell responses. Selective ablation of *Ptgs2* expression in lung fibroblasts abrogated their suppressive functions. Interestingly, neutrophil-derived IL-1β further reinforced the inflammatory phenotype of $Ptgs2^+$ lung fibroblasts, underscoring

the link between cancer-promoting inflammation and immune dysfunction (Gong et al., 2022).

Given its involvement in several mechanisms contributing to immune evasion, PGE_2 emerges as a valuable therapeutic target. However, PGE_2 blockade alone has shown limited effectiveness in reducing tumor progression (Pelly et al., 2021). Combining PGE_2 inhibition with immune checkpoint blockade (ICB) and/or chemotherapy has demonstrated improved anti-tumor efficacy in various cancer models Bell et al., 2022; Bonavita et al., 2020; Gong et al., 2022; Pelly et al., 2021; Zelenay et al., 2015). In addition, even broad anti-inflammatory drugs like corticosteroids have shown enhanced anti-tumor responses when combined with ICB, in line with the role of inflammation in supporting tumor progression (Pelly et al., 2021). Interestingly, cytotoxic therapies, such as chemotherapies, were found to increase the production of PGE_2 by tumor cells (Bell et al., 2022). Several murine and human cancer cell lines showed this behavior, irrespective of the mechanisms of action of the chemotherapeutic drug employed. This suggests that it might be a conserved mechanism by which, paradoxically, cytotoxic drugs might fuel tumor progression. Pharmacological inhibition of COX-2 improved the efficacy of chemotherapy and ICB combinations, reducing tumor relapse and spontaneous metastatic spread in a poorly immunogenic breast cancer model (Bell et al., 2022).

In summary, PGE_2 exerts complex activities in the TME, by enhancing the production of inflammatory mediators while suppressing the anti-tumor immune response. As a result, PGE_2 emerges as a key player in shifting the inflammatory balance of the TME and represents an ideal therapeutic target.

2. AIM OF THE WORK

With a dismal prognosis and an overall survival of less than 5 years, PDAC is among the most aggressive solid tumors and represents a strong unmet medical need. The complexity and heterogeneity of the PDAC microenvironment contribute to its resistance to treatments and pose significant challenges. Classified as immunologically cold, the PDAC TME is highly infiltrated by suppressive immune cells which fuel a pathogenic inflammation and inhibit anti-tumor responses. Notably, inflammation can cooperate with oncogenic mutations accelerating cancer progression.

In this complex picture, TAMs represent one of the most abundant population of leukocytes in PDAC and have been linked to reduced patient survival. While TAMs have been considered as potential therapeutic targets to halt tumor progression, strategies aimed at targeting their survival or recruitment have shown limitations in terms of safety and efficacy. This is, in part, because they do not account for the remarkable heterogeneity and the diverse roles of macrophages in the TME. This underscores the importance and the need of a more comprehensive investigation into the diversity of TAMs and their contributions to pathogenic inflammation in PDAC. This research is critical for identifying novel therapeutic targets. Consequently, this study aims to achieve the following:

1. Investigate the heterogeneity of TAMs at the single-cell level in both human PDAC patients and relevant mouse models of pancreatic cancer.
2. Mechanistically dissect how TAMs drive pathogenic inflammation and tumor progression in PDAC.
3. Identify new therapeutic targets and assess their efficacy in mouse models, as well as their relevance in human PDAC.

By addressing these points, we aim to improve our understanding of the mechanisms of immune dysfunction in PDAC and advance its therapeutic treatment.

3. RESULTS

3.1. *IL1B*$^{+}$ TAMs correlate with poor prognosis in human PDAC

To elucidate macrophage heterogeneity in human PDAC, we performed scRNA-seq of freshly dissociated resected tumor samples from either naïve (n=4) or chemotherapy-treated patients (n=6). Specifically, we analyzed PDAC samples from patients treated with gemcitabine and nab-paclitaxel (n=3), FOLFIRINOX (n=2) and PAXG (n=1). We decided to include different kind of chemo-treatments as well as male and female patients, with no specific limitations on their ages, in order to have the broadest possible representation of macrophages in human pancreatic cancer. The resulting dataset contained 59,569 single-cell transcriptomes comprising tumor, epithelial, stromal, and immune compartments, with variable frequencies across patients but no significant differences between naïve and chemo-treated patients (Fig. 1. A-D). Sub-clustering of mononuclear phagocytes (MNPs) highlighted the presence of distinct subsets of monocytes (classical and non-classical), cDCs (cDC1, cDC2 and mregDCs) and macrophages (Fig. 1. E,F).

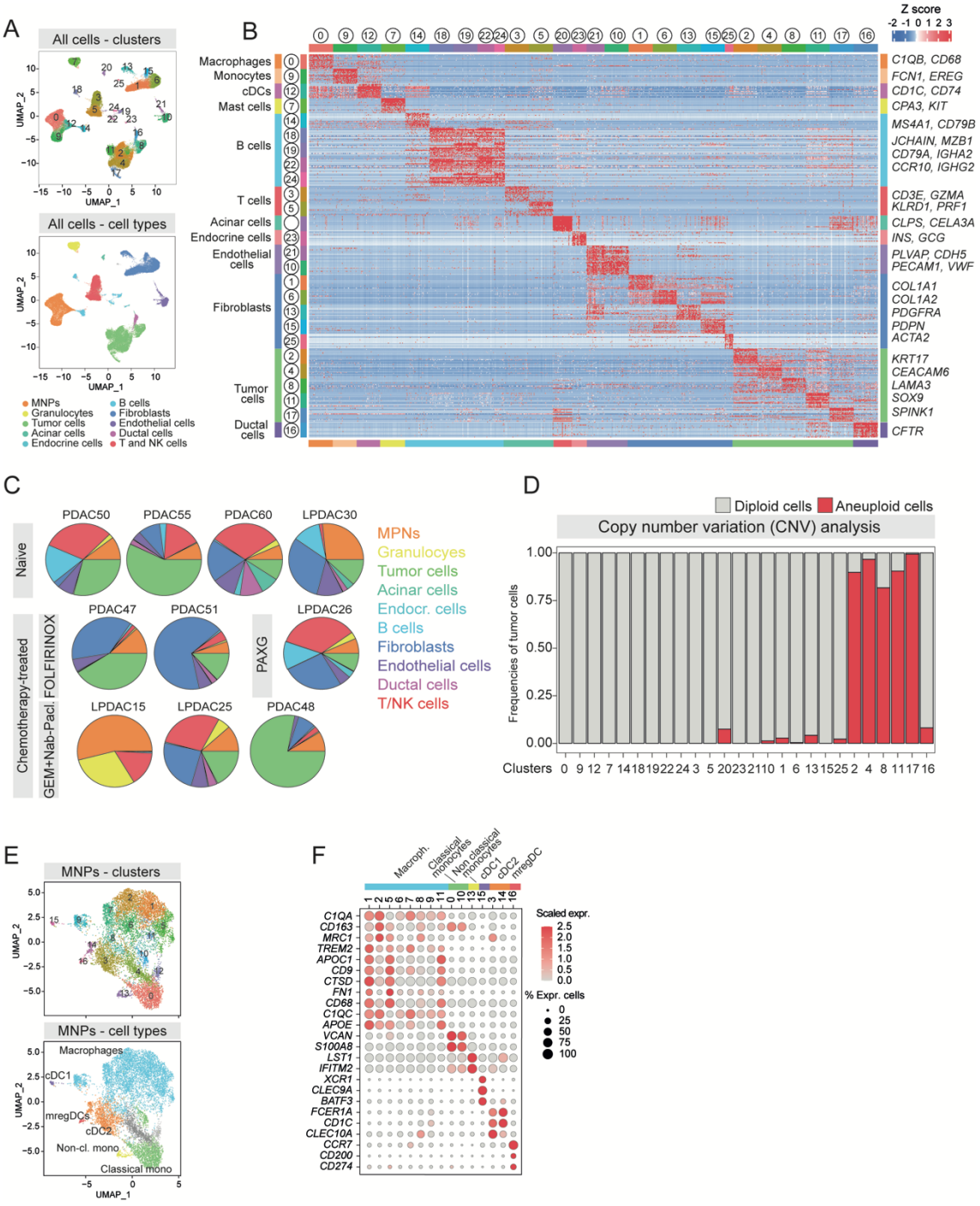

Figure 1. scRNAseq analysis of human PDAC patients.

A. *UMAP plot showing all cells of the human scRNAseq dataset colored by cluster (upper panel) and by annotation of major cell types (lower panel).* ***B.*** *Heatmap showing scaled gene expression of top 25 marker genes for each cluster. Clusters are grouped according to their annotation (as shown in panel* ***A****). Selected marker genes for major populations are reported.* ***C.*** *Pie charts showing abundance of major cell types for each patient sample. Patients are grouped according to the treatment: naïve; Gemcitabine + Nab-Paclitaxel; FOLFIRINOX; PAXG (cisplatin, nab-paclitaxel, capecitabine, gemcitabine).* ***D.*** *Bar plot showing frequencies of aneuploid cells (putative tumor cells) for each cluster. Aneuploid cells (red) were annotated performing copy*

number variation analysis with CopyKAT on each patient sample. ***E.*** *UMAP plot showing mononuclear phagocytes of the human scRNAseq dataset colored by cluster (upper panel) and by annotation of cell types (lower panel).* ***F.*** *Dot plot showing scaled gene expression (negative values are set to zero) of selected genes for each mononuclear phagocyte cluster, annotated as shown in panel* ***C.***

Re-clustering of TAMs, which are the most abundant population of MNPs, revealed various transcriptional states of macrophages whose frequencies were comparable between naïve and chemotherapy-treated patients (Fig. 2. A-C). In addition, differential gene expression analysis showed only a small number of genes whose expression is modulated by the treatment, suggesting that chemotherapy does not strongly affect their transcriptional profiles (Fig. 2. D). Nevertheless, gene set enrichment analyses (GSEA) showed that all subsets of macrophages in patients treated with chemotherapy have an enrichment in gene ontology terms related to interferon (Fig. 2. E). This heightened IFN response could be triggered either by the direct effects of the chemotherapy drugs on the macrophages or by the cellular death and tissue damage occurring in the TME post-treatment.

Analysis of the macrophages identified *SPP1*$^{+}$ TAMs that expressed lipid metabolism (*FBP1*, *APOC1*) and phagocytic receptor (*MARCO*, *MERTK*) genes and they corresponded to populations previously described in liver, colorectal and non-small cell lung cancer (Casanova-Acebes et al., 2021; Maynard et al., 2020; Sharma et al., 2020; L. Zhang et al., 2020). *FOLR2*$^{+}$ TAMs expressed non-canonical myeloid markers (*LYVE1, SELENOP*) and matched *bona fide* resident macrophages in normal tissues and human tumors (Chakarov et al., 2019; Dick et al., 2022; Guilliams et al., 2022; Nalio Ramos et al., 2022; Sharma et al., 2020). We also identified clusters of TAMs expressing metallothionein (*MT1G*, *MT1X*, *MT1E*), heat-shock protein (*HSP*), or cell cycle (*TOP2A*, *MKI67*) genes (Fig. 2A-B, F).

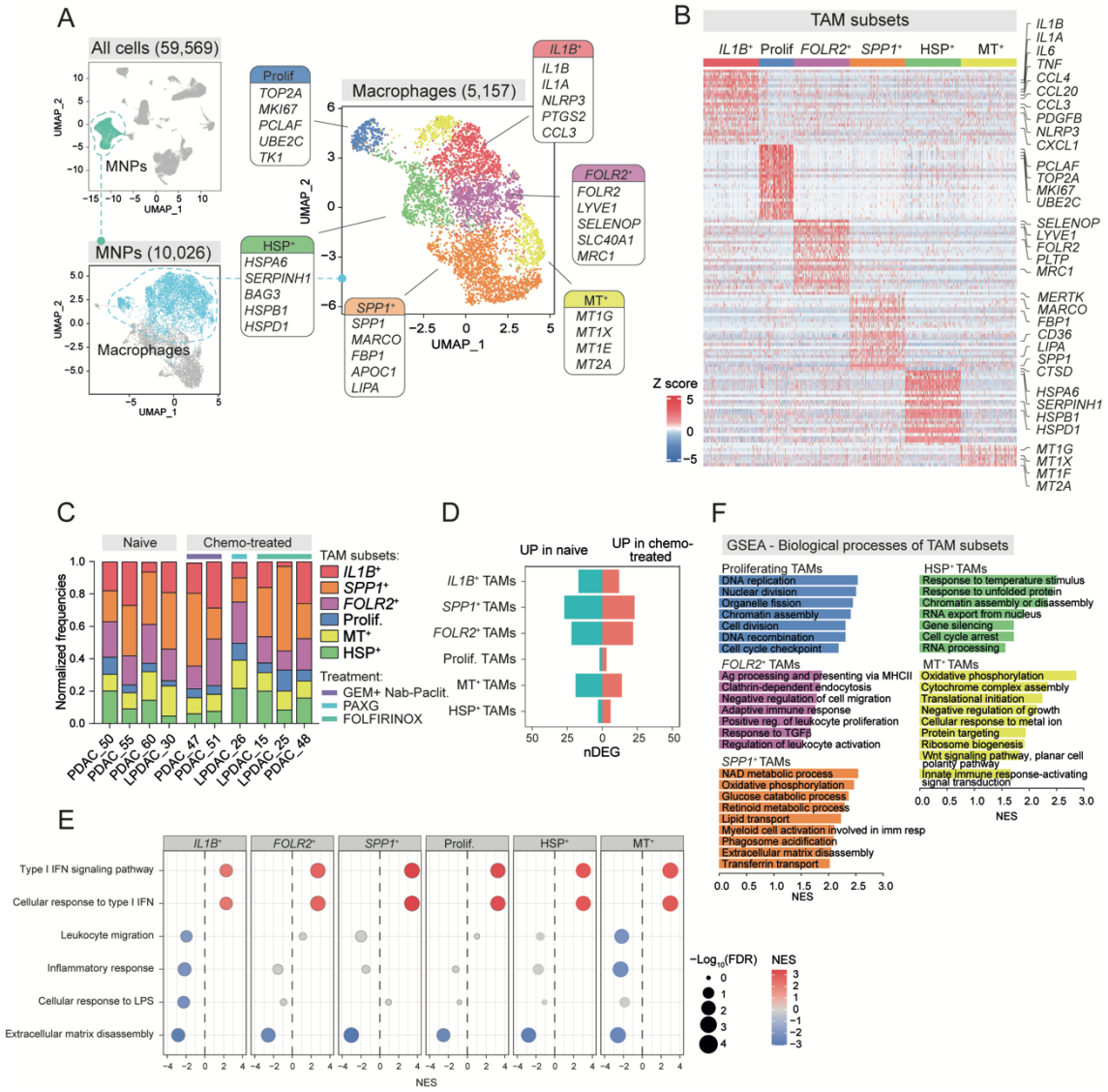

Figure 2. scRNAseq analysis of human PDAC patients uncovers IL1B$^+$ TAMs.
A. *UMAP clustering of scRNA-Seq data from the complete dataset (upper left panel), mononuclear phagocytes (MNPs – lower left panel) and macrophages (right panel). Selected marker genes for each macrophage cluster are shown.* ***B.*** *Heatmap showing scaled gene expression of top 25 marker genes for each cluster of tumor-associated macrophages (ranked for log_2FC). Selected gene names are shown.* ***C.*** *Bar plot showing normalized frequencies of TAM subsets in each patient sample. Samples are grouped according to treatment.* ***D.*** *Bar plot showing the number of differentially expressed genes (DEG) between chemotherapy-treated and naïve PDAC samples for all TAM subsets.* ***E.*** *Gene set enrichment analysis (GSEA) performed on genes expressed by TAM subsets ranked by log_2FC in the comparison between each cluster from chemo-naïve patients vs the same cluster from chemo-treated patient. Gene ontologies-biological processes (GO-BP) were used as gene sets.* ***F.*** *GSEA performed on genes expressed by TAM subsets ranked by log_2FC in the comparison between each cluster vs the other TAM clusters. Gene ontologies-biological processes (GO-BP) were used as gene sets. Normalized enrichment scores (NES) for selected significant terms are reported.*

Our analysis uncovered *IL1B*$^{+}$ TAMs, a discrete subset of PDAC macrophages expressing high levels of transcripts belonging to inflammatory response (*IL1B, TNF, NLRP3, PTGS2*), leukocyte recruitment (*CXCL1, CXCL2, CCL3*), and angiogenesis (*VEGFA, THBS1, PDGFB*) programs. Furthermore, the transcriptome of *IL1B*$^{+}$ TAMs was depleted of interferon (IFN) response and antigen presentation gene ontology (GO) terms (Fig. 3. A-B). We also evaluated whether any of the identified TAM states corresponded to M1 or M2-like cells, by examining the expression of gene signatures derived from *in vitro* polarized macrophages (Martinez & Gordon, 2014). All subsets co-expressed both signatures to varying degree, underscoring that the M1 and M2 classification is overly simplistic and it does not account for the extensive heterogeneity that characterize macrophages *in vivo* (Fig. 3. C).

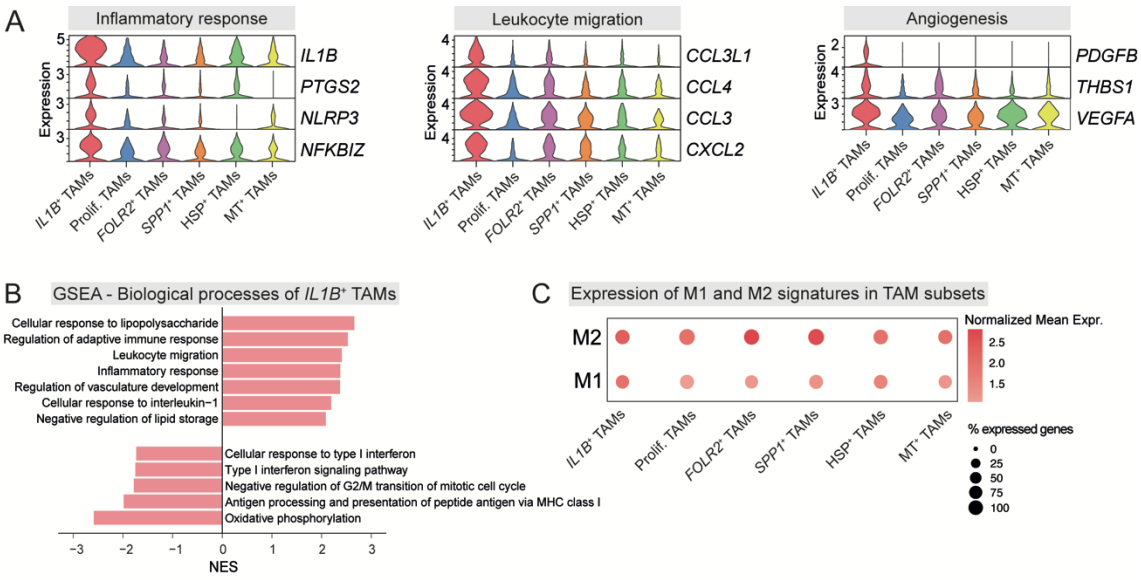

Figure 3. IL1B*$^{+}$ *TAMs showed an inflammatory profile while being depleted of antigen presentation and IFN-related signatures.
A. *Violin plots showing expression values of selected genes associated to inflammatory response, leukocyte migration and angiogenesis.* ***B.*** *Gene set enrichment analysis (GSEA) performed on all genes expressed by TAMs ranked by log$_2$FC between IL1B*$^{+}$ *TAMs vs other TAM clusters. We used gene ontologies-biological processes (GO-BP) as gene sets. Normalized enrichment scores (NES) for selected significant terms are reported.* ***C.*** *Normalized mean expression of M1 and M2 signatures in the TAM subsets identified by scRNAseq analysis of PDAC patients.*

We next assessed the impact of each TAM subset on the survival of PDAC patients, by taking advantage of bulk tumor RNA-Seq and clinical follow-up data of PDAC patients from The Cancer Genome Atlas (TCGA). To this end, we generated gene signatures

specific for each TAM clusters by performing differential gene expression analysis (each TAM cluster versus the others) and retaining only transcripts with selective expression in MNPs. To take into account variability of the macrophage content in the analyzed samples, the mean expression of each signature was normalized by CD68 expression, a known marker of macrophages. While we were not able to identify MNP-specific marker genes for proliferating TAMs, we did not obtain marker genes significantly associated with PDAC prognosis for *MT*$^{+}$ and *HSP*$^{+}$ TAMs. Instead, gene signatures for *SPP1*$^{+}$ and *FOLR2*$^{+}$ TAM subsets were associated with good prognosis (Fig. 4. A). Notably, we obtained a 6-genes signature of *IL1B*$^{+}$ TAMs (*IL1A*, *CCL20, CXCL3, IL1R2, EREG, PLAUR*) whose expression level was correlated with poor PDAC prognosis but not with overall macrophage abundance. Indeed, stratification of PDAC patients based on the *IL1B*-gene signature showed that patients expressing lower levels of such gene signature were associated with a better prognosis (Fig 4. B,C). These data uncover *IL1B*$^{+}$ TAMs as a subset of PDAC macrophages characterized by inflammatory and non-cytotoxic transcriptional programs, whose predicted abundance correlated with poor patient prognosis.

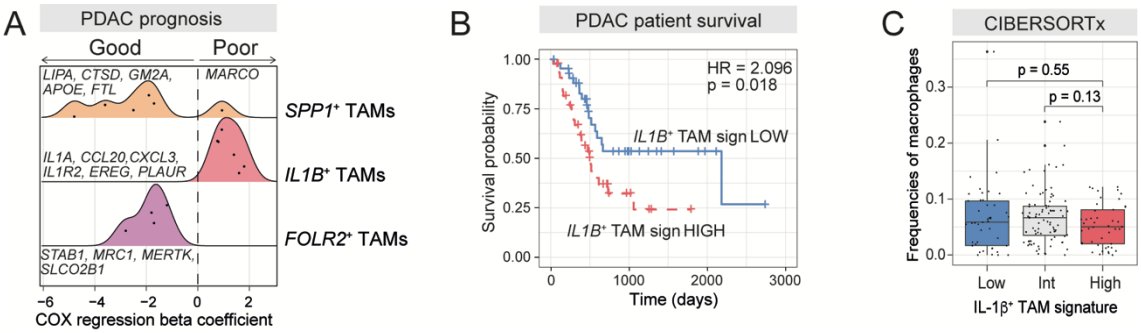

Figure 4. IL1B^{+} TAMs correlate with poor prognosis in human PDAC.
A. *Density plot showing prognostic values of TAM marker genes for the TCGA cohort of PDAC patients. Only genes with significant values are reported. No marker gene for MT*$^{+}$ *and HSP*$^{+}$ *TAMs was significantly associated with PDAC prognosis.* ***B.*** *Kaplan-Meier plot showing survival probability of PDAC patients (TCGA), stratified based on high or low expression of the IL1B*$^{+}$ *TAM 6-gene prognostic signature (shown in panel A). Hazard ratio (HR) and p-value of Cox regression fit are reported.* ***C.*** *Box plot showing the frequencies of macrophages in TCGA PDAC cohort, predicted by CIBERSORTx deconvolution. Patients are stratified according to the expression of IL1B*$^{+}$ *TAM 6-gene prognostic signature.*

3.2. Characterization of *Il1b*$^{+}$ TAMs in mouse models of pancreatic cancer

We next profiled a mouse model of pancreatic cancer whereby *Kras*$^{G12D/+}$ *Trp53*$^{R172H/+}$ *Pdx1*$^{Cre/+}$ (KPC) cells are injected orthotopically in immune-competent recipients (Hingorani et al., 2005). Cells from blood, pancreas and tumors at day 10, 20 and 30 post inoculation were subjected to scRNA-Seq, followed by clustering and annotation of 51,276 single cells spanning the tumor, epithelial, stromal, and immune compartments (Fig. 5. A,B).

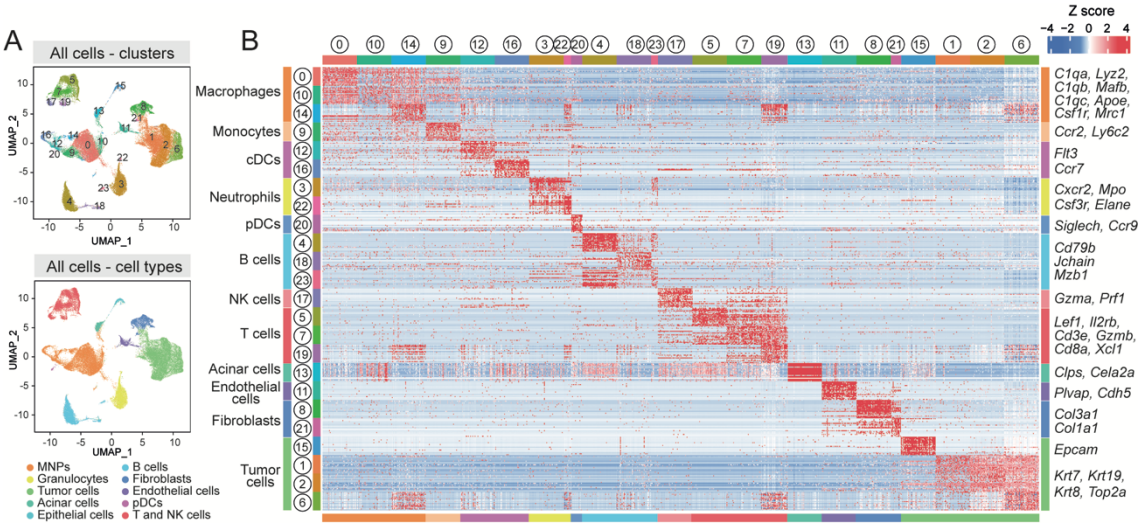

Figure 5. scRNAseq analysis of KPC-derived mouse PDAC model.
A. *UMAP of scRNA-Seq of all cells from mouse PDAC (orthotopic KPC). Colors and numbers indicate scRNA-Seq clusters (upper panel) or cell type annotations (lower panel)* ***B.*** *Heatmap showing scaled gene expression of top 25 marker genes for each cluster. Clusters are grouped according to their annotation (as shown in panel* ***A****). Selected genes for major cell types are reported.*

Similar to our analysis in human PDAC patients, we sub-clustered first MNPs and then macrophages, annotating 6,996 macrophage transcriptomes (Fig. 6. A,B). In order to identify specie-specific and cross-species conserved subsets of macrophages, we performed GSEA between human and murine TAMs. Specifically, we first defined the marker genes for each human TAM subset, we converted them into their murine orthologs and we assessed their enrichment in the genes expressed by the murine TAM subsets, ranked by $\log_2$FC (each TAM cluster vs the others). We found that key marker genes and transcriptional programs of *Il1b*$^{+}$ TAMs, as well as of *Folr2*$^{+}$, *Spp1*$^{+}$, and proliferating TAMs, were conserved between human and mice, while the other TAM subsets, both human and murine, appeared to be specie-specific (Fig. 6. C,D).

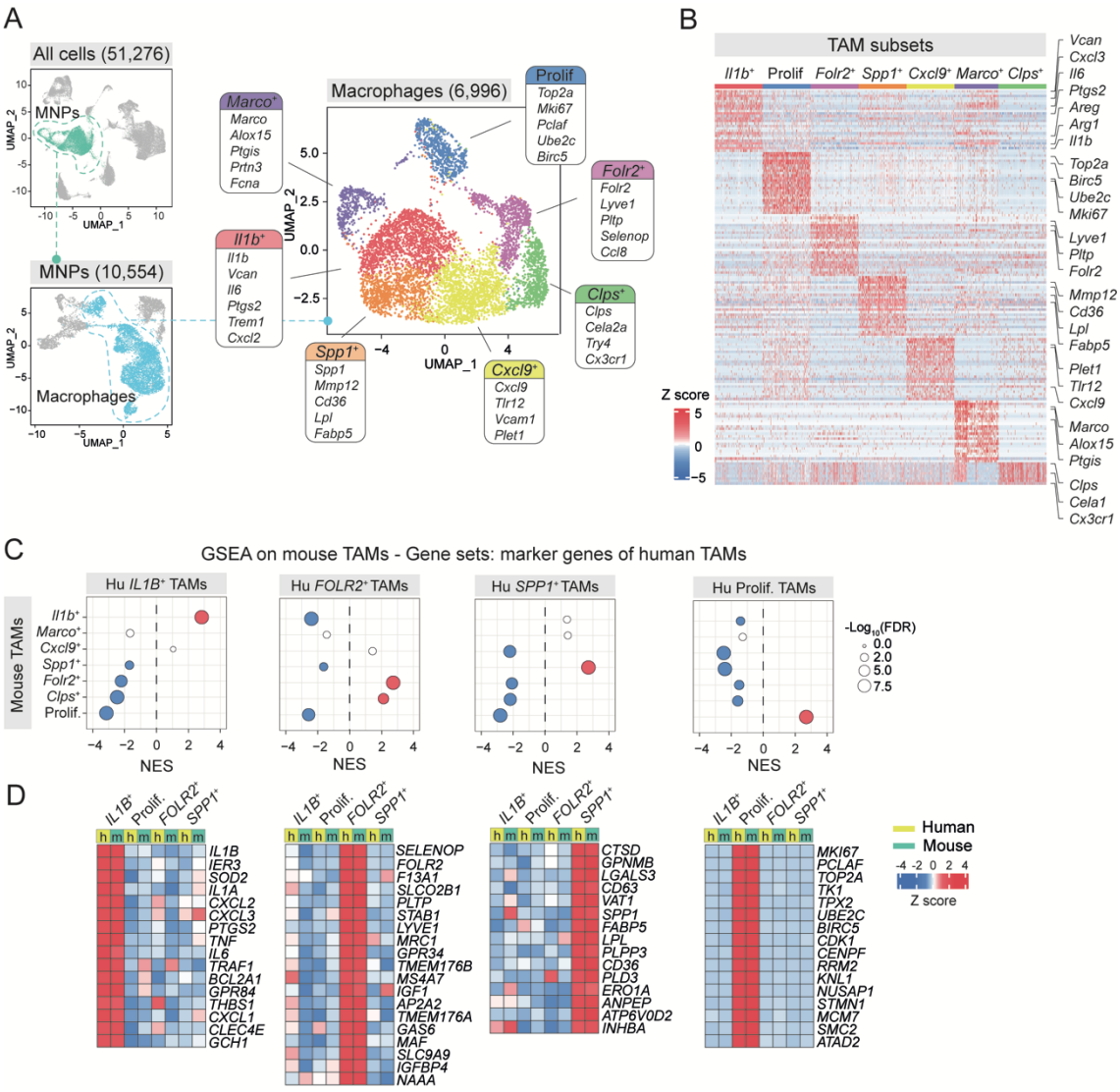

Figure 6. IL-1β⁺ TAMs are conserved in mouse models of pancreatic cancer.
A. *UMAP clustering of scRNA-Seq data from the complete dataset (upper left panel), mononuclear phagocytes (MNPs – lower left panel) and macrophages (right panel). Selected marker genes for each macrophage cluster are shown.* ***B.*** *Heatmap showing scaled gene expression of top 25 marker genes for each cluster of tumor-associated macrophages (ranked for log_2FC). Selected gene names are shown.* ***C.*** *GSEA performed on genes expressed by mouse TAM subsets (ranked by log_2FC vs other TAM clusters), using the marker genes of human TAM subsets as gene sets. NES and significance are reported for each comparison.* ***D***. *Heatmap showing scaled gene expression of marker genes conserved between mouse and human TAM subsets. Only clusters of TAMs conserved between species are reported.*

Next, we set out to define the dynamics of the macrophage subsets during tumor progression. Interestingly, we found that *Il1b*$^+$ macrophages are completely absent in healthy pancreas, while showing an early and persistent accumulation in mouse PDAC already 10 days after tumor inoculation. In contrast, other subsets, such as *Folr2*$^+$ macrophages, were already present in healthy pancreas and persisted during tumor

growth (Fig. 7. A). In keeping with scRNA-Seq analyses, flow cytometry staining showed a detectable population of FOLR2^{+} macrophages both in healthy pancreas, as well as in late stage orthotopic tumors. On the other hand, IL-1β expression was undetectable in pancreatic macrophages from control mice whereas a substantial fraction of TAMs expressed IL-1β in late stage orthotopic PDAC (Fig. 7. B). Moreover, we found no detectable IL-1β expression in macrophages from distal organs, such as spleen, bone marrow and lung either in control or tumor-bearing mice (Fig- 7. C).

In order to further corroborate our data, we performed scRNAseq of additional relevant pancreatic mouse models, that are orthotopic or subcutaneous $Kras^{G12D/WT}$ $Pdx1^{Cre/WT}$ (KC) models as well as autochthonous tumors from KPC mice. In all these cases, we were able to identify *Il1b*$^{+}$ TAMs as well as the other TAM subsets conserved between human and mouse (Fig. 7. D). Furthermore, flow cytometry staining revealed the presence of a distinct and detectable IL-1β^{+} TAM population in various PDAC models generated by orthotopic or subcutaneous inoculation of pancreatic cell lines: KC- (DT6606) or KPC-derived (K8484, 5M7101, K4651, Ximbio) as well as chemically induced (Panc 02) (Fig. 7. E).

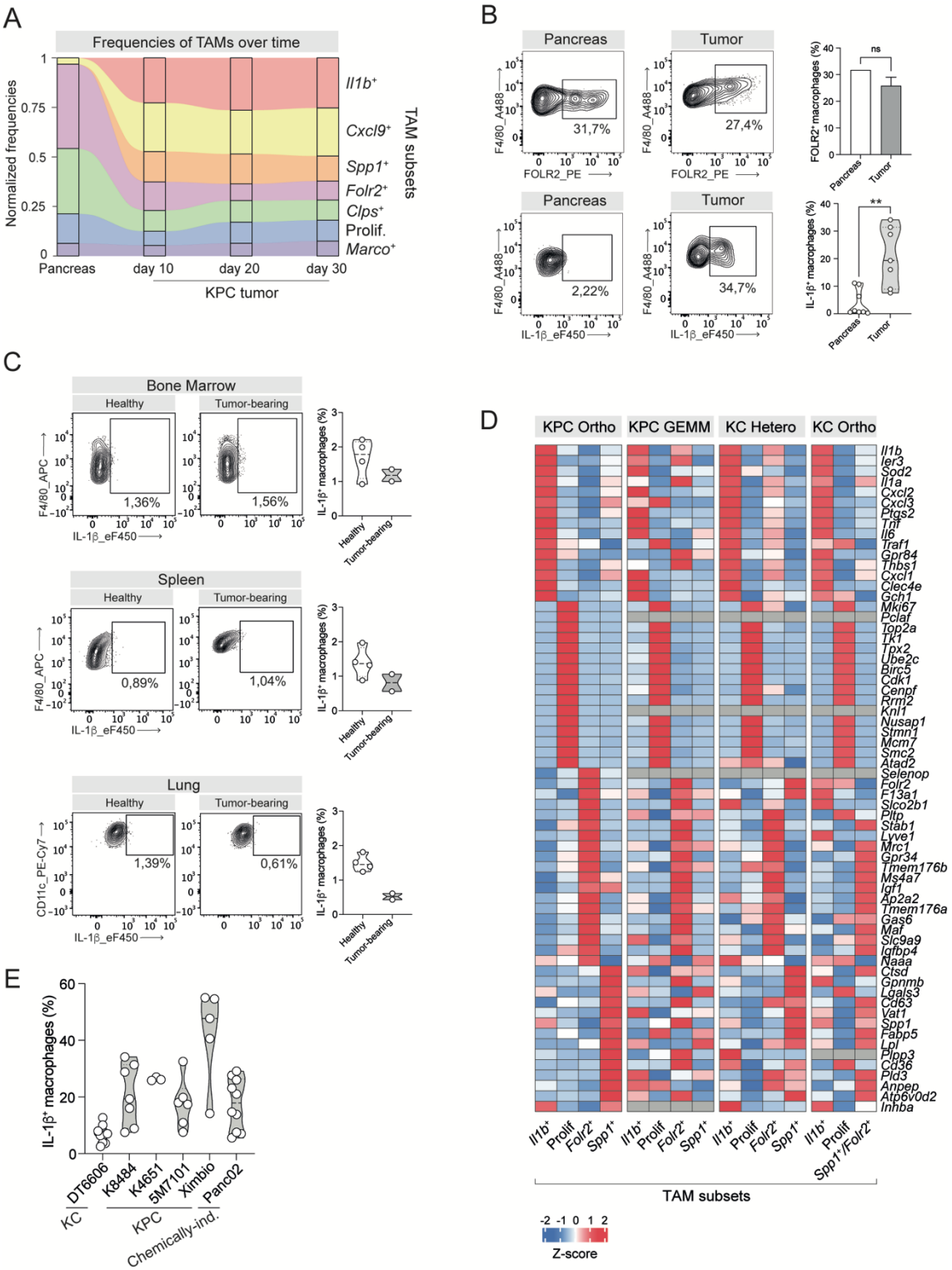

Figure 7. IL-1β⁺ macrophages accumulate early during tumor progression and are conserved in multiple murine PDAC models.

A. *Alluvial plot showing normalized frequencies from scRNA-seq data of TAM subsets from control pancreas (Ctrl) and PDAC (orthotopic KPC) at the indicated time points of tumor progression.* ***B.*** *Representative contour plots and frequencies of mouse FOLR2⁺and IL-1β⁺ macrophages in control pancreas (Pancreas) (n=3 for FOLR2⁺ macrophages; n=8 for IL-1β⁺ macrophages) and PDAC tissues (orthotopic PDAC) (n=4 for FOLR2⁺ macrophages; n=7 for*

*IL-1β$^+$ macrophages). Statistical significance was measured by two-tailed Student's t test. **p < 0.01.* ***C.*** *Representative contour plots and frequencies of IL-1β$^+$ macrophages from BM, spleen and lung of healthy (n=4) or tumor-bearing mice (n=2).* ***D.*** *Heatmap showing scaled gene expression of marker genes conserved between mouse and human TAM subsets (as in panel* ***6D****) in macrophages from multiple PDAC mouse models.* ***E.*** *Frequencies of IL-1β$^+$ macrophages in multiple PDAC cell lines (DT6606 n=10, subcutaneous; K8484 n=7, orthotopic; K4651 n=3, subcutaneous; 5M7101 n=6, subcutaneous; Ximbio n=5, subcutaneous; Panc02 n=10, subcutaneous).*

We then defined the surface phenotype of IL-1β$^+$ TAMs with a panel of antibodies against markers of macrophage identity and/or function. While F4/80, CD11b, Ly6C and PDL2 were expressed at similar levels between IL-1β$^+$ and IL-1β$^-$ TAMs, IL-1β$^+$ TAMs were characterized by high expression of CD64, CD11c, MHC II and costimulatory molecules CD80 and CD86, together with known markers of immune dysfunction in cancer such as CD206, ARG1 and the immune checkpoint inhibitor PD-L1 (Fig. 8. A,B).

Additionally, we assessed the expression of active caspase 1, a key player of inflammasome activation and IL-1β maturation and release (Barnett et al., 2023), by employing a fluorescent labeled inhibitor that specifically recognize and bind to active caspase 1 (named FLICA). We found increased expression of active caspase 1 in the fraction of CD64^{high} TAMs, that is enriched in IL-1β$^+$ macrophages (Fig. 8. C-E).

These data establish IL-1β$^+$ TAMs as a conserved macrophage population, that accumulates early during tumor growth and co-express inflammatory and immune inhibitory markers.

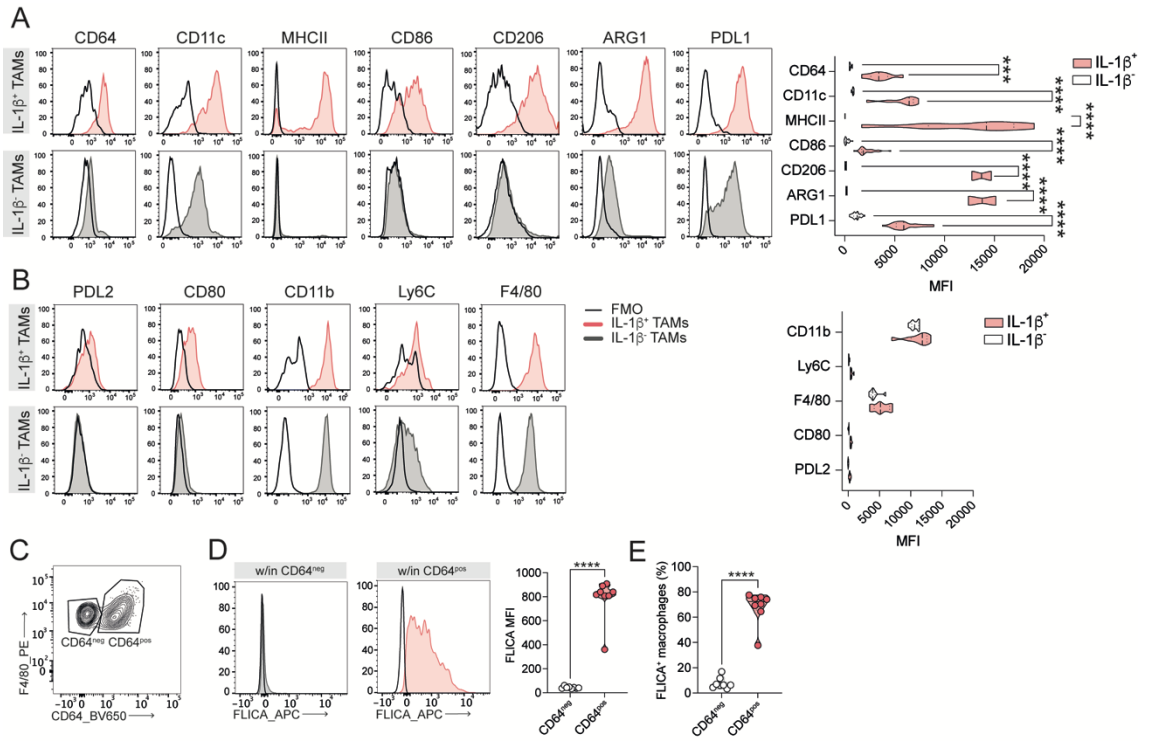

Figure 8. Immunophenotypic analysis of IL-1β⁺ TAMs.

A,B. *Expression of the indicated markers by IL-1β⁺ TAMs (upper panel, red histograms) and IL-1β⁻ TAMs (lower panel, grey histograms) (subcutaneous PDAC). Representative histograms and median fluorescence intensity (MFI) values are shown. Black lines represent fluorescence minus one control (FMO). Statistical significance was measured using 2-way ANOVA. ***p < 0.001, ****p < 0.0001.* ***C.*** *Representative contour plots of $CD64^{neg}$ and $CD64^{pos}$ macrophages.* ***D,E.*** *Expression of FLICA by $CD64^{neg}$ TAMs (left panel, grey histograms) and $CD64^{pos}$ TAMs (right panel, red histograms) (orthotopic PDAC, n=8). Representative histograms (**D**), MFI values (**D**) and frequencies (**E**) are shown. Black lines represent fluorescence minus one control (FMO). Statistical significance was measured using unpaired two-tailed Student's t test. ****p < 0.0001.*

3.3. Monocytes differentiate into IL-1β⁺ TAMs upon exposure to TME factors

Time-resolved scRNA-Seq datasets of mouse monocytes and macrophages from blood, pancreas, and tumors were integrated and subjected to CellRank analysis that, by combining RNA velocity and transcriptional similarities, infer cell-cell transition probabilities (Lange et al., 2022). We found a trajectory linking tumor-infiltrating monocytes and *Il1b*⁺ TAMs, supporting a monocytic origin for these TAMs (Fig. 9. A-C). In line with this, marker genes of *Il1b*⁺ TAMs, such as *Il1b*, *Ptgs2* and *Cxcl2*, among others, ranked as top driver genes of this transition, and their expression increased as monocytes entered the tumor (Fig. 9. D).

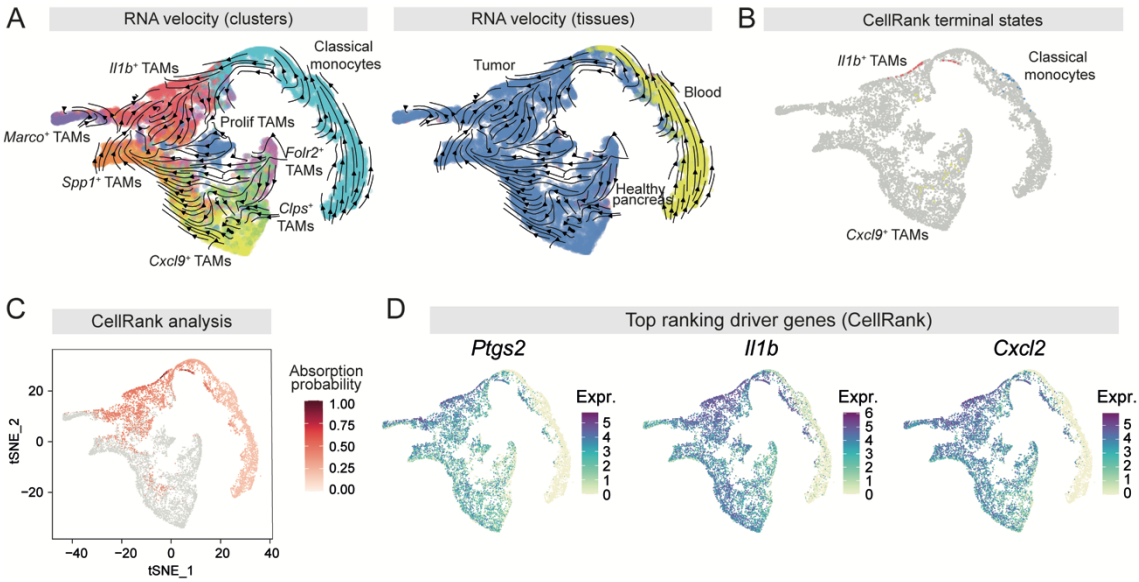

Figure 9. CellRank analysis identify tumor-infiltrating monocytes as bona fide precursors of IL-1β+ TAMs.
A. *RNA velocity vectors of macrophages and monocytes from blood, pancreas and PDAC (orthotopic PDAC) samples computed on tSNE embedding based on diffusion maps. Cells are colored by cluster identity (left) or tissue of origin (right).* ***B.*** *tSNE embedding of mouse macrophages and monocytes from blood, pancreas and PDAC (orthotopic PDAC) samples. Steady state cells identified as terminal states by CellRank analysis are shown.* ***C.*** *Absorption probability of each cell to transit towards Il1b+ TAMs, identified as terminal state by CellRank.* ***D.*** *Expression values of the top-ranking genes driving the trajectory from tumor-infiltrating monocytes towards Il1b+ TAMs.*

Furthermore, *Il1b*$^{+}$ TAM marker genes were poorly expressed in circulating and in healthy pancreatic monocytes, but they were promptly induced in tumor-infiltrating monocytes and in *Il1b*$^{+}$ TAMs (Fig. 10. A-B, D-E). Accordingly, protein levels of IL-1β were low in circulating monocytes from control and tumor-bearing mice but increased substantially upon recruitment to tumors (Fig. 10. C). In collaboration with the laboratory of Florent Ginhoux, we next performed lineage tracing experiments with *Ms4a3*^{Cre}-*Rosa*^{TdT} mice, in which granulocyte-monocyte precursors (GMP) and their progeny are irreversibly marked by tdTomato (Z. Liu et al., 2019). Flow cytometry staining of end-stage orthotopic tumors revealed that the vast majority of IL-1β^{+} TAMs was tdTomato^{+}, indicating that these cells originate from circulating monocytes that infiltrate the tumor and become exposed to local factors in the TME (Fig. 10. F).

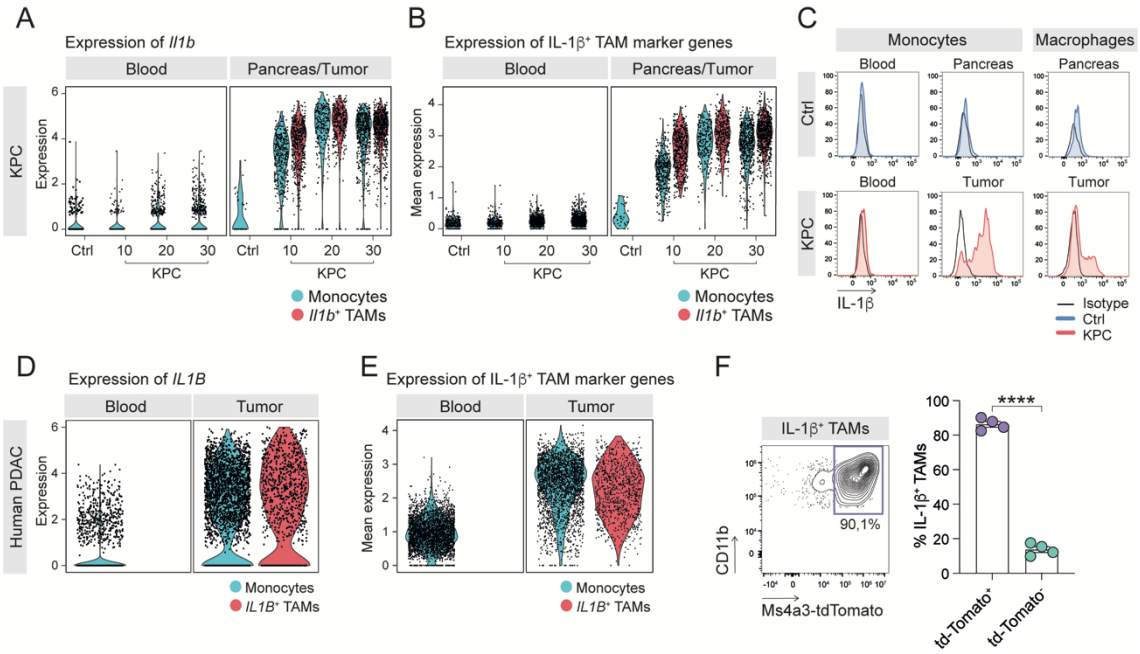

Figure 10. Monocytes differentiate into IL-1β$^+$ TAMs upon exposure to TME factors. ***A,B.*** *Violin plots showing expression (scRNAseq) of Il1b (**A**) and the marker genes of Il1b$^+$ TAMs (**B**), in mouse monocytes and Il1b$^+$ TAMs from control pancreas (Ctrl) and PDAC (orthotopic KPC) at the indicated time points.* ***C.*** *Representative histograms of IL-1β intracellular staining of monocytes and macrophages in the indicated conditions. Cells from control mice are represented in blue, cells from tumor-bearing animals in red. Black lines represent isotype controls.* ***D,E.*** *Violin plots showing expression of IL1B (**D**) and marker genes of IL1B$^+$ TAMs (**E**) in human monocytes and IL1B$^+$ TAMs in blood and PDAC samples.* ***F.*** *Frequencies of tdTomato$^+$ and tdTomato$^-$ IL-1β$^+$ TAMs from PDAC (orthotopic KPC, end-stage, n=4). ****p<0.0001, unpaired student's two tailed t-test.*

3.4. PGE$_2$ and TNF-α cooperatively elicit the IL-1β$^+$ TAM state

In the attempt to identify local factors responsible for the acquisition of the IL-1β$^+$ TAM state, we performed GSEA and observed an enrichment of IL-1 and TNF response GO terms within driver genes of the monocyte-to-IL-1β$^+$ TAM transition (Fig. 11. A). Consistently, the transcriptome of IL-1β$^+$ TAMs was selectively enriched in genes induced by IL-1β or TNF-α in mouse macrophages (Ostuni et al., 2013), and both molecules were detectable in human PDAC, with their levels increasing compared to those in plasma (Fig. 11. B,C). However, treatment of mouse bone marrow-derived macrophages (BMDMs) with IL-1β or TNF-α did not elicit IL-1β synthesis, highlighting a requirement for additional factors (Fig. 11. D).

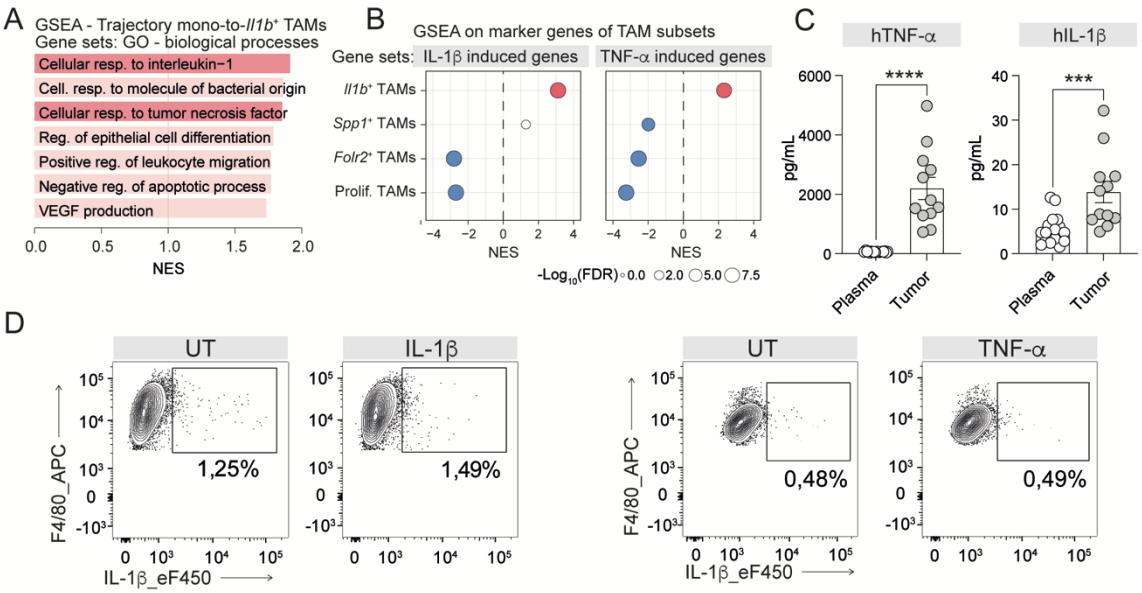

Figure 11. Investigation of local factors eliciting the Il1b$^+$ TAM phenotype.
A. *GSEA performed on genes ranked by correlation with absorption probability of the monocyte-to-Il1b$^+$ TAM transition, using biological processes gene ontologies (GO) as gene sets. Significant selected terms are reported.* ***B.*** *GSEA performed on genes expressed by mouse TAM subsets (ranked by log$_2$FC between each cluster vs other TAMs), using IL-1β- or TNF-α-induced genes as gene sets.* ***C.*** *Concentration (mean±SEM) of TNF-α (n=18) and IL-1β (n=17) in plasma and tumor of PDAC patients (n=12). ***p<0.001 ****p<0.0001 (unpaired student's two-tailed t test).* ***D.*** *Expression of IL-1β (intracellular staining) in mouse BMDMs treated for 6 hours with IL-1β or TNF-α.*

Previous studies found that the eicosanoid prostaglandin E2 (PGE_2), a known regulator of the immune TME, can stimulate IL-1β production while suppressing IFN responses in macrophages (Böttcher et al., 2018; Cilenti et al., 2021; Perkins et al., 2018; Zasłona et al., 2017; Zelenay et al., 2015). Mass spectrometry (performed by the proteomics and metabolomics facility) and ELISA assay revealed high levels of PGE_2 in biopsies of human and mouse PDAC and in culture supernatant of PDAC cell lines (Fig. 12. A-C). Additionally, PGE_2-induced genes (Cilenti et al., 2021) were over-represented selectively in IL-1β$^+$ TAMs (Fig. 12. D).

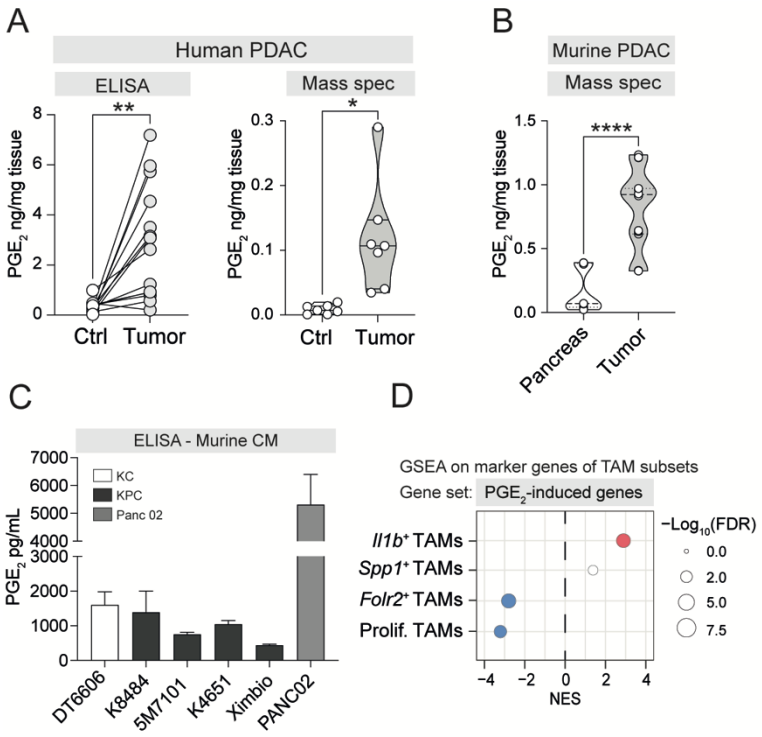

Figure 12. PGE_2 is highly expressed in human and mouse PDAC.
A. *Left: ELISA quantification of PGE_2 in human PDAC (n=14) and normal adjacent tissue (Ctrl) (n=14) **p<0.01paired student's two-tailed t test; right: quantification of PGE_2 in human PDAC samples and control (Ctrl) matched normal adjacent tissue (n=7/group) by mass spectrometry. *p<0.05 Unpaired student's two-tailed t test* ***B.*** *Quantification of PGE_2 in mouse control pancreas (n=3) and PDAC (orthotopic KPC, end-stage) (n=5) by mass spectrometry analysis. ****p<0.0001 Unpaired student's two-tailed t test.* ***C.*** *Quantification of PGE_2 in culture supernatants of KC (DT6606, n=10), KPC (K8484 n=14, 5M7101 n=3, K4651 n=3, Ximbio n=3) and PANC02 (n=3) PDAC cells by ELISA (mean±SD).* ***D.*** *GSEA (PGE_2-induced genes) on genes ranked by log_2FC between each mouse TAM subset versus other TAMs (orthotopic KPC).*

We thus tested whether PGE_2 contributed to elicit the IL-1β$^+$ TAM state. Similar to the effects of TNF-α or IL-1β stimulation, PGE_2 alone had limited effects on *Il1b* expression. However, both BMDMs and monocytes co-exposed to PGE_2 and TNF-α exhibited a significant increase of *Il1b* transcript levels (Fig. 13. A,B). Co-administration of PGE_2 and IL-1β, instead, had more moderate effects (Fig. 13. C). These findings were consistent at protein level, as evidenced by the quantification of intracellular accumulation of IL-1β, as well as IL-1β secretion upon inflammasome activation (Fig. Fig. 13. D-H).

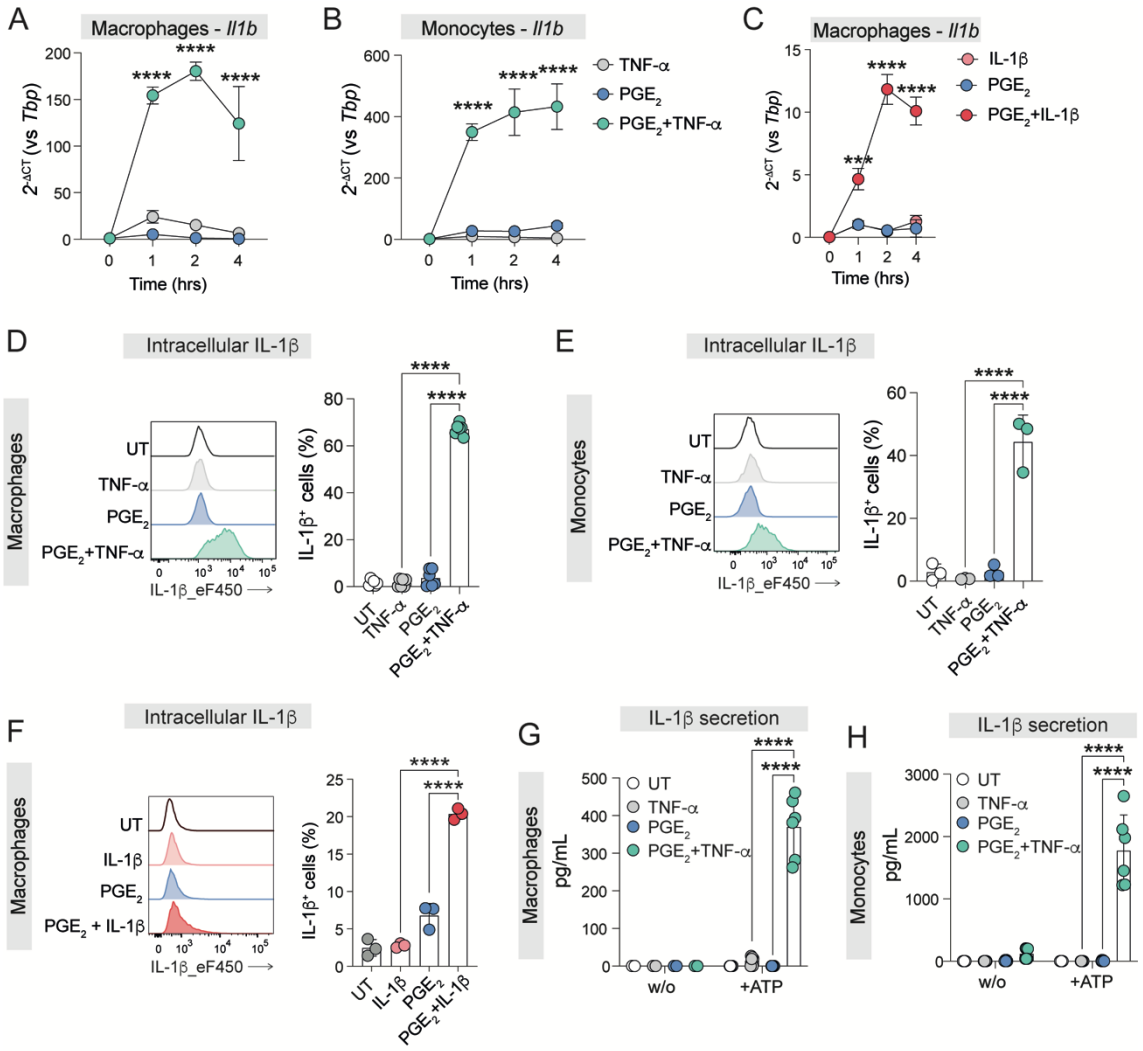

Figure 13. PGE_2 and TNF-α synergistically induce Il1b expression in mouse macrophages and monocytes.

A,B. *Real time qPCR analysis showing expression of Il1b in BMDMs (**A**) or BM-monocytes (**B**) stimulated with TNF-α, PGE_2 or PGE_2+TNF-α for the indicated time points. ****p<0.0001 calculated with two-way ANOVA.* ***C.*** *Real time qPCR analysis showing expression of Il1b in BMDMs stimulated with IL-1β, PGE_2 or PGE_2+IL-1β for the indicated time points. ***p<0.001, ****p<0.0001 calculated with two-way ANOVA.* ***D,E.*** *Intracellular staining of IL-1β in BMDMs (**D**, n=6/group) or monocytes (**E**, n=3/group) stimulated for 5 hours as indicated. Representative histograms (left) and frequencies of IL-1β$^+$ BMDMs or monocytes (right) are reported. Bar plots represent the mean ± SD. ****p<0.0001 calculated with ordinary one-way ANOVA.* ***F.*** *Intracellular staining of IL-1β in BMDMs stimulated for 6 hours as indicated. Representative histograms (left) and frequencies of IL-1β$^+$ BMDMs (right) are reported. Bar plots represent the mean ±SD (n=3). ****p<0.0001 calculated with ordinary one-way ANOVA.* ***G,H.*** *Quantification of IL-1β secretion from BMDMs (**G**) or monocytes (**H**) stimulated as indicated. ATP was added for the last 30 minutes of stimulation. Bar plots represent the mean±SD (n=6/group). ****p<0.0001 calculated with ordinary one-way ANOVA.*

Notably, additional *Il1b*$^+$ TAM marker genes - such as *Ptgs2*, *Il6* and *Il10* – showed increased expression in cells co-exposed to PGE_2 and TNF-α (Fig. 14. A). We next

performed RNA-seq analyses in BMDMs left untreated, stimulated with PGE_2 or TNF-α and co-stimulated with PGE_2+TNF-α. We identified dozens of transcripts synergistically induced by PGE_2+TNF-α, which were over-represented in IL-1β$^+$ TAMs and within the driver genes of monocyte-to-IL-1β$^+$ TAM transition; these genes encoded for factors that elicit tumor-promoting inflammation (*Il1b*, *Il6*), suppress cytotoxic immunity (*Il10*), or stimulate prostaglandin synthesis (*Ptges, Ptgs2*), myeloid cell recruitment (*Cxcl1, Cxcl2, Cxcl3*), and tissue repair (*Areg, Arg2, Wnt11, Il33*) (Fig. 14. B-D). Multiplexed ELISA analyses of secreted proteins confirmed elevated synthesis of IL-6 and IL-10 by co-stimulated macrophages, while revealing PGE_2-driven suppression of CCL5, CXCL10, CXCL11, and CXCL16 – chemokines with key roles in cytotoxic T and NK cell recruitment (Fig. 14. E). These data identify PGE_2 and TNF-α as TME factors able to cooperatively elicit the IL-1β$^+$ TAM state in PDAC.

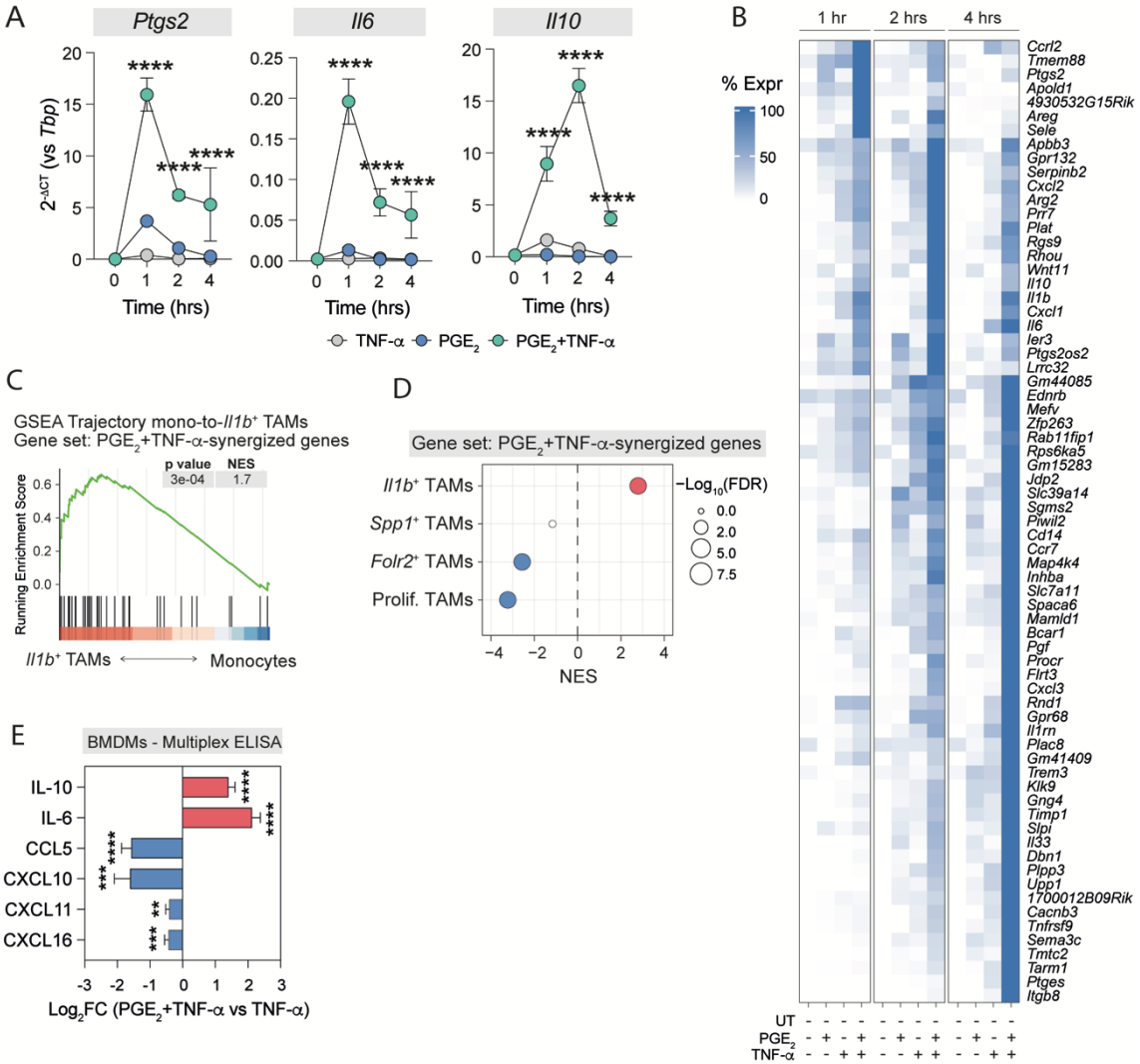

Figure 14. PGE_2 and TNF-α cooperatively elicit the IL-1β$^+$ TAM state.
A. *RT-PCR of Ptgs2, Il6 and Il10 in BMDMs stimulated with TNF-α; PGE_2 or PGE_2+TNF-α for the indicated time points. Dot plots represent mean ± SD (n=3). ****p<0.0001 calculated with two-way ANOVA.* ***B.*** *Heatmap showing gene expression (rescaled in percentage of expression for each gene) of PGE_2+TNF-α synergized genes for all the experimental conditions and time point analyzed.* ***C.*** *GSEA (Gene set: PGE_2+TNF-α synergized genes) on genes ranked by correlation with absorption probability of the monocyte-to-Il1b$^+$ TAM trajectory (**C**) or on genes ranked by log_2FC between TAM subsets versus other TAMs (**D**).* ***E.*** *Quantification (ELISA, mean±SD) of the indicated proteins in the supernatant of BMDMs (n=3), shown as log_2FC of concentration values in PGE_2+TNF-α versus TNF-α.*

PGE_2 can bind to four different receptors, leading in this way to the activation of distinct downstream signaling pathways. Macrophages mainly express EP2 and EP4 that, upon PGE_2 binding, activate the adenylyl cyclase leading to cAMP accumulation. To understand the mechanisms underlying the synergistic effects of PGE_2, we stimulated BMDMs with either an activator of the adenylyl cyclase (forskolin) or with a cell-

permeable analog of cAMP (dibutyryl-cAMP, db-cAMP), with or without LPS. LPS is a paradigmatic inflammatory stimulus and its administration to BMDMs in the presence of PGE_2 mimicked the synergic effects of PGE_2 and TNF-α, resulting in increased expression of *Il1b* and other relevant IL-1β$^+$ TAM marker genes, such as *Il10*, *Il6* and *Ptgs2* (Fig. 15. A,B). Notably, when we replaced PGE_2 with forskolin or db-cAMP, we still observed a synergistic upregulation of *Il1b* and other significant IL-1β$^+$ TAM marker genes (Fig. 15. C). The synergic activity between forskolin/db-cAMP and LPS was further confirmed by the increased secretion of IL-1β into the supernatant of co-stimulated BMDMs following inflammasome activation (Fig. 15. D). In conclusion, activation of cAMP signaling pathway was able to phenocopy PGE_2-synergistic activities when combined with LPS at both the transcriptional and protein level. These findings suggest that the modulation of inflammatory response in macrophages by PGE_2 may be dependent on the cAMP signaling pathway.

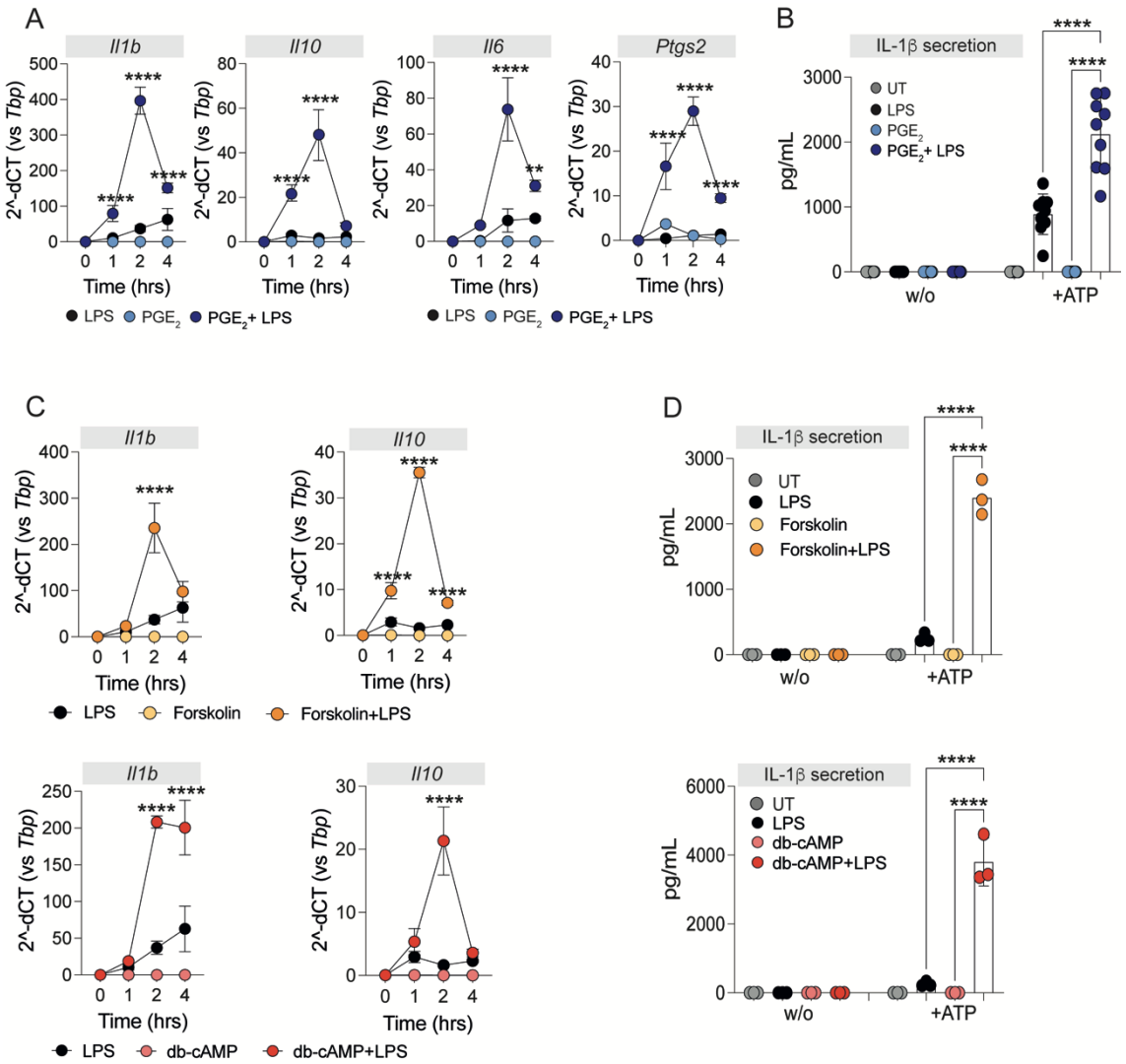

Figure 15. cAMP is able to phenocopy PGE_2-dependent synergistic activity with inflammatory stimuli.

A. *RT-PCR of Il1b, Il10, Il6 and Ptgs2 in BMDMs stimulated with LPS; PGE_2 or PGE_2+LPS for the indicated time points. Dot plots represent mean ± SD (n=3). **p>0.01 ****p<0.0001 calculated with two-way ANOVA.* ***B.*** *Quantification of IL-1β secretion from BMDMs stimulated as indicated. ATP was added for the last 30 minutes of stimulation. Bar plots represent the mean±SD (n=9/group). ****p<0.0001 calculated with ordinary one-way ANOVA.* ***C.*** *RT-PCR of Il1b and Il10 in BMDMs stimulated with LPS; forskolin; db-cAMP; forskolin+LPS or db-cAMP+LPS for the indicated time points. Dot plots represent mean ± SD (n=3). ****p<0.0001 calculated with two-way ANOVA.* ***D.*** *Quantification of IL-1β secretion from BMDMs stimulated as indicated. ATP was added for the last 30 minutes of stimulation. Bar plots represent the mean±SD (n=3/group). ****p<0.0001 calculated with ordinary one-way ANOVA.*

3.5. PDAC-derived PGE_2 elicits IL-1β$^+$ TAMs and promotes tumor growth

To assess the role of PGE_2 in PDAC, we treated immune competent mice with celecoxib, a selective inhibitor of the prostaglandin biosynthetic enzyme COX-2, concomitant with tumor challenge. As assessed by mass spectrometry analysis performed

on end-stage tumors, celecoxib-treated mice showed reduced PGE_2 levels in tumors, concomitantly with delayed tumor growth (Fig. 16. A,B). In addition, this treatment decreased accumulation of IL-1β$^+$ TAMs and monocytes, increased infiltration of cytotoxic GZMB$^+$ CD8$^+$ T cells and increased activation of NK and CD8$^+$ T cells in tumor-draining lymph nodes (Fig. 16. C-E).

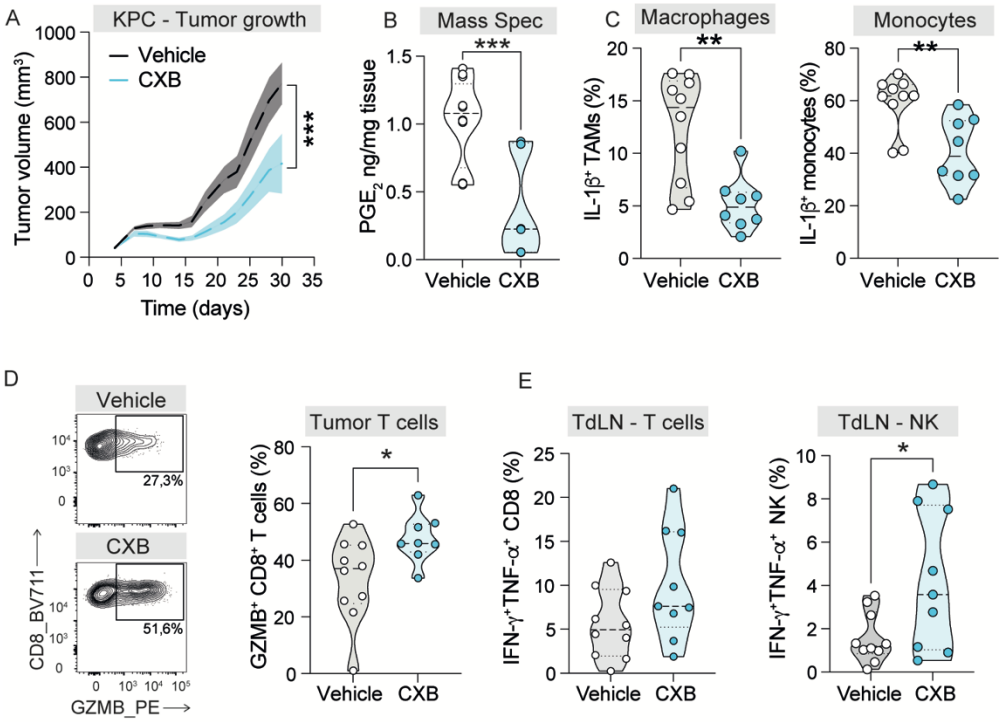

Figure 16. Inhibition of COX-2 reduces PDAC progression.
A,E. *Treatment of KPC-bearing mice with Celecoxib (CXB, COX2 inhibitor; 400μg/mouse). Mice were treated daily starting from day 0.* ***A.*** *Tumor growth in mice treated with vehicle or CXB. Data represent mean±SEM. Statistical analysis was performed using two-way ANOVA. ***p < 0.001.* ***B.*** *Quantification by mass spectrometry of PGE_2 abundance in lysates of end stage tumors (day 30) treated with Celecoxib (CXB, n=3) or vehicle (n=4). Each sample was analyzed using technical triplicates. Statistical significance was measured by unpaired t test. ***p < 0.001.* ***C.*** *Frequencies of IL-1β$^+$ macrophages and IL-1β$^+$ monocytes in tumors treated with CXB (n=8) or vehicle (n=10). Significance was determined by unpaired t test. **p < 0.01.* ***D.*** *Representative plots and frequencies of GZMB$^+$ CD8 T cells in tumors treated with CXB (n=8) or vehicle (n=10). Significance was determined by unpaired t test. *p < 0.05.* ***E.*** *Frequencies of IFN-γ$^+$ TNF-α$^+$ CD8$^+$ T cells and NK cells in tumor-draining lymph node (TdLN). Significance was determined by unpaired t test. *p < 0.05.*

Because cancer cells produce high levels of PGE_2 (Fig. 12. C), we generated COX-2 KO clones of multiple PDAC cell lines. Western blot and ELISA analyses confirmed the absence of the COX-2 and the inability to produce PGE_2, respectively (Fig. 17. A,B).

Additionally, these cells showed no defects in viability or proliferation *in vitro* (Fig. 17. C,D).

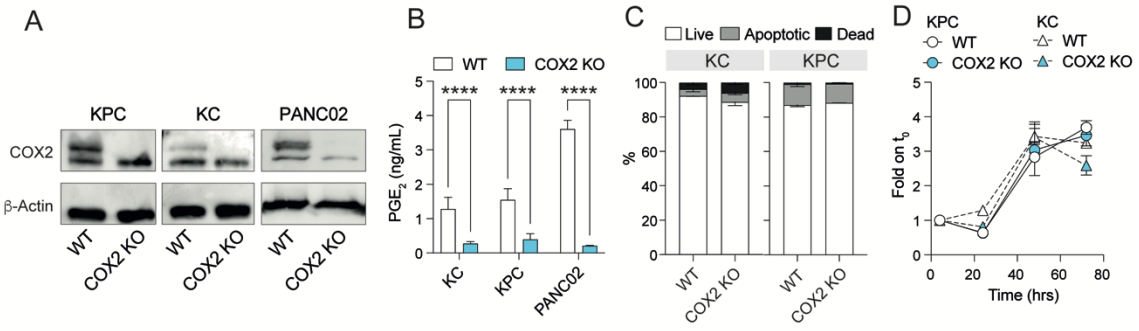

Figure 17. Disruption of Ptgs2 in tumor cells impairs PGE_2 production without affecting their vitality and proliferation in vitro.
A. *Western blot analysis of COX2 and b-Actin in WT and COX2 KO PDAC cell lines.* ***B.*** *Quantification of PGE_2 (ELISA, mean±SD) in the culture supernatant of the indicated control (KC, n=6; KPC, n=6; PANC02, n=2) and COX-2 KO (KC, n=5; KPC, n=5; PANC02, n=2) mouse PDAC cell lines . ****p < 0.0001 (2-way ANOVA).* ***C.*** *Annexin V and 7AAD staining in WT and COX2 KO PDAC cell lines.* ***D.*** *In vitro proliferation of WT and COX2 KO cell lines measured by WST-1 assay.*

COX-2 KO PDAC cells efficiently engrafted but exhibited an impaired tumor growth, both in subcutaneous and orthotopic models (Fig. 18. A). Flow cytometry analyses revealed a predominantly similar immune cell composition between control and COX-2 KO tumors at early disease stages, with only decreased frequencies of infiltrating neutrophils and a slight increase in T cells (Fig. 18. B). Nevertheless, when we examined the expression of IL-1β in the TME, we observed reduced frequencies of IL-1β$^+$ monocytes in COX-2 KO tumors, providing further support for the pivotal role of PGE_2 in promoting IL-1β expression (Fig. 18. C). Additionally, we detected increased lymphocyte and NK cell activation in tumor-draining lymph nodes of COX-2 KO tumors (Fig. 18. D). Similar results were obtained also by orthotopically transplanting spheroids derived from KPC WT or KPC COX-2 KO tumor cells. The latter showed reduced tumor growth compared to WT spheroids, concomitantly with reduced frequencies of IL-1β$^+$ monocytes and TAMs as well as increased activation of NK and CD8$^+$ T cells in the tumor-draining lymph nodes (Fig. 18. F-H). Notably, the depletion of CD8$^+$ and NK cells prevented the rejection of COX-2 KO tumors (Fig. 18. I,J). Moreover, flowcytometry analyses of end-stage tumors revealed that NK-depleted mice harbored reduced

infiltration of $CD8^+$ T cells (Fig. 18. K). Overall, these data underscored the central role of CD8 and NK cells in preventing tumor progression in the absence of PGE_2.

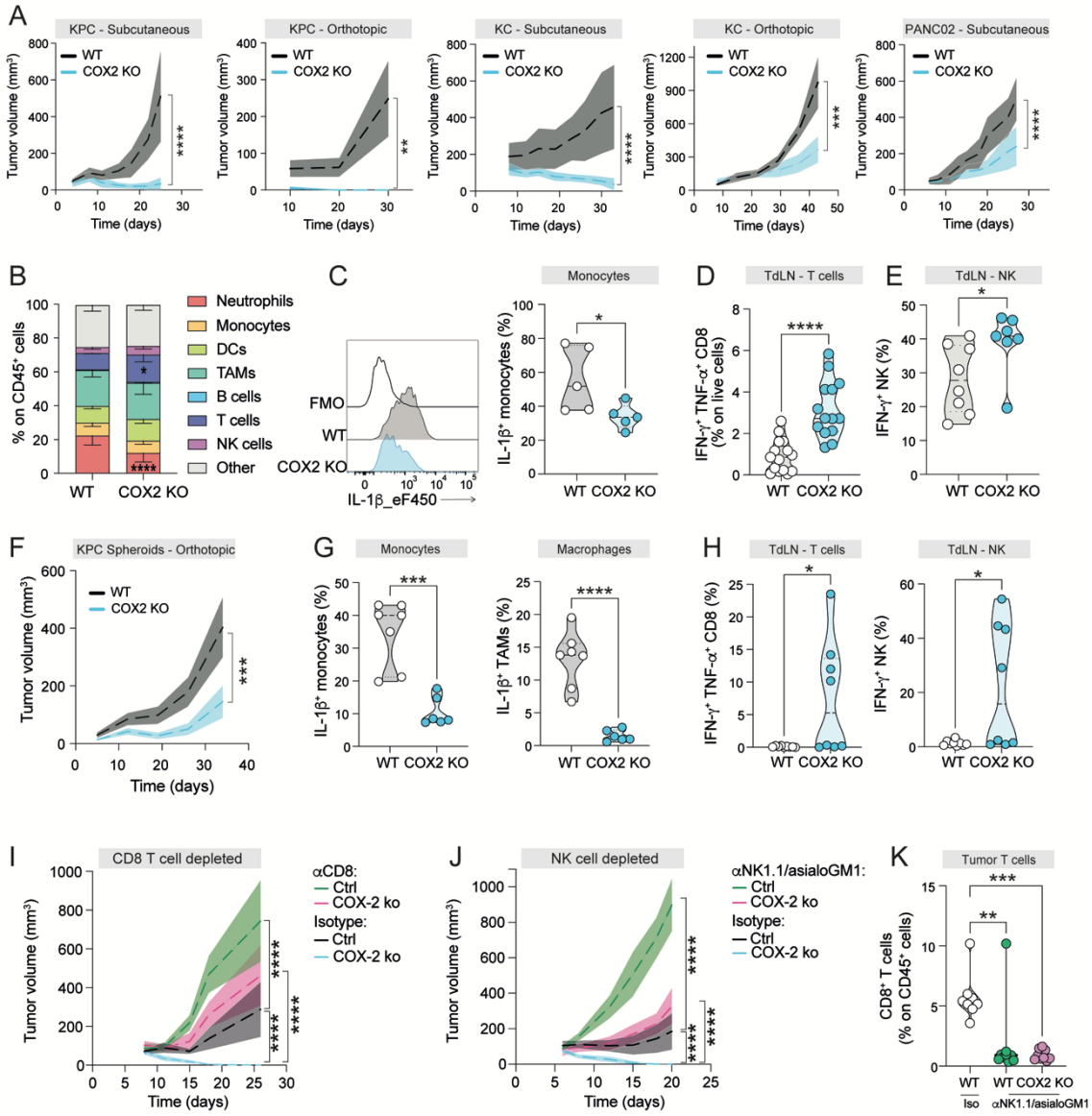

Figure 18. COX2 KO tumors show impaired tumor growth in immunocompetent mice.
A. *Growth curves (mean±SEM) of control (subcutaneous KPC, n=5; orthotopic KPC, n=5; subcutaneous KC, n=8; orthotopic KC, n=4; subcutaneous PANC02, n=10) and COX-2 KO PDAC cells (subcutaneous KPC, n=5; orthotopic KPC, n=5; subcutaneous KC, n=10; orthotopic KC, n=4 subcutaneous PANC02, n=7) in wild-type mice. **p < 0.01, ***p < 0.001 ****p < 0.0001 (two-way ANOVA).* ***B.*** *Bar plot showing frequencies of immune cell populations infiltrating WT and COX2 KO KPC tumors at day 6 p.i. analyzed by flow cytometry. Statistical analysis was performed using two-way ANOVA. *p < 0.05, ****p < 0.0001.* ***C****. Representative histograms (left) and frequencies (right) of IL-1β⁺ monocytes in WT and COX2 KO subcutaneous KPC tumors (n=5/group) at day 5 p.i. Statistical significance was performed using unpaired t test *p>0.05.* ***D****. Quantification of IFN-γ⁺ TNF-α⁺ CD8 T cells in WT (n=15) and COX2 KO (n=14) tumor-draining lymph nodes (TdLNs). Significance was determined by unpaired t test. ****p < 0.0001.* ***E.*** *Quantification of IFN-γ⁺ NK cells in WT (n=8) and COX2 KO (n=7) tumor-*

*draining lymph nodes. Significance was determined by unpaired t test. *p < 0.05.* ***F.*** *Growth curves of WT and COX2 KO KPC spheroids inoculated orthotopically in immune competent mice. Data represent the mean±SEM. n=9 mice/group. Significance was determined by two way ANOVA. ***p < 0.001.* ***G.*** *Frequencies of IL-1β$^+$ monocytes and IL-1β$^+$ macrophages in WT (n=7) and COX2 KO (n=6) tumors. Significance was determined by unpaired t test. ***p < 0.001 ****p < 0.0001.* ***H.*** *Quantification of IFN-γ$^+$ TNF-α$^+$ CD8 T cells (left) and of IFN-γ$^+$ NK cells in WT (n=9) and COX2 KO (n=8) tumor-draining lymph nodes. Significance was determined by unpaired t test. *p < 0.05.* ***I.*** *Growth curves of WT and COX2 KO KPC cells subcutaneously injected in immune competent mice treated with antibody targeting CD8$^+$ T cells or isotype control. Data are represented as mean±SD; statistical analysis was performed using two-way ANOVA. ****p < 0.0001, *p < 0.05. n=5 mice/group* ***J.*** *Growth curves of WT and COX2 KO KPC cells subcutaneously injected in immune competent mice treated with antibody targeting NK cells (aNK1.1+aASIALO GM-1) or isotype control. Data are represented as mean±SD; statistical analysis was performed using two-way ANOVA. ****p < 0.0001. n=9 mice/group.* ***K.*** *Quantification of CD8+ T cells in isotype-treated WT tumors (n=8) or NK-depleted tumors (WT n=9, COX2 KO n=9). Statistical significance was assessed by one way ANOVA. **p<0.01 ***p<0.001.*

Next, to further investigate the impact of PGE_2 on the pancreatic TME, we performed scRNA-Seq of WT and COX-2 KO tumors at an early time point, 7 days after tumor inoculation. We did not observe major differences in the composition of the TME , with the exception of a neutrophil reduction, in line with our flow cytometry data (Fig. 19. A). Nevertheless, we observed significant changes in gene expression within relevant cell populations, including macrophages, activated T cells and fibroblasts (Fig. 19. B). Specifically, fibroblasts retrieved from WT tumors showed increased expression of transcripts related to inflammatory response (*Il1b*, *Cxlc1*, *Ptgs2*), angiogenesis (*Thbs1*) and hypoxia (*Hif1a*). COX-2 KO tumor-infiltrating T cells showed higher expression of genes associated to cytotoxicity (*Gzma*, *Gzmk*), in line with flow cytometry results that indicated their increased activation (Fig. 19. C). Finally, IL-1β$^+$ TAMs from COX-2 KO tumors displayed a marked transcriptional rewiring. They exhibited reduced expression of key identity and inflammatory response genes while acquiring signatures related to type I and II IFN response (Fig. 19. D-E). However, COX-2 KO tumors were still controlled in mice lacking a crucial subunit of the IFN-α/β receptor (*Ifnar1*$^{-/-}$) (Fig. 19. F). Overall, these data highlight a key role of tumor-derived PGE_2 in shaping the TME and, importantly, in driving the IL-1β$^+$ TAM state *in vivo*. Targeting COX-2 leads to TME reprogramming and disease control in an IFN-independent manner.

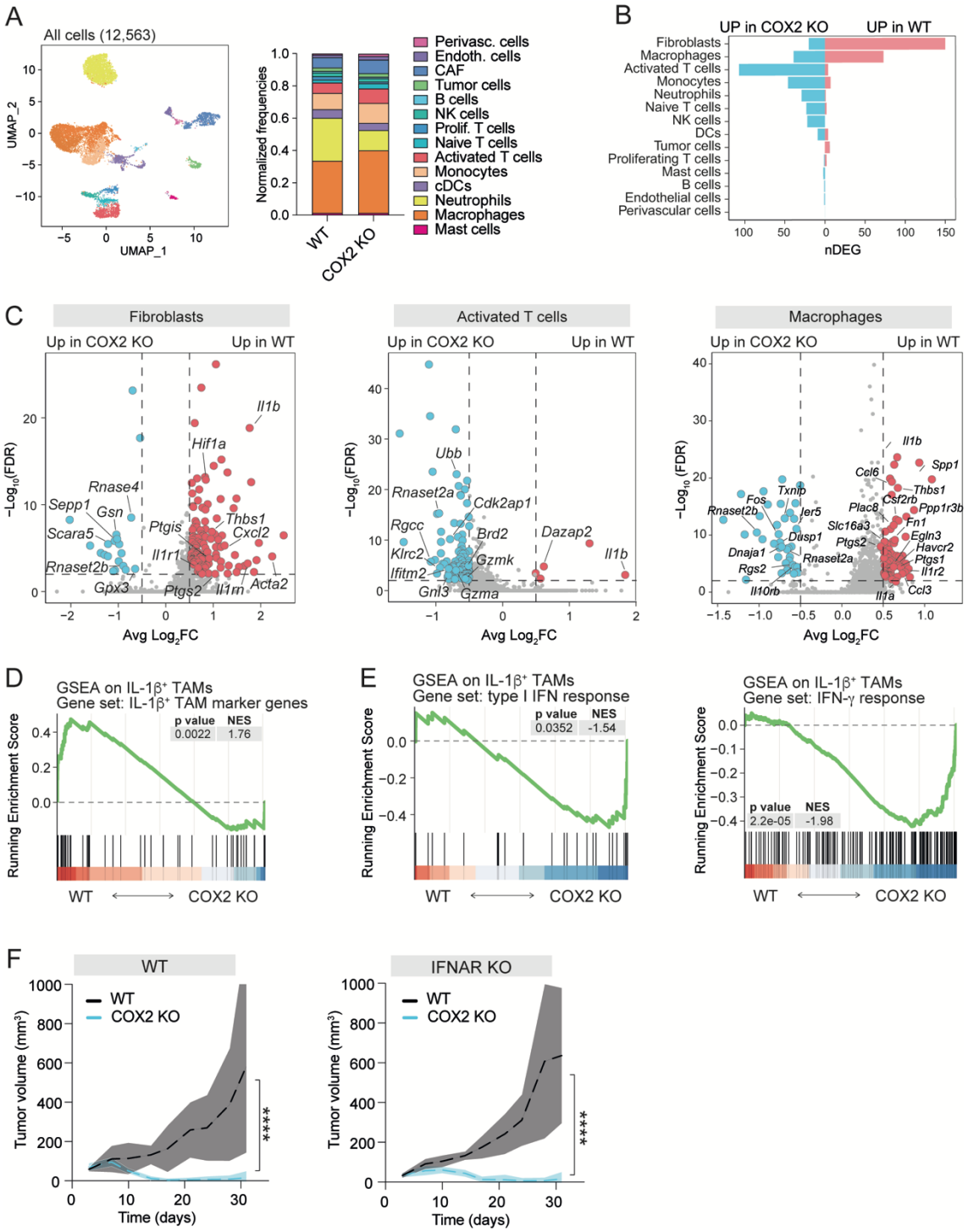

Figure 19. PDAC-derived PGE_2 elicits the IL-1β$^+$ TAM phenotype.

A. *UMAP representing transcriptome of cells from WT and COX-2 KO tumors (subcutaneous KPC, day 7 p.i.) colored by annotation for major cell types (left). Sample composition colored by cell type annotation is shown on the right.* ***B.*** *Bar plot showing the number of differentially expressed genes (DEG) in the comparison between WT vs COX2 KO for major cell types.* ***C.*** *Volcano plot showing differentially expressed genes in WT (red) vs COX2-KO (blue) comparison within fibroblast (left), activated T cells (middle) and macrophages (right). Relevant genes are reported.* ***D.*** *GSEA (IL-1β$^+$ TAM marker genes) genes ranked by log_2FC between Il1b$^+$ TAMs from WT versus COX-2 KO PDAC.* ***E.*** *GSEA performed on genes ranked by log_2FC in WT vs*

COX2-KO comparison of Il1b^{+} TAMs, using type I IFN response (left) or IFN-γ-response genes (Hallmarks) as gene set. ***F.*** *Growth curves (mean±SD) of WT and COX-2 KO PDAC cells (subcutaneous KPC) in wild-type mice (n=4 WT, n=5 COX-2 KO, left) or Ifnar1$^{-/-}$ (n=5 WT, n=5 COX-2 ko, right) mice. ****p < 0.0001 (two-way ANOVA).*

3.6. IL-1β signaling in PDAC cells promotes tumor growth

After identifying tumor-derived PGE_2 as a critical factor supporting PDAC growth, we examined the impact of IL-1β on PDAC and its ability to modulate the tumor microenvironment. To do this, we treated tumor-bearing mice with an IL-1β neutralizing antibody. Antibody-mediated neutralization of IL-1β *in vivo* led to delayed PDAC growth, concomitant with reduced expression of IL-1β by monocytes and TAMs, and with increased activation of cytotoxic T cells in tumor-draining lymph nodes (Fig. 20. A-C). Delayed tumor growth was also observed in NLRP3 KO mice, who lack a crucial component of the inflammasome, necessary for IL-1β maturation and release (Fig. 20 D). Consistently, culture supernatants of NLRP3 KO tumors showed reduced IL-1β content (Fig. 20. E).

Re-analysis of patient scRNA-Seq data highlighted tumor monocytes and *IL1B*$^{+}$ TAMs as the major sources of IL-1β, with subsets of dendritic cells and neutrophils expressing much lower transcript levels (Fig. 20. F).

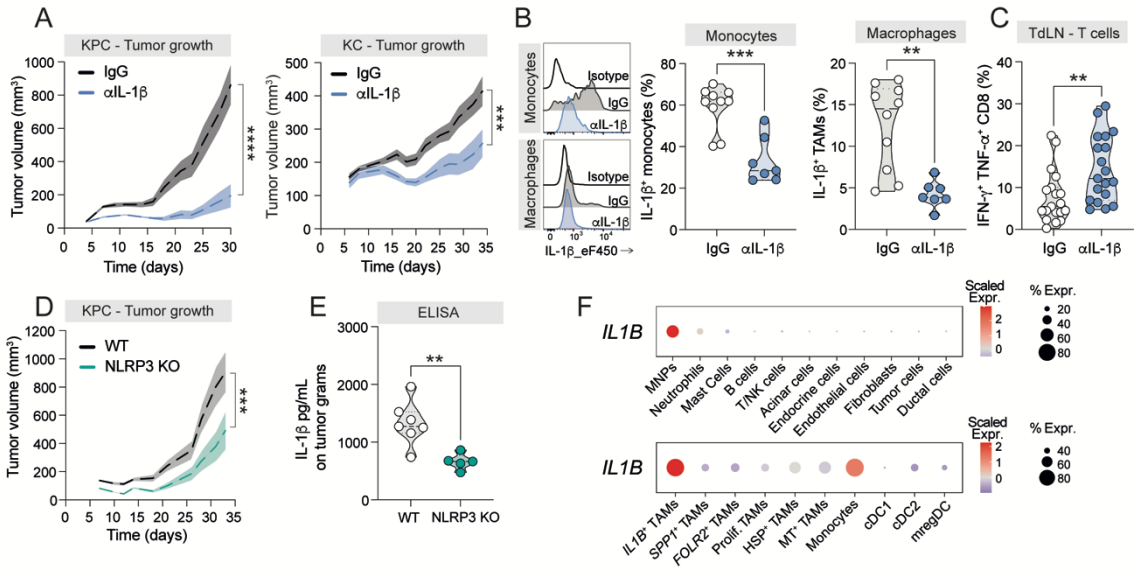

Figure 20. Neutralization of IL-1β impairs PDAC growth.
A. *Growth curves (mean±SEM) of PDAC cells (left, subcutaneous KPC, right subcutaneous KC, n=10 mice/group) in mice treated with anti-IL-1β or isotype control (IgG). ***p < 0.001 ****p < 0.0001 (two-way ANOVA).* ***B.*** *Representative histograms and frequencies of IL-1β^{+} monocytes*

*(left) and IL-1β$^+$ macrophages (right) (IgG n=10; αIL-1β n=7). **p<0.01 ***p<0.001 (unpaired student's two-tailed t test).* ***C.*** *Frequencies of IFN-γ$^+$ TNF-α$^+$ CD8 T cells in tumor-draining lymph nodes. n=19 mice/group. Statistical analysis with unpaired student's two-tailed t test. **p<0.01. D. Growth curves (mean±SEM) of PDAC cells (subcutaneous KPC) inoculated in WT (n=9) or NLRP3 KO (n=9) mice. ***p < 0.001 (two-way ANOVA).* ***E.*** *IL-1β quantification by ELISA analysis of TCM from WT (n=7) and NLRP3 KO (n=5) tumors. **p<0.01. Significance assessed by unpaired t test student* ***F.*** *Upper panel: dot plot showing scaled IL1B expression in immune and non-immune populations infiltrating human PDAC samples. Lower panel: dot plot showing scaled IL1B expression in human TAM subsets, monocytes and DC populations infiltrating PDAC samples.*

To determine the cellular targets of IL-1β in PDAC, we challenged WT and *Il1r1*$^{-/-}$ mice and found no differences in tumor growth (Fig. 21. A). To better dissect the effects of IL-1β on the immune and stromal compartments, we performed tumor challenge experiments in haemato-chimeric mice. In particular, bone marrow (BM) cells from *Il1r1*$^{-/-}$ donors, which lack a key signaling subunit of the IL-1 receptor, or from wild-type control were transplanted into irradiated wild-type or *Il1r1*$^{-/-}$ recipients, respectively (Fig. 21. B). No defect in tumor growth was observed in the two groups, indicating that the cancer-promoting effects of IL-1β are not driven by signaling in hematopoietic or stromal cells (Fig. 21. B).

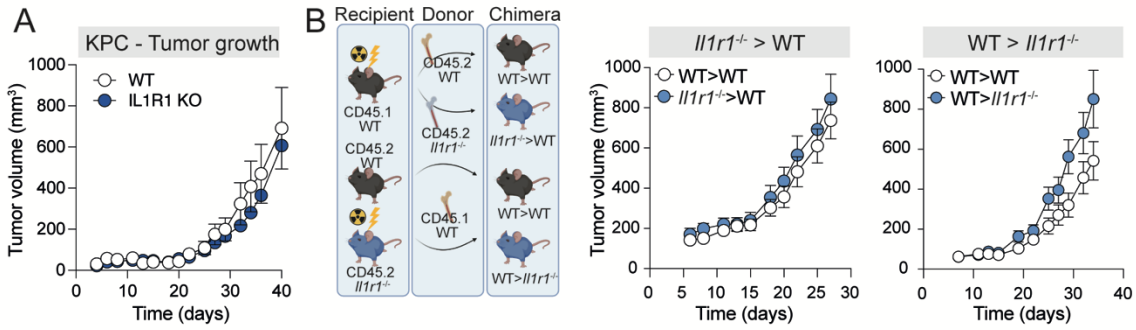

Figure 21. Inhibition of IL-1β signaling in stromal or hematopoietic cells does not alter PDAC growth.
A. *Tumor growth curves of subcutaneous KPC cells injected in WT or IL1R1 KO mice.* ***B.*** *Left: schematic representation of the generation of BM chimeras. Lethally irradiated recipient mice (WT or Il1r1*$^{-/-}$ *mice) were transplanted with 5x10*^{6} *donor BM cells (WT or Il1r1*$^{-/-}$*). Image was created with Biorender. Right: tumor growth curves of subcutaneous KPC cells injected in BM-chimeric mice. Data represent mean ± SEM (n=10 mice/group).*

Western blot analyses revealed that PDAC cell lines express IL1R1 (Fig. 22. A). In order to assess a possible direct effect of IL-1β on tumor cells, we generated IL1R1 KO KPC cells. We confirmed the absence of the receptor on IL1R1 KO clones and we functionally

assessed their inability to respond to IL-1β stimulation by measuring IkBα degradation (Fig. 22. B-C). Interestingly, IL1R1 KO KPC cells showed drastically reduced capacity to form tumors in immune competent mice, concomitant with reduced infiltration of IL-1β^{+} monocytes and increased activation of CD8^{+} T cells (Fig. 22. E-H). CD8 T cell depletion restored tumor growth of IL1R1 KO (Fig. 22. I). In addition, re-expression of IL1R1 in gene-targeted PDAC cells rescued their tumorigenic potential *in vivo* (Fig. 22. D,J).

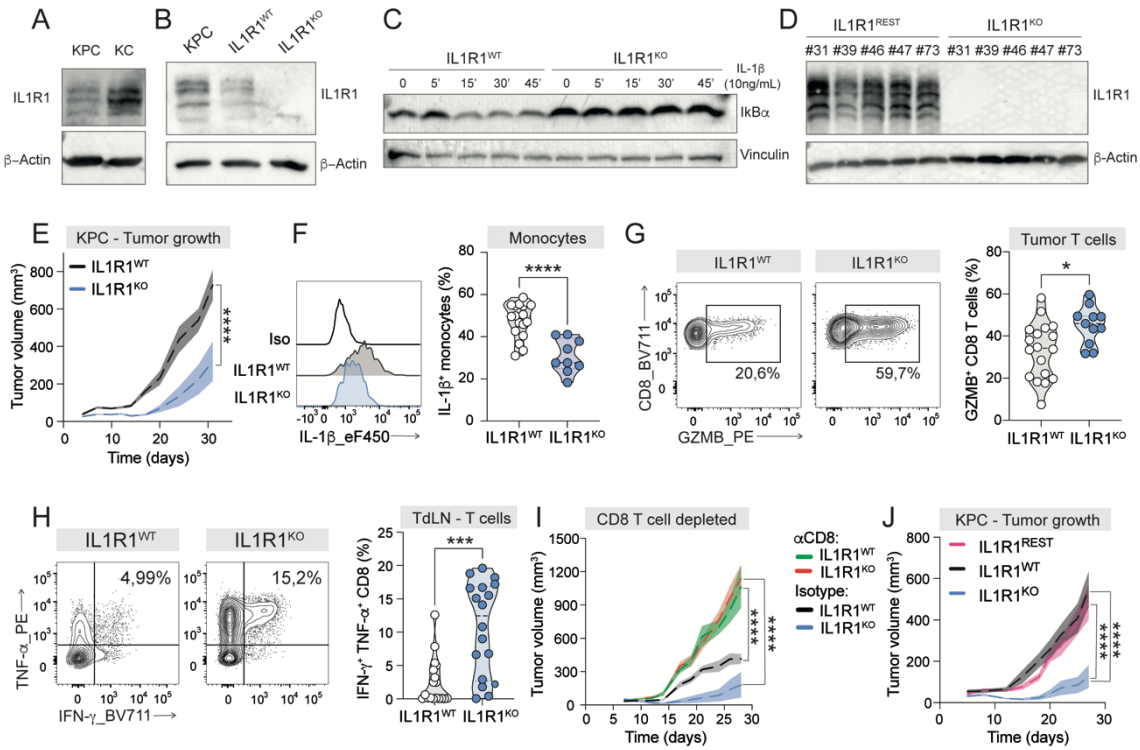

Figure 22. IL-1β signaling in PDAC cells is critical for tumor growth.
A,B. *Western Blot analyses of IL1R1 and β-Actin in whole cell extracts from KPC and KC parental cell lines (**A**), IL1R1^{WT} and Il1R1^{KO} edited KPC cells (**B**).* ***C.*** *Western Blot analyses of IkBα and Vinculin in whole cell extracts of IL1R1^{WT} and IL1R1^{KO} KPC cells, stimulated with IL-1β (10ng/mL) for the indicated time points.* ***D.*** *Western Blot analyses of IL1R1 and β-Actin in whole cell extracts from IL1R1-reconstituted (IL1R1^{REST}) and IL1R1^{KO} KPC clones (# clone ID).* ***E.*** *Growth curves of subcutaneous IL1R1^{WT} and IL1R1^{KO} PDAC cells. Data represent mean±SEM (n=8 mice/group).. Statistical analysis was performed using two-way ANOVA. ****p<0.0001.* ***F.*** *Representative histograms and frequencies of IL-1β^{+} monocytes (IL1R1^{WT} n=18; IL1R1^{KO} n=9). Statistical analysis was performed using unpaired student's two-tailed t test. ****p<0.0001* ***G.*** *Representative plots (left) and frequencies (right) of GZMB^{+} CD8 T cells. (IL1R1^{WT} n=18; IL1R1^{KO} n=11). Statistical analysis was performed using unpaired student's two-tailed t test. *p<0.05.* ***H.*** *Representative plots and frequencies of IFN-γ^{+} TNF-α^{+} CD8 T cells. (n=18 mice/group). Statistical analysis was performed using unpaired student's two-tailed t test. ***p<0.001.* ***I.*** *Growth curves of WT and IL1R1 KO KPC cells subcutaneously injected in immune competent mice treated with antibody targeting CD8^{+} T cells or isotype control. Data*

*are represented as mean±SEM; isotype-treated IL1R1^{WT}, n=5; isotype-treated IL1R1^{KO}, n=6; αCD8-treated IL1R1^{WT}, n=5; αCD8-treated IL1R1^{KO}, n=6. Statistical analysis was performed using two-way ANOVA. ****p < 0.0001.* ***J.*** *Growth curves of IL1R1^{WT}, IL1R1^{KO} or IL1R1^{REST} PDAC cells inoculated subcutaneously. Data represent mean±SEM. n=10 mice/group. Significance was assessed by 2-way ANOVA, ****p<0.0001.*

To further evaluate the impact of IL-1β on cancer cells, in collaboration with the laboratory of Carla Taveggia, we explanted IL1R1 WT and KO tumors eleven days after subcutaneous inoculation in immunocompetent mice and we cultured them in matrigel domes. After six days, explants of IL1R1 KO tumors showed a defective organoid-forming efficiency compared to the WT counterpart (Fig. 23. A). Additionally, we treated established IL1R1 WT and KO organoids with IL-1β and we observed that IL-1β signaling significantly expanded the number of IL1R1 WT but not IL1R1 KO organoids (Fig. 23. B).

Overall, these data highlight a critical role of tumor cell-intrinsic IL-1β signaling for PDAC growth.

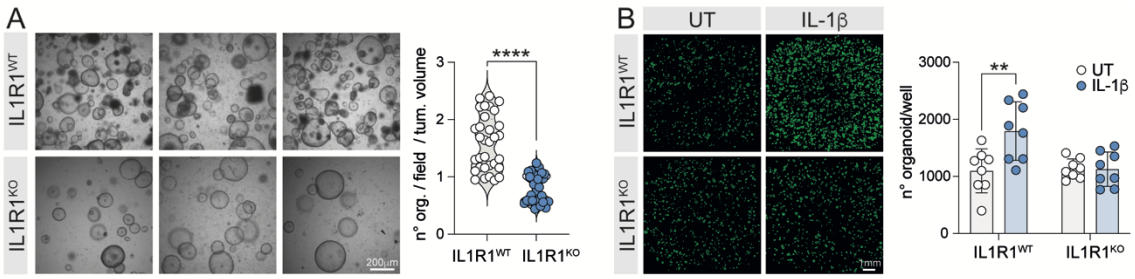

Figure 23. IL-1β intrinsic signaling affects organoid-forming efficiency of tumor cells.
A. *Organoid-forming efficiency (organoids/field/tumor volume) of explanted control (Ctrl) and IL-1R1 ko PDAC (subcutaneous KPC, day 11). Tumors (n=4/group) were plated in 8 wells, 4 fields/well were counted. ****p<0.0001 (unpaired student's two-tailed t test with Welch's correction).* ***B.*** *Representative images and quantification of IL1R1^{WT} and IL1R1^{KO} organoids treated with IL-1β for 5 days or left untreated. Each dot represents the mean number of organoid/well for the WT (white dots) and IL1R1^{KO} tumors (blue dots). Significance was assessed by paired student's two-tailed t test, *p<0.05.*

3.7. IL-1β signaling in PDAC cells sustains TAM recruitment and conditioning

In order to comprehensively assess the effects of IL-1β on tumor cells, we performed RNA-Seq analyses of KPC cells treated with IL-1β. We found marked up-regulation of genes encoding for myeloid growth factors (*Csf1*, *Csf2*), chemokines (*Ccl2*, *Cxcl1*),

cytokines (*Tnfa*, *Il6*), as well as for enzymes with immune regulatory functions (*Ptgs2*, *Nos2*) (Fig. 24. A). These results were confirmed by quantification of proteins in the supernatant of tumor cells, where IL-1β treatment robustly induced immunomodulatory molecules (IL-10), neutrophil-recruiting chemokines (CXCL1), together with factors involved in monocyte recruitment (CCL2) and mono/macrophage proliferation and differentiation (CSF-1) (Fig. 24. B). To assess the functional relevance of these two latter molecules, we performed tumor challenge experiments in *Ccr2*$^{-/-}$ mice, which lack the CCL2 receptor, or in wild-type mice treated with a neutralizing antibody against CSF-1. Interestingly, WT tumor cells failed to grow when implanted in *Ccr2*$^{-/-}$ mice, highlighting the critical role of monocyte-derived macrophages in supporting PDAC growth (Fig. 24. C). On the same line, neutralization of CSF-1 delayed tumor progression (Fig. 24. D).

We next focused on IL-1β-induced factors driving macrophage conditioning. Among the most enriched GO terms in the transcriptome of IL-1β-treated tumor cells were cytokine and prostaglandin secretion, in line with the finding that stimulation of KPC cells with IL-1β led to increased production of PGE_2 and TNF-α (Fig. 24. B,E-F). To further assess their role in shaping macrophage phenotype we performed supernatant transfer experiments (Fig. 24. G). We found that, while tumor-conditioned media (TCM) from untreated KPC cells (KPC^{UT}) did not induce *Il1b* expression in macrophages, TCM from KPC cells treated for 24hrs with IL-1β ($KPC^{IL\text{-}1\beta}$) strongly upregulated *Il1b* expression by BMDMs (Fig. 24. G). However, this induction was reduced when KPC cells were concomitantly treated with IL-1β and a COX-2 inhibitor ($KPC^{IL\text{-}1\beta+Cox\text{-}2i}$) for 24hrs (Fig. 24. G). Additionally, *Il1b* upregulation by BMDMs was strongly reduced in the presence of a TNF-α neutralizing antibody, further suggesting the key role of PGE_2 and inflammatory molecules, such as TNF-α, in promoting *Il1b* expression in macrophages (Fig. 24. G). These data highlight a self-sustaining loop between PDAC cells and macrophages. In this loop, IL-1β triggers in tumor cells the release of factors that recruit monocytes to tumors and elicit the development of IL-1β$^+$ TAMs at least in part through PGE_2 and TNF-α.

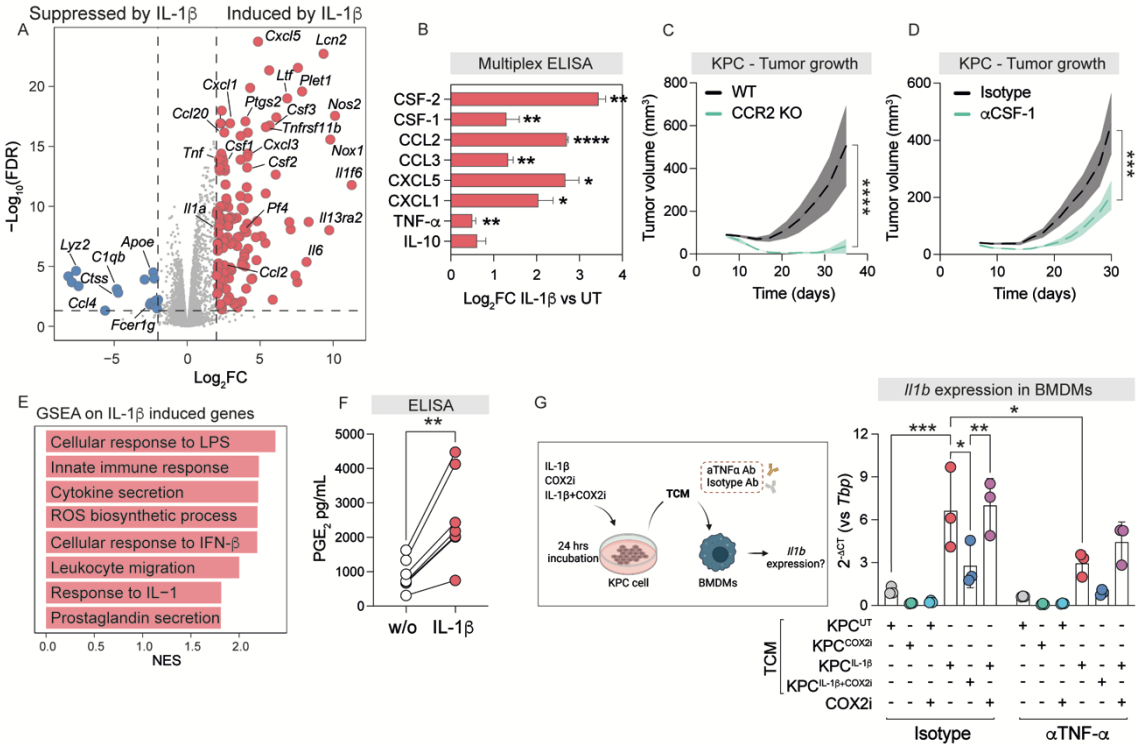

Figure 24. IL-1β signaling induces an inflammatory reprogramming of tumor cells.
A. *Volcano plot (left) of genes up-regulated (red) or down-regulated (blue) in PDAC (KPC) cells treated with IL-1β for 24 hours (UT n=3, IL-1β n=2). Selected genes are highlighted.* ***B.*** *Quantification (Multiplex ELISA) of the indicated cytokines (mean±SD, n=3) in the supernatant of PDAC cells (KPC) treated with IL-1β for 24 hours. Significance was assessed with unpaired two-tailed student's t test *p<0.5, **p<0.01, ****p < 0.0001.* ***C,D.*** *Growth curves (mean±SEM) of PDAC cells (subcutaneous KPC) in wild-type and Ccr2$^{-/-}$ mice (**C**) (n=5/group) or (**D**) in wild-type mice treated with an anti-CSF-1 antibody (aCSF-1, n=8) or isotype control (IgG, n=10). ***p<0.001 ****p < 0.0001 (two-way ANOVA).* ***E.*** *GSEA on genes ranked by log$_2$FC between PDAC cells (KPC) treated with IL-1b versus untreated controls.* ***F.*** *Quantification (ELISA) of PGE$_2$ (n=7) in the supernatant of PDAC cells (KPC) treated with IL-1β for 24 hours. Significance was assessed with paired two-tailed student's t test. **p< 0.01.* ***G.*** *Scheme of the experiment (left, created with Biorender) and expression of Il1b (RT-qPCR, mean±SD) in BMDMs treated for 2 hours with tumor-conditioned media (TCM) of mouse PDAC cells (KPC) from the following conditions: untreated (KPC^{UT}) or treated for 24 hours with a COX-2 inhibitor (KPC^{COX2i}), IL-1β (KPC$^{IL-1β}$), IL-1β+COX-2 inhibitor (KPC$^{IL-1β+COX2i}$). A control condition of BMDMs stimulated with vehicle or COX-2 inhibitor (COX2i) is shown. Isotype control or an anti-TNF-α antibody (αTNF-α) groups were included for each condition (n=3). *p<0.05 **p<0.01 ***p<0.001 (two-way ANOVA).*

3.8. Inflammatory reprogramming occurs early during pancreatic tumorigenesis

To broadly assess the effects of IL-1β on tumor cells, we performed transcriptomic analyses of PDAC cell lines as well as of KPC-derived organoids left untreated or stimulated with IL-1β at different time points. By integrating our RNA-seq data, we

defined a core signature of 57 genes, hereafter referred to as tumor-intrinsic IL-1β response signature (T1RS), which were commonly upregulated by IL-1β stimulation in at least one timepoint in all our datasets (Fig. 25. A,B). After defining their human orthologs, we found that this gene module correlated with predicted abundance of IL-1β^{+} TAMs in PDAC patients and with a poor patient survival in TCGA data (Fig. 25. C,D). In addition, T1RS was enriched in the transcriptome of human (Peng et al., 2019) and mouse (Alonso-Curbelo et al., 2021) malignant cells compared to the normal adjacent or healthy counterpart, respectively (Fig. 25. E,F).

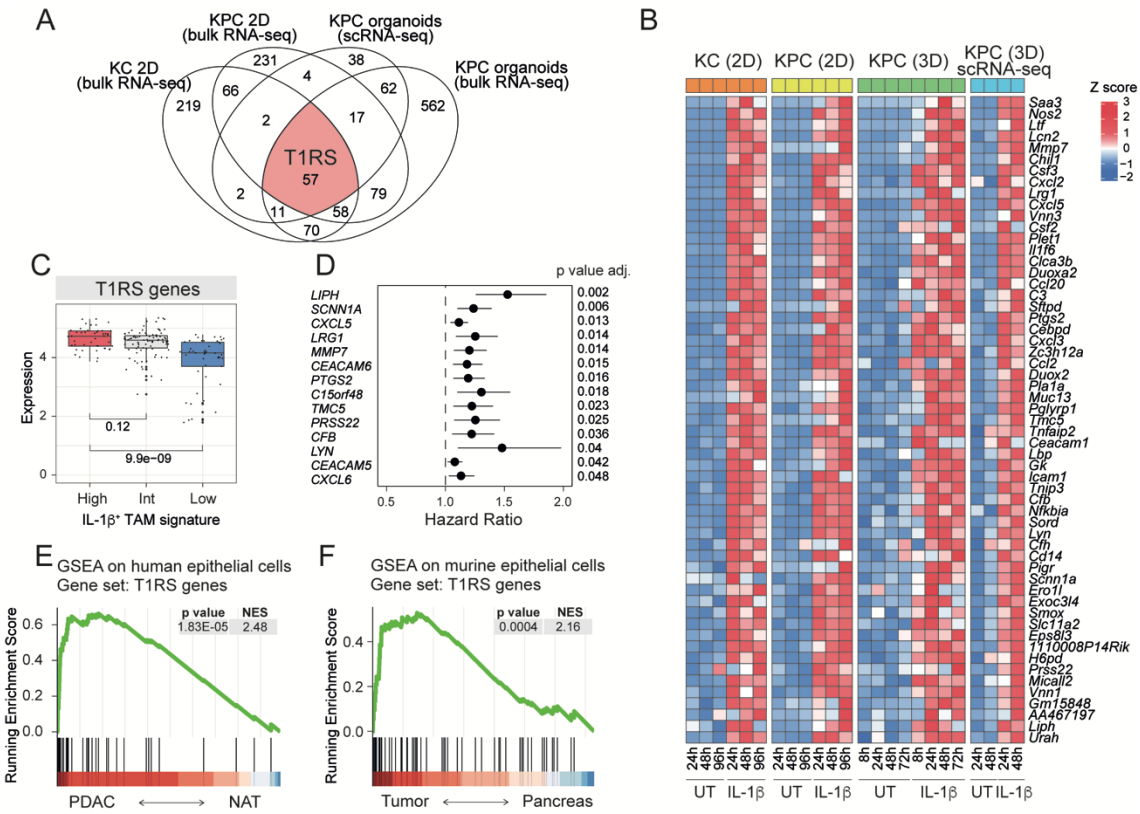

Figure 25. T1RS is associated with IL-1β^{+} TAMs abundance and poor prognosis in PDAC patients.

A. *Venn diagram of genes up-regulated (bulk RNA-Seq or scRNA-Seq) upon treatment with IL-1β in the indicated mouse PDAC models. The tumor-intrinsic IL-1β response signature (T1RS) is composed by the 57 genes commonly up-regulated by IL-1β in all conditions.* ***B.*** *Heatmap of scaled expression (bulk RNA-Seq or scRNA-Seq) of T1RS genes in the indicated mouse PDAC models, left untreated or stimulated with IL-1β for the indicated time points.* ***C.*** *Mean expression of human orthologs of T1RS genes in PDAC patients (TCGA) stratified for the levels of expression of the IL1B^{+} TAM signature.* ***D.*** *Hazard ratios obtained by fitting univariate Cox model on gene expression of T1RS genes in TCGA PDAC cohort. Only genes with significant adjusted p-values are reported.* ***E,F.*** *GSEA (T1RS genes) on genes ranked by log$_2$FC between*

*human PDAC and normal adjacent tissue (NAT) (**E**) or between mouse PDAC and control pancreas (**F**).*

Longitudinal analyses of PDAC cells orthotopically injected in experimental animals revealed an upregulation of T1RS at early time points (day 10 post inoculation, p.i.). Although at lower levels, T1RS was still expressed at later disease stages (day 20-30 p.i.) (Fig. 26. A). Interestingly, GSEA performed 10, 20 and 30 days after tumor inoculation, revealed that T1RS expression anticipated acquisition by tumor cells of biological programs closely related to tumor malignancy, such as proliferation and EMT (Fig. 26. B). To assess inflammatory reprogramming of tumor cells during the different stages of pancreatic tumorigenesis, we analyzed available gene expression data from GEMMs (Burdziak et al., 2023). These studies revealed that activating mutation of *Kras* oncogene in pre-neoplastic lesions correlated with T1RS expression (Fig. 26. C). However, the highest expression of T1RS resulted in the stage of PanINs, with levels of the signature remaining still elevated in established PDAC and distal metastasis (Fig. 26. C). Similarly, T1RS genes were highly expressed in PanINs from healthy donor and PDAC patients and maintained in tumor lesions too, as assessed by re-analysis of a publicly available spatial transcriptome dataset (Fig. 26. D) (Carpenter et al., 2023).

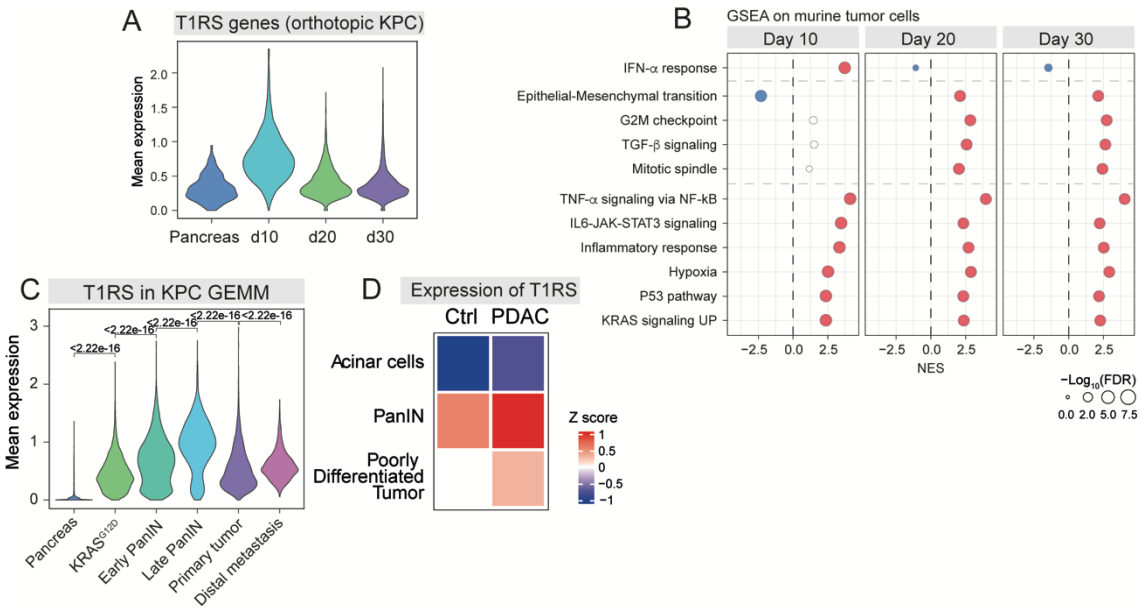

Figure 26. Inflammatory reprogramming occurs early during pancreatic tumorigenesis.
A. *Mean expression (scRNA-Seq) of T1RS genes in pancreatic epithelial cells and tumor cells from control pancreas or mouse PDAC (orthotopic KPC) in the indicated time points.* ***B.*** *GSEA (MSigDB hallmark genes) on genes ranked by log_2FC between tumor versus healthy pancreas*

cells at the indicated time points (orthotopic KPC). ***C.*** *Expression of T1RS in pancreatic cells from the indicated mouse models of tumorigenesis. Significance was assessed by two-sided Mann-Whitney test* ***D.*** *Heatmap of scaled mean expression (GeoMx) of human orthologs of T1RS genes in the indicated regions of interest (ROIs) of healthy donors and PDAC patients.*

Recently, several studies showed that inflammation may cooperate with oncogene activation by fueling tumor progression at any stage of carcinogenesis (Alonso-Curbelo et al., 2021; Del Poggetto et al., 2021; Hill et al., 2023; Weeden et al., 2023).

In this context, by re-analyzing available scRNAseq data from hereditary or idiopathic pancreatitis patients, we were able to identify macrophage populations transcriptionally resembling the TAM subsets identified in PDAC patients. In particular, we found a subset of macrophages displaying a gene expression profile comparable to that of IL-1β^+ TAMs (Fig. 27. A,B) (Lee et al., 2022). In line with this, re-analyses of available RNA-seq data revealed that murine epithelial cells undergoing tissue damage induced by cerulein administration upregulate T1RS (Fig. 27. C). Additionally, as previously described, activating mutation of *Kras* oncogene induced T1RS in epithelial cells at higher levels compared to cerulein administration alone. However, the highest T1RS expression was achieved by combination of cerulein-induced inflammation and *Kras* activating mutations (Fig. 27. C). Similarly, mice treated with the alarmin IL-33, which mediates tissue damage responses in the pancreas, upregulated T1RS expression in epithelial cells, but combination of oncogene activation and IL-33 administration further increased its expression (Fig. 27. D) (Alonso-Curbelo et al., 2021). Finally, pancreatic spheroids derived from cerulein-treated mice, months after resolution of the injury, retained higher T1RS expression compared to spheroids derived from control animals (Fig. 27. E) (Del Poggetto et al., 2021). We conclude that inflammatory reprogramming is an early event in pancreatic tumorigenesis, leading to persistent transcriptional changes that associate with disease progression and poor patient outcome.

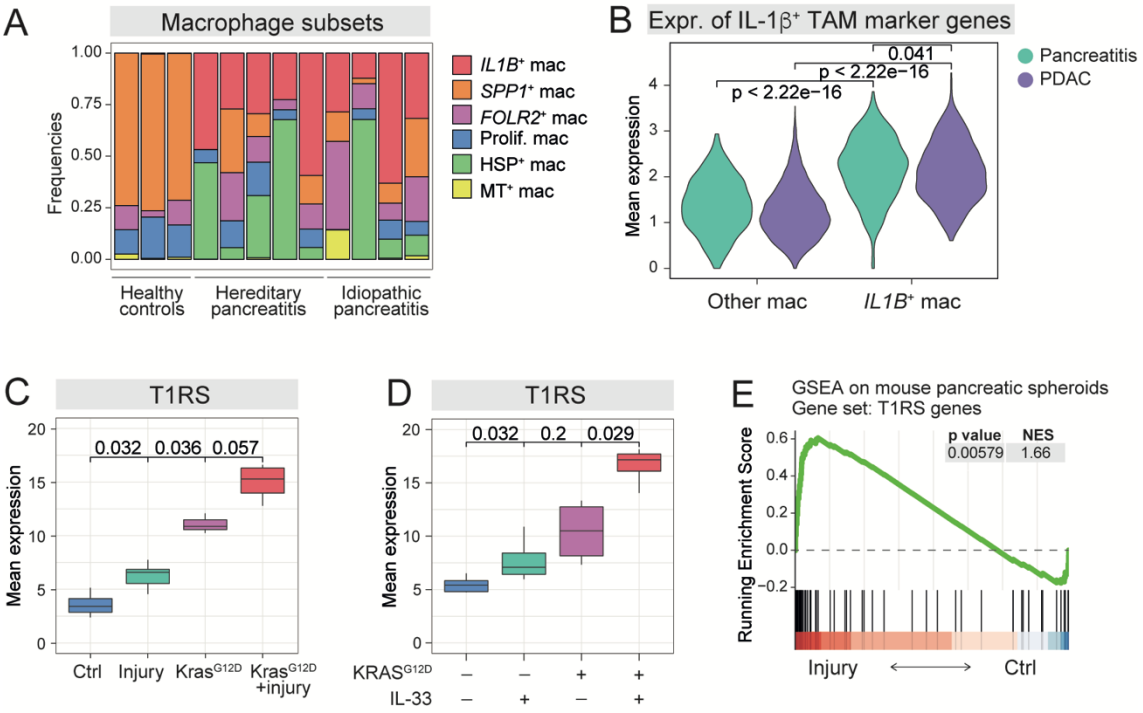

Figure 27. Tissue damage and oncogene activation cooperatively promotes inflammatory reprogramming of pancreatic cells.
A. *Frequencies (scRNA-Seq) of the indicated macrophage subsets in the pancreas of healthy controls or patient with hereditary or idiopathic pancreatitis.* ***B.*** *Mean expression (scRNA-Seq) of IL-1β⁺ TAM marker genes in IL-1β⁺ TAMs (or other TAMs) from PDAC patients and in macrophages corresponding to IL-1β⁺ TAMs (or other macrophages) in pancreatitis patients. Significance is computed by two-sided Mann-Whitney test.* ***C.*** *Mean expression of T1RS genes in pancreatic epithelial cells from the following conditions: control mice (Ctrl), mice treated with cerulein (Injury), mice harboring mutated Kras ($Kras^{G12D}$), mice harboring mutated Kras and treated with cerulein ($Kras^{G12D}$ + Injury). Significance was assessed with two-sided Mann-Whitney test.* ***D.*** *Mean expression of T1RS genes in pancreatic epithelial cells from the following conditions: control mice, mice treated with IL-33, mice harboring mutated Kras ($Kras^{G12D}$), mice harboring mutated Kras and treated with IL-33. Significance was assessed with two-sided Mann-Whitney test.* ***E.*** *GSEA (T1RS genes) on genes ranked by log_2FC between spheroids generated from injured or control pancreas.*

3.9. IL-1β⁺ TAMs spatially colocalize with T1RS⁺ PDAC cells in patients

We next asked whether local interactions with IL-1β⁺ TAMs underlie transcriptional heterogeneity and inflammatory reprogramming of tumor cells. Analyses of scRNAseq data from PDAC patients uncovered subsets of tumor cells expressing T1RS at high levels (Fig. 28. A,B). After re-clustering, pseudotime analyses (Street et al., 2018) identified these T1RS⁺ PDAC cells as end points of a transcriptional trajectory driven by increasing expression of the T1RS itself (Fig. 28. C,D). The predicted transition correlated with higher levels of known IL-1β target genes, such as *NFKBIA*, *IL1RN*, and *CXCL1*, as well

as of known tumor markers, such as *CEACAM6*, *CEACAM7*, *KRT19* (Fig. 28. E). Moreover, GSEA revealed an enrichment of GO terms associated to pancreatic tumorigenesis - *Kras* signaling, hypoxia, EMT, p53 pathway, and TGF-β signaling, among others – within the driver genes of the predicted trajectory (Fig. 28. F). These data highlight an intrinsic correlation between inflammatory reprogramming and acquisition of pathogenic programs by tumor cells.

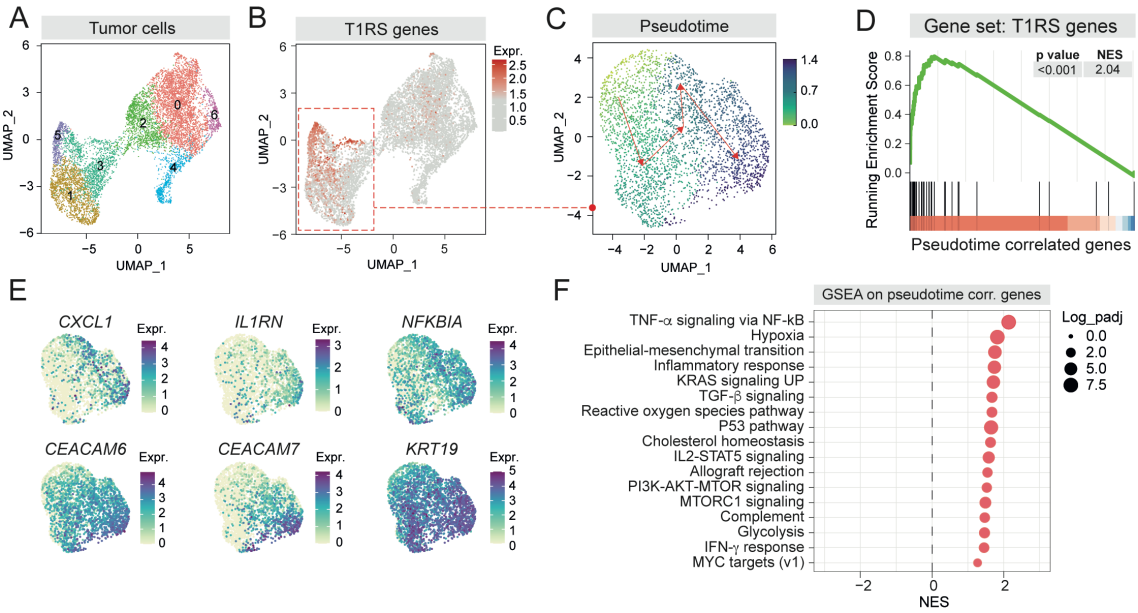

Figure 28. Identification of T1RS^{+} PDAC cells in human PDAC patients.
A. *UMAP plot of scRNA-Seq data of PDAC cells from chemotherapy-naïve patients. Colors and numbers indicate cluster identity.* ***B.*** *UMAP plot showing mean expression of T1RS genes in human PDAC cells.* ***C.*** *Pseudotime analysis of T1RS+ PDAC cells.* ***D.*** *GSEA (T1RS genes) on pseudotime-ordered genes of the computed developmental trajectory of T1RS^{+} PDAC cells.* ***E.*** *Expression of selected pseudotime-correlated T1RS genes and/or IL-1β targets in PDAC cells.* ***F.*** *GSEA (MSigDB hallmark genes) on pseudotime-ordered genes of the computed developmental trajectory of T1RS^{+} PDAC cells.*

To assess the role of macrophages in this process, we performed single-cell spatial gene expression analyses in human PDAC samples. Highly multiplexed *in situ* RNA hybridization (Guilliams et al., 2022) with a custom panel of 98 gene probes identified IL-1β^{+}, FOLR2^{+} and SPP1^{+} TAMs, as well as subsets of tumor, stromal, and immune cells; co-expression of *CXCL1* and *KRT19* was used as proxy to detect T1RS^{+} PDAC cells (Fig. 29. A,B). We next set out to elucidate local cellular interactions between macrophages and tumor cells, by performing spatial neighborhood analyses. First, we found that *IL1B*$^{+}$ TAMs, rather than being scattered in the tumor, tend to be localized in

specific areas of tumor tissue, representing the most enriched population in their own neighborhood. Interestingly, the second cluster to be significantly enriched in their spatial neighborhood corresponds to T1RS$^+$ PDAC cells (Fig. 29. C). Similarly, T1RS$^+$ PDAC cells tend to cluster together and *IL1B*$^+$ TAMs are significantly enriched in their spatial neighborhood (Fig. 29. C). Representative images of PDAC patients clearly show their co-localization in specific areas of tumor tissue (Fig. 29. D). These data highlight a spatially confined cross-talk between IL-1β$^+$ TAMs and T1RS$^+$ PDAC cells sustained by the PGE_2-IL-1β axis.

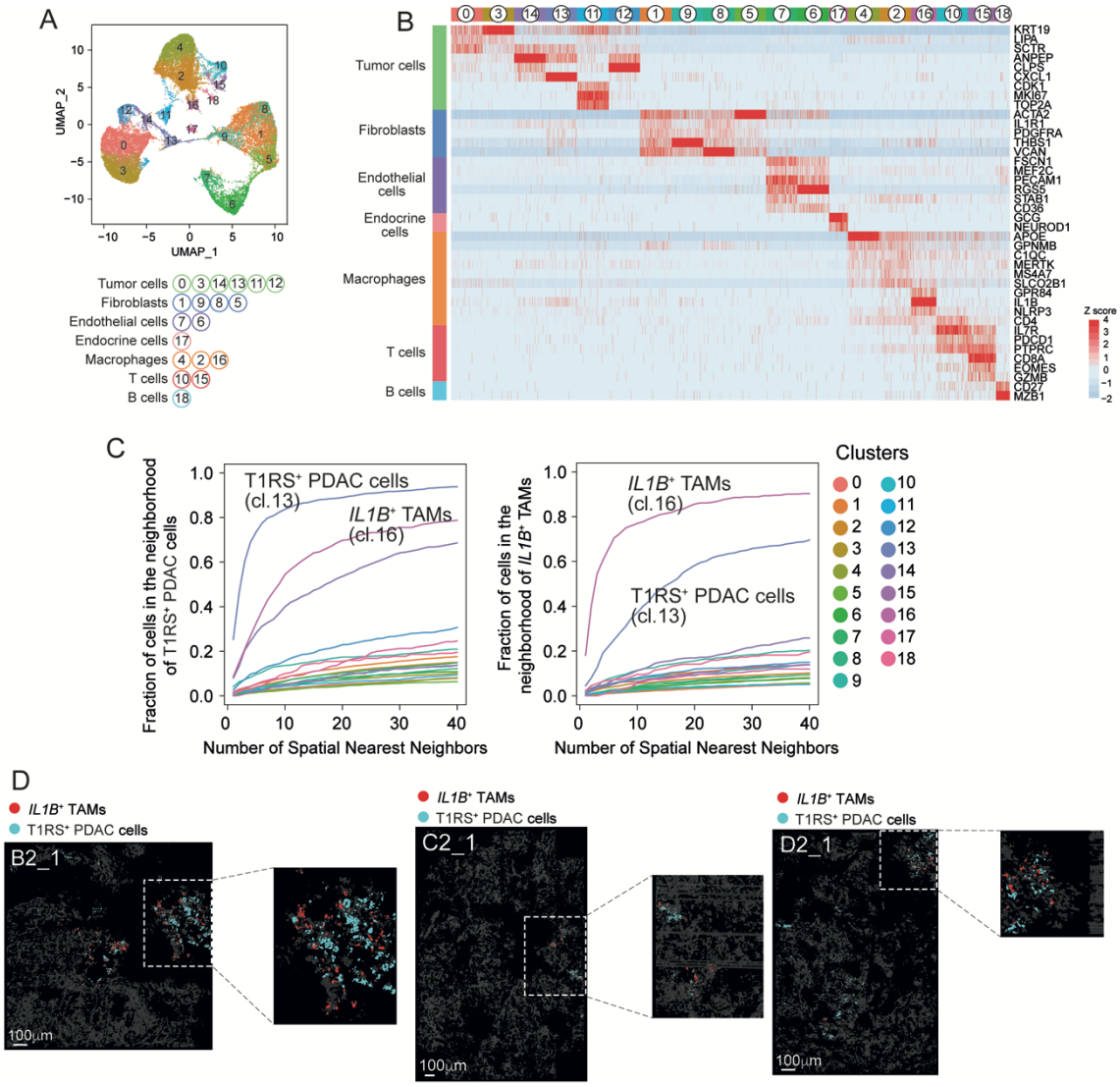

Figure 29. IL-1β$^+$ TAMs spatially colocalize with T1RS$^+$ PDAC cells in patients.
A. *UMAP of spatial gene expression data (Molecular Cartography) of cells from all sections collected from patient LPDAC30. Colors and numbers indicate cluster identity and corresponding annotations.* ***B.*** *Heatmap of scaled expression (in situ RNA hybridization) of marker genes for clusters identified by spatial transcript analyses. Numbers refer to cluster*

identity. (T1RS^{+} PDAC cells cluster 13 and IL-1β^{+} TAMs cluster 16). ***C.*** *Fraction of cells belonging to each cluster identified by spatial transcript analyses found in the spatial neighborhood of IL-1β^{+} TAMs (left) or T1RS^{+} PDAC cells (right). Numbers and colors refer to cluster identity.* ***D.*** *Selected regions of interest (LPDAC30 B2_1, left, LPDAC30 C2_1, middle and LPDAC30 D2_1, right) showing co-localization of IL-1β^{+} TAMs (red) and T1RS^{+} PDAC cells (light blue) in spatial gene expression analyses.*

4. DISCUSSION

By combining genomic and functional studies, we identified a population of TAMs expressing high levels of transcripts belonging to inflammatory response and tissue repair programs, but depleted of antigen presentation and interferon-related gene ontology terms. Enrichment analyses revealed that *IL1B*$^{+}$ TAMs co-expressed M1 and M2 signatures, similar to findings in head and neck squamous carcinoma (Bill et al., 2023), highlighting the complex heterogeneity of macrophages *in vivo*. Interrogation of the TCGA dataset revealed a negative correlation between the expression of *IL1B*$^{+}$ TAM signature and PDAC patient survival, suggesting their pathogenic activities. In line, broad neutralization of IL-1β reduced tumor progression in multiple murine models of pancreatic cancer. This was associated with decreased production of IL-1β by tumor-infiltrating monocytes and TAMs, together with increased cytotoxic activation of NK and T cells. Similarly, blocking IL-1β activity reduced the formation of lung adenocarcinoma, where a subset of IL-1β-producing TAMs, induced by local inflammation, accumulated and promoted tumor progression (Hill et al., 2023). Consistent with a previous study in pancreatic cancer (Daley et al., 2017), even NLRP3 KO mice exhibited reduced tumor progression, further supporting the tumor-promoting role of IL-1β. However, broad neutralization of IL-1β appears to have greater therapeutic potential compared to inhibiting inflammasome activation. This might be due to the ability of certain cell populations to process and release IL-1β in an inflammasome-independent manner (Afonina et al., 2015; Netea et al., 2015), or to the presence of additional inflammasome-dependent anti-tumor activities that could be impaired in NLRP3 KO mice (Zhivaki et al., 2020; Zhivaki & Kagan, 2021). To properly compare the efficacy of these two therapeutic approaches, parallel experiments should be conducted using antibodies to neutralize IL-1β and small molecules to inhibit NLRP3 activation.

While macrophages represent a key source of IL-1β, subsets of tumor cells in pancreatic cancer participate to IL-1β secretion. Indeed, selective interference of *Il1b* production or release by tumor cells correlated with reduced tumor progression and a reprogramming of the TME toward an immune-stimulatory phenotype (Das et al., 2020). Altogether, our and other studies highlight the multifaced tumor-promoting roles of IL-1β, supporting a broad targeting of its activity in order to avoid compensatory effects by other populations in the TME (Daley et al., 2017; Das et al., 2020; Dmitrieva-Posocco et al., 2019; Garlanda

& Mantovani, 2021; Hill et al., 2023). Nevertheless, to properly tackle the contribution of mono/macrophage-derived IL-1β in our model, selective genetic deletion should be carried out.

Longitudinal scRNAseq analyses coupled with flow cytometry data, revealed that *Il1b*$^{+}$ macrophages are nearly absent in the healthy pancreas. However, these macrophages accumulate during the early stages of tumor development and persist as the tumor progresses. Fate mapping experiments further confirmed that these TAMs originate from monocytic cells. Specifically, local exposure to PGE_2 and inflammatory molecules – such as TNF-α – prompts circulating monocytes to adopt the *Il1b*$^{+}$ TAM state and produce IL-1β.

Recent studies have emphasized the critical role of PGE_2 in driving tumor progression by fostering a pathogenic inflammation that hinders the recruitment and activation of cytotoxic and antigen-presenting cells in the TME (Bayerl et al., 2023; Bonavita et al., 2020; Böttcher et al., 2018; Gong et al., 2022; Zelenay et al., 2015). In line with these findings, our study showed that selective inhibition of COX-2 delayed tumor growth, reducing the accumulation of IL-1β^{+} macrophages while enhancing T cell activity. Furthermore, genetic disruption of *Ptgs2* in tumor cells had a profound impact on their tumor-forming potential *in vivo*. COX-2 KO tumors exhibited delayed growth or complete rejection in immunocompetent mice, and this effect was dependent on NK cells and CD8^{+} T cells. Notably, NK-depleted mice displayed reduced infiltration of CD8^{+} T cells, consistent with studies in melanoma cancer, where NK cells were found to play a pivotal role in promoting the accumulation and activation of cytotoxic lymphocytes (Bonavita et al., 2020).

To comprehensively explore the effects of PGE_2 on the TME, we performed scRNAseq analyses of COX-2 KO tumors. Ablation of tumor-derived PGE_2 correlated with decreased expression of inflammatory genes in CAFs and increased expression of cytotoxic-related genes in tumor-infiltrating T cells, in line with their involvement in the rejection of COX-2 KO tumors. Notably, we observed significant changes in the gene expression profile of *Il1b*$^{+}$ TAMs upon PGE_2 ablation. Specifically, their key marker genes were downregulated, while genes related to type I and II interferon responses were upregulated. Surprisingly, COX2 KO tumors were still rejected when implanted in *Ifnar*

$^{-/-}$ mice. This is in contrast to findings in melanoma cancer models where a type I IFN-dependent immune response restricts the growth of *Ptgs*$^{-/-}$ tumors, at least in the early stages of the disease (Zelenay et al., 2015). These results suggest that the inhibited growth of PGE_2-deficient pancreatic tumors is not specifically linked to type I interferon-dependent responses but rather reflects a more extensive inflammatory reprogramming of the TME.

Our data suggest that the complex biological effects of PGE_2 reflect divergent control of gene modules in macrophages. On the one hand, PGE_2 suppresses the expression of genes encoding key molecules associated with anti-tumor immunity, including chemokines involved in recruiting NK and T cells (Bonavita et al., 2020; Böttcher et al., 2018), and type I interferon and interferon-stimulated genes, whose expression requires the transcription factor MEF2A (Cilenti et al., 2021). On the other hand, PGE_2, in cooperation with inflammatory stimuli, triggers expression of immunomodulatory molecules like IL-10 (Cilenti et al., 2021), alongside with inflammatory factors that support tumor growth and tissue repair. While the molecular mechanisms governing these synergistic activities induced by PGE_2 remain to be elucidated, it is worth noting that PGE_2-sensitive regions have a less permissive chromatin structure characterized by low H3K27Ac (Cilenti et al., 2021). We anticipate that these synergized regions might share common genomic features, enabling their robust expression upon co-stimulation with PGE_2 and inflammatory signals.

Additionally, the observation that PGE_2-dependent synergistic activity is phenocopied by cAMP is particularly intriguing, as cAMP is a second messenger induced in response to various environmental stimuli, such as acidification of the TME or agonists of the β2-adrenergic receptors or the neuropeptide CGRP (Bohn et al., 2018; Chu et al., 2020). Notably, cAMP intracellular accumulation was found to reduce type I IFN production in LPS-stimulated BMDMs (Cilenti et al., 2021) and to polarize macrophages towards an anti-inflammatory phenotype, that hinders the anti-tumor responses (Bohn et al., 2018; Luan et al., 2015). Consistent with this, inhibiting the *de novo* synthesis of cAMP reduced tumor progression in a melanoma mouse model (Bohn et al., 2018). As a result, it will be important to investigate whether other cAMP-inducing signals can synergize with inflammatory stimuli and shape the inflammatory activation of macrophages.

Furthermore, it is worth exploring whether inhibiting cAMP could effectively reprogram the inflammatory environment and restore anti-tumor immunity in pancreatic cancer.

Next, we set out to investigate the cellular targets of IL-1β-dependent pro-tumor activities. Tumor challenge experiments with IL1R1 KO mice or BM chimeras revealed no differences in tumor growth. Nevertheless, we cannot exclude the possibility of IL-1β playing opposing roles in different cell types. For instance, the production of IL-1β by hyperactivated dendritic cells in draining lymph nodes has been shown instrumental in promoting the generation of antigen-specific $CD8^+$ T cells, the trafficking of cytotoxic T cells in the TME and the tumor eradication (Zhivaki et al., 2020). Additionally, a granular analysis during colorectal carcinogenesis unraveled cell-type specific responses to IL-1β (Dmitrieva-Posocco et al., 2019). While whole-body or hematopoietic-specific ablation of IL1R1 expression had limited effects on CRC progression, selective deletion of IL1R1 in epithelial or T cells was associated with reduced tumor burden. Specifically, abolishing IL-1β signaling in epithelial cells led to reduced tumor cell proliferation, while IL1R1 deletion in T cells resulted in decreased production of inflammatory cytokines that support tumor growth. Intriguingly, selective removal of IL1R1 in neutrophils was linked to an increased presence of intratumor bacteria, which fueled pathogenic inflammation and facilitated tumor progression. Given the complex and contrasting roles of IL-1β, we propose that genetic deletion of *Il1r1* in specific hematopoietic and stromal cell populations should be performed to comprehensively evaluate and dissect the activities of IL-1β in the pancreatic TME.

However, genetic disruption of *Il1r1* in tumor cells, led to a significant reduction in tumor progression. This reduction correlated with a decreased accumulation of IL-$1\beta^+$ monocytes and an increased T-cell activation. Explants of IL1R1 KO tumors showed an impaired ability to form organoids upon *ex vivo* culture, highlighting the critical role of intrinsic IL-1β signaling in tumor cells. Additionally, IL-1β stimulation increased the number of tumor organoids, similar to lung cancer models, where treatment of *EGFR*-mutant lung epithelial cells with IL-1β resulted in the formation of larger organoids (Hill et al., 2023). Indeed, several studies have highlighted the crucial roles of IL-1β in epithelial cells. Prolonged exposure of lung cancer cells to IL-1β promotes chemo-resistance and the transition toward a mesenchymal state, which persists even after the

withdrawal of IL-1β. This transition is associated with the acquisition of an EMT memory-like state driven by epigenetic modifications (Rui Li et al., 2020). Similarly, IL-1β signaling in colorectal cancer cells plays a critical role during the early stages of tumorigenesis, sustaining NF-kB activation and cancer cell proliferation (Dmitrieva-Posocco et al., 2019). Additionally, the IL1-IL1R1 axis is essential for intestinal regeneration by indirectly promoting the proliferation of epithelial progenitors and the maintenance of stem cells (Cox et al., 2021).

Here, we found that IL-1β triggers an inflammatory reprogramming of pancreatic tumor cells, increasing the production of molecules involved in monocyte recruitment – such as CSF1 and CCL2 – or in macrophage polarization – namely, PGE_2 and TNF-α. This establishes a self-sustaining loop between *Il1b*$^+$ TAMs and PDAC cells, hindering its therapeutic targeting in advanced disease stages. Interestingly, a similar interplay between PGE_2 and IL-1β was described also in the lung, where neutrophil-derived IL-1β reinforces the inflammatory phenotype of a subset of *Ptgs2*$^+$ fibroblasts, sustaining metastatic seeding of tumor cells in the lung (Gong et al., 2022). Thus, it is important to investigate whether the PGE_2-IL-1β axis also plays a role in the metastatic dissemination of PDAC.

Spatial analyses of PDAC patients revealed that *IL1B*$^+$ TAMs are not randomly scattered in the tissue. Instead, they localize in specific niches where they closely interact with a subset of PDAC cells expressing the IL-1β response signature (T1RS). Notably, we observed that T1RS$^+$ PDAC cells express genes in common with the *IL1B*$^+$ TAMs transcriptional program, such as *CXCL1* as well as *IL1B* itself, although at low levels. This is in line with a recent study describing distinct spatial niches characterized by a coordinated and harmonized gene expression across different cell types in the TME (Bill et al., 2023). A defined spatial localization was also observed in microarray analyses of pancreatic cancer reporting a population of *IL1B*-expressing macrophages enriched in stromal and cancer regions (Moncada et al., 2020). Similarly, spatial analyses of kidney cancer patients identified a specific subset of *IL1B*$^+$ macrophages situated at the interface between normal and tumor tissues. These macrophages were found in close proximity to a subset of tumor cells that exhibited an enrichment of EMT-related processes (Ruoyan Li et al., 2022). This observation further supports the pivotal role of IL-1β in sustaining

inflammatory reprogramming and promoting tumor malignancy. However, numerous clinical trials targeting IL-1β, or even COX-2 activity, have shown limited therapeutic effectiveness, failing to halt tumor progression or increase patient survival (Garlanda & Mantovani, 2021; D. Wang & DuBois, 2018). Despite these outcomes, our findings support the notion of broadly targeting the PGE_2-IL-1β axis, as it represents a main driver of transcriptional heterogeneity in PDAC and it underlies the acquisition of a pathogenic inflammatory state associated with poor patient survival. Finally, combination therapies targeting the PGE_2-IL-1β axis and ICB should be considered in order to further improve the activation of the adaptive immune system and boost the overall anti-tumor response. On this line, we will perform *in vivo* functional experiments in order to assess the efficacy of different combination approaches within a therapeutic framework. Notably, clinical investigations involve several early phase or on going trials targeting IL-1β activity in PDAC. Among them, the trial NCT02550327 combines anakinra with gemcitabine, nab-paclitaxel, and cisplatin, while a second trial (NCT04581343) combines canakinumab - an IL-1β-targeting antibody - with anti-PD1 antibody, FOLFIRINOX, and nab-paclitaxel.

Inflammatory signaling in epithelial cells can enhance tumorigenesis upon oncogene activation (Alonso-Curbelo et al., 2021; Del Poggetto et al., 2021; Hill et al., 2023; Weeden et al., 2023). We found that pancreatic tissue damage or *Kras* activation alone induce expression of the T1RS in epithelial cells. However, when combined, the expression of this signature is significantly increased, highlighting the cooperation between inflammation and oncogenic mutations. Reanalysis of available datasets has shown that the T1RS is induced at high levels in preneoplastic lesions, both in humans and mice, before rapid cancer growth and the acquisition of malignancy-related programs. On the same line, we identified a subset of macrophages in pancreatitis patients with a transcriptional profile similar to that of $IL1B^+$ TAMs. These findings suggest that the PGE_2-IL-1β axis is readily induced during tissue damage and co-opted by cancer to drive its progression. Notably, constitutive IL-1β expression in the pancreas is linked to the development of chronic pancreatitis, a known risk factor for PDAC. This condition is characterized by atrophy of the pancreas, increased inflammatory infiltration, and fibrosis (Marrache et al., 2008). Therefore, targeting the PGE_2-IL-1β axis in a preventive manner may enhance therapeutic effectiveness. This notion is supported by the recent phase 3

CANTOS trial, where the administration of the anti-IL-1β antibody canakinumab significantly reduced the incidence of lung cancer (Ridker et al., 2017). Similarly, a meta-analysis encompassing multiple trials revealed that the daily intake of aspirin, primarily used for preventing vascular events, decreased the number of deaths due to solid tumors, especially those affecting the gastrointestinal tract, including pancreatic cancer (Rothwell et al., 2011).

In conclusion, mechanistic studies in genetically engineered mouse models of pancreatic cancer will be performed in order to assess the therapeutic potential and the roles of PGE_2 and IL-1β during pancreatic tissue damage and tumorigenesis. At the same time, we plan to conduct spatial transcriptomic analyses on patients diagnosed with IPMN. This aims to reinforce the identification of IL-1β$^+$ TAMs and the expression of the T1RS within preneoplastic lesions and to correlate their abundance with disease progression and the survival rates of patients.

In conclusion, we identified a population of monocyte-derived IL-1β$^+$ TAMs, expressing inflammatory but not cytotoxic programs and locally elicited by the synergistic activity of PGE_2 and TNF-α. Spatial analyses revealed a specific co-localization between *IL1B*$^+$ TAMs and a subset of PDAC cells that acquire an inflammatory phenotype associated with poor patient survival. Blocking PGE_2 or IL-1β reprograms *Il1b*$^+$ TAMs and delays tumor progression. Given the prominent role of the PGE_2-IL-1β axis in sustaining pathogenic inflammation and disease progression in PDAC, its therapeutic targeting may efficiently reshape the pancreatic TME leading to effective anti-tumor responses in the clinic. Finally, it will be of crucial importance to assess the role of such axis in additional tumors.

5. MATERIAL AND METHODS

5.1. Patient samples

Human samples from resected primary PDAC as well as peripheral blood (PB) samples were obtained from the Pancreatic Surgery Unit at the Pancreas Translational and Clinical Center of San Raffaele Hospital (Milan, Italy). The study was compliant with the Declaration of Helsinki and the General Data Protection Regulation and was approved by San Raffaele Hospital ethic committee (protocols: NEU-IPMN and LiMeT). Tissue specimens were confirmed to be tumor or adjacent-normal tissue based on pathologist assessment. Informed consent was obtained by all participants, which received no compensation. Age and sex, as well as anonymized clinical information of participants are reported below:

ID	age	sex	Site of lesion	Chemotherapy schedule	Grading	TNM	Tissue	Down Stream Analysis
PDAC47	78	M	Head	FOLFIRINOX	G2	T2; N2; M0	Tumor Resection (fresh)	scRNA Seq
							Peripheral Blood	scRNA Seq
							Tissue culture, surnatant (NAT and Tumor)	Bioplex: IL-1B
PDAC48	61	M	Head	GEMCITABINA + NAB PACLITAXEL	G2	T2; N2; M0	Tumor Resection (fresh)	scRNA Seq
							Peripheral Blood	scRNA Seq
							Tissue culture, surnatant (NAT and Tumor)	Bioplex: IL-1B
PDAC50	72	M	Uncinated process	NA	G3	T2; N2	Tumor Resection (fresh)	scRNA Seq
							Peripheral Blood	scRNA Seq
							Tissue culture, surnatant (NAT and Tumor)	ELISA: PGE2; Bioplex: TNF
							Tissue Snap Frozen (NAT and Tumor)	Mass Spectrometry PGE2
PDAC51	68	F	Head, Uncinated process	FOLFIRINOX	G2	T2; N2; M0	Tumor Resection (fresh)	scRNA Seq
							Peripheral Blood	scRNA Seq
							Tissue culture, surnatant (NAT and Tumor)	ELISA: PGE2; Bioplex: TNF, IL-1B
PDAC55	62	M	Head	NA	G3	T2; N1	Tumor Resection (fresh)	scRNA Seq
							Peripheral Blood	scRNA Seq
							Tissue culture, surnatant (NAT and Tumor)	ELISA: PGE2; Bioplex: TNF, IL-1B
							Tissue Snap Frozen (NAT and Tumor)	Mass Spectrometry PGE2
PDAC56	83	F	Isthmus	NA	G3	T1c; N0	Tissue culture, surnatant (NAT and Tumor)	ELISA: PGE2; Bioplex: TNF, IL-1B
PDAC57	80	F	Head, Isthmus	NA	G3	T3; N2	Tissue culture, surnatant (NAT and Tumor)	ELISA: PGE2; Bioplex: TNF, IL-1B
PDAC58	48	M	Head, Isthmus	FOLFIRINOX	G2	T2; N1	Tissue culture, surnatant (NAT and Tumor)	ELISA: PGE2; Bioplex: TNF
							Tissue Snap Frozen (NAT and Tumor)	Mass Spectrometry PGE2
PDAC59	65	F	Body, Isthmus	NA	G2	pT1c, pN0	Tissue culture, surnatant (NAT and Tumor)	ELISA: PGE2; Bioplex: TNF, IL-1B
							Tissue Snap Frozen (NAT and Tumor)	Mass Spectrometry PGE2
PDAC60	71	F	Head, Uncinated process	NA	G2	pT1c, pN2	Tumor Resection (fresh)	scRNA Seq
							Peripheral Blood	scRNA Seq
							Tissue culture, surnatant (NAT and Tumor)	ELISA: PGE2; Bioplex: TNF, IL-1B
PDAC61	82	F	Head	NA	G3	pT2, pN2	Tissue culture, surnatant (NAT and Tumor)	ELISA: PGE2
PDAC62	63	F	Head	FOLFIRINOX	NA	NA	Tissue culture, surnatant (NAT and Tumor)	ELISA: PGE2; Bioplex: TNF, IL-1B
PDAC63	79	M	Tail	NA	G3	pT1; M0	Tissue culture, surnatant (NAT and Tumor)	ELISA: PGE2; Bioplex: TNF, IL-1B
							Tissue Snap Frozen (NAT and Tumor)	Mass Spectrometry PGE2
PDAC64	70	F	Body, Tail	PAXG	G3	T3; N1; M0	Tissue culture, surnatant (NAT and Tumor)	ELISA: PGE2; Bioplex: TNF, IL-1B
							Tissue Snap Frozen (NAT and Tumor)	Mass Spectrometry PGE2
PDAC65	50	F	Head	PAXG	G2	T2; N0; M0	Tissue culture, surnatant (NAT and Tumor)	ELISA: PGE2; Bioplex: TNF, IL-1B
							Tissue Snap Frozen (NAT and Tumor)	Mass Spectrometry PGE2
LPDAC15	72	F	Head	GEMCITABINA + NAB PACLITAXEL	G3	T2; N1; M0	Tumor Resection (fresh)	scRNA Seq
LPDAC17	69	M	Head	GEMCITABINA + NAB PACLITAXEL	G2	T3; M2; N0	Tissue culture, surnatant (NAT and Tumor)	ELISA: PGE2
LPDAC21	71	F	Head, Uncinated process	GEMCITABINA + NAB PACLITAXEL	G3	T2; N2; M0	Tissue Snap Frozen (NAT and Tumor)	Mass Spectrometry PGE2
LPDAC23	61	F	Uncinated process	GEMCITABINA + NAB PACLITAXEL	G2	T2; N2; M0	Tissue Snap Frozen (NAT and Tumor)	Mass Spectrometry PGE2
LPDAC25	63	F	Head	GEMCITABINA + NAB PACLITAXEL	G2	T2; N1; M0	Tumor Resection (fresh)	scRNA Seq
LPDAC26	58	M	Body	PAXG	G3	T2; N2; M0	Tumor Resection (fresh)	scRNA Seq
LPDAC27	66	F	Head	PAXG	G3	T2; N2; M0	Tissue culture, surnatant (NAT and Tumor)	ELISA: PGE2
LPDAC30	69	F	Head	NA	G2	T2; N2; M0	Tumor Resection (fresh)	scRNASeq
							Cryopreserved tumor resection	Molecular Cartography
							Tissue Snap Frozen (NAT and Tumor)	Mass Spectrometry PGE2
22LIMET10	66	F	Body, Tail	NA	G2	T2; N0; M0	Cryopreserved tumor resection	Molecular Cartography
21LIMET49	67	F	Head, Uncinated process	NA	G3	T2; N1; M0	Cryopreserved tumor resection	Molecular Cartography
LIMET139	64	F	Head	NA	G3	T2; N1; M0	Cryopreserved tumor resection	Molecular Cartography
							Formalin-fixed, paraffin-embedded tumor resection	IHC staining
22LIMET162	62	M	Head	FOLFIRINOX	G2	T1a; N0; M0	Cryopreserved tumor resection	Molecular Cartography
21LIMET163	77	F	Head	NA	G2	T2; N2; M0	Cryopreserved tumor resection	Molecular Cartography
22LIMET165	82	F	Tail	NA	G1	T1c; N0; M0	Cryopreserved tumor resection	Molecular Cartography
21LIMET325	56	M	Head, Uncinated process	NA	NA	NA	Cryopreserved tumor resection	Molecular Cartography

5.2. Mouse PDAC

KC (DT6606) and KPC (K8484; 5M7101; K4651; Ximbio) cell lines were previously established from tumors arising in genetically engineered mouse models carrying the G12D oncogenic mutation in the *Kras* gene ($Kras^{LSL\text{-}G12D/+}$;$Pdx1^{Cre/WT}$ for KC) and the

missense point R720H mutation in the *Tpr53* gene (*Kras*$^{LSL\text{-}G12D/+}$;*Tpr53*$^{LSL\text{-}R270H/+}$;*Pdx1*$^{Cre/WT}$ for KPC) (Hingorani et al., 2003, 2005). Panc02 cell line is derived from a methylcholanthrene-induced pancreatic ductal adenocarcinoma (Corbett et al., 1984). DT6606, K8484 and Panc02 cell lines were kindly provided by Piemonti Lorenzo; 5M7101 and K4651 were kindly provided by Mondino Anna; KPC-Ximbio were purchased from Ximbio. All the cell lines were cultured under standard conditions, and periodically tested for mycoplasma.

5.3. CRISPR-Cas9-mediated gene targeting

Single guide RNAs (sgRNAs) were designed using CHOPCHOP (Labun et al., 2019) and synthetized by *in vitro* transcription using GeneArt™ Precision gRNA Synthesis Kit (Invitrogen), following manufacturer's instructions. Ribonucleoprotein complexes (RNPs: Cas9-sgRNA) were generated by incubating 12µg of sgRNA with 5µg of Cas9 for 15 min at RT. KPC (K8484), KC (DT6606) or Panc02 cells (2.5 x 10^4) were resuspended in SF solution of SF Cell Line 4D Nucleofector™ X Kit S, mixed with RNPs and electroporated using EP-100 program of the 4D-Nucleofector System (Lonza). Three days after nucleofection, single clones were FACS-sorted in 96 well plates. Single cell clones were screened to evaluate Non-Homologous End Joining (NHEJ) efficiency on the targeted site with T7 endonuclease assay. Briefly, genomic DNA was extracted using QuickExtract™ DNA Extraction Solution and targeted regions were amplified by PCR. PCR products were purified with Ampure XP beads and quantified by Nanodrop 8000. Purified PCR products were mixed 1:1 with corresponding products from wild-type cells. Annealed PCR products (400 ng) were digested with T7 Endonuclease for 30 min at 37°C and subjected to capillary electrophoresis using D1000 TapeStation kit (Agilent 4200 TapeStation). NHEJ efficiency was defined by calculating the percentage of PCR product cleavage. Gene-edited clones were validated by Sanger Sequencing using PCR products encompassing the target sequence. Polyclonal KO pools were generated mixing an equal amount of at least 5 validated clones. The absence of the targeted protein was further validated by western-blot analyses. A complete list of sgRNAs and primer pairs used for the NHEJ assay is reported below:

Oligonucleotides	Sequence	Assay
sgRNA_Ptgs2_FW	TTGGGCAGTCATCTGCTACG	Gene editing
sgRNA_Ptgs2_RV	CGTAGCAGATGACTGCCCAA	Gene editing
NHEJ_Ptgs2_FW	CTAGGGTTTGGGTCAGAAGAGA	Non-Homologous End Joining assay
NHEJ_Ptgs2_RV	TTCTAGGTACACACCCAAGCCT	Non-Homologous End Joining assay

Oligonucleotides	Sequence	Assay
sgRNA_IL1R1_FW	CTTCGATCGTCTCATTCCGA	Gene editing
sgRNA_IL1R1_RV	TCGGAATGAGACGATCGAAG	Gene editing
NHEJ_IL1R1_FW	CTCCTGCTGTACTTGAGGGACT	Non-Homologous End Joining assay
NHEJ_IL1R1_RV	TGATCCGTACATGACAGAAAGG	Non-Homologous End Joining assay

5.4. *In vivo* animal studies

All experiments and procedures were performed according to protocols approved by the Institutional Animal Care and Use Committee (IACUC) at San Raffaele Scientific Institute animal facilities and authorized by the Italian Ministry of Health in accordance with the Italian Laws (D.L.vo 116/92), which enforce the EU 86/609 Directive (approval number #449/2018-PR; #962/2020-PR and #908/2021-PR). C57BL/6N mice were purchased from Charles River Italy; IFNAR KO and CCR2 KO mice were obtained from Matteo Iannacone (IRCCS San Raffaele Scientific Institute, Milan, Italy); NLRP3 KO mice were kindly provided by Alessandra Mortellaro (IRCCS San Raffaele Scientific Institute, Milan, Italy); IL1R1 KO mice were kindly provided by Cecilia Garlanda (Humanitas Research Hospital, Milan, Italy). All animals were maintained under pathogen-free conditions at the animal facility of San Raffaele Scientific Institute with a 12h/12h dark/light cycle and standardized temperature (22 +/- 2°C) and humidity (55 +/- 5%). *Ms4a3*^{Cre}-*Rosa*^{TdT} mice were maintained under pathogen-free conditions at Institute Gustave Roussy. Pancreatic tissue samples from genetically engineered mouse models of PDAC (*Kras*$^{LSL\text{-}G12D/+}$;*Tpr53*$^{LSL\text{-}R270H/+}$;*Pdx1*$^{Cre/WT}$) were kindly provided by Francesco Novelli (Department of Molecular Biotechnology and Health Sciences, University of Turin, Turin, Italy). No statistical method was used to predetermine sample size. Sample sizes were estimated based on preliminary experiments. Mice were allocated randomly to the experimental groups. Blinding was used to measure tumor growth curves, both when using digital caliper and ultrasound analyses.

5.5. Orthotopic tumors

To establish orthotopic models, 6- to 9-weeks old female mice (for K8484) or male mice (for DT6606) were anesthetized with isoflurane and subjected to surgical procedure. After left abdominal incision, pancreatic tails were exposed and injected with 5 x 10^5 tumor cells resuspended in cold PBS mixed at 1:4 dilution with Matrigel (Corning) in a final volume of 50µL. Mice were monitored with ultrasound imaging to measure tumor progression. Experiments were terminated when tumors reached a size of 1,000 mm^3, as per IACUC limit.

5.6. Heterotopic tumors

To establish heterotopic tumors, a total of 2 x 10^6 cancer cells were resuspended in 200uL of endotoxin-free PBS and injected subcutaneously in the right flank of female (K8484, 5M7101 and Ximbio) or male (DT6606, K4651, Panc 02) mice. Tumor growth was monitored using a digital caliper. Tumor volume was estimated assuming ellipsoidal shape as $(a \bullet b)^2 \bullet \pi/6$, where a=major diameter while b=minor diameter. Experiments were terminated when tumors reached a size of 1,000 mm^3, as per IACUC limit.

5.7. *In vivo* treatments

The COX2 inhibitor, Celecoxib, was prepared at a concentration of 2 mg/mL in a solution of 10% DMSO, 50% Poly(ethylene glycol) - Average Mn 400 (PEG400) (Sigma) - and 40% Cell Culture Grade Water (Corning) and 200 µL (400µg/mouse) were administered daily through oral gavage (Pelly et al., 2021). For IL-1β neutralization, mice were intraperitoneally injected with 50µg/mouse of anti-IL-1β monoclonal antibody (Clone B122, InVivoMAb, BioXCell) or isotype control (Polyclonal Armenian Hamster IgG, InVivoMAb, BioXCell) on the day of tumor inoculation and on day 1 post inoculation (p.i.). Starting from day 4 p.i., mice were injected three times a week for the entire duration of the experiment. $CD8^+$ T cells depletion was achieved by injecting mice intraperitoneally with 300 µg/mouse of anti-mouse CD8α (Clone 2.43, BioXCell) antibody or isotype control (Clone LTF-2, BioXCell) two days before tumor injection. Starting from day 4 p.i., mice were treated twice a week with 200 µg/mouse of antibody or isotype control for the entire duration of the experiment. Depletion of $CD8^+$ T cells

was confirmed by FACS analysis on blood and tumor samples. NK cells depletion was achieved by injecting the mice with a combination of 200 μg/mouse of anti-mouse NK1.1 (clone PK136, BioXCell) and 50 μL/mouse of anti-ASIALO GM-1 (clone Poly21460, BioLegend) or isotype control (clone C1.18.4, BioXCell) one day before and one day after tumor inoculation. Starting from day 4 p.i., mice were injected twice a week for the entire duration of the experiment. Depletion of NK cells was confirmed by FACS analysis on blood and tumor samples. For CSF-1 neutralization, mice were intraperitoneally injected with 1mg/mouse of anti-mouse CSF1 monoclonal antibody (Clone 5A1, BioXCell) or isotype control (clone HRPN, BioXCell) 3 days before tumor inoculation. Starting from day 1 p.i., mice were injected with 500 μg/mouse every 5 days. Depletion of monocytes was assessed by FACS analysis on blood and tumor samples.

5.8. Bone Marrow (BM) chimeras.

Recipient mice were lethally irradiated with two doses of radiations for a total of 935 cGy. The following day, irradiated mice were transplanted with 5 x 10^6 total BM cells by intravenous injections. BM chimerism was checked by measuring the percentage of CD45.1/CD45.2 cells in blood samples by flow cytometry 4- and 10-weeks post transplantation. BM chimeras were inoculated with K8484 cells 12-weeks post transplantation.

5.9. Tissue processing

Human and murine PB samples were incubated with Red Blood Cell (RBC) lysis buffer (Biolegend) for 10 min on ice and washed with Phosphate Buffered Saline (PBS). Cells were centrifuged for 5 min at 450 x g and resuspended in the appropriate buffer for down-stream application. Freshly resected human PDAC samples were minced in small pieces and digested with the Tumor Dissociation kit, human (Miltenyi Biotec). Similarly, murine healthy pancreas and tumors were manually minced in small pieces and dissociated with the Tumor Dissociation kit, mouse (Miltenyi Biotec) following manufacturer's instructions. Healthy lungs were perfused with PBS and then collected, minced in small pieces, resuspended in Liberase (Roche) and then dissociated with the gentleMACS Octo Dissociator. Spleens and bone marrows were collected and manually smashed or crushed, respectively. The obtained single cells suspensions were filtered on

70µm cell strainers, incubated with RBC lysis buffer for 10 min on ice and resuspended in the appropriate buffer for cell counting and down-stream application. In selected experiments, murine tumor-draining lymph nodes were smashed, filtered through a 70µm cell strainers, and resuspended in the appropriate buffer for down-stream application. For the collection of plasma samples, an aliquot of 300 µl of blood collected into EDTA tubes was centrifuged 5 min at 10,000 x g. Plasma was transferred into a clean tube and re-centrifuged 5 min at 10,000 x g. Plasma samples were frozen and stored at −80 °C until use. Supernatants of human PDAC and normal adjacent tissues were generated by culturing weighted tissues (1 to 30mg) in 1mL of complete media in a 48 well-plate. After 48 hours, supernatants were collected, centrifuged for 5 min at 450 x g to remove cellular debris and stored at -80°C until use. For mass-spectrometry experiments, tissue samples were chopped, weighted and immediately snap-frozen at -80°C.

5.10. Culture of mouse monocytes and macrophages

Bone marrow cells were collected by crushing the hips, femurs, and tibias of female mice in 50 mL of sterile PBS, filtered through a 70µm cell strainer, and centrifuged for 5 min at 450 x g. Red blood cells were lysed using 0,2% NaCl solution, followed by 1,6% NaCl solution. BM cells were filtered through a 70µm cell strainers and centrifuged for 5 min at 450 x g. For BMDM differentiation, cells were counted and seeded in IMDM supplemented with 20% FBS, 20% L929-conditioned media containing M-CSF, antibiotics (penicillin G 100 U/ml and streptomycin sulfate 100 U/ml), 2 mM L-glutamine and 5 µM 2-mercaptoethanol. Four days after culture, fresh medium was added to the cells. At day 7 after plating, cells were stimulated as described below. Monocytes were isolated from total BM cells using the mouse Monocyte Isolation Kit (BM, Miltenyi Biotec), following manufacturer's instructions. At the end of the isolation procedure, cells were > 90-95% $CD11b^{+}Ly6G^{-}Ly6C^{+}$ as assessed by flow cytometry. Monocytes were counted and seeded in U-bottom 96 well-plates at a density of 1 x 10^5 cells/well in RPMI supplemented with 10% FBS, antibiotics (penicillin G 100 U/ml and streptomycin sulfate 100 U/ml) and 2 mM L-glutamine. One hour after plating, monocytes were stimulated as described below.

5.11. *Ex vivo* stimulation of mouse cells

Cells were stimulated with LPS (10ng/mL), TNF-α (10 ng/mL), PGE_2 (1μM), IL-1β (10 ng/mL), Forskolin (50 μM, 30 minutes of pre-treatment), db-cAMP (50 μM, 30 minutes of pre-treatment). For stimulation with Tumor Conditioned Medium (TCM), KPC (K8484) cells were stimulated or not for 24 hours with either IL-1β (10 ng/mL), Cox2-inhibitor SC-236 (Cayman Chemical) (10μM), or their combination. At the end of the stimulation, TCM were collected, centrifuged for 5 min at 450 x g to remove cellular debris, filtered through 0,22μm strainer and stored at -80°C. Before BMDMs stimulation, thawed TCM were incubated at 37°C for 30 min with anti-TNF-α antibody (25μg/mL; Clone XT3.11, InVivoMAb, BioXCell) or isotype control rat IgG1 anti-horseradish peroxidase (25μg/mL; Clone HRPN, InVivoMAb, BioXCell). To rule out any carryover effect of Cox2-inhibitor, fresh SC-236 (10μM) was added to the TCM before stimulating BMDMs.

5.12. Generation and culture of mouse PDAC spheroids

For the establishment of mouse pancreatic tumor spheroid culture, 1 x 10^4 WT and COX2-KO KPC (K8484) cells were resuspended in 50 μL Matrigel, plated in 4-well culture plates (Nunc) and grew in Mouse Complete Medium (Advanced DMEM/F12) supplemented with 10 mM HEPES, antibiotics (penicillin G 100 U/ml and streptomycin sulfate 100 U/ml), 1% GlutaMax, B-27 Supplement, 10 mM Nicotinamide, 1.25 mM N–Acetylcysteine, 10 ng/mL recombinant human R–Spondin1, 100 ng/mL recombinant human FGF10, 100 ng/mL recombinant human Noggin, 500nM A83–01, 50 ng/mL recombinant human EGF, 10 nM Gastrin1, and 10.5 μM Y–27632). Spheroid cultures were split at confluence by dissolving Matrigel in cold Splitting Medium (Advanced DMEM/F12 supplemented with 10mM Hepes, 1% GlutaMAX and antibiotics (penicillin G 100 U/ml and streptomycin sulfate 100 U/ml)). Spheroids were then mechanically disrupted with a 21 Gauge needle syringe, centrifuged for 5 min at 300G, and washed with Splitting Medium. After a second centrifugation, dissociated spheroids were resuspended in Matrigel and spotted as domes (50 μL/dome) in 4-well culture plates with Mouse Complete Medium. For orthotopic injections, WT and COX2-KO K8484-derived spheroids were collected after 6 passages in cold Splitting Medium and centrifuged at 300G for 5 min at 8°C. Spheroids were then mechanically dissociated, centrifuged at

300G for 5 min, and resuspended in a solution of 25% Matrigel in PBS. Dissociated spheroids (1 x 10^6 cells in 50 µL) were injected orthotopically in immune-competent mice as described above.

5.13. Generation and culture of mouse PDAC organoids

Murine PDAC organoids from IL1R1 WT or IL1R1 KO KPC (K8484) cells were generated according to previously published protocol (Baker & Tuveson, 2019). Briefly, IL1R1 WT or IL1R1 KO KPC cells were subcutaneously injected into C57BL/6N mice as described above. 11 days p.i., tumors were explanted and manually minced into 1-2 mm^3 pieces in Splitting Medium, incubated for 1-2 hours at 37°C in pre-warmed Digestion Solution (Splitting Medium supplemented with 0.125 mg/mL Collagenase type I, 0.125 mg/mL Dispase II and 0.1 mg/mL DNase I), and further mechanically dissociated by vigorously pipetting. Dissociated samples were then filtered through a 70 µm Cell Strainer and washed with cold Wash Medium (DMEM high glucose supplemented with 1% FBS and antibiotics (penicillin G 100 U/ml and streptomycin sulfate 100 U/ml)). Cells were pelleted at 300G for 5 min at 8°C and washed twice with Wash Medium. Finally, tumor cells were resuspended in cold Matrigel, plated into 50 µL dome/well. After Matrigel solidification, 500µL of warm Mouse Complete Medium supplemented with 10.5 µM Rock Inhibitor were added to each well.

5.14. *In vitro* stimulation of murine PDAC organoids

Four domes of organoids (passage 3) obtained from either IL1R1 WT (n=4) or IL1R1 KO (n=4) tumors were incubated in Dispase solution (Splitting Medium supplemented with 2mg/mL Dispase II) for 20 min at 37°C, to allow matrix dissociation. Matrix-free organoids were centrifuged at 300 x g for 5 min at 8°C, and dissociated by incubation with TrypLE digestion enzyme at 37°C for 10 min, followed by addition of Dispase Solution supplemented with 0.1 mg/mL DNase I for 10 min. Cells were counted and seeded at 5 x 10^3 single cells/well in 4 wells of 8-Well Glass Bottom µ-Slides (Ibidi) in a final volume of 100 µL Matrigel/well. Cultures were maintained in Mouse Complete Medium supplemented with 10.5 µM Rock Inhibitor and stimulated with 10 ng/mL IL-1β where indicated, replacing the medium and the stimulus every 72 hours for a total of five days.

5.15. Analysis of organoid-forming efficiency

For freshly prepared organoids, the forming efficiency was assessed after 6 days of culture. Each tumor (n=4/group) was plated in 8 domes, and for each dome four different brightfield images were captured to allow the counting of live organoids. Then, the mean number of organoids per field, normalized for the volume of the tumor of origin, was calculated.

For organoids stimulated with IL-1β, samples were fixed for 20 min in 4% PFA at 37°C and processed for immunofluorescence analysis. Briefly, after fixation, organoid cultures were permeabilized with PBS + 0.5% Triton X-100 at 37°C for 30 min and then incubated in blocking buffer (PBS + 5% BSA + 10% Donkey Serum (Jackson Immunoresearch) + 0.5% Triton X-100) at 37°C for 30 min. Samples were then incubated with Alexa Fluor™ 488 Phalloidin (Invitrogen A12379, 1:200) in 1% BSA for 3 hours at room temperature. Nuclei were counterstained with DAPI for 10 min at room temperature. Samples were imaged on an Olympus FluoVIEW 3000 RS confocal laser scanning system using UPLXAPO 4X/0.16 objective, by acquiring 3 x 3 grids and optical sections of 33µm each (1,95AU) were collected for each well to cover the entire Matrigel area.

Data processing. Image segmentation was performed using the Machine Learning Tool of the Arivis Vision 4D software (ZeissAG) using annotated regions of interest as training input. Identified image objects were filtered by sphericity (> 0.6) and volume (> 10^3 μm^3). The volume and the number of organoids for each well were calculated and exported for statistical analyses. The same parameters for organoid identification were applied to all the imaged samples.

5.16. *In vitro* stimulation of tumor cells and organoids with IL-1β for gene expression analysis.

KC (DT6606), KPC (K8484) cell lines (2D) and KPC-derived organoids (3D) were cultured as described above and stimulated with IL-1β to the final concentration of 10ng/mL for the indicated time points or left untreated. At the end of the stimulation, KPC organoids were dissolved in cold Cell Recovery Solution (Gibco) at 4°C for 20 min in agitation, centrifuged at 400g for 5 min at 4°C, and resuspended in Lysis buffer (ReliaPrep RNA Cell Miniprep System, Promega). Bulk and scRNA-Seq were performed as described below.

5.17. Lentiviral transduction of KPC cells

Il1r1 cDNA was synthetized and cloned in the pCCLsin.PPT.hPGK.GFP.wpre plasmid by GenScript DNA Synthesis service. Lentiviral vectors (LV) were produced, concentrated and titrated as previously described (Milani et al., 2017). For KPC (K8484) transduction, single IL1R1 KO clones (2 x 10^5 cells) were transduced with a multiplicity of infection (MOI) of 10. Two weeks after transduction, IL1R1$^+$ cells were sorted (FACSAria instrument; BD Biosciences) and expanded *in vitro* for tumor inoculation. Polyclonal IL1R1-reconstituted pools were generated mixing an equal amount of 5 validated clones. The presence of the targeted protein was further validated by western-blot analyses.

5.18. Flow cytometry

If not differently stated, single cell suspensions were incubated with anti-mouse FcgIII/II receptor (CD16/CD32) blocking antibody for 10 min on ice and pelleted by centrifugation. Cell viability was assessed by Aqua Live/Dead staining, applied for 30 min at 4°C. Surface staining was then performed with fluorophore-conjugated primary antibodies for 30 min at 4°C. For intracellular staining, samples were fixed with IC Fixation Buffer (Biolegend) and permeabilized with Intracellular Staining Perm Wash Buffer 10X (Biolegend) according to manufacturer's instructions. For detection of active caspase 1, FLICA staining was performed as first step according to manufacturer's instructions. Briefly, a 30X working solution was prepared and added to the samples for 30 min at 37°C; after two washes, samples were fixed and then stained as described above. For detection of intracellular IFN-γ and TNF-α, tumor-draining lymph nodes were processed as described above. Single cell suspensions were incubated in a 96 well-plate with Cell Activation Cocktail with Brefeldin A (Biolegend) for 3 hours at 37°C, and then stained as described above. To assess cell apoptosis and viability, KC (DT6606) and KPC (K8484) cells (WT and COX-2 KO) were washed with cold PBS and resuspended in AnnexinV binding buffer (PE AnnexinV Apoptosis Detection kit, Biolegend). Cells were stained following manufacturer's instructions. For the quantification of the intracellular IL-1β in monocytes, total BM cells were seeded in a 48 well-plate at a density of 2 x 10^6 cells/well in IMDM supplemented with 10% FBS, antibiotics (penicillin G 100 U/mL and streptomycin sulfate 100 U/mL) and 2 mM L-glutamine and stimulated as indicated. After

stimulation, samples were processed for flow cytometry analysis as reported. After exclusion of doublets and dead cells, monocytes were gated as $CD11b^+$ $Ly6G^-$ $Ly6C^+$. Absolute cell count was performed using Precision Count Beads™ (Biolegend), following manufacturer's instructions. All samples were acquired on BD FACSymphony and FACSCanto II using DIVA software v.8.0.2 (BD Biosciences). Data were analyzed with FlowJo Software (v. 10.8.1). A complete list of antibodies is reported below:

Rat anti-mouse Arginase 1 Monoclonal Antibody (A1exF5), PE-Cyanine7; eBioscience, Thermo Fischer Scientific; Cat# 25-3697-82; 1:300
Hamster anti-mouse CD3e Monoclonal Antibody (145-2C11), BV650; BD Bioscience; Cat# 564378; 1:100
Hamster anti-mouse CD3e Monoclonal Antibody (145-1C11), APC; BioLegend; Cat# 100312; 1:100
Rat anti-mouse CD4 Monoclonal Antibody (GK1.5), PE-Cyanine7; eBioscience, Thermo Fischer Scientific; Cat# 25-0041-82; 1:300
Rat anti-mouse CD8a Monoclonal Antibody (53-6.7), FITC; BD Bioscience; Cat# 553030; 1:200
Rat anti-mouse CD8a Monoclonal Antibody (53-6.7), BV711; BD Bioscience; Ca# 563046; 1:100
Rat anti mouse CD11b Monoclonal Antibody (M1/70), BUV737; BD Bioscience; Cat# 612801; 1:200
Rat anti mouse CD11b Monoclonal Antibody (M1/70), APC; BioLegend; Cat# 101212; 1:200
Hamster anti-mouse CD11c Monoclonal Antibody (N418), PE-Cyanine7; eBioscience, Thermo Fischer Scientific; Cat# 25-0114-82; 1:200
Hamster anti-mouse CD11c Monoclonal Antibody (N418), BUV395; BD Bioscience; Cat# 744180; 1:200
Rat anti mouse CD16/CD32 Monoclonal Antibody (93), TruStain FcX; BioLegend; Cat# 101320; 1:100
Rat anti-mouse CD19 Monoclonal Antibody (6D5), FITC; BioLegend; Cat# 115505; 1:200
Rat anti-mouse CD19 Monoclonal Antibody (6D5), PE; BioLegend; Cat# 115508; 1:200

Rat anti-mouse CD45 Monoclonal Antibody (30-F11), FITC; BD Bioscience; Cat# 553079; 1:200

Rat anti-mouse CD45 Monoclonal Antibody (30-F11), PerCP-Cyanine5.5; eBioscience, Thermo Fischer Scientific; Cat# 45-0451-80; 1:200

Rat anti-mouse CD45 Monoclonal Antibody (30-F11), BUV395; BD Bioscience; Cat# 564279; 1:100

Mouse anti-mouse CD45.1 Monoclonal Antibody (A20), BV650; BioLegend; Cat# 110735; 1:100

Mouse anti-mouse CD45.2 Monoclonal Antibody (104), BV786; BD Bioscience; Cat# 563686; 1:100

Mouse anti-mouse CD45.2 Monoclonal Antibody (104), BUV737; BD Bioscience; Cat# 612778; 1:100

Mouse anti-mouse CD64 Monoclonal Antibody (X54-5/7.1), BV650; BD Bioscience; Cat# 740622; 1:100

Hamster anti-mouse CD80 Monoclonal Antibody (16-10A1), APC/Fire 750; BioLegend; Cat# 104740; 1:100

Rat anti-mouse CD86 Monoclonal Antibody (GL1), PE; eBioscience, Thermo Fischer Scientific; Cat# 12-0862-82; 1:100

Rat anti-mouse CD115 (CSF-1R) Monoclonal Antibody (AFS98), PE/Dazzle 594; BioLegend; Cat# 135528; 1:100

Rat anti-mouse CD206 (MMR) Monoclonal Antibody (C068C2), Alexa Fluor 647; BioLegend; Cat# 141712; 1:200

Rat anti-mouse CD273 (PDL2) Monoclonal Antibody (122), PerCP-eFluor710; eBioscience, Thermo Fischer Scientific; Cat# 46-9972-82; 1:100

Rat anti-mouse CD274 (PDL1) Monoclonal Antibody (MIH5), PE-CF594; BD Bioscience; Cat# 567032; 1:100

Rat anti-mouse F4/80 Monoclonal Antibody (BM8), APC; eBioscience, Thermo Fischer Scientific; Cat# 17480182; 1:50

Rat anti-mouse F4/80 Monoclonal Antibody (BM8), PE; eBioscience, Thermo Fischer Scientific; Cat# 12480182; 1:50

Rat anti-mouse I-A/I-E (MHCII) Monoclonal Antibody (M5/114.15.2), BV785; BioLegend; Cat# 107645; 1:400

Mouse anti-human Granzyme B Monoclonal Antibody (GB12), PE; Thermo Fischer Scientific; Cat# MHGB04; 1:50

Rat anti-mouse IFNg Monoclonal Antibody (XMG1.2), BV711; BioLegend; Cat# 505836; 1:100

Rat anti-mouse IL1b (Pro-Form) Monoclonal Antibody (NJTEN3), eFluor450; eBioscience, Thermo Fischer Scientific; Cat# 48-7114-82; 1:100

Rat IgG1 kappa Isotype Control (eBRG1), eFluor450; eBioscience, Thermo Fischer Scientific; Cat# 48-4301-82; 1:100

Rat anti-mouse Ly6C Monoclonal Antibody (HK1.4), BV711; BioLegend; Cat# 128037; 1:500

Rat anti-mouse Ly6C Monoclonal Antibody (HK1.4), APC-eFluor 780; BioLegend; Cat# 47-5932-82; 1:200

Rat anti-mouse Ly6G Monoclonal Antibody (1A8), FITC; BD Bioscience; Cat# 561105; 1:200

Rat anti-mouse Ly6G Monoclonal Antibody (1A8), APC-Cyanine7; BioLegend; Cat# 127624; 1:200

Mouse anti-mouse NK1.1 Monoclonal Antibody (PK136), BV785; BioLegend; Cat# 108749; 1:100

Mouse anti-mouse NK1.1 Monoclonal Antibody (PK136), BUV395; BD Bioscience; Cat# 564144; 1:100

Rat anti-mouse Siglec-F Monoclonal Antibody (E50-2440), PerCP-Cyanine5.5; BD Bioscience; Cat# 565526; 1:100

Rat anti-mouse TNFa Monoclonal Antibody (MP6-XT22), PE; BioLegend; Cat# 506306; 1:100

Mouse anti-human CD45 Monoclonal Antibody (HI30), PE; BioLegend; Cat# 304008; 1:200

Mouse anti-human CD19 Monoclonal Antibody (HIB19), BV510; BioLegend; Cat# 302242; 1:50

Mouse anti-human CD3 Monoclonal Antibody (OKT3), BV510; BioLegend; Cat# 317332; 1:100

5.19. Cell proliferation assay

KC (DT6606) or KPC (K8484) cells were seeded in a 96 well-plate at a density of 1 x 10^4 cells/well in technical triplicate. After 4, 24, 48, and 72 hours of culture, 10µL/well of WST-1 reagent (Abcam) was added and cells were incubated for 30 min in standard culture conditions. After incubation, OD values (450nm) were acquired at Multiskan GO Microplate Spectrophotometer (Thermo Scientific) and proliferation was calculated as fold-change over the 4 hours.

5.20. RT-qPCR

Total RNA was extracted using the ReliaPrep RNA Cell Miniprep System (Promega) and quantified with NanoDrop 8000. Single-stranded cDNA was synthesized using ImProm-II Reverse Transcription System (Promega) starting from 400-500 ng total RNA. For monocytes isolated from total BM, cDNA was synthesized using SuperScript II (Thermo Scientific), amplified via PCR with KAPA HiFi HotStart (Roche) and purified with AMPure XP beads (Thermo Scientific). Sample concentration was assessed by Qubit 3.0 and size distribution by an Agilent 4200 Tapestation system. Amplification of target genes was performed with Fast SYBR Master Mix on a ViiA7 Real-Time PCR System. A complete list of primer pairs used is reported below:

Oligonucleotides	Sequence	Assay
mouse_Il1b_FW	GACCTTCCAGGATGAGGACA	qRT-PCR
mouse_Il1b_RV	TCCATTGAGGTGGAGAGCTT	qRT-PCR
mouse_Ptgs2_FW	CCACTTCAAGGGAGTCTGGA	qRT-PCR
mouse_Ptgs2_RV	AGTCATCTGCTACGGGAGGA	qRT-PCR
mouse_Il6_FW	CCATAGCTACCTGGAGTACATG	qRT-PCR
mouse_Il6_RV	TGGAAATTGGGGTAGGAAGGAC	qRT-PCR
mouse_Il10_FW	CCAAGCCTTATCGGAAATGA	qRT-PCR
mouse_Il10_RV	TCACTCTTCACCTGCTCCAC	qRT-PCR

5.21. Analyses of cell culture supernatant

Murine BMDMs, BM monocytes and tumor cells were stimulated as indicated. For quantification of IL-1β, murine BMDMs and BM monocytes were stimulated for 4hrs as indicated and ATP (5mM) was added for the last 30 min of stimulation. Supernatants

were collected and centrifuged to remove cellular debris. IL-1β (Mouse IL-1 beta Uncoated ELISA, Invitrogen) and M-CSF (DuoSet ELISA Mouse M-CSF; R&D) were measured following manufacturer's instructions. Absorbance was measured on a Multiskan GO Microplate Spectrophotometer. Other human and murine cytokines were measured using Bio-Plex Pro™ Mouse Chemokine 31-Plex Assays (Bio-Rad) and Bio-Plex Pro Human Cytokine Screening Panel, 48-Plex (Bio-Rad), according to the manufacturer's indications. Acquisition was performed using Luminex instruments and analyzed with Bio-plex manager (Bio-Rad) software.

PGE_2 levels were quantified either in the supernatants of human tissue samples, obtained as described above, or in the supernatants of KC (DT6606), KPC (K8484, 5M7101, K4651, Ximbio) and Panc02 cell lines. PDAC cells were seeded at 1 x 10^6 cells per 10 cm dish and cultured for 24-48 hours in 6 mL of complete medium. Supernatants were collected and centrifuged to remove cellular debris. PGE_2 (Prostaglandin E_2 Express ELISA kit, Cayman Chemical) was measured following manufacturer's instructions. Absorbance was measured on a Multiskan GO Microplate Spectrophotometer. When indicated, PGE_2 levels were normalized on tissue weight.

5.22. Extraction of prostaglandins (PGs) by SPE (C-18) purification

PGs were extracted as previously described with minor modifications (Golovko & Murphy, 2008). Briefly, 35 mg of tissue was homogenized in 3 ml of 15% methanol in water at pH 3 (containing formic acid 0.04%) containing PGE_2-d4 and PGD_2-d4 (40 ng each) as internal standards and 0.005% BHT to prevent PGs oxidation, using an electric pestle. The homogenate was then vortexed for 5 min and subjected to 10 min of centrifugation (2,000 x g) at 4°C to remove the precipitated proteins. The supernatant was loaded onto an OASIS HLB prime vac Cartridge (3cc) and allowed to completely enter the packing material. The cartridge was washed with 3 ml 15% methanol and 3 ml water. The PGs were eluted from the cartridge with 3 ml ethyl acetate containing 1% methanol. The eluted samples were dried under nitrogen and resuspended with 50 µl acetonitrile/water (1:2) and stored at -20 °C until LC-MS/MS analysis. For PGE_2 and PGD_2 absolute quantification, calibration curves were prepared by spiking increasing amount of PGA1 (from 0.0625 ng to 625 ng) in the same sample matrix (murine or human control sample). The calibration curve point samples were then processed as described

above, including the addition of PGE_2-d4 and PGD_2-d4 (40 ng each) for the extraction yield correction.

5.23. Chromatographic separation of PGE2 and PGD2 and their LC-MS/MS detection

Samples were directly analysed using the UPLC 1290 (Agilent Technologies) coupled to the TripleTOF 5600+ mass spectrometer (SCIEX) (ProMeFa, Proteomics and Metabolomics Facility, Ospedale San Raffaele, Milan, Italy). Chromatographic separations occurred on C18 column (ACQUITY UPLC HSS T3 Column, Waters, 1.8 µm, 2.1 mm x 100 mm) by directly injecting 10 µl of samples (1/5 of the original sample). Metabolites were separated using a flow rate set at 0.4 ml/min and a gradient of solvent A (water, 0.1% formic acid) and solvent B (acetonitrile, 0.1% formic acid). The gradient, in negative mode, started from 25% B hold for 2 min; increased up to 40 % B in 16 min; increased again up to 90% in 1 min; maintained constant at 90% B for 4 min; decreased to 25% B in 1 min and maintained at 25% for 2 min. The column was set at 50°C while the samples were kept at 4°C. Full scan spectra were acquired in the mass range from *m*/*z* 50 to 500. Automated calibration was performed using an external calibrant delivery system (CDS) which infuses APCI negative calibration solution every 5 samples injection. A product ion experiment mode was used to monitor PGE_2 and PGD_2 mass (at 351.2 m/z) as well as internal standards PGE_2-d4 and PGD_2-d4 (355.4 m/z). PGA1 at 335.4 m/z was followed for the calibration curves. The source parameters were: Gas 1: 33 psi, Gas 2: 58 psi, Curtain gas: 25 psi, Temperature: 500 °C and ISVF (IonSpray Voltage Floating): -4500 V, DP: -80 V, CE: 44 V.

5.24. Western Blot analyses

Cells were lysed in a radioimmunoprecipitation assay (RIPA) lysis buffer, containing 10 mM Tris-HCl pH 8, 1 mM EDTA pH 8, 140 mM NaCl, 1% Triton X-100, 0.1% SDS, 0.1% deoxycholate and protease/phosphatase inhibitors. Protein concentrations were measured with the Pierce™ BCA Protein Assay Kit. Lysates were then electrophoresed on Tris-glycine sodium dodecyl sulfate/polyacrylamide gel electrophoresis (SDS/PAGE) gels and transferred on Nitrocellulose membranes (Amersham™ Protran™ Premium 0.45 µm NC). Membranes were blocked in PBS-T buffer added with 5% BSA or 5% Milk

(1 hour at room temperature), followed by overnight incubation with primary antibodies at 4°C: anti-IkBa (#9242S, Cell signaling, 1:1000), anti-IL1R1 (ab229051, Abcam, 1:1000) and anti-COX2 (160106, Cayman Chemical, 1:100). The following day, membranes were washed and incubated for 1 hour at room temperature with HRP-conjugated secondary antibody. Membranes were developed either with Clarity™ Western ECL Substrate (BIO-RAD) or Westar Supernova (CYANAGEN). Protein loading was assessed by detecting anti-b-actin (A1978, Sigma-Aldrich, 1:2000) or anti-Vinculin (#13901S, Cell Signaling, 1:1000). Western blot analyses were performed using Image Lab Software v6.1.

5.25. Generation of and processing of single-cell RNA-Seq data

5.25.1. Data generation

Human and murine samples were collected and dissociated as described above. For the patient LiMeT PDAC15, cells were enriched in the myeloid fraction as $CD45^+CD3^-CD19^-$ by sorting (FACSAria, BD Biosciences). For heterotopic and orthotopic KC (DT6606) tumors, cells were enriched in the myeloid fraction as $CD45^+Cd11b^+$ via sorting and scRNA-Seq libraries generated using the Chromium Single Cell 3' Reagent Kit v2, according to the manufacturers' instructions. For murine KPC organoids, Matrigel domes containing the organoids were dissolved in Cell Recovery Solution (Gibco) for 30 min on ice, manually inverting the tubes every 5 min. After addition of cold Splitting Medium, organoid suspension was centrifuged and supernatant was removed prior to incubation in TrypLE Express (Gibco) for 20 min on an orbital shaker at 37°C. The larger cellular aggregates were allowed to settle by gravity, and the single cell suspension was collected from the supernatant without interfering with the lower fraction. Upon centrifugation at 400 g for 5 min at 4°C, cells were resuspended in ultrapure BSA (400ug/mL) (Invitrogen) for downstream processing.

If not differently stated, scRNA-Seq libraries were generated using a microfluidics-based approach on Chromium Single-Cell Controller (10X Genomics) using the Chromium Single Cell 3′ Reagent Kit v3.1, according to the manufacturers' instructions. Briefly, single cells were partitioned in Gel Beads in Emulsion (GEMs) and lysed, followed by RNA barcoding, reverse transcription and PCR amplification (13-15 cycles). The concentration of the scRNA-seq libraries was determined using Qubit 3.0 and size

distribution was assessed using an Agilent 4200 TapeStation system. Libraries were sequenced on an Illumina NovaSeq 6000 instrument (paired-end, 150bp read length).

5.25.2. Data processing

Fastq files were processed with Cell Ranger (v 4.0.0) (Zheng et al., 2017), using default parameters. Reads were aligned to reference genome mm10 for mouse samples and hg38 for human samples (references version 2020-A, 10X Genomics). Only confidently mapped reads with valid barcodes and unique molecular identifiers (UMIs) were retained to compute a gene expression matrix containing the number of UMI for every cell and gene. Gene counts were imported in R environment (v 4.0.3) and processed with Seurat (v 4.0.3). When creating the Seurat object, genes expressed in less than 3 cells were removed. Putative doublets were identified and discarded using scDblFinder R package (v 1.4.0) (Germain et al., 2021) by imputing doublet rates (dbr) equal to 0.07 for mouse sample and 0.05 for human samples. Dbr were established in agreement with the number of loaded cells and following the 10X Genomics guidelines. Cells expressing less than 1000 UMI counts were discarded. Cells expressing less than 200 genes (mouse sample), or less than 500 genes (human sample) were also excluded. Lastly, cells with a ratio of mitochondrial versus endogenous genes expression exceeding 0.25 (mouse sample) or 0.40 (human sample) were discarded. Raw expression data were normalized applying $\log_2$ transformation with NormalizeData function, scaled using ScaleData function, regressing on percentage of mitochondrial gene expression and cell cycle scores, previously computed using CellCycleScoring function. Top 3,000 genes with the highest standardized variance were computed using FindVariableFeatures function (selection.method = "vst"). Principal component analysis (PCA) was computed using RunPCA function with default parameters.

5.25.3. Batch correction

PCA embeddings were corrected for sample batch by applying alternative algorithms to the same Seurat object through the Seurat Wrapper package (v 0.3.0). For both human and mouse data, when analyzing the whole or tumor cells dataset, batch effect was corrected employing matching mutual nearest neighbor (MNN) algorithm (Haghverdi et al., 2018), implemented by RunFastMNN function using default parameters. For the analysis of mononuclear-phagocytes and tumor-associated macrophages, batch correction was achieved with the Harmony algorithm (v 0.1.0) (Korsunsky et al., 2019),

implemented by RunHarmony function using the first 30 PCA dimensions and default theta (theta=3 for human dataset).

5.25.4. Graph-based clustering and differential gene expression analyses.

Shared Nearest Neighbor (SNN) graph was computed using the FindNeighbors function, taking as input the first 20 PCA dimensions. Cell clusters were defined using Louvain algorithm with the FindCluster function. For visualization in 2 dimensions uniform manifold approximation and projection (UMAP) (Becht et al., 2019) was used. Cluster-specific genes were identified using FindAllMarkers function with option only.pos = TRUE and min.pct=0.1, setting a cut-off of FDR < 0.01.

5.25.5. Inference of copy-number variants (CNV)

Single-cell CNVs were inferred using CopyKAT R package (v 1.0.5) (Gao et al., 2021). CopyKAT estimates the genome copy number profile of single cells employing an integrative Bayesian segmentation approach combined with hierarchical clustering to identify putative aneuploid cells. CopyKAT was run separately on each human sample, taking the raw count matrix of all cells as input and adjusting the segmentation parameter KS.cut to either 0.1 or 0.15 according to data quality.

5.25.6. Human-mouse comparison of TAM clusters

We performed a pre-ranked GSEA analysis with clusterProfiler R package (v 3.18.1) (Yu et al., 2012) on mouse TAM genes ranked by log_2FC (each TAM subset vs other TAMs) using as gene sets mouse orthologs of human TAMs marker genes obtained using biomaRt (v 2.46.3) (Durinck et al., 2009) database. To identify shared signatures for each human and mouse TAM cluster, we computed overlaps between marker genes identified using logfc.threshold = 0.8.

5.25.7. RNA Velocity and single-cell trajectories

Mouse classical monocytes and tumor-associated macrophages from pancreatic and blood samples were analyzed together as previously described. Batch effect correction was performed by matching mutual nearest neighbor (MNN) algorithm, using the RunFastMNN function with default parameters. The first 20 MNN-corrected principal components were used to compute the two-dimensional embedding using the diffusion map-based algorithm Palantir (Setty et al., 2019), implemented with the RunPalantirDiffusionMap function from SeuratExtend R package (v 0.4.2). Cell clusters were defined according to marker-based manual annotation previously done on each

dataset. The Seurat object was then converted into Scanpy format (v 1.6.0) (Wolf et al., 2018) using SeuratDisk (v 0.0.0.9019) and the following analyses were performed in Python environment (v 3.6.10). To annotate spliced and unspliced reads, cell-barcode sorted bam files from Cell Ranger output were processed using Velocyto pipeline (v 0.17.17) (La Manno et al., 2018). The scVelo Python package (v 0.2.2) (Bergen et al., 2020) was used to compute RNA velocity vectors for each gene, employing dynamical modeling to estimate splicing kinetics. Using CellRank package (v 1.2.0) (Lange et al., 2022), RNA velocity and transcriptomic similarity information were combined in single kernel to compute a cell-cell transition matrix. Generalized Perron Cluster Cluster Analysis (GPCCA) (Reuter et al., 2018) estimator was used to identify macrostates. Terminal states were inferred by inspecting the coarse-grained transition matrix and were then used to compute absorption probabilities. Focusing on the Classical Monocyte - *Il1b*$^{+}$ TAMs lineage, genes whose expression correlates with absorption probabilities towards Il1b+ TAMs terminal state were identified as potential lineage drivers.

5.25.8. Gene set enrichment analysis (GSEA)

Hallmarks gene sets were retrieved from msigdbr (v 7.5.1) (Liberzon et al., 2015). For Gene Ontology biological processes gene sets, we used org.Hs.eg.db (v 3.12.0) and org.Mm.eg.db (v 3.12.0) as genome wide annotations for human and mouse respectively. Gene sets of cytokine-induced signatures were derived from *in vitro* stimulation experiments on mouse bone marrow-derived macrophages (Cilenti et al., 2021; Ostuni et al., 2013).

5.25.9. IL1B gene expression in human cell types.

To evaluate the expression of *IL1B* across all human cell types, we reanalyzed scRNA-Seq data including neutrophils in the dataset. Neutrophils were retrieved lowering the cutoffs on UMI counts and genes per cell to 500 and 100, respectively. Data were processed as previously described, with the exception that counts were normalized with SCTransform function in Seurat.

5.25.10. Reanalysis of human PDAC cells in Naïve samples.

Tumor cells from untreated patients were analyzed separately as previously described. We computed new embedding and clustering on cells showing variable expression of the T1RS signature (clusters 1,3,5 at resolution 0.3) and then we performed trajectory analysis with slingshot (v. 1.8.0) (Street et al., 2018) on the MNN space. We correlated

gene expression with pseudotime, computed with slingPseudotime function. To evaluate if cell trajectory reflected the acquisition of the expression of T1RS signature we performed GSEA analyses on gene list ranked by correlation values.

5.25.11. scRNA-Seq datasets collected in this study

We collected published scRNA-seq data on human pancreatic ductal adenocarcinoma and normal adjacent tissue (CRA001160) (Peng et al., 2019); immune cells from idiopathic or hereditary pancreatitis and normal pancreas (GSE165045) (Lee et al., 2022); pancreatic epithelial cells from GEMMs of PDAC progression (GSE207943) (Burdziak et al., 2023). For these datasets we downloaded: raw fastqs, raw count matrices and normalized counts, respectively. Data were processed as previously described.

5.25.12. scRNA-Seq dataset from pancreatitis patients

Raw counts matrices of immune cells from idiopathic or hereditary pancreatitis and normal pancreata were filtered to discard cells expressing less than 200 genes, less than 1000 UMIs and with a ratio of mitochondrial versus endogenous genes expression exceeding 0.20. Cells were processed as previously described, using 2000 variable features. For the analysis of macrophages, anchoring-based transfer learning (Stuart et al., 2019) was used to perform annotation, using our tumor-associated macrophage dataset as reference. Anchors for transfer learning were computed using the FindTransferAnchors Seurat function. Reference labels were then projected onto query macrophages using the TransferData function. Macrophages from pancreatitis and donor pancreata were annotated according to our reference classification if the prediction score exceeded 0.75, otherwise were left unlabeled.

5.25.13. scRNA-Seq datasets from other mouse models

scRNA-Seq datasets from GEMM mouse models and WT and COX-2 KO KPC were processed as previously described. For scRNA-Seq data derived from heterotopic and orthotopic KC tumors we corrected batch effect employing Harmony algorithm (v 0.1.0), implemented by RunHarmony function using the first 30 PCA dimensions and theta=1. For the reclustering of mononuclear-phagocytes, batch correction was achieved with the Harmony algorithm (v 0.1.0) on the first 30 PCA dimensions and default theta. Differentially expressed genes in the comparison between cells from WT and COX-2 KO tumors were computed using FindAllMarkers function with option only.pos = FALSE, min.pct=0.1, setting a cut-off of FDR < 0.01 and average $\log_2$FC>0.5.

5.26. Generation and processing of spatial transcriptomic (ST) data

Molecular Cartography™ data

5.26.1. Data generation

10-µm sections were collected from fresh frozen PDAC tissues, placed within the capture areas of cold slides, and sent to Resolve Biosciences on dry ice for sample processing. Upon arrival, tissue sections were thawed, fixed with 4% Formaldehyde (Sigma-Aldrich F8775) in PBS for 20 min at 4 °C, and used for Molecular Cartography™ (100-plex combinatorial single molecule fluorescence in-situ hybridization) according to the manufacturer's instructions (protocol 1.3; available for download from Resolve's website for registered users). Briefly, tissue sections were hybridized at 37°C for 24 hours with oligonucleotides probes specific for the selected target genes (a complete list of the probes is reported below). Probes were designed using Resolve's proprietary algorithm, as previously reported (Guilliams et al., 2022). Afterwards, probe binding was revealed with fluorescent tags in a multi-step automated imaging process, repeating color development, imaging and decolorization for a total of 8 cycles on a Zeiss Celldiscoverer 7 instrument, using a 50x water immersion objective. The resulting raw data images were preprocessed for background correction, aligned to perform spot segmentation, analyzed to decode the resulting signals and to finally assign each detected transcript to a *x*-*y*-*z* coordinates, as previously reported (Guilliams et al., 2022).

PROBE LIST ID	Species	Gene_ID	Gene_Name
KGJ1L	Homo Sapiens	ENSG00000081237	PTPRC
KGJ1L	Homo Sapiens	ENSG00000139193	CD27
KGJ1L	Homo Sapiens	ENSG00000156738	MS4A1
KGJ1L	Homo Sapiens	ENST00000302125	MZB1
KGJ1L	Homo Sapiens	ENSG00000167286	CD3D
KGJ1L	Homo Sapiens	ENSG00000010610	CD4
KGJ1L	Homo Sapiens	ENSG00000153563	CD8A
KGJ1L	Homo Sapiens	ENSG00000188389	PDCD1
KGJ1L	Homo Sapiens	ENSG00000135077	HAVCR2
KGJ1L	Homo Sapiens	ENSG00000089692	LAG3
KGJ1L	Homo Sapiens	ENSG00000163599	CTLA4
KGJ1L	Homo Sapiens	ENSG00000163600	ICOS
KGJ1L	Homo Sapiens	ENSG00000163508	EOMES
KGJ1L	Homo Sapiens	ENSG00000111537	IFNG
KGJ1L	Homo Sapiens	ENSG00000181847	TIGIT
KGJ1L	Homo Sapiens	ENSG00000049249	TNFRSF9
KGJ1L	Homo Sapiens	ENSG00000168685	IL7R
KGJ1L	Homo Sapiens	ENSG00000188404	SELL
KGJ1L	Homo Sapiens	ENSG00000049768	FOXP3
KGJ1L	Homo Sapiens	ENSG00000134460	IL2RA
KGJ1L	Homo Sapiens	ENSG00000100453	GZMB
KGJ1L	Homo Sapiens	ENSG00000105374	NKG7
KGJ1L	Homo Sapiens	ENST00000355819	CLEC9A
KGJ1L	Homo Sapiens	ENST00000309285	XCR1
KGJ1L	Homo Sapiens	ENST00000368170	CD1C
KGJ1L	Homo Sapiens	ENSG00000132514	CLEC10A
KGJ1L	Homo Sapiens	ENSG00000126353	CCR7
KGJ1L	Homo Sapiens	ENST00000382361	FSCN1
KGJ1L	Homo Sapiens	ENST00000296046	CPA3
KGJ1L	Homo Sapiens	ENSG00000130203	APOE
KGJ1L	Homo Sapiens	ENSG00000159189	C1QC
KGJ1L	Homo Sapiens	ENSG00000177575	CD163
KGJ1L	Homo Sapiens	ENSG00000129226	CD68
KGJ1L	Homo Sapiens	ENSG00000203747	FCGR3A
KGJ1L	Homo Sapiens	ENSG00000204482	LST1
KGJ1L	Homo Sapiens	ENSG00000038427	VCAN
KGJ1L	Homo Sapiens	ENSG00000121807	CCR2
KGJ1L	Homo Sapiens	ENSG00000120217	CD274
KGJ1L	Homo Sapiens	ENST00000397747	PDCD1LG2
KGJ1L	Homo Sapiens	ENSG00000232629	HLA-DQB2
KGJ1L	Homo Sapiens	ENSG00000204287	HLA-DRA
KGJ1L	Homo Sapiens	ENSG00000119535	CSF3R
KGJ1L	Homo Sapiens	ENSG00000162747	FCGR3B
KGJ1L	Homo Sapiens	ENST00000361566	KRT19
KGJ1L	Homo Sapiens	ENST00000019103	SCTR
KGJ1L	Homo Sapiens	ENSG00000137392	CLPS
KGJ1L	Homo Sapiens	ENSG00000162992	NEUROD1
KGJ1L	Homo Sapiens	ENSG00000261371	PECAM1
KGJ1L	Homo Sapiens	ENSG00000134853	PDGFRA
KGJ1L	Homo Sapiens	ENSG00000107796	ACTA2
KGJ1L	Homo Sapiens	ENSG00000115594	IL1R1
KGJ1L	Homo Sapiens	ENST00000264870	F13A1
KGJ1L	Homo Sapiens	ENSG00000165457	FOLR2
KGJ1L	Homo Sapiens	ENSG00000171659	GPR34
KGJ1L	Homo Sapiens	ENSG00000133800	LYVE1
KGJ1L	Homo Sapiens	ENSG00000178573	MAF
KGJ1L	Homo Sapiens	ENSG00000260314	MRC1
KGJ1L	Homo Sapiens	ENSG00000166927	MS4A7
KGJ1L	Homo Sapiens	ENST00000321725	STAB1
KGJ1L	Homo Sapiens	ENSG00000137491	SLCO2B1
KGJ1L	Homo Sapiens	ENSG00000153208	MERTK
KGJ1L	Homo Sapiens	ENST00000395761	CXCL1
KGJ1L	Homo Sapiens	ENSG00000115008	IL1A
KGJ1L	Homo Sapiens	ENSG00000125538	IL1B
KGJ1L	Homo Sapiens	ENSG00000136244	IL6
KGJ1L	Homo Sapiens	ENST00000260356	THBS1
KGJ1L	Homo Sapiens	ENSG00000232810	TNF
KGJ1L	Homo Sapiens	ENST00000367468	PTGS2
KGJ1L	Homo Sapiens	ENSG00000100311	PDGFB
KGJ1L	Homo Sapiens	ENSG00000162711	NLRP3
KGJ1L	Homo Sapiens	ENSG00000139572	GPR84
KGJ1L	Homo Sapiens	ENST00000296026	CXCL3
KGJ1L	Homo Sapiens	ENSG00000166523	CLEC4E
KGJ1L	Homo Sapiens	ENST00000300060	ANPEP
KGJ1L	Homo Sapiens	ENSG00000135218	CD36
KGJ1L	Homo Sapiens	ENSG00000136235	GPNMB
KGJ1L	Homo Sapiens	ENSG00000122641	INHBA
KGJ1L	Homo Sapiens	ENSG00000175445	LPL
KGJ1L	Homo Sapiens	ENSG00000183019	MCEMP1
KGJ1L	Homo Sapiens	ENST00000327097	MARCO
KGJ1L	Homo Sapiens	ENSG00000107798	LIPA
KGJ1L	Homo Sapiens	ENSG00000164687	FABP5
KGJ1L	Homo Sapiens	ENSG00000133063	CHIT1
KGJ1L	Homo Sapiens	ENSG00000130208	APOC1
KGJ1L	Homo Sapiens	ENSG00000148773	MKI67
KGJ1L	Homo Sapiens	ENSG00000170312	CDK1
KGJ1L	Homo Sapiens	ENST00000423485	TOP2A
KGJ1L	Homo Sapiens	ENSG00000121351	IAPP
KGJ1L	Homo Sapiens	ENSG00000115263	GCG
KGJ1L	Homo Sapiens	ENSG00000068305	MEF2A
KGJ1L	Homo Sapiens	ENSG00000081189	MEF2C
KGJ1L	Homo Sapiens	ENSG00000116604	MEF2D
KGJ1L	Homo Sapiens	ENST00000292513	PTGER1
KGJ1L	Homo Sapiens	ENSG00000125384	PTGER2
KGJ1L	Homo Sapiens	ENSG00000050628	PTGER3
KGJ1L	Homo Sapiens	ENST00000302472	PTGER4
KGJ1L	Homo Sapiens	ENSG00000123560	PLP1
KGJ1L	Homo Sapiens	ENSG00000143248	RGS5

5.26.2. Cell Segmentation

We segmented cell nuclei in the DAPI image with Cellpose (v. 2.2) (Stringer et al., 2021) using the pre-trained nuclei model, with automated estimation of diameter parameter. Subsequently, cells were segmented on transcript coordinates with Baysor (v. 0.5.0) (Petukhov et al., 2022) using DAPI segments as prior with the following parameters: --n-clusters 1 --prior-segmentation-confidence 0.2 -m 3. Finally, we computed cells outlines by applying the convex hull algorithm, using chull R function, on transcripts assigned to each individual cell by Baysor.

5.26.3. Cell filtering and annotation

We imported Baysor output files and segmentation into a Seurat object with a custom function. Cells expressing less than 4 genes or more then 25 genes, along with cells with less than 10 transcripts were discarded. Gene counts were normalized with SCTransform Seurat function with clip.range set form -10 to 10. Then, we performed PCA and we computed clustering and dimensionality reduction as previously described for scRNA-Seq data. Finally, we computed markers for all cluster and annotated cell types.

5.26.4. Spatial neighborhood analysis

For each cluster we defined a set of cells in its spatial neighborhood, then we computed which clusters were significatively overrepresented in this neighborhood set. Briefly, for each cell we computed k-nearest neighbors within spatial coordinates space using kNN function from dbscan R package (v. 1.1-11) (Hahsler et al., 2019), with k set to 40 and maximum distance set to 400 pixels. We selected the set of nearest neighbors of all cells belonging to the same cluster and we counted the number of cells from all different cluster within this set of nearest neighbors. We then computed significance using randomly annotated data as null distribution. Specifically, we reannotated cells randomly 1000 times, maintaining cluster dimensionality and, for each randomization, we computed again the number of cells from all clusters in the set of nearest neighbors of each cluster.

5.26.5. ST datasets collected in this study.

We downloaded raw count matrices of published GeoMX data (GSE226829) (Carpenter et al., 2023). We performed normalization with voom function of limma R package (v. 3.46.0) (Ritchie et al., 2015).

5.27. Generation and processing of bulk RNA-Seq data

5.27.1. Data generation

Total RNA was purified using the ReliaPrep RNA Cell Miniprep System and RNA-Seq libraries were generated using the Smart-seq2 method with minor modification. Briefly, 5ng of RNA were retrotranscribed, cDNA was PCR-amplified (15 cycles) and purified with AMPure XP beads. After purification, the concentration was determined using Qubit 3.0 and size distribution was assessed using Agilent 4200 TapeStation system. Then, the tagmentation reaction was performed starting from 0.5 ng of cDNA for 30 min at 55°C and the enrichment PCR was carried out using 12 cycles. Libraries were then purified with AMPure XP beads, quantified using Qubit 3.0, assessed for fragment size distribution on an Agilent 4200 TapeStation system. Sequencing was performed on an Illumina NovaSeq6000 (single-end, 75bp read length) following manufacturer's instruction.

5.27.2. Data processing

Reads were aligned to the mm10 reference genome using STAR aligner (v STAR_2.5.3a) (Dobin et al., 2013). Read counts matrices were computed using the featureCounts function from Rsubread package (v 2.0.1) (Liao et al., 2019), using RefSeq *Mus musculus* transcriptome (mm10) annotation (Pruitt et al., 2007), setting minMQS option to 255. Further analyses were performed in R environment (v 3.6.3) with edgeR R package (v 3.28.1) (Robinson Mark et al., 2010). Expressed genes read counts were normalized using the calcNormFactors function, with the Trimmed Mean of M-values (TMM) method (Robinson & Oshlack, 2010). The estimateDisp function was used to estimate dispersion. Differential gene expression across conditions was computed by fitting a negative binomial generalized linear model, with the glmQLFit function, followed by a quasi-likelihood (QL) F-test, with the glmQLFTest function, including sample replicates as covariates in the design matrix. Reads per kilo base per million (RPKM) values were computed for each gene with the rpkm function.

5.27.3. Definition of TNF-α+PGE$_2$ synergized genes.

RNA-Seq data were generated and pre-processed as described above. Genes not passing the expression cut-off of RPKM > 1 in at least two samples in the dataset were filtered out. For each timepoint we defined TNF-α-PGE$_2$-inducible genes comparing expression levels in the TNF-α+PGE$_2$ condition versus UT, PGE$_2$ alone or TNF-α alone

conditions, setting log_2FC(RPKM) ≥ 1.5 and FDR < 0.01 as cut-offs. We also filtered out genes not reaching RPKM > 1.5 in at least two samples within each comparison. Finally, for each timepoint, we defined PGE_2-TNF-α synergized genes selecting genes passing previously defined cut-offs in all tested comparisons. For GSEA analysis we considered genes defined as PGE_2-TNF-a synergized in at least one timepoint.

5.27.4. Definition of tumor-intrinsic IL-1β response signature (T1RS) gene signature.

We analyzed bulk and single-cell RNA-seq data on KC (DT6606), KPC (K8484) cells and KPC organoids stimulated with IL-1b *in vitro*. For each timepoint of stimulation, we defined IL-1b -inducible genes comparing expression levels in the IL-1b condition versus UT, setting log_2FC(RPKM) ≥ 1 and FDR < 0.05 as cut-offs. For each experimental condition we defined lists of IL-1b-inducible genes, selecting genes passing the defined cut-offs in at least one timepoint. Intersection of these gene lists led us to the identification of a set of genes commonly induced by IL-1b in all experimental conditions, namely the T1RS signature.

5.27.5. RNA-Seq datasets collected in this study.

We collected published RNA-Seq data on pancreatic epithelial cells from *Kras*-wild type and mutant *Kras* mice treated either with Caerulein or IL-33 or left untreated (GSE132326, GSE154543) (Alonso-Curbelo et al., 2021); mouse pancreatic spheroids derived from pancreas either pre-exposed or not exposed to inflammation (GSE180211) (Del Poggetto et al., 2021). For these datasets raw count matrices were downloaded and analyzed as previously described.

5.27.6. TCGA data analyses.

Using the TCGAbiolinks R package (v 2.23.2) (Colaprico et al., 2016), we downloaded transcriptomic data and clinical data from PAAD cohort for pancreatic cancer (n=178). Survival analysis on primary tumor samples was performed using the survival (v 3.2-10) and survminer (v 0.4.9) R packages.

5.27.7. Survival analysis of TAM markers and T1RS genes in PAAD cohort.

To evaluate the prognostic significance of TAM marker genes, we obtained TAM cluster-specific genes by performing differential gene expression analysis (each TAM cluster vs other TAM clusters) and filtering for log_2FC≥1. On such gene lists, we evaluated MNP-specificity by differential gene expression analysis, selecting genes with log_2FC≥2 in MNP compared to other cell types identified in our scRNA-Seq data. Impact

on patient prognosis was assessed by Cox beta regression coefficient on genes for which the fit was significant according to Wald test p-values corrected for multiple testing. Univariate Cox regression model was fit for the expression of each gene or for the expression of each gene normalized for CD68 expression as continuous variables, for the evaluation of T1RS signature or TAM marker genes respectively.

5.27.8. Survival analysis on IL1B$^+$ TAMs gene signature.

The 6-gene prognostic signature for *IL1B*$^+$ TAMs, obtained as previously described, was used to stratified patients for survival analysis. The mean expression of the signature, normalized by CD68 expression, was used to group samples into high and low groups according to the upper and the lower quartile respectively. Cox regression model was fit to compare the high group against the low group, extracting the hazard ratio and its associated p-value.

5.27.9. Association of T1RS and IL1B$^+$ TAMs signatures

Using the TCGAbiolinks R package (v 2.28.3), we downloaded transcriptomic data and clinical data from the aforementioned cohort. We grouped patients based on the mean expression of the 6-gene IL1B+ TAMs signature normalized by CD68 expression into high, intermediate and low groups according to the upper and the lower quartile of the score distribution. To examine association between IL1B+ TAMs and T1RS signature, we then computed the mean of log2-transformed expression values of T1RS signature genes for each group of patients.

5.27.10. Cell type deconvolution of TCGA PDAC samples

To estimate macrophage proportion in TCGA samples we used CIBERSORTx online tool to deconvolute cell fractions using our annotated scRNA-Seq human PDAC dataset as reference. To build the signature matrix file, we first down-sampled our scRNA-Seq human PDAC dataset, randomly selecting 200 cells for each annotated cell type. We then ran CIBERSORTx to generate cell-type signature matrices and impute the relative cell fractions in each tumor sample, enabling S-mode batch correction.

5.28. Quantification and statistical analyses

Results are illustrated as mean ± SD or mean ± SEM. Graphs show data from at least two independent repeats. Significance was defined as $p < 0.05$. Statistical analysis was conducted either using GraphPad Prism v9.0 (GraphPad Software) or R v3.4.1 (R

project). Statistical tests, exact value of n, what n represents are mentioned in the Fig. legends.

6. BIBLIOGRAPHY

Afonina, I. S., Müller, C., Martin, S. J., & Beyaert, R. (2015). Proteolytic Processing of Interleukin-1 Family Cytokines: Variations on a Common Theme. In *Immunity*. https://doi.org/10.1016/j.immuni.2015.06.003

Aguirre, A. J., Nowak, J. A., Camarda, N. D., Moffitt, R. A., Ghazani, A. A., Hazar-Rethinam, M., Raghavan, S., Kim, J., Brais, L. K., Ragon, D., Welch, M. W., Reilly, E., McCabe, D., Marini, L., Anderka, K., Helvie, K., Oliver, N., Babic, A., Da Silva, A., … Wolpin, B. M. (2018). Real-time genomic characterization of advanced pancreatic cancer to enable precision medicine. *Cancer Discovery*. https://doi.org/10.1158/2159-8290.CD-18-0275

Alliot, F., Godin, I., & Pessac, B. (1999). Microglia derive from progenitors, originating from the yolk sac, and which proliferate in the brain. *Developmental Brain Research*. https://doi.org/10.1016/S0165-3806(99)00113-3

Alonso-Curbelo, D., Ho, Y. J., Burdziak, C., Maag, J. L. V., Morris, J. P., Chandwani, R., Chen, H. A., Tsanov, K. M., Barriga, F. M., Luan, W., Tasdemir, N., Livshits, G., Azizi, E., Chun, J., Wilkinson, J. E., Mazutis, L., Leach, S. D., Koche, R., Pe'er, D., & Lowe, S. W. (2021). A gene–environment-induced epigenetic program initiates tumorigenesis. *Nature*. https://doi.org/10.1038/s41586-020-03147-x

Amit, I., Winter, D. R., & Jung, S. (2016). The role of the local environment and epigenetics in shaping macrophage identity and their effect on tissue homeostasis. In *Nature Immunology*. https://doi.org/10.1038/ni.3325

Aung, K. L., Fischer, S. E., Denroche, R. E., Jang, G. H., Dodd, A., Creighton, S., Southwood, B., Liang, S. Ben, Chadwick, D., Zhang, A., O'Kane, G. M., Albaba, H., Moura, S., Grant, R. C., Miller, J. K., Mbabaali, F., Pasternack, D., Lungu, I. M., Bartlett, J. M. S., … Knox, J. J. (2018). Genomics-driven precision medicine for advanced pancreatic cancer: Early results from the COMPASS trial. *Clinical Cancer Research*. https://doi.org/10.1158/1078-0432.CCR-17-2994

Baer, J. M., Zuo, C., Kang, L. I., de la Lastra, A. A., Borcherding, N. C., Knolhoff, B. L., Bogner, S. J., Zhu, Y., Yang, L., Laurent, J., Lewis, M. A., Zhang, N., Kim, K. W., Fields, R. C., Yokoyama, W. M., Mills, J. C., Ding, L., Randolph, G. J., & DeNardo, D. G. (2023). Fibrosis induced by resident macrophages has divergent roles in pancreas inflammatory injury and PDAC. *Nature Immunology*, *24*(September).

https://doi.org/10.1038/s41590-023-01579-x

Bailey, P., Chang, D. K., Nones, K., Johns, A. L., Patch, A. M., Gingras, M. C., Miller, D. K., Christ, A. N., Bruxner, T. J. C., Quinn, M. C., Nourse, C., Murtaugh, L. C., Harliwong, I., Idrisoglu, S., Manning, S., Nourbakhsh, E., Wani, S., Fink, L., Holmes, O., … Grimmond, S. M. (2016). Genomic analyses identify molecular subtypes of pancreatic cancer. *Nature*. https://doi.org/10.1038/nature16965

Bain, C. C., Bravo-Blas, A., Scott, C. L., Gomez Perdiguero, E., Geissmann, F., Henri, S., Malissen, B., Osborne, L. C., Artis, D., & Mowat, A. M. I. (2014). Constant replenishment from circulating monocytes maintains the macrophage pool in the intestine of adult mice. *Nature Immunology*. https://doi.org/10.1038/ni.2967

Baker, L. A., & Tuveson, D. A. (2019). Generation and culture of tumor and metastatic organoids from murine models of pancreatic ductal adenocarcinoma. In *Methods in Molecular Biology*. https://doi.org/10.1007/978-1-4939-8879-2_10

Balachandran, V. P., Łuksza, M., Zhao, J. N., Makarov, V., Moral, J. A., Remark, R., Herbst, B., Askan, G., Bhanot, U., Senbabaoglu, Y., Wells, D. K., Cary, C. I. O., Grbovic-Huezo, O., Attiyeh, M., Medina, B., Zhang, J., Loo, J., Saglimbeni, J., Abu-Akeel, M., … Bassi, C. (2017). Identification of unique neoantigen qualities in long-term survivors of pancreatic cancer. *Nature*. https://doi.org/10.1038/nature24462

Barnett, K. C., Li, S., Liang, K., & Ting, J. P. Y. (2023). A 360° view of the inflammasome: Mechanisms of activation, cell death, and diseases. In *Cell*. https://doi.org/10.1016/j.cell.2023.04.025

Barriga, F. M., Tsanov, K. M., Ho, Y. J., Sohail, N., Zhang, A., Baslan, T., Wuest, A. N., Del Priore, I., Meškauskaitė, B., Livshits, G., Alonso-Curbelo, D., Simon, J., Chaves-Perez, A., Bar-Sagi, D., Iacobuzio-Donahue, C. A., Notta, F., Chaligne, R., Sharma, R., Pe'er, D., & Lowe, S. W. (2022). MACHETE identifies interferon-encompassing chromosome 9p21.3 deletions as mediators of immune evasion and metastasis. *Nature Cancer*. https://doi.org/10.1038/s43018-022-00443-5

Bärthel, S., Falcomatà, C., Rad, R., Theis, F. J., & Saur, D. (2023). Single-cell profiling to explore pancreatic cancer heterogeneity, plasticity and response to therapy. In *Nature Cancer*. https://doi.org/10.1038/s43018-023-00526-x

Bayerl, F., Meiser, P., Donakonda, S., Hirschberger, A., Lacher, S. B., Pedde, A. M., Hermann, C. D., Elewaut, A., Knolle, M., Ramsauer, L., Rudolph, T. J., Grassmann,

S., Öllinger, R., Kirchhammer, N., Trefny, M., Anton, M., Wohlleber, D., Höchst, B., Zaremba, A., … Böttcher, J. P. (2023). Tumor-derived prostaglandin E2 programs cDC1 dysfunction to impair intratumoral orchestration of anti-cancer T cell responses. *Immunity*. https://doi.org/10.1016/j.immuni.2023.05.011

Bayne, L. J., Beatty, G. L., Jhala, N., Clark, C. E., Rhim, A. D., Stanger, B. Z., & Vonderheide, R. H. (2012). Tumor-Derived Granulocyte-Macrophage Colony-Stimulating Factor Regulates Myeloid Inflammation and T Cell Immunity in Pancreatic Cancer. *Cancer Cell*. https://doi.org/10.1016/j.ccr.2012.04.025

Bear, A. S., Vonderheide, R. H., & O'Hara, M. H. (2020). Challenges and Opportunities for Pancreatic Cancer Immunotherapy. In *Cancer Cell*. https://doi.org/10.1016/j.ccell.2020.08.004

Becht, E., McInnes, L., Healy, J., Dutertre, C. A., Kwok, I. W. H., Ng, L. G., Ginhoux, F., & Newell, E. W. (2019). Dimensionality reduction for visualizing single-cell data using UMAP. *Nature Biotechnology*. https://doi.org/10.1038/nbt.4314

Bell, C. R., Pelly, V. S., Moeini, A., Chiang, S. C., Flanagan, E., Bromley, C. P., Clark, C., Earnshaw, C. H., Koufaki, M. A., Bonavita, E., & Zelenay, S. (2022). Chemotherapy-induced COX-2 upregulation by cancer cells defines their inflammatory properties and limits the efficacy of chemoimmunotherapy combinations. *Nature Communications*. https://doi.org/10.1038/s41467-022-29606-9

Berenblum, I., & Shubik, P. (1949). The persistence of latent tumour cells induced in the mouse's skin by a single application of 9: Io-dimethyl-1:2-benzanthracene. *British Journal of Cancer*. https://doi.org/10.1038/bjc.1949.42

Bergen, V., Lange, M., Peidli, S., Wolf, F. A., & Theis, F. J. (2020). Generalizing RNA velocity to transient cell states through dynamical modeling. *Nature Biotechnology*. https://doi.org/10.1038/s41587-020-0591-3

Biffi, G., Oni, T. E., Spielman, B., Hao, Y., Elyada, E., Park, Y., Preall, J., & Tuveson, D. A. (2019). Il1-induced Jak/STAT signaling is antagonized by TGFβ to shape CAF heterogeneity in pancreatic ductal adenocarcinoma. *Cancer Discovery*. https://doi.org/10.1158/2159-8290.CD-18-0710

Bill, R., Wirapati, P., Messemaker, M., Roh, W., Zitti, B., Duval, F., Kiss, M., Park, J. C., Saal, T. M., Hoelzl, J., Tarussio, D., Benedetti, F., Tissot, S., Kandalaft, L.,

Varrone, M., Ciriello, G., McKee, T. A., Monnier, Y., Mermod, M., … Pittet, M. J. (2023). CXCL9:SPP1 macrophage polarity identifies a network of cellular programs that control human cancers. In *Science* (Vol. 381, Issue 6657, pp. 515–524). https://doi.org/10.1126/science.ade2292

Binnewies, M., Mujal, A. M., Pollack, J. L., Combes, A. J., Hardison, E. A., Barry, K. C., Tsui, J., Ruhland, M. K., Kersten, K., Abushawish, M. A., Spasic, M., Giurintano, J. P., Chan, V., Daud, A. I., Ha, P., Ye, C. J., Roberts, E. W., & Krummel, M. F. (2019). Unleashing Type-2 Dendritic Cells to Drive Protective Antitumor CD4+ T Cell Immunity. *Cell*. https://doi.org/10.1016/j.cell.2019.02.005

Binnewies, M., Roberts, E. W., Kersten, K., Chan, V., Fearon, D. F., Merad, M., Coussens, L. M., Gabrilovich, D. I., Ostrand-Rosenberg, S., Hedrick, C. C., Vonderheide, R. H., Pittet, M. J., Jain, R. K., Zou, W., Howcroft, T. K., Woodhouse, E. C., Weinberg, R. A., & Krummel, M. F. (2018). Understanding the tumor immune microenvironment (TIME) for effective therapy. *Nature Medicine*. https://doi.org/10.1038/s41591-018-0014-x

Blackford, A., Serrano, O. K., Wolfgang, C. L., Parmigiani, G., Jones, S., Zhang, X., Parsons, D. W., Lin, J. C. H., Leary, R. J., Eshleman, J. R., Goggins, M., Jaffee, E. M., Iacobuzio-Donahue, C. A., Maitra, A., Cameron, J. L., Olino, K., Schulick, R., Winter, J., Herman, J. M., … Hruban, R. H. (2009). SMAD4 gene mutations are associated with poor prognosis in pancreatic cancer. *Clinical Cancer Research*. https://doi.org/10.1158/1078-0432.CCR-09-0227

Blériot, C., Chakarov, S., & Ginhoux, F. (2020). Determinants of Resident Tissue Macrophage Identity and Function. In *Immunity*. https://doi.org/10.1016/j.immuni.2020.05.014

Blériot, C., Dupuis, T., Jouvion, G., Eberl, G., Disson, O., & Lecuit, M. (2015). Liver-Resident Macrophage Necroptosis Orchestrates Type 1 Microbicidal Inflammation and Type-2-Mediated Tissue Repair during Bacterial Infection. *Immunity*. https://doi.org/10.1016/j.immuni.2014.12.020

Bohn, T., Rapp, S., Luther, N., Klein, M., Bruehl, T. J., Kojima, N., Aranda Lopez, P., Hahlbrock, J., Muth, S., Endo, S., Pektor, S., Brand, A., Renner, K., Popp, V., Gerlach, K., Vogel, D., Lueckel, C., Arnold-Schild, D., Pouyssegur, J., … Bopp, T. (2018). Tumor immunoevasion via acidosis-dependent induction of regulatory

tumor-associated macrophages. *Nature Immunology*. https://doi.org/10.1038/s41590-018-0226-8

Bonavita, E., Bromley, C. P., Jonsson, G., Pelly, V. S., Sahoo, S., Walwyn-Brown, K., Mensurado, S., Moeini, A., Flanagan, E., Bell, C. R., Chiang, S. C., Chikkanna-Gowda, C. P., Rogers, N., Silva-Santos, B., Jaillon, S., Mantovani, A., Reis e Sousa, C., Guerra, N., Davis, D. M., & Zelenay, S. (2020). Antagonistic Inflammatory Phenotypes Dictate Tumor Fate and Response to Immune Checkpoint Blockade. *Immunity*. https://doi.org/10.1016/j.immuni.2020.10.020

Böttcher, J. P., Bonavita, E., Chakravarty, P., Blees, H., Cabeza-Cabrerizo, M., Sammicheli, S., Rogers, N. C., Sahai, E., Zelenay, S., & Reis e Sousa, C. (2018). NK Cells Stimulate Recruitment of cDC1 into the Tumor Microenvironment Promoting Cancer Immune Control. *Cell*. https://doi.org/10.1016/j.cell.2018.01.004

Brahmer, J. R., Tykodi, S. S., Chow, L. Q. M., Hwu, W.-J., Topalian, S. L., Hwu, P., Drake, C. G., Camacho, L. H., Kauh, J., Odunsi, K., Pitot, H. C., Hamid, O., Bhatia, S., Martins, R., Eaton, K., Chen, S., Salay, T. M., Alaparthy, S., Grosso, J. F., … Wigginton, J. M. (2012). Safety and Activity of Anti–PD-L1 Antibody in Patients with Advanced Cancer. *New England Journal of Medicine*. https://doi.org/10.1056/nejmoa1200694

Brenneis, C., Coste, O., Altenrath, K., Angioni, C., Schmidt, H., Schuh, C. D., Zhang, D. D., Henke, M., Weigert, A., Brüne, B., Rubin, B., Nusing, R., Scholich, K., & Geisslinger, G. (2011). Anti-inflammatory role of microsomal prostaglandin e synthase-1 in a model of neuroinflammation. *Journal of Biological Chemistry*. https://doi.org/10.1074/jbc.M110.157362

Burdziak, C., Alonso-Curbelo, D., Walle, T., Reyes, J., Barriga, F. M., Haviv, D., Xie, Y., Zhao, Z., Zhao, C. J., Chen, H. A., Chaudhary, O., Masilionis, I., Choo, Z. N., Gao, V., Luan, W., Wuest, A., Ho, Y. J., Wei, Y., Quail, D. F., … Pe'er, D. (2023). Epigenetic plasticity cooperates with cell-cell interactions to direct pancreatic tumorigenesis. In *Science (New York, N.Y.)* (Vol. 380, Issue 6645, p. eadd5327). https://doi.org/10.1126/science.add5327

Burris, H. A., Moore, M. J., Andersen, J., Green, M. R., Rothenberg, M. L., Modiano, M. R., Cripps, M. C., Portenoy, R. K., Storniolo, A. M., Tarassoff, P., Nelson, R., Dorr, F. A., Stephens, C. D., & Von Hoff, D. D. (1997). Improvements in survival and

clinical benefit with gemcitabine as first- line therapy for patients with advanced pancreas cancer: A randomized trial. *Journal of Clinical Oncology*. https://doi.org/10.1200/JCO.1997.15.6.2403

Caligiuri, G., & Tuveson, D. A. (2023). Activated fibroblasts in cancer: Perspectives and challenges. In *Cancer Cell*. https://doi.org/10.1016/j.ccell.2023.02.015

Candido, J. B., Morton, J. P., Bailey, P., Campbell, A. D., Karim, S. A., Jamieson, T., Lapienyte, L., Gopinathan, A., Clark, W., McGhee, E. J., Wang, J., Escorcio-Correia, M., Zollinger, R., Roshani, R., Drew, L., Rishi, L., Arkell, R., Evans, T. R. J., Nixon, C., … Sansom, O. J. (2018). CSF1R+ Macrophages Sustain Pancreatic Tumor Growth through T Cell Suppression and Maintenance of Key Gene Programs that Define the Squamous Subtype. *Cell Reports*. https://doi.org/10.1016/j.celrep.2018.03.131

Caronni, N., La Terza, F., Vittoria, F. M., Barbiera, G., Mezzanzanica, L., Cuzzola, V., Barresi, S., Pellegatta, M., Canevazzi, P., Dunsmore, G., Leonardi, C., Montaldo, E., Lusito, E., Dugnani, E., Citro, A., Ng, M. S. F., Schiavo Lena, M., Drago, D., Andolfo, A., … Ostuni, R. (2023). IL-1β+ macrophages fuel pathogenic inflammation in pancreatic cancer. *Nature*, *623*(7986), 415–422. https://doi.org/10.1038/s41586-023-06685-2

Caronni, N., Montaldo, E., Mezzanzanica, L., Cilenti, F., Genua, M., & Ostuni, R. (2021). Determinants, mechanisms, and functional outcomes of myeloid cell diversity in cancer. In *Immunological Reviews*. https://doi.org/10.1111/imr.12944

Carpenter, E. S., Elhossiny, A. M., Kadiyala, P., Li, J., McGue, J., Griffith, B. D., Zhang, Y., Edwards, J., Nelson, S., Lima, F., Donahue, K. L., Du, W., Bischoff, A. C., Alomari, D., Watkoske, H. R., Mattea, M., The, S., Espinoza, C. E., Barrett, M., … Pasca di Magliano, M. (2023). Analysis of Donor Pancreata Defines the Transcriptomic Signature and Microenvironment of Early Neoplastic Lesions. *Cancer Discovery*, *13*(6), 1324–1345. https://doi.org/10.1158/2159-8290.CD-23-0013

Casanova-Acebes, M., Dalla, E., Leader, A. M., LeBerichel, J., Nikolic, J., Morales, B. M., Brown, M., Chang, C., Troncoso, L., Chen, S. T., Sastre-Perona, A., Park, M. D., Tabachnikova, A., Dhainaut, M., Hamon, P., Maier, B., Sawai, C. M., Agulló-Pascual, E., Schober, M., … Merad, M. (2021). Tissue-resident macrophages

provide a pro-tumorigenic niche to early NSCLC cells. *Nature*. https://doi.org/10.1038/s41586-021-03651-8

Cassetta, L., & Pollard, J. W. (2018). Targeting macrophages: Therapeutic approaches in cancer. In *Nature Reviews Drug Discovery*. https://doi.org/10.1038/nrd.2018.169

Cha, R. S., Thilly, W. G., & Zarbl, H. (1994). N-nitroso-N-methylurea-induced rat mammary tumors arise from cells with preexisting oncogenic Hras1 gene mutations. *Proceedings of the National Academy of Sciences of the United States of America*. https://doi.org/10.1073/pnas.91.9.3749

Chakarov, S., Lim, H. Y., Tan, L., Lim, S. Y., See, P., Lum, J., Zhang, X. M., Foo, S., Nakamizo, S., Duan, K., Kong, W. T., Gentek, R., Balachander, A., Carbajo, D., Bleriot, C., Malleret, B., Tam, J. K. C., Baig, S., Shabeer, M., … Ginhoux, F. (2019). Two distinct interstitial macrophage populations coexist across tissues in specific subtissular niches. *Science*. https://doi.org/10.1126/science.aau0964

Cheng, H., Huang, H., Guo, Z., Chang, Y., & Li, Z. (2021). Role of prostaglandin E2 in tissue repair and regeneration. In *Theranostics*. https://doi.org/10.7150/thno.63396

Cheng, S., Li, Z., Gao, R., Xing, B., Gao, Y., Yang, Y., Qin, S., Zhang, L., Ouyang, H., Du, P., Jiang, L., Zhang, B., Yang, Y., Wang, X., Ren, X., Bei, J. X., Hu, X., Bu, Z., Ji, J., & Zhang, Z. (2021). A pan-cancer single-cell transcriptional atlas of tumor infiltrating myeloid cells. *Cell*. https://doi.org/10.1016/j.cell.2021.01.010

Christofides, A., Strauss, L., Yeo, A., Cao, C., Charest, A., & Boussiotis, V. A. (2022). The complex role of tumor-infiltrating macrophages. In *Nature Immunology*. https://doi.org/10.1038/s41590-022-01267-2

Chu, C., Artis, D., & Chiu, I. M. (2020). Neuro-immune Interactions in the Tissues. In *Immunity*. https://doi.org/10.1016/j.immuni.2020.02.017

Cilenti, F., Barbiera, G., Caronni, N., Iodice, D., Montaldo, E., Barresi, S., Lusito, E., Cuzzola, V., Vittoria, F. M., Mezzanzanica, L., Miotto, P., Di Lucia, P., Lazarevic, D., Cirillo, D. M., Iannacone, M., Genua, M., & Ostuni, R. (2021). A PGE2-MEF2A axis enables context-dependent control of inflammatory gene expression. *Immunity*. https://doi.org/10.1016/j.immuni.2021.05.016

Colaprico, A., Silva, T. C., Olsen, C., Garofano, L., Cava, C., Garolini, D., Sabedot, T. S., Malta, T. M., Pagnotta, S. M., Castiglioni, I., Ceccarelli, M., Bontempi, G., & Noushmehr, H. (2016). TCGAbiolinks: An R/Bioconductor package for integrative

analysis of TCGA data. *Nucleic Acids Research*. https://doi.org/10.1093/nar/gkv1507

Collins, M. A., Bednar, F., Zhang, Y., Brisset, J. C., Galbán, S., Galbán, C. J., Rakshit, S., Flannagan, K. S., Adsay, N. V., & Pasca Di Magliano, M. (2012). Oncogenic Kras is required for both the initiation and maintenance of pancreatic cancer in mice. *Journal of Clinical Investigation*. https://doi.org/10.1172/JCI59227

Collins, M. A., Brisset, J. C., Zhang, Y., Bednar, F., Pierre, J., Heist, K. A., Galbán, C. J., Galbán, S., & di Magliano, M. P. (2012). Metastatic Pancreatic Cancer Is Dependent on Oncogenic Kras in Mice. *PLoS ONE*. https://doi.org/10.1371/journal.pone.0049707

Collisson, E. A., Bailey, P., Chang, D. K., & Biankin, A. V. (2019). Molecular subtypes of pancreatic cancer. In *Nature Reviews Gastroenterology and Hepatology*. https://doi.org/10.1038/s41575-019-0109-y

Collisson, E. A., Sadanandam, A., Olson, P., Gibb, W. J., Truitt, M., Gu, S., Cooc, J., Weinkle, J., Kim, G. E., Jakkula, L., Feiler, H. S., Ko, A. H., Olshen, A. B., Danenberg, K. L., Tempero, M. A., Spellman, P. T., Hanahan, D., & Gray, J. W. (2011). Subtypes of pancreatic ductal adenocarcinoma and their differing responses to therapy. *Nature Medicine*. https://doi.org/10.1038/nm.2344

Conroy, T., Desseigne, F., Ychou, M., Bouché, O., Guimbaud, R., Bécouarn, Y., Adenis, A., Raoul, J.-L., Gourgou-Bourgade, S., de la Fouchardière, C., Bennouna, J., Bachet, J.-B., Khemissa-Akouz, F., Péré-Vergé, D., Delbaldo, C., Assenat, E., Chauffert, B., Michel, P., Montoto-Grillot, C., & Ducreux, M. (2011). FOLFIRINOX versus Gemcitabine for Metastatic Pancreatic Cancer. *New England Journal of Medicine*. https://doi.org/10.1056/nejmoa1011923

Corbett, T. H., Roberts, B. J., Leopold, W. R., Peckham, J. C., Wilkoff, L. J., Griswold, D. P., & Schabel, F. M. (1984). Induction and chemotherapeutic response of two transplantable ductal adenocarcinomas of the pancreas in C57BL/6 mice. *Cancer Research*.

Coulombe, F., Jaworska, J., Verway, M., Tzelepis, F., Massoud, A., Gillard, J., Wong, G., Kobinger, G., Xing, Z., Couture, C., Joubert, P., Fritz, J. H., Powell, W. S., & Divangahi, M. (2014). Targeted prostaglandin E2 inhibition enhances antiviral immunity through induction of type I interferon and apoptosis in macrophages.

Immunity. https://doi.org/10.1016/j.immuni.2014.02.013

Coussens, L. M., Zitvogel, L., & Palucka, A. K. (2013). Neutralizing tumor-promoting chronic inflammation: A magic bullet? In *Science*. https://doi.org/10.1126/science.1232227

Cox, C. B., Storm, E. E., Kapoor, V. N., Chavarria-Smith, J., Lin, D. L., Wang, L., Li, Y., Kljavin, N., Ota, N., Bainbridge, T. W., Anderson, K., Roose-Girma, M., Warming, S., Arron, J. R., Turley, S. J., De Sauvage, F. J., & Van Lookeren Campagne, M. (2021). IL-1R1-dependent signaling coordinates epithelial regeneration in response to intestinal damage. *Science Immunology*. https://doi.org/10.1126/sciimmunol.abe8856

Daley, D., Mani, V. R., Mohan, N., Akkad, N., Balasubramania Pandian, G. S. D., Savadkar, S., Lee, K. B., Torres-Hernandez, A., Aykut, B., Diskin, B., Wang, W., Farooq, M. S., Mahmud, A. I., Werba, G., Morales, E. J., Lall, S., Wadowski, B. J., Rubin, A. G., Berman, M. E., … Miller, G. (2017). NLRP3 signaling drives macrophage-induced adaptive immune suppression in pancreatic carcinoma. *Journal of Experimental Medicine*. https://doi.org/10.1084/jem.20161707

Daley, D., Zambirinis, C. P., Seifert, L., Akkad, N., Mohan, N., Werba, G., Barilla, R., Torres-Hernandez, A., Hundeyin, M., Mani, V. R. K., Avanzi, A., Tippens, D., Narayanan, R., Jang, J. E., Newman, E., Pillarisetty, V. G., Dustin, M. L., Bar-Sagi, D., Hajdu, C., & Miller, G. (2016). γδ T Cells Support Pancreatic Oncogenesis by Restraining αβ T Cell Activation. *Cell*. https://doi.org/10.1016/j.cell.2016.07.046

Das, S., Shapiro, B., Vucic, E. A., Vogt, S., & Bar-Sagi, D. (2020). Tumor cell-derived IL1β promotes desmoplasia and immune suppression in pancreatic cancer. *Cancer Research*. https://doi.org/10.1158/0008-5472.CAN-19-2080

Del Poggetto, E., Ho, I. L., Balestrieri, C., Yen, E. Y., Zhang, S., Citron, F., Shah, R., Corti, D., Diaferia, G. R., Li, C. Y., Loponte, S., Carbone, F., Hayakawa, Y., Valenti, G., Jiang, S., Sapio, L., Jiang, H., Dey, P., Gao, S., … Viale, A. (2021). Epithelial memory of inflammation limits tissue damage while promoting pancreatic tumorigenesis. *Science*. https://doi.org/10.1126/science.abj0486

DeNardo, D. G., & Ruffell, B. (2019). Macrophages as regulators of tumour immunity and immunotherapy. In *Nature Reviews Immunology*. https://doi.org/10.1038/s41577-019-0127-6

Dey, P., Li, J., Zhang, J., Chaurasiya, S., Strom, A., Wang, H., Liao, W. T., Cavallaro, F., Denz, P., Bernard, V., Yen, E. Y., Genovese, G., Gulhati, P., Liu, J., Chakravarti, D., Deng, P., Zhang, T., Carbone, F., Chang, Q., … DePinho, R. A. (2020). Oncogenic KRAS-driven metabolic reprogramming in pancreatic cancer cells utilizes cytokines from the tumor microenvironment. *Cancer Discovery*. https://doi.org/10.1158/2159-8290.CD-19-0297

Dick, S. A., Wong, A., Hamidzada, H., Nejat, S., Nechanitzky, R., Vohra, S., Mueller, B., Zaman, R., Kantores, C., Aronoff, L., Momen, A., Nechanitzky, D., Li, W. Y., Ramachandran, P., Crome, S. Q., Becher, B., Cybulsky, M. I., Billia, F., Keshavjee, S., … Epelman, S. (2022). Three tissue resident macrophage subsets coexist across organs with conserved origins and life cycles. *Science Immunology*. https://doi.org/10.1126/sciimmunol.abf7777

Dmitrieva-Posocco, O., Dzutsev, A., Posocco, D. F., Hou, V., Yuan, W., Thovarai, V., Mufazalov, I. A., Gunzer, M., Shilovskiy, I. P., Khaitov, M. R., Trinchieri, G., Waisman, A., & Grivennikov, S. I. (2019). Cell-Type-Specific Responses to Interleukin-1 Control Microbial Invasion and Tumor-Elicited Inflammation in Colorectal Cancer. *Immunity*. https://doi.org/10.1016/j.immuni.2018.11.015

Dobin, A., Davis, C. A., Schlesinger, F., Drenkow, J., Zaleski, C., Jha, S., Batut, P., Chaisson, M., & Gingeras, T. R. (2013). STAR: Ultrafast universal RNA-seq aligner. *Bioinformatics*. https://doi.org/10.1093/bioinformatics/bts635

DuBois, R. N., Abramson, S. B., Crofford, L., Gupta, R. A., Simon, L. S., Putte, L. B. A., & Lipsky, P. E. (1998). Cyclooxygenase in biology and disease. *The FASEB Journal*. https://doi.org/10.1096/fasebj.12.12.1063

Dudziak, D., Kamphorst, A. O., Heidkamp, G. F., Buchholz, V. R., Trumpfheller, C., Yamazaki, S., Cheong, C., Liu, K., Lee, H. W., Chae, G. P., Steinman, R. M., & Nussenzweig, M. C. (2007). Differential antigen processing by dendritic cell subsets in vivo. *Science*. https://doi.org/10.1126/science.1136080

Durinck, S., Spellman, P. T., Birney, E., & Huber, W. (2009). Mapping identifiers for the integration of genomic datasets with the R/ Bioconductor package biomaRt. *Nature Protocols*. https://doi.org/10.1038/nprot.2009.97

Dvorak, H. F. (1986). Tumors: wounds that do not heal. Similarities between tumor stroma generation and wound healing. *The New England Journal of Medicine*.

https://doi.org/10.1056/NEJM198612253152606

Egeblad, M., Rasch, M. G., & Weaver, V. M. (2010). Dynamic interplay between the collagen scaffold and tumor evolution. In *Current Opinion in Cell Biology*. https://doi.org/10.1016/j.ceb.2010.08.015

Elyada, E., Bolisetty, M., Laise, P., Flynn, W. F., Courtois, E. T., Burkhart, R. A., Teinor, J. A., Belleau, P., Biffi, G., Lucito, M. S., Sivajothi, S., Armstrong, T. D., Engle, D. D., Yu, K. H., Hao, Y., Wolfgang, C. L., Park, Y., Preall, J., Jaffee, E. M., … Tuveson, D. A. (2019). Cross-species single-cell analysis of pancreatic ductal adenocarcinoma reveals antigen-presenting cancer-associated fibroblasts. In *Cancer Discovery*. https://doi.org/10.1158/2159-8290.CD-19-0094

Escobar-Hoyos, L. F., Penson, A., Kannan, R., Cho, H., Pan, C. H., Singh, R. K., Apken, L. H., Hobbs, G. A., Luo, R., Lecomte, N., Babu, S., Pan, F. C., Alonso-Curbelo, D., Morris, J. P., Askan, G., Grbovic-Huezo, O., Ogrodowski, P., Bermeo, J., Saglimbeni, J., … Leach, S. D. (2020). Altered RNA Splicing by Mutant p53 Activates Oncogenic RAS Signaling in Pancreatic Cancer. *Cancer Cell*. https://doi.org/10.1016/j.ccell.2020.05.010

Ferris, S. T., Durai, V., Wu, R., Theisen, D. J., Ward, J. P., Bern, M. D., Davidson, J. T., Bagadia, P., Liu, T., Briseño, C. G., Li, L., Gillanders, W. E., Wu, G. F., Yokoyama, W. M., Murphy, T. L., Schreiber, R. D., & Murphy, K. M. (2020). cDC1 prime and are licensed by CD4+ T cells to induce anti-tumour immunity. *Nature*. https://doi.org/10.1038/s41586-020-2611-3

Fujikura, K., Hosoda, W., Felsenstein, M., Song, Q., Reiter, J. G., Zheng, L., Beleva Guthrie, V., Rincon, N., Dal Molin, M., Dudley, J., Cohen, J. D., Wang, P., Fischer, C. G., Braxton, A. M., Noë, M., Jongepier, M., Fernández-Del Castillo, C., Mino-Kenudson, M., Schmidt, C. M., … Wood, L. D. (2021). Multiregion whole-exome sequencing of intraductal papillary mucinous neoplasms reveals frequent somatic KLF4 mutations predominantly in low-grade regions. *Gut*. https://doi.org/10.1136/gutjnl-2020-321217

Fukunaga, A., Miyamoto, M., Cho, Y., Murakami, S., Kawarada, Y., Oshikiri, T., Kato, K., Kurokawa, T., Suzuoki, M., Nakakubo, Y., Hiraoka, K., Itoh, T., Morikawa, T., Okushiba, S., Kondo, S., & Hiroyuki, K. (2004). CD8+tumor-infiltrating lymphocytes together with CD4+tumor-infiltrating lymphocytes and dendritic cells

improve the prognosis of patients with pancreatic adenocarcinoma. *Pancreas*. https://doi.org/10.1097/00006676-200401000-00023

Funk, C. D. (2001). Prostaglandins and leukotrienes: Advances in eicosanoid biology. In *Science*. https://doi.org/10.1126/science.294.5548.1871

Gao, R., Bai, S., Henderson, Y. C., Lin, Y., Schalck, A., Yan, Y., Kumar, T., Hu, M., Sei, E., Davis, A., Wang, F., Shaitelman, S. F., Wang, J. R., Chen, K., Moulder, S., Lai, S. Y., & Navin, N. E. (2021). Delineating copy number and clonal substructure in human tumors from single-cell transcriptomes. *Nature Biotechnology*. https://doi.org/10.1038/s41587-020-00795-2

Garber, M., Yosef, N., Goren, A., Raychowdhury, R., Thielke, A., Guttman, M., Robinson, J., Minie, B., Chevrier, N., Itzhaki, Z., Blecher-Gonen, R., Bornstein, C., Amann-Zalcenstein, D., Weiner, A., Friedrich, D., Meldrim, J., Ram, O., Cheng, C., Gnirke, A., … Amit, I. (2012). A High-Throughput Chromatin Immunoprecipitation Approach Reveals Principles of Dynamic Gene Regulation in Mammals. *Molecular Cell*. https://doi.org/10.1016/j.molcel.2012.07.030

Garlanda, C., & Mantovani, A. (2021). Interleukin-1 in tumor progression, therapy, and prevention. *Cancer Cell*. https://doi.org/10.1016/j.ccell.2021.04.011

Garris, C. S., Arlauckas, S. P., Kohler, R. H., Trefny, M. P., Garren, S., Piot, C., Engblom, C., Pfirschke, C., Siwicki, M., Gungabeesoon, J., Freeman, G. J., Warren, S. E., Ong, S. F., Browning, E., Twitty, C. G., Pierce, R. H., Le, M. H., Algazi, A. P., Daud, A. I., … Pittet, M. J. (2018). Successful Anti-PD-1 Cancer Immunotherapy Requires T Cell-Dendritic Cell Crosstalk Involving the Cytokines IFN-γ and IL-12. *Immunity*. https://doi.org/10.1016/j.immuni.2018.09.024

Gautiar, E. L., Shay, T., Miller, J., Greter, M., Jakubzick, C., Ivanov, S., Helft, J., Chow, A., Elpek, K. G., Gordonov, S., Mazloom, A. R., Ma'Ayan, A., Chua, W. J., Hansen, T. H., Turley, S. J., Merad, M., Randolph, G. J., Best, A. J., Knell, J., … Benoist, C. (2012). Gene-expression profiles and transcriptional regulatory pathways that underlie the identity and diversity of mouse tissue macrophages. *Nature Immunology*. https://doi.org/10.1038/ni.2419

Gautier, E. L., Ivanov, S., Williams, J. W., Huang, S. C. C., Marcelin, G., Fairfax, K., Wang, P. L., Francis, J. S., Leone, P., Wilson, D. B., Artyomov, M. N., Pearce, E. J., & Randolph, G. J. (2014). Gata6 regulates aspartoacylase expression in resident

peritoneal macrophages and controls their survival. *Journal of Experimental Medicine*. https://doi.org/10.1084/jem.20140570

Germain, P. L., Lun, A., Macnair, W., & Robinson, M. D. (2021). Doublet identification in single-cell sequencing data using scDblFinder. *F1000Research*. https://doi.org/10.12688/f1000research.73600.1

Ghisletti, S., Barozzi, I., Mietton, F., Polletti, S., De Santa, F., Venturini, E., Gregory, L., Lonie, L., Chew, A., Wei, C. L., Ragoussis, J., & Natoli, G. (2010). Identification and Characterization of Enhancers Controlling the Inflammatory Gene Expression Program in Macrophages. *Immunity*. https://doi.org/10.1016/j.immuni.2010.02.008

Ginhoux, F., Greter, M., Leboeuf, M., Nandi, S., See, P., Gokhan, S., Mehler, M. F., Conway, S. J., Ng, L. G., Stanley, E. R., Samokhvalov, I. M., & Merad, M. (2010). Fate mapping analysis reveals that adult microglia derive from primitive macrophages. *Science*. https://doi.org/10.1126/science.1194637

Ginhoux, F., & Guilliams, M. (2016). Tissue-Resident Macrophage Ontogeny and Homeostasis. In *Immunity*. https://doi.org/10.1016/j.immuni.2016.02.024

Glass, C. K., & Natoli, G. (2016). Molecular control of activation and priming in macrophages. In *Nature Immunology*. https://doi.org/10.1038/ni.3306

Golovko, M. Y., & Murphy, E. J. (2008). An improved LC-MS/MS procedure for brain prostanoid analysis using brain fixation with head-focused microwave irradiation and liquid-liquid extraction. *Journal of Lipid Research*. https://doi.org/10.1194/jlr.D700030-JLR200

Gomez Perdiguero, E., Klapproth, K., Schulz, C., Busch, K., Azzoni, E., Crozet, L., Garner, H., Trouillet, C., De Bruijn, M. F., Geissmann, F., & Rodewald, H. R. (2015). Tissue-resident macrophages originate from yolk-sac-derived erythro-myeloid progenitors. *Nature*. https://doi.org/10.1038/nature13989

Gong, Z., Li, Q., Shi, J., Wei, J., Li, P., Chang, C. H., Shultz, L. D., & Ren, G. (2022). Lung fibroblasts facilitate pre-metastatic niche formation by remodeling the local immune microenvironment. *Immunity*. https://doi.org/10.1016/j.immuni.2022.07.001

Groot, V. P., Rezaee, N., Wu, W., Cameron, J. L., Fishman, E. K., Hruban, R. H., Weiss, M. J., Zheng, L., Wolfgang, C. L., & He, J. (2018). Patterns, Timing, and Predictors of Recurrence Following Pancreatectomy for Pancreatic Ductal Adenocarcinoma.

Annals of Surgery. https://doi.org/10.1097/SLA.0000000000002234

Grünwald, B. T., Devisme, A., Andrieux, G., Vyas, F., Aliar, K., McCloskey, C. W., Macklin, A., Jang, G. H., Denroche, R., Romero, J. M., Bavi, P., Bronsert, P., Notta, F., O'Kane, G., Wilson, J., Knox, J., Tamblyn, L., Udaskin, M., Radulovich, N., … Khokha, R. (2021). Spatially confined sub-tumor microenvironments in pancreatic cancer. *Cell*. https://doi.org/10.1016/j.cell.2021.09.022

Gschwend, J., Sherman, S. P. M., Ridder, F., Feng, X., Liang, H. E., Locksley, R. M., Becher, B., & Schneider, C. (2021). Alveolar macrophages rely on GM-CSF from alveolar epithelial type 2 cells before and after birth. *Journal of Experimental Medicine*. https://doi.org/10.1084/jem.20210745

Guerra, C., Schuhmacher, A. J., Cañamero, M., Grippo, P. J., Verdaguer, L., Pérez-Gallego, L., Dubus, P., Sandgren, E. P., & Barbacid, M. (2007). Chronic Pancreatitis Is Essential for Induction of Pancreatic Ductal Adenocarcinoma by K-Ras Oncogenes in Adult Mice. *Cancer Cell*. https://doi.org/10.1016/j.ccr.2007.01.012

Guilliams, M., Bonnardel, J., Haest, B., Vanderborght, B., Wagner, C., Remmerie, A., Bujko, A., Martens, L., Thoné, T., Browaeys, R., De Ponti, F. F., Vanneste, B., Zwicker, C., Svedberg, F. R., Vanhalewyn, T., Gonçalves, A., Lippens, S., Devriendt, B., Cox, E., … Scott, C. L. (2022). Spatial proteogenomics reveals distinct and evolutionarily conserved hepatic macrophage niches. *Cell*. https://doi.org/10.1016/j.cell.2021.12.018

Guilliams, M., & Scott, C. L. (2017). Does niche competition determine the origin of tissue-resident macrophages? In *Nature Reviews Immunology*. https://doi.org/10.1038/nri.2017.42

Haghverdi, L., Lun, A. T. L., Morgan, M. D., & Marioni, J. C. (2018). Batch effects in single-cell RNA-sequencing data are corrected by matching mutual nearest neighbors. *Nature Biotechnology*. https://doi.org/10.1038/nbt.4091

Hahsler, M., Piekenbrock, M., & Doran, D. (2019). Dbscan: Fast density-based clustering with R. *Journal of Statistical Software*. https://doi.org/10.18637/jss.v091.i01

Halbrook, C. J., Lyssiotis, C. A., Pasca di Magliano, M., & Maitra, A. (2023). Pancreatic cancer: Advances and challenges. *Cell*, *186*(8), 1729–1754. https://doi.org/10.1016/j.cell.2023.02.014

Haldar, M., Kohyama, M., So, A. Y. L., Kc, W., Wu, X., Briseño, C. G., Satpathy, A. T.,

Kretzer, N. M., Arase, H., Rajasekaran, N. S., Wang, L., Egawa, T., Igarashi, K., Baltimore, D., Murphy, T. L., & Murphy, K. M. (2014). Heme-mediated SPI-C induction promotes monocyte differentiation into iron-recycling macrophages. *Cell*. https://doi.org/10.1016/j.cell.2014.01.069

Hallin, J., Bowcut, V., Calinisan, A., Briere, D. M., Hargis, L., Engstrom, L. D., Laguer, J., Medwid, J., Vanderpool, D., Lifset, E., Trinh, D., Hoffman, N., Wang, X., David Lawson, J., Gunn, R. J., Smith, C. R., Thomas, N. C., Martinson, M., Bergstrom, A., … Christensen, J. G. (2022). Anti-tumor efficacy of a potent and selective non-covalent KRASG12D inhibitor. *Nature Medicine*. https://doi.org/10.1038/s41591-022-02007-7

Hanahan, D. (2022). Hallmarks of Cancer: New Dimensions. In *Cancer Discovery*. https://doi.org/10.1158/2159-8290.CD-21-1059

Hegde, S., Krisnawan, V. E., Herzog, B. H., Zuo, C., Breden, M. A., Knolhoff, B. L., Hogg, G. D., Tang, J. P., Baer, J. M., Mpoy, C., Lee, K. B., Alexander, K. A., Rogers, B. E., Murphy, K. M., Hawkins, W. G., Fields, R. C., DeSelm, C. J., Schwarz, J. K., & DeNardo, D. G. (2020). Dendritic Cell Paucity Leads to Dysfunctional Immune Surveillance in Pancreatic Cancer. *Cancer Cell*. https://doi.org/10.1016/j.ccell.2020.02.008

Heinz, S., Benner, C., Spann, N., Bertolino, E., Lin, Y. C., Laslo, P., Cheng, J. X., Murre, C., Singh, H., & Glass, C. K. (2010). Simple Combinations of Lineage-Determining Transcription Factors Prime cis-Regulatory Elements Required for Macrophage and B Cell Identities. *Molecular Cell*. https://doi.org/10.1016/j.molcel.2010.05.004

Heinz, S., & Glass, C. K. (2012). Roles of lineage-determining transcription factors in establishing open chromatin: Lessons from high-throughput studies. *Current Topics in Microbiology and Immunology*. https://doi.org/10.1007/82_2011_142

Henderson, N. C., Rieder, F., & Wynn, T. A. (2020). Fibrosis: from mechanisms to medicines. In *Nature*. https://doi.org/10.1038/s41586-020-2938-9

Hessmann, E., Buchholz, S. M., Demir, I. E., Singh, S. K., Gress, T. M., Ellenrieder, V., Neesse, A., Hessmann, E., Buchholz, S. M., Demir, I. E., Singh, S. K., Gress, T. M., Ellenrieder, V., & Neesse, A. (2020). Microenvironmental determinants of pancreatic cancer. In *Physiological Reviews*. https://doi.org/10.1152/physrev.00042.2019

Hill, W., Lim, E. L., Weeden, C. E., Lee, C., Augustine, M., Chen, K., Kuan, F. C., Marongiu, F., Evans, E. J., Moore, D. A., Rodrigues, F. S., Pich, O., Bakker, B., Cha, H., Myers, R., van Maldegem, F., Boumelha, J., Veeriah, S., Rowan, A., … Swanton, C. (2023). Lung adenocarcinoma promotion by air pollutants. *Nature*, *616*(7955), 159–167. https://doi.org/10.1038/s41586-023-05874-3

Hingorani, S. R., Petricoin, E. F., Maitra, A., Rajapakse, V., King, C., Jacobetz, M. A., Ross, S., Conrads, T. P., Veenstra, T. D., Hitt, B. A., Kawaguchi, Y., Johann, D., Liotta, L. A., Crawford, H. C., Putt, M. E., Jacks, T., Wright, C. V. E., Hruban, R. H., Lowy, A. M., & Tuveson, D. A. (2003). Preinvasive and invasive ductal pancreatic cancer and its early detection in the mouse. *Cancer Cell*. https://doi.org/10.1016/S1535-6108(03)00309-X

Hingorani, S. R., Wang, L., Multani, A. S., Combs, C., Deramaudt, T. B., Hruban, R. H., Rustgi, A. K., Chang, S., & Tuveson, D. A. (2005). Trp53R172H and KrasG12D cooperate to promote chromosomal instability and widely metastatic pancreatic ductal adenocarcinoma in mice. *Cancer Cell*. https://doi.org/10.1016/j.ccr.2005.04.023

Hoeffel, G., Chen, J., Lavin, Y., Low, D., Almeida, F. F., See, P., Beaudin, A. E., Lum, J., Low, I., Forsberg, E. C., Poidinger, M., Zolezzi, F., Larbi, A., Ng, L. G., Chan, J. K. Y., Greter, M., Becher, B., Samokhvalov, I. M., Merad, M., & Ginhoux, F. (2015). C-Myb+ Erythro-Myeloid Progenitor-Derived Fetal Monocytes Give Rise to Adult Tissue-Resident Macrophages. *Immunity*. https://doi.org/10.1016/j.immuni.2015.03.011

Hofmann, M. H., Gerlach, D., Misale, S., Petronczki, M., & Kraut, N. (2022). Expanding the Reach of Precision Oncology by Drugging All KRAS Mutants. In *Cancer Discovery*. https://doi.org/10.1158/2159-8290.CD-21-1331

Hoggatt, J., Singh, P., Sampath, J., & Pelus, L. M. (2009). Prostaglandin E2 enhances hematopoietic stem cell homing, survival, and proliferation. *Blood*. https://doi.org/10.1182/blood-2009-01-201335

Huang, H., Wang, Z., Zhang, Y., Pradhan, R. N., Ganguly, D., Chandra, R., Murimwa, G., Wright, S., Gu, X., Maddipati, R., Müller, S., Turley, S. J., & Brekken, R. A. (2022). Mesothelial cell-derived antigen-presenting cancer-associated fibroblasts induce expansion of regulatory T cells in pancreatic cancer. *Cancer Cell*.

https://doi.org/10.1016/j.ccell.2022.04.011

Hutton, C., Heider, F., Blanco-Gomez, A., Banyard, A., Kononov, A., Zhang, X., Karim, S., Paulus-Hock, V., Watt, D., Steele, N., Kemp, S., Hogg, E. K. J., Kelly, J., Jackstadt, R. F., Lopes, F., Menotti, M., Chisholm, L., Lamarca, A., Valle, J., … Jørgensen, C. (2021). Single-cell analysis defines a pancreatic fibroblast lineage that supports anti-tumor immunity. *Cancer Cell*. https://doi.org/10.1016/j.ccell.2021.06.017

Ino, Y., Yamazaki-Itoh, R., Shimada, K., Iwasaki, M., Kosuge, T., Kanai, Y., & Hiraoka, N. (2013). Immune cell infiltration as an indicator of the immune microenvironment of pancreatic cancer. *British Journal of Cancer*. https://doi.org/10.1038/bjc.2013.32

Jacobetz, M. A., Chan, D. S., Neesse, A., Bapiro, T. E., Cook, N., Frese, K. K., Feig, C., Nakagawa, T., Caldwell, M. E., Zecchini, H. I., Lolkema, M. P., Jiang, P., Kultti, A., Thompson, C. B., Maneval, D. C., Jodrell, D. I., Frost, G. I., Shepard, H. M., Skepper, J. N., & Tuveson, D. A. (2013). Hyaluronan impairs vascular function and drug delivery in a mouse model of pancreatic cancer. *Gut*. https://doi.org/10.1136/gutjnl-2012-302529

Jänne, P. A., Riely, G. J., Gadgeel, S. M., Heist, R. S., Ou, S.-H. I., Pacheco, J. M., Johnson, M. L., Sabari, J. K., Leventakos, K., Yau, E., Bazhenova, L., Negrao, M. V., Pennell, N. A., Zhang, J., Anderes, K., Der-Torossian, H., Kheoh, T., Velastegui, K., Yan, X., … Spira, A. I. (2022). Adagrasib in Non–Small-Cell Lung Cancer Harboring a KRAS G12C Mutation . *New England Journal of Medicine*. https://doi.org/10.1056/nejmoa2204619

Kamei, D., Yamakawa, K., Takegoshi, Y., Mikami-Nakanishi, M., Nakatani, Y., Oh-Ishi, S., Yasui, H., Azuma, Y., Hirasawa, N., Ohuchi, K., Kawaguchi, H., Ishikawa, Y., Ishii, T., Uematsu, S., Akira, S., Murakami, M., & Kudo, I. (2004). Reduced pain hypersensitivity and inflammation in mice lacking microsomal prostaglandin E synthase-1. *Journal of Biological Chemistry*. https://doi.org/10.1074/jbc.M400199200

Kanda, M., Matthaei, H., Wu, J., Hong, S. M., Yu, J., Borges, M., Hruban, R. H., Maitra, A., Kinzler, K., Vogelstein, B., & Goggins, M. (2012). Presence of somatic mutations in most early-stage pancreatic intraepithelial neoplasia. *Gastroenterology*. https://doi.org/10.1053/j.gastro.2011.12.042

Kapoor, A., Yao, W., Ying, H., Hua, S., Liewen, A., Wang, Q., Zhong, Y., Wu, C. J., Sadanandam, A., Hu, B., Chang, Q., Chu, G. C., Al-Khalil, R., Jiang, S., Xia, H., Fletcher-Sananikone, E., Lim, C., Horwitz, G. I., Viale, A., … Depinho, R. A. (2014). Yap1 activation enables bypass of oncogenic KRAS addiction in pancreatic cancer. *Cell*. https://doi.org/10.1016/j.cell.2014.06.003

Kemp, S. B., Cheng, N., Markosyan, N., Sor, R., Kim, I. K., Hallin, J., Shoush, J., Quinones, L., Brown, N. V., Bassett, J. B., Joshi, N., Yuan, S., Smith, M., Vostrejs, W. P., Perez-Vale, K. Z., Kahn, B., Mo, F., Donahue, T. R., Radu, C. G., … Stanger, B. Z. (2023). Efficacy of a Small-Molecule Inhibitor of KrasG12D in Immunocompetent Models of Pancreatic Cancer. *Cancer Discovery*. https://doi.org/10.1158/2159-8290.CD-22-1066

Kim, D., Xue, J. Y., & Lito, P. (2020). Targeting KRAS(G12C): From Inhibitory Mechanism to Modulation of Antitumor Effects in Patients. In *Cell*. https://doi.org/10.1016/j.cell.2020.09.044

Klichinsky, M., Ruella, M., Shestova, O., Lu, X. M., Best, A., Zeeman, M., Schmierer, M., Gabrusiewicz, K., Anderson, N. R., Petty, N. E., Cummins, K. D., Shen, F., Shan, X., Veliz, K., Blouch, K., Yashiro-Ohtani, Y., Kenderian, S. S., Kim, M. Y., O'Connor, R. S., … Gill, S. (2020). Human chimeric antigen receptor macrophages for cancer immunotherapy. *Nature Biotechnology*. https://doi.org/10.1038/s41587-020-0462-y

Kloosterman, D. J., & Akkari, L. (2023). Macrophages at the interface of the co-evolving cancer ecosystem. In *Cell*. https://doi.org/10.1016/j.cell.2023.02.020

Kohyama, M., Ise, W., Edelson, B. T., Wilker, P. R., Hildner, K., Mejia, C., Frazier, W. A., Murphy, T. L., & Murphy, K. M. (2009). Role for Spi-C in the development of red pulp macrophages and splenic iron homeostasis. *Nature*. https://doi.org/10.1038/nature07472

Korsunsky, I., Millard, N., Fan, J., Slowikowski, K., Zhang, F., Wei, K., Baglaenko, Y., Brenner, M., Loh, P. ru, & Raychaudhuri, S. (2019). Fast, sensitive and accurate integration of single-cell data with Harmony. *Nature Methods*. https://doi.org/10.1038/s41592-019-0619-0

Kourtzelis, I., Hajishengallis, G., & Chavakis, T. (2020). Phagocytosis of Apoptotic Cells in Resolution of Inflammation. In *Frontiers in Immunology*.

https://doi.org/10.3389/fimmu.2020.00553

Kurahara, H., Shinchi, H., Mataki, Y., Maemura, K., Noma, H., Kubo, F., Sakoda, M., Ueno, S., Natsugoe, S., & Takao, S. (2011). Significance of M2-polarized tumor-associated macrophage in pancreatic cancer. *Journal of Surgical Research*. https://doi.org/10.1016/j.jss.2009.05.026

La Manno, G., Soldatov, R., Zeisel, A., Braun, E., Hochgerner, H., Petukhov, V., Lidschreiber, K., Kastriti, M. E., Lönnerberg, P., Furlan, A., Fan, J., Borm, L. E., Liu, Z., van Bruggen, D., Guo, J., He, X., Barker, R., Sundström, E., Castelo-Branco, G., … Kharchenko, P. V. (2018). RNA velocity of single cells. *Nature*. https://doi.org/10.1038/s41586-018-0414-6

Labun, K., Montague, T. G., Krause, M., Torres Cleuren, Y. N., Tjeldnes, H., & Valen, E. (2019). CHOPCHOP v3: Expanding the CRISPR web toolbox beyond genome editing. *Nucleic Acids Research*. https://doi.org/10.1093/nar/gkz365

Lacobuzio-Donahue, C. A., Fu, B., Yachida, S., Luo, M., Abe, H., Henderson, C. M., Vilardell, F., Wang, Z., Keller, J. W., Banerjee, P., Herman, J. M., Cameron, J. L., Yeo, C. J., Halushka, M. K., Eshleman, J. R., Raben, M., Klein, A. P., Hruban, R. H., Hidalgo, M., & Laheru, D. (2009). DPC4 gene status of the primary carcinoma correlates with patterns of failure in patients with pancreatic cancer. *Journal of Clinical Oncology*. https://doi.org/10.1200/JCO.2008.17.7188

Lange, M., Bergen, V., Klein, M., Setty, M., Reuter, B., Bakhti, M., Lickert, H., Ansari, M., Schniering, J., Schiller, H. B., Pe'er, D., & Theis, F. J. (2022). CellRank for directed single-cell fate mapping. *Nature Methods*. https://doi.org/10.1038/s41592-021-01346-6

Lavie, D., Ben-Shmuel, A., Erez, N., & Scherz-Shouval, R. (2022). Cancer-associated fibroblasts in the single-cell era. In *Nature Cancer*. https://doi.org/10.1038/s43018-022-00411-z

Lavin, Y., Winter, D., Blecher-Gonen, R., David, E., Keren-Shaul, H., Merad, M., Jung, S., & Amit, I. (2014). Tissue-resident macrophage enhancer landscapes are shaped by the local microenvironment. *Cell*. https://doi.org/10.1016/j.cell.2014.11.018

Lee, B., Namkoong, H., Yang, Y., Huang, H., Heller, D., Szot, G. L., Davis, M. M., Husain, S. Z., Pandol, S. J., Bellin, M. D., & Habtezion, A. (2022). Single-cell sequencing unveils distinct immune microenvironments with CCR6-CCL20

crosstalk in human chronic pancreatitis. *Gut*. https://doi.org/10.1136/gutjnl-2021-324546

Lévy, P., & Rebours, V. (2019). Cystic Neoplasms of the Pancreas. *Encyclopedia of Gastroenterology, Second Edition*, 790–798. https://doi.org/10.1016/B978-0-12-801238-3.65867-1

Li, Rui, Ong, S. L., Tran, L. M., Jing, Z., Liu, B., Park, S. J., Huang, Z. L., Walser, T. C., Heinrich, E. L., Lee, G., Salehi-Rad, R., Crosson, W. P., Pagano, P. C., Paul, M. K., Xu, S., Herschman, H., Krysan, K., & Dubinett, S. (2020). Chronic IL-1β-induced inflammation regulates epithelial-to-mesenchymal transition memory phenotypes via epigenetic modifications in non-small cell lung cancer. *Scientific Reports*. https://doi.org/10.1038/s41598-019-57285-y

Li, Ruoyan, Ferdinand, J. R., Loudon, K. W., Bowyer, G. S., Laidlaw, S., Muyas, F., Mamanova, L., Neves, J. B., Bolt, L., Fasouli, E. S., Lawson, A. R. J., Young, M. D., Hooks, Y., Oliver, T. R. W., Butler, T. M., Armitage, J. N., Aho, T., Riddick, A. C. P., Gnanapragasam, V., … Mitchell, T. J. (2022). Mapping single-cell transcriptomes in the intra-tumoral and associated territories of kidney cancer. *Cancer Cell*. https://doi.org/10.1016/j.ccell.2022.11.001

Liao, Y., Smyth, G. K., & Shi, W. (2019). The R package Rsubread is easier, faster, cheaper and better for alignment and quantification of RNA sequencing reads. *Nucleic Acids Research*. https://doi.org/10.1093/nar/gkz114

Liberzon, A., Birger, C., Thorvaldsdóttir, H., Ghandi, M., Mesirov, J. P., & Tamayo, P. (2015). The Molecular Signatures Database Hallmark Gene Set Collection. *Cell Systems*. https://doi.org/10.1016/j.cels.2015.12.004

Lin, J. H., Huffman, A. P., Wattenberg, M. M., Walter, D. M., Carpenter, E. L., Feldser, D. M., Beatty, G. L., Furth, E. E., & Vonderheide, R. H. (2020). Type 1 conventional dendritic cells are systemically dysregulated early in pancreatic carcinogenesis. *Journal of Experimental Medicine*. https://doi.org/10.1084/jem.20190673

Liu, X., Hogg, G. D., Zuo, C., Borcherding, N. C., Baer, J. M., Lander, V. E., Kang, L. I., Knolhoff, B. L., Ahmad, F., Osterhout, R. E., Galkin, A. V., Bruey, J. M., Carter, L. L., Mpoy, C., Vij, K. R., Fields, R. C., Schwarz, J. K., Park, H., Gupta, V., & DeNardo, D. G. (2023). Context-dependent activation of STING-interferon signaling by CD11b agonists enhances anti-tumor immunity. *Cancer Cell*.

https://doi.org/10.1016/j.ccell.2023.04.018

Liu, Z., Gu, Y., Chakarov, S., Bleriot, C., Kwok, I., Chen, X., Shin, A., Huang, W., Dress, R. J., Dutertre, C. A., Schlitzer, A., Chen, J., Ng, L. G., Wang, H., Liu, Z., Su, B., & Ginhoux, F. (2019). Fate Mapping via Ms4a3-Expression History Traces Monocyte-Derived Cells. *Cell*. https://doi.org/10.1016/j.cell.2019.08.009

Liudahl, S. M., Betts, C. B., Sivagnanam, S., Morales-Oyarvide, V., Silva, A. Da, Yuan, C., Hwang, S., Grossblatt-Wait, A., Leis, K. R., Larson, W., Lavoie, M. B., Robinson, P., Costa, A. D., Väyrynen, S. A., Clancy, T. E., Rubinson, D. A., Link, J., Keith, D., Horton, W., … Coussens, L. M. (2021). Leukocyte heterogeneity in pancreatic ductal adenocarcinoma: Phenotypic and spatial features associated with clinical outcome. *Cancer Discovery*. https://doi.org/10.1158/2159-8290.CD-20-0841

Lo, A., Wang, L. C. S., Scholler, J., Monslow, J., Avery, D., Newick, K., O'Brien, S., Evans, R. A., Bajor, D. J., Clendenin, C., Durham, A. C., Buza, E. L., Vonderheide, R. H., June, C. H., Albelda, S. M., & Pure, E. (2015). Tumor-promoting desmoplasia is disrupted by depleting FAP-expressing stromal cells. *Cancer Research*. https://doi.org/10.1158/0008-5472.CAN-14-3041

Luan, B., Yoon, Y. S., Lay, J. Le, Kaestner, K. H., Hedrick, S., & Montminy, M. (2015). CREB pathway links PGE2 signaling with macrophage polarization. *Proceedings of the National Academy of Sciences of the United States of America*. https://doi.org/10.1073/pnas.1519644112

Ma, R. Y., Black, A., & Qian, B. Z. (2022). Macrophage diversity in cancer revisited in the era of single-cell omics. In *Trends in Immunology*. https://doi.org/10.1016/j.it.2022.04.008

Mahadevan, K. K., McAndrews, K. M., LeBleu, V. S., Yang, S., Lyu, H., Li, B., Sockwell, A. M., Kirtley, M. L., Morse, S. J., Moreno Diaz, B. A., Kim, M. P., Feng, N., Lopez, A. M., Guerrero, P. A., Paradiso, F., Sugimoto, H., Arian, K. A., Ying, H., Barekatain, Y., … Kalluri, R. (2023). KRASG12D inhibition reprograms the microenvironment of early and advanced pancreatic cancer to promote FAS-mediated killing by CD8+ T cells. *Cancer Cell*. https://doi.org/10.1016/j.ccell.2023.07.002

Maier, B., Leader, A. M., Chen, S. T., Tung, N., Chang, C., LeBerichel, J., Chudnovskiy,

A., Maskey, S., Walker, L., Finnigan, J. P., Kirkling, M. E., Reizis, B., Ghosh, S., D'Amore, N. R., Bhardwaj, N., Rothlin, C. V., Wolf, A., Flores, R., Marron, T., … Merad, M. (2020). A conserved dendritic-cell regulatory program limits antitumour immunity. *Nature*. https://doi.org/10.1038/s41586-020-2134-y

Maitra, A., Adsay, N. V., Argani, P., Iacobuzio-Donahue, C., De Marzo, A., Cameron, J. L., Yeo, C. J., & Hruban, R. H. (2003). Multicomponent analysis of the pancreatic adenocarcinoma progression model using a pancreatic intraepithelial neoplasia tissue microarray. *Modern Pathology*. https://doi.org/10.1097/01.MP.0000086072.56290.FB

Majety, M., Runza, V., Lehmann, C., Hoves, S., & Ries, C. H. (2018). A drug development perspective on targeting tumor-associated myeloid cells. In *FEBS Journal*. https://doi.org/10.1111/febs.14277

Mantovani, A., Allavena, P., Sica, A., & Balkwill, F. (2008). Cancer-related inflammation. In *Nature*. https://doi.org/10.1038/nature07205

Mantovani, A., Marchesi, F., Malesci, A., Laghi, L., & Allavena, P. (2017). Tumour-associated macrophages as treatment targets in oncology. In *Nature Reviews Clinical Oncology*. https://doi.org/10.1038/nrclinonc.2016.217

Mantovani, A., Sozzani, S., Locati, M., Allavena, P., & Sica, A. (2002). Macrophage polarization: Tumor-associated macrophages as a paradigm for polarized M2 mononuclear phagocytes. In *Trends in Immunology*. https://doi.org/10.1016/S1471-4906(02)02302-5

Markovič, T., Jakopin, Ž., Dolenc, M. S., & Mlinarič-Raščan, I. (2017). Structural features of subtype-selective EP receptor modulators. In *Drug Discovery Today*. https://doi.org/10.1016/j.drudis.2016.08.003

Marrache, F., Tu, S. P., Bhagat, G., Pendyala, S., Österreicher, C. H., Gordon, S., Ramanathan, V., Penz-Österreicher, M., Betz, K. S., Song, Z., & Wang, T. C. (2008). Overexpression of Interleukin-1β in the Murine Pancreas Results in Chronic Pancreatitis. *Gastroenterology*. https://doi.org/10.1053/j.gastro.2008.06.078

Martinez, F. O., & Gordon, S. (2014). The M1 and M2 paradigm of macrophage activation: Time for reassessment. *F1000Prime Reports*. https://doi.org/10.12703/P6-13

Masetti, M., Carriero, R., Portale, F., Marelli, G., Morina, N., Pandini, M., Iovino, M.,

Partini, B., Erreni, M., Ponzetta, A., Magrini, E., Colombo, P., Elefante, G., Simone Colombo, F., den Haan, J. M. M., Peano, C., Cibella, J., Termanini, A., Kunderfranco, P., … Di Mitri, D. (2021). Lipid-loaded tumor-associated macrophages sustain tumor growth and invasiveness in prostate cancer. *Journal of Experimental Medicine*. https://doi.org/10.1084/jem.20210564

Matthaei, H., Schulick, R. D., Hruban, R. H., & Maitra, A. (2011). Cystic precursors to invasive pancreatic cancer. In *Nature Reviews Gastroenterology and Hepatology*. https://doi.org/10.1038/nrgastro.2011.2

Mattiuz, R., Brousse, C., Ambrosini, M., Cancel, J. C., Bessou, G., Mussard, J., Sanlaville, A., Caux, C., Bendriss-Vermare, N., Valladeau-Guilemond, J., Dalod, M., & Crozat, K. (2021). Type 1 conventional dendritic cells and interferons are required for spontaneous CD4+ and CD8+ T-cell protective responses to breast cancer. *Clinical and Translational Immunology*. https://doi.org/10.1002/cti2.1305

Maynard, A., McCoach, C. E., Rotow, J. K., Harris, L., Haderk, F., Kerr, D. L., Yu, E. A., Schenk, E. L., Tan, W., Zee, A., Tan, M., Gui, P., Lea, T., Wu, W., Urisman, A., Jones, K., Sit, R., Kolli, P. K., Seeley, E., … Bivona, T. G. (2020). Therapy-Induced Evolution of Human Lung Cancer Revealed by Single-Cell RNA Sequencing. *Cell*. https://doi.org/10.1016/j.cell.2020.07.017

McAllister, F., Bailey, J. M., Alsina, J., Nirschl, C. J., Sharma, R., Fan, H., Rattigan, Y., Roeser, J. C., Lankapalli, R. H., Zhang, H., Jaffee, E. M., Drake, C. G., Housseau, F., Maitra, A., Kolls, J. K., Sears, C. L., Pardoll, D. M., & Leach, S. D. (2014). Oncogenic kras activates a hematopoietic-to-epithelial IL-17 signaling axis in preinvasive pancreatic neoplasia. *Cancer Cell*. https://doi.org/10.1016/j.ccr.2014.03.014

Merad, M., Sathe, P., Helft, J., Miller, J., & Mortha, A. (2013). The dendritic cell lineage: Ontogeny and function of dendritic cells and their subsets in the steady state and the inflamed setting. In *Annual Review of Immunology*. https://doi.org/10.1146/annurev-immunol-020711-074950

Metschnikoff, E. (1891). Lecture on phagocytosis and immunity. *British Medical Journal*. https://doi.org/10.1136/bmj.1.1570.213

Milani, M., Annoni, A., Bartolaccini, S., Biffi, M., Russo, F., Di Tomaso, T., Raimondi, A., Lengler, J., Holmes, M. C., Scheiflinger, F., Lombardo, A., Cantore, A., &

Naldini, L. (2017). Genome editing for scalable production of alloantigen-free lentiviral vectors for in vivo gene therapy . *EMBO Molecular Medicine*. https://doi.org/10.15252/emmm.201708148

Mills, C. D., Kincaid, K., Alt, J. M., Heilman, M. J., & Hill, A. M. (2000). M-1/M-2 Macrophages and the Th1/Th2 Paradigm. *The Journal of Immunology*. https://doi.org/10.4049/jimmunol.164.12.6166

Moffitt, R. A., Marayati, R., Flate, E. L., Volmar, K. E., Loeza, S. G. H., Hoadley, K. A., Rashid, N. U., Williams, L. A., Eaton, S. C., Chung, A. H., Smyla, J. K., Anderson, J. M., Kim, H. J., Bentrem, D. J., Talamonti, M. S., Iacobuzio-Donahue, C. A., Hollingsworth, M. A., & Yeh, J. J. (2015). Virtual microdissection identifies distinct tumor- and stroma-specific subtypes of pancreatic ductal adenocarcinoma. *Nature Genetics*. https://doi.org/10.1038/ng.3398

Molgora, M., & Colonna, M. (2021). Turning enemies into allies—reprogramming tumor-associated macrophages for cancer therapy. In *Med*. https://doi.org/10.1016/j.medj.2021.05.001

Moncada, R., Barkley, D., Wagner, F., Chiodin, M., Devlin, J. C., Baron, M., Hajdu, C. H., Simeone, D. M., & Yanai, I. (2020). Integrating microarray-based spatial transcriptomics and single-cell RNA-seq reveals tissue architecture in pancreatic ductal adenocarcinomas. *Nature Biotechnology*. https://doi.org/10.1038/s41587-019-0392-8

Montaldo, E., Lusito, E., Bianchessi, V., Caronni, N., Scala, S., Basso-Ricci, L., Cantaffa, C., Masserdotti, A., Barilaro, M., Barresi, S., Genua, M., Vittoria, F. M., Barbiera, G., Lazarevic, D., Messina, C., Xue, E., Marktel, S., Tresoldi, C., Milani, R., … Ostuni, R. (2022). Cellular and transcriptional dynamics of human neutrophils at steady state and upon stress. *Nature Immunology*. https://doi.org/10.1038/s41590-022-01311-1

Morris, J. P., Yashinskie, J. J., Koche, R., Chandwani, R., Tian, S., Chen, C. C., Baslan, T., Marinkovic, Z. S., Sánchez-Rivera, F. J., Leach, S. D., Carmona-Fontaine, C., Thompson, C. B., Finley, L. W. S., & Lowe, S. W. (2019). α-Ketoglutarate links p53 to cell fate during tumour suppression. *Nature*. https://doi.org/10.1038/s41586-019-1577-5

Morris, L., Graham, C. F., & Gordon, S. (1991). Macrophages in haemopoietic and other

tissues of the developing mouse detected by the monoclonal antibody F4/80. *Development*. https://doi.org/10.1242/dev.112.2.517

Mossadegh-Keller, N., Sarrazin, S., Kandalla, P. K., Espinosa, L., Richard Stanley, E., Nutt, S. L., Moore, J., & Sieweke, M. H. (2013). M-CSF instructs myeloid lineage fate in single haematopoietic stem cells. *Nature*. https://doi.org/10.1038/nature12026

Mulder, K., Patel, A. A., Kong, W. T., Piot, C., Halitzki, E., Dunsmore, G., Khalilnezhad, S., Irac, S. E., Dubuisson, A., Chevrier, M., Zhang, X. M., Tam, J. K. C., Lim, T. K. H., Wong, R. M. M., Pai, R., Khalil, A. I. S., Chow, P. K. H., Wu, S. Z., Al-Eryani, G., … Ginhoux, F. (2021). Cross-tissue single-cell landscape of human monocytes and macrophages in health and disease. *Immunity*. https://doi.org/10.1016/j.immuni.2021.07.007

Murray, P. J., & Wynn, T. A. (2011). Protective and pathogenic functions of macrophage subsets. In *Nature Reviews Immunology*. https://doi.org/10.1038/nri3073

Nalio Ramos, R., Missolo-Koussou, Y., Gerber-Ferder, Y., Bromley, C. P., Bugatti, M., Núñez, N. G., Tosello Boari, J., Richer, W., Menger, L., Denizeau, J., Sedlik, C., Caudana, P., Kotsias, F., Niborski, L. L., Viel, S., Bohec, M., Lameiras, S., Baulande, S., Lesage, L., … Helft, J. (2022). Tissue-resident FOLR2+ macrophages associate with CD8+ T cell infiltration in human breast cancer. *Cell*. https://doi.org/10.1016/j.cell.2022.02.021

Narumiya, S. (2009). Prostanoids and inflammation: a new concept arising from receptor knockout mice. In *Journal of molecular medicine (Berlin, Germany)*. https://doi.org/10.1007/s00109-009-0500-1

Natoli, G., & Ostuni, R. (2019). Adaptation and memory in immune responses. In *Nature Immunology*. https://doi.org/10.1038/s41590-019-0399-9

Netea, M. G., Van De Veerdonk, F. L., Van Der Meer, J. W. M., Dinarello, C. A., & Joosten, L. A. B. (2015). Inflammasome-independent regulation of IL-1-family cytokines. *Annual Review of Immunology*. https://doi.org/10.1146/annurev-immunol-032414-112306

North, T. E., Goessling, W., Walkley, C. R., Lengerke, C., Kopani, K. R., Lord, A. M., Weber, G. J., Bowman, T. V., Jang, I. H., Grosser, T., Fitzgerald, G. A., Daley, G. Q., Orkin, S. H., & Zon, L. I. (2007). Prostaglandin E2 regulates vertebrate

haematopoietic stem cell homeostasis. *Nature*. https://doi.org/10.1038/nature05883

O'Reilly, E. M., Oh, D. Y., Dhani, N., Renouf, D. J., Lee, M. A., Sun, W., Fisher, G., Hezel, A., Chang, S. C., Vlahovic, G., Takahashi, O., Yang, Y., Fitts, D., & Philip, P. A. (2019). Durvalumab with or Without Tremelimumab for Patients with Metastatic Pancreatic Ductal Adenocarcinoma: A Phase 2 Randomized Clinical Trial. *JAMA Oncology*. https://doi.org/10.1001/jamaoncol.2019.1588

Öhlund, D., Handly-Santana, A., Biffi, G., Elyada, E., Almeida, A. S., Ponz-Sarvise, M., Corbo, V., Oni, T. E., Hearn, S. A., Lee, E. J., Chio, I. I. C., Hwang, C. Il, Tiriac, H., Baker, L. A., Engle, D. D., Feig, C., Kultti, A., Egeblad, M., Fearon, D. T., … Tuveson, D. A. (2017). Distinct populations of inflammatory fibroblasts and myofibroblasts in pancreatic cancer. *The Journal of Experimental Medicine*. https://doi.org/10.1084/jem.20162024

Ortega-Gómez, A., Perretti, M., & Soehnlein, O. (2013). Resolution of inflammation: An integrated view. In *EMBO Molecular Medicine*. https://doi.org/10.1002/emmm.201202382

Ostuni, R., & Natoli, G. (2013). Lineages, cell types and functional states: A genomic view. In *Current Opinion in Cell Biology*. https://doi.org/10.1016/j.ceb.2013.07.006

Ostuni, R., Piccolo, V., Barozzi, I., Polletti, S., Termanini, A., Bonifacio, S., Curina, A., Prosperini, E., Ghisletti, S., & Natoli, G. (2013). Latent enhancers activated by stimulation in differentiated cells. *Cell*. https://doi.org/10.1016/j.cell.2012.12.018

Overbeek, K. A., Cahen, D. L., Canto, M. I., & Bruno, M. J. (2016). Surveillance for neoplasia in the pancreas. In *Best Practice and Research: Clinical Gastroenterology*. https://doi.org/10.1016/j.bpg.2016.10.013

Özdemir, B. C., Pentcheva-Hoang, T., Carstens, J. L., Zheng, X., Wu, C. C., Simpson, T. R., Laklai, H., Sugimoto, H., Kahlert, C., Novitskiy, S. V., DeJesus-Acosta, A., Sharma, P., Heidari, P., Mahmood, U., Chin, L., Moses, H. L., Weaver, V. M., Maitra, A., Allison, J. P., … Kalluri, R. (2014). Depletion of carcinoma-associated fibroblasts and fibrosis induces immunosuppression and accelerates pancreas cancer with reduced survival. *Cancer Cell*. https://doi.org/10.1016/j.ccr.2014.04.005

Paolicelli, R. C., Bolasco, G., Pagani, F., Maggi, L., Scianni, M., Panzanelli, P., Giustetto, M., Ferreira, T. A., Guiducci, E., Dumas, L., Ragozzino, D., & Gross, C. T. (2011). Synaptic pruning by microglia is necessary for normal brain development. *Science*.

https://doi.org/10.1126/science.1202529

Park, M. D., Silvin, A., Ginhoux, F., & Merad, M. (2022). Macrophages in health and disease. In *Cell*. https://doi.org/10.1016/j.cell.2022.10.007

Pelly, V. S., Moeini, A., Roelofsen, L. M., Bonavita, E., Bell, C. R., Hutton, C., Blanco-Gomez, A., Banyard, A., Bromley, C. P., Flanagan, E., Chiang, S. C., Jørgensen, C., Schumacher, T. N., Thommen, D. S., & Zelenay, S. (2021). Anti-inflammatory drugs remodel the tumor immune environment to enhance immune checkpoint blockade efficacy. *Cancer Discovery*. https://doi.org/10.1158/2159-8290.CD-20-1815

Peng, J., Sun, B. F., Chen, C. Y., Zhou, J. Y., Chen, Y. S., Chen, H., Liu, L., Huang, D., Jiang, J., Cui, G. S., Yang, Y., Wang, W., Guo, D., Dai, M., Guo, J., Zhang, T., Liao, Q., Liu, Y., Zhao, Y. L., … Wu, W. (2019). Single-cell RNA-seq highlights intra-tumoral heterogeneity and malignant progression in pancreatic ductal adenocarcinoma. *Cell Research*. https://doi.org/10.1038/s41422-019-0195-y

Perkins, D. J., Richard, K., Hansen, A. M., Lai, W., Nallar, S., Koller, B., & Vogel, S. N. (2018). Autocrine–paracrine prostaglandin E 2 signaling restricts TLR4 internalization and TRIF signaling. *Nature Immunology*. https://doi.org/10.1038/s41590-018-0243-7

Perusina Lanfranca, M., Zhang, Y., Girgis, A., Kasselman, S., Lazarus, J., Kryczek, I., Delrosario, L., Rhim, A., Koneva, L., Sartor, M., Sun, L., Halbrook, C., Nathan, H., Shi, J., Crawford, H. C., Pasca di Magliano, M., Zou, W., & Frankel, T. L. (2020). Interleukin 22 Signaling Regulates Acinar Cell Plasticity to Promote Pancreatic Tumor Development in Mice. *Gastroenterology*. https://doi.org/10.1053/j.gastro.2019.12.010

Petukhov, V., Xu, R. J., Soldatov, R. A., Cadinu, P., Khodosevich, K., Moffitt, J. R., & Kharchenko, P. V. (2022). Cell segmentation in imaging-based spatial transcriptomics. *Nature Biotechnology*. https://doi.org/10.1038/s41587-021-01044-w

Piccolo, V., Curina, A., Genua, M., Ghisletti, S., Simonatto, M., Sabò, A., Amati, B., Ostuni, R., & Natoli, G. (2017). Opposing macrophage polarization programs show extensive epigenomic and transcriptional cross-talk. *Nature Immunology*. https://doi.org/10.1038/ni.3710

Pittet, M. J., Michielin, O., & Migliorini, D. (2022). Clinical relevance of tumour-associated macrophages. In *Nature Reviews Clinical Oncology*. https://doi.org/10.1038/s41571-022-00620-6

Pruitt, K. D., Tatusova, T., & Maglott, D. R. (2007). NCBI reference sequences (RefSeq): A curated non-redundant sequence database of genomes, transcripts and proteins. *Nucleic Acids Research*. https://doi.org/10.1093/nar/gkl842

Puleo, F., Nicolle, R., Blum, Y., Cros, J., Marisa, L., Demetter, P., Quertinmont, E., Svrcek, M., Elarouci, N., Iovanna, J., Franchimont, D., Verset, L., Galdon, M. G., Devière, J., de Reyniès, A., Laurent-Puig, P., Van Laethem, J. L., Bachet, J. B., & Maréchal, R. (2018). Stratification of Pancreatic Ductal Adenocarcinomas Based on Tumor and Microenvironment Features. *Gastroenterology*. https://doi.org/10.1053/j.gastro.2018.08.033

Pylayeva-Gupta, Y., Lee, K. E., Hajdu, C. H., Miller, G., & Bar-Sagi, D. (2012). Oncogenic Kras-Induced GM-CSF Production Promotes the Development of Pancreatic Neoplasia. *Cancer Cell*. https://doi.org/10.1016/j.ccr.2012.04.024

Rahib, L., Smith, B. D., Aizenberg, R., Rosenzweig, A. B., Fleshman, J. M., & Matrisian, L. M. (2014). Projecting cancer incidence and deaths to 2030: The unexpected burden of thyroid, liver, and pancreas cancers in the united states. In *Cancer Research*. https://doi.org/10.1158/0008-5472.CAN-14-0155

Rahib, L., Wehner, M. R., Matrisian, L. M., & Nead, K. T. (2021). Estimated Projection of US Cancer Incidence and Death to 2040. *JAMA Network Open*. https://doi.org/10.1001/jamanetworkopen.2021.4708

Reuter, B., Weber, M., Fackeldey, K., Röblitz, S., & Garcia, M. E. (2018). Generalized Markov State Modeling Method for Nonequilibrium Biomolecular Dynamics: Exemplified on Amyloid β Conformational Dynamics Driven by an Oscillating Electric Field. *Journal of Chemical Theory and Computation*. https://doi.org/10.1021/acs.jctc.8b00079

Riabov, V., Gudima, A., Wang, N., Mickley, A., Orekhov, A., & Kzhyshkowska, J. (2014). Role of tumor associated macrophages in tumor angiogenesis and lymphangiogenesis. In *Frontiers in Physiology*. https://doi.org/10.3389/fphys.2014.00075

Ricciotti, E., & Fitzgerald, G. A. (2011). Prostaglandins and inflammation.

Arteriosclerosis, Thrombosis, and Vascular Biology. https://doi.org/10.1161/ATVBAHA.110.207449

Ridker, P. M., MacFadyen, J. G., Thuren, T., Everett, B., Libby, P., Glynn, R. J., Lorenzatti, A., Krum, H., Varigos, J., Siostrzonek, P., Sinnaeve, P., Fonseca, F., Nicolau, J., Gotcheva, N., Genest, J., Yong, H., Urina-Triana, M., Milicic, D., Cifkova, R., … Gersh, B. (2017). Effect of interleukin-1β inhibition with canakinumab on incident lung cancer in patients with atherosclerosis: exploratory results from a randomised, double-blind, placebo-controlled trial. *The Lancet*. https://doi.org/10.1016/S0140-6736(17)32247-X

Ritchie, M. E., Phipson, B., Wu, D., Hu, Y., Law, C. W., Shi, W., & Smyth, G. K. (2015). Limma powers differential expression analyses for RNA-sequencing and microarray studies. *Nucleic Acids Research*. https://doi.org/10.1093/nar/gkv007

Robinson, M. D., & Oshlack, A. (2010). A scaling normalization method for differential expression analysis of RNA-seq data. *Genome Biology*. https://doi.org/10.1186/gb-2010-11-3-r25

Robinson Mark, D., McCarthy Davis, J., & Smyth Gordon, K. (2010). edgeR: a Bioconductor package for differential expression analysis of digital gene expression data. *Bioinformatics*.

Rojas, L. A., Sethna, Z., Soares, K. C., Olcese, C., Pang, N., Patterson, E., Lihm, J., Ceglia, N., Guasp, P., Chu, A., Yu, R., Chandra, A. K., Waters, T., Ruan, J., Amisaki, M., Zebboudj, A., Odgerel, Z., Payne, G., Derhovanessian, E., … Balachandran, V. P. (2023). Personalized RNA neoantigen vaccines stimulate T cells in pancreatic cancer. *Nature*. https://doi.org/10.1038/s41586-023-06063-y

Rosas, M., Davies, L. C., Giles, P. J., Liao, C. Te, Kharfan, B., Stone, T. C., O'Donnell, V. B., Fraser, D. J., Jones, S. A., & Taylor, P. R. (2014). The transcription factor Gata6 links tissue macrophage phenotype and proliferative renewal. *Science*. https://doi.org/10.1126/science.1251414

Rothwell, P. M., Fowkes, F. G. R., Belch, J. F., Ogawa, H., Warlow, C. P., & Meade, T. W. (2011). Effect of daily aspirin on long-term risk of death due to cancer: Analysis of individual patient data from randomised trials. *The Lancet*. https://doi.org/10.1016/S0140-6736(10)62110-1

Roulis, M., Kaklamanos, A., Schernthanner, M., Bielecki, P., Zhao, J., Kaffe, E.,

Frommelt, L. S., Qu, R., Knapp, M. S., Henriques, A., Chalkidi, N., Koliaraki, V., Jiao, J., Brewer, J. R., Bacher, M., Blackburn, H. N., Zhao, X., Breyer, R. M., Aidinis, V., … Flavell, R. A. (2020). Paracrine orchestration of intestinal tumorigenesis by a mesenchymal niche. *Nature*. https://doi.org/10.1038/s41586-020-2166-3

Royal, R. E., Levy, C., Turner, K., Mathur, A., Hughes, M., Kammula, U. S., Sherry, R. M., Topalian, S. L., Yang, J. C., Lowy, I., & Rosenberg, S. A. (2010). Phase 2 trial of single agent ipilimumab (Anti-CTLA-4) for locally advanced or metastatic pancreatic adenocarcinoma. *Journal of Immunotherapy*. https://doi.org/10.1097/CJI.0b013e3181eec14c

Sadik, A., Somarribas Patterson, L. F., Öztürk, S., Mohapatra, S. R., Panitz, V., Secker, P. F., Pfänder, P., Loth, S., Salem, H., Prentzell, M. T., Berdel, B., Iskar, M., Faessler, E., Reuter, F., Kirst, I., Kalter, V., Foerster, K. I., Jäger, E., Guevara, C. R., … Opitz, C. A. (2020). IL4I1 Is a Metabolic Immune Checkpoint that Activates the AHR and Promotes Tumor Progression. *Cell*. https://doi.org/10.1016/j.cell.2020.07.038

Schalck, A., Sakellariou-Thompson, D., Forget, M. A., Sei, E., Hughes, T. G., Reuben, A., Bai, S., Hu, M., Kumar, T., Hurd, M. W., Katz, M. H. G., Tzeng, C. W. D., Pant, S., Javle, M., Fogelman, D. R., Maitra, A., Haymaker, C. L., Kim, M. P., Navin, N. E., & Bernatchez, C. (2022). Single-Cell Sequencing Reveals Trajectory of Tumor-Infiltrating Lymphocyte States in Pancreatic Cancer. *Cancer Discovery*. https://doi.org/10.1158/2159-8290.CD-21-1248

Schneider, C., Nobs, S. P., Kurrer, M., Rehrauer, H., Thiele, C., & Kopf, M. (2014). Induction of the nuclear receptor PPAR-γ 3 by the cytokine GM-CSF is critical for the differentiation of fetal monocytes into alveolar macrophages. *Nature Immunology*. https://doi.org/10.1038/ni.3005

Schumacher, T. N., & Schreiber, R. D. (2015). Neoantigens in cancer immunotherapy. In *Science*. https://doi.org/10.1126/science.aaa4971

Schyns, J., Bai, Q., Ruscitti, C., Radermecker, C., De Schepper, S., Chakarov, S., Farnir, F., Pirottin, D., Ginhoux, F., Boeckxstaens, G., Bureau, F., & Marichal, T. (2019). Non-classical tissue monocytes and two functionally distinct populations of interstitial macrophages populate the mouse lung. *Nature Communications*.

https://doi.org/10.1038/s41467-019-11843-0

Scott, C. L., Zheng, F., De Baetselier, P., Martens, L., Saeys, Y., De Prijck, S., Lippens, S., Abels, C., Schoonooghe, S., Raes, G., Devoogdt, N., Lambrecht, B. N., Beschin, A., & Guilliams, M. (2016). Bone marrow-derived monocytes give rise to self-renewing and fully differentiated Kupffer cells. *Nature Communications*. https://doi.org/10.1038/ncomms10321

Sears, R., Nuckolls, F., Haura, E., Taya, Y., Tamai, K., & Nevins, J. R. (2000). Multiple Ras-dependent phosphorylation pathways regulate Myc protein stability. *Genes and Development*. https://doi.org/10.1101/gad.836800

Setty, M., Kiseliovas, V., Levine, J., Gayoso, A., Mazutis, L., & Pe'er, D. (2019). Characterization of cell fate probabilities in single-cell data with Palantir. *Nature Biotechnology*. https://doi.org/10.1038/s41587-019-0068-4

Sharma, A., Seow, J. J. W., Dutertre, C. A., Pai, R., Blériot, C., Mishra, A., Wong, R. M. M., Singh, G. S. N., Sudhagar, S., Khalilnezhad, S., Erdal, S., Teo, H. M., Khalilnezhad, A., Chakarov, S., Lim, T. K. H., Fui, A. C. Y., Chieh, A. K. W., Chung, C. P., Bonney, G. K., … DasGupta, R. (2020). Onco-fetal Reprogramming of Endothelial Cells Drives Immunosuppressive Macrophages in Hepatocellular Carcinoma. *Cell*. https://doi.org/10.1016/j.cell.2020.08.040

Sherman, M. H., & Beatty, G. L. (2023). Tumor Microenvironment in Pancreatic Cancer Pathogenesis and Therapeutic Resistance. In *Annual Review of Pathology: Mechanisms of Disease*. https://doi.org/10.1146/annurev-pathmechdis-031621-024600

Singhi, A. D., George, B., Greenbowe, J. R., Chung, J., Suh, J., Maitra, A., Klempner, S. J., Hendifar, A., Milind, J. M., Golan, T., Brand, R. E., Zureikat, A. H., Roy, S., Schrock, A. B., Miller, V. A., Ross, J. S., Ali, S. M., & Bahary, N. (2019). Real-Time Targeted Genome Profile Analysis of Pancreatic Ductal Adenocarcinomas Identifies Genetic Alterations That Might Be Targeted With Existing Drugs or Used as Biomarkers. *Gastroenterology*. https://doi.org/10.1053/j.gastro.2019.02.037

Singhi, A. D., Koay, E. J., Chari, S. T., & Maitra, A. (2019). Early Detection of Pancreatic Cancer: Opportunities and Challenges. *Gastroenterology*. https://doi.org/10.1053/j.gastro.2019.01.259

Sohn, T. A., Yeo, C. J., Cameron, J. L., Iacobuzio-Donahue, C. A., Hruban, R. H., &

Lillemoe, K. D. (2001). Intraductal papillary mucinous neoplasms of the pancreas: An increasingly recognized clinicopathologic entity. *Annals of Surgery*. https://doi.org/10.1097/00000658-200109000-00005

Street, K., Risso, D., Fletcher, R. B., Das, D., Ngai, J., Yosef, N., Purdom, E., & Dudoit, S. (2018). Slingshot: Cell lineage and pseudotime inference for single-cell transcriptomics. *BMC Genomics*. https://doi.org/10.1186/s12864-018-4772-0

Strickler, J. H., Satake, H., George, T. J., Yaeger, R., Hollebecque, A., Garrido-Laguna, I., Schuler, M., Burns, T. F., Coveler, A. L., Falchook, G. S., Vincent, M., Sunakawa, Y., Dahan, L., Bajor, D., Rha, S.-Y., Lemech, C., Juric, D., Rehn, M., Ngarmchamnanrith, G., … Hong, D. S. (2023). Sotorasib in KRAS p.G12C–Mutated Advanced Pancreatic Cancer . *New England Journal of Medicine*. https://doi.org/10.1056/nejmoa2208470

Stringer, C., Wang, T., Michaelos, M., & Pachitariu, M. (2021). Cellpose: a generalist algorithm for cellular segmentation. *Nature Methods*. https://doi.org/10.1038/s41592-020-01018-x

Strobel, O., Neoptolemos, J., Jäger, D., & Büchler, M. W. (2019). Optimizing the outcomes of pancreatic cancer surgery. In *Nature Reviews Clinical Oncology*. https://doi.org/10.1038/s41571-018-0112-1

Stuart, T., Butler, A., Hoffman, P., Hafemeister, C., Papalexi, E., Mauck, W. M., Hao, Y., Stoeckius, M., Smibert, P., & Satija, R. (2019). Comprehensive Integration of Single-Cell Data. *Cell*. https://doi.org/10.1016/j.cell.2019.05.031

Tanaka, N., Lin, J. J., Li, C., Ryan, M. B., Zhang, J., Kiedrowski, L. A., Michel, A. G., Syed, M. U., Fella, K. A., Sakhi, M., Baiev, I., Juric, D., Gainor, J. F., Klempner, S. J., Lennerz, J. K., Siravegna, G., Bar-Peled, L., Hata, A. N., Heist, R. S., & Corcoran, R. B. (2021). Clinical acquired resistance to krasg12c inhibition through a novel kras switch-ii pocket mutation and polyclonal alterations converging on ras–mapk reactivation. *Cancer Discovery*. https://doi.org/10.1158/2159-8290.CD-21-0365

Tang, C. H., Yang, R. Sen, & Fu, W. M. (2005). Prostaglandin E2 stimulates fibronectin expression through EP1 receptor, phospholipase C, protein kinase Cα, and c-Src pathway in primary cultured rat osteoblasts. *Journal of Biological Chemistry*. https://doi.org/10.1074/jbc.M500130200

The Cancer Genome Atlas Research Network, & Raphael, B. J. (2017). Integrated

Genomic Characterization of Pancreatic Ductal Adenocarcinoma The Cancer Genome Atlas Research Network *. *Cancer Cell*.

Theurl, I., Hilgendorf, I., Nairz, M., Tymoszuk, P., Haschka, D., Asshoff, M., He, S., Gerhardt, L. M. S., Holderried, T. A. W., Seifert, M., Sopper, S., Fenn, A. M., Anzai, A., Rattik, S., McAlpine, C., Theurl, M., Wieghofer, P., Iwamoto, Y., Weber, G. F., … Swirski, F. K. (2016). On-demand erythrocyte disposal and iron recycling requires transient macrophages in the liver. *Nature Medicine*. https://doi.org/10.1038/nm.4146

Thumkeo, D., Punyawatthananukool, S., Prasongtanakij, S., Matsuura, R., Arima, K., Nie, H., Yamamoto, R., Aoyama, N., Hamaguchi, H., Sugahara, S., Takeda, S., Charoensawan, V., Tanaka, A., Sakaguchi, S., & Narumiya, S. (2022). PGE2-EP2/EP4 signaling elicits immunosuppression by driving the mregDC-Treg axis in inflammatory tumor microenvironment. *Cell Reports*. https://doi.org/10.1016/j.celrep.2022.110914

Trebino, C. E., Stock, J. L., Gibbons, C. P., Naiman, B. M., Wachtmann, T. S., Umland, J. P., Pandher, K., Lapointe, J. M., Saha, S., Roach, M. L., Carter, D., Thomas, N. A., Durtschi, B. A., McNeish, J. D., Hambor, J. E., Jakobsson, P. J., Carty, T. J., Perez, J. R., & Audoly, L. P. (2003). Impaired inflammatory and pain responses in mice lacking an inducible prostaglandin E synthase. *Proceedings of the National Academy of Sciences of the United States of America*. https://doi.org/10.1073/pnas.1332766100

Tsai, Y. S., Woodcock, M. G., Azam, S. H., Thorne, L. B., Kanchi, K. L., Parker, J. S., Vincent, B. G., & Pecot, C. V. (2022). Rapid idiosyncratic mechanisms of clinical resistance to KRAS G12C inhibition. *Journal of Clinical Investigation*. https://doi.org/10.1172/JCI155523

Tu, M., Klein, L., Espinet, E., Georgomanolis, T., Wegwitz, F., Li, X., Urbach, L., Danieli-Mackay, A., Küffer, S., Bojarczuk, K., Mizi, A., Günesdogan, U., Chapuy, B., Gu, Z., Neesse, A., Kishore, U., Ströbel, P., Hessmann, E., Hahn, S. A., … Singh, S. K. (2021). TNF-α-producing macrophages determine subtype identity and prognosis via AP1 enhancer reprogramming in pancreatic cancer. *Nature Cancer*. https://doi.org/10.1038/s43018-021-00258-w

van de Laar, L., Saelens, W., De Prijck, S., Martens, L., Scott, C. L., Van Isterdael, G.,

Hoffmann, E., Beyaert, R., Saeys, Y., Lambrecht, B. N., & Guilliams, M. (2016). Yolk Sac Macrophages, Fetal Liver, and Adult Monocytes Can Colonize an Empty Niche and Develop into Functional Tissue-Resident Macrophages. *Immunity*. https://doi.org/10.1016/j.immuni.2016.02.017

Van Hove, H., Martens, L., Scheyltjens, I., De Vlaminck, K., Pombo Antunes, A. R., De Prijck, S., Vandamme, N., De Schepper, S., Van Isterdael, G., Scott, C. L., Aerts, J., Berx, G., Boeckxstaens, G. E., Vandenbroucke, R. E., Vereecke, L., Moechars, D., Guilliams, M., Van Ginderachter, J. A., Saeys, Y., & Movahedi, K. (2019). A single-cell atlas of mouse brain macrophages reveals unique transcriptional identities shaped by ontogeny and tissue environment. *Nature Neuroscience*. https://doi.org/10.1038/s41593-019-0393-4

Varol, C., Mildner, A., & Jung, S. (2015). Macrophages: Development and tissue specialization. In *Annual Review of Immunology*. https://doi.org/10.1146/annurev-immunol-032414-112220

Von Hoff, D. D., Ervin, T., Arena, F. P., Chiorean, E. G., Infante, J., Moore, M., Seay, T., Tjulandin, S. A., Ma, W. W., Saleh, M. N., Harris, M., Reni, M., Dowden, S., Laheru, D., Bahary, N., Ramanathan, R. K., Tabernero, J., Hidalgo, M., Goldstein, D., … Renschler, M. F. (2013). Increased Survival in Pancreatic Cancer with nab-Paclitaxel plus Gemcitabine. *New England Journal of Medicine*. https://doi.org/10.1056/nejmoa1304369

Vonderheide, R. H. (2018). The Immune Revolution: A Case for Priming, Not Checkpoint. In *Cancer Cell*. https://doi.org/10.1016/j.ccell.2018.03.008

Waddell, N., Pajic, M., Patch, A. M., Chang, D. K., Kassahn, K. S., Bailey, P., Johns, A. L., Miller, D., Nones, K., Quek, K., Quinn, M. C. J., Robertson, A. J., Fadlullah, M. Z. H., Bruxner, T. J. C., Christ, A. N., Harliwong, I., Idrisoglu, S., Manning, S., Nourse, C., … Grimmond, S. M. (2015). Whole genomes redefine the mutational landscape of pancreatic cancer. *Nature*. https://doi.org/10.1038/nature14169

Wang, D., & Dubois, R. N. (2010). Eicosanoids and cancer. In *Nature Reviews Cancer*. https://doi.org/10.1038/nrc2809

Wang, D., & DuBois, R. N. (2018). Role of prostanoids in gastrointestinal cancer. In *Journal of Clinical Investigation*. https://doi.org/10.1172/JCI97953

Wang, M., Zukas, A. M., Hui, Y., Ricciotti, E., Puré, E., & FitzGerald, G. A. (2006).

Deletion of microsomal prostaglandin E synthase-1 augments prostacyclin and retards atherogenesis. *Proceedings of the National Academy of Sciences of the United States of America*. https://doi.org/10.1073/pnas.0606586103

Waters, A. M., & Der, C. J. (2018). KRAS: The critical driver and therapeutic target for pancreatic cancer. *Cold Spring Harbor Perspectives in Medicine*. https://doi.org/10.1101/cshperspect.a031435

Weeden, C. E., Hill, W., Lim, E. L., Grönroos, E., & Swanton, C. (2023). Impact of risk factors on early cancer evolution. *Cell*, *186*(8), 1541–1563. https://doi.org/10.1016/j.cell.2023.03.013

Weissmueller, S., Manchado, E., Saborowski, M., Morris IV, J. P., Wagenblast, E., Davis, C. A., Moon, S. H., Pfister, N. T., Tschaharganeh, D. F., Kitzing, T., Aust, D., Markert, E. K., Wu, J., Grimmond, S. M., Pilarsky, C., Prives, C., Biankin, A. V., & Lowe, S. W. (2014). Mutant p53 drives pancreatic cancer metastasis through cell-autonomous PDGF receptor β signaling. *Cell*. https://doi.org/10.1016/j.cell.2014.01.066

Whitsett, J. A., Wert, S. E., & Weaver, T. E. (2010). Alveolar surfactant homeostasis and the pathogenesis of pulmonary disease. In *Annual Review of Medicine*. https://doi.org/10.1146/annurev.med.60.041807.123500

Wolf, F. A., Angerer, P., & Theis, F. J. (2018). SCANPY: Large-scale single-cell gene expression data analysis. *Genome Biology*. https://doi.org/10.1186/s13059-017-1382-0

Wright, J. R. (1990). Clearance and recycling of pulmonary surfactant. In *American Journal of Physiology - Lung Cellular and Molecular Physiology*. https://doi.org/10.1152/ajplung.1990.259.2.l1

Wynn, T. A., & Vannella, K. M. (2016). Macrophages in Tissue Repair, Regeneration, and Fibrosis. In *Immunity*. https://doi.org/10.1016/j.immuni.2016.02.015

Yachida, S., Jones, S., Bozic, I., Antal, T., Leary, R., Fu, B., Kamiyama, M., Hruban, R. H., Eshleman, J. R., Nowak, M. A., Velculescu, V. E., Kinzler, K. W., Vogelstein, B., & Iacobuzio-Donahue, C. A. (2010). Distant metastasis occurs late during the genetic evolution of pancreatic cancer. *Nature*. https://doi.org/10.1038/nature09515

Ying, H., Kimmelman, A. C., Lyssiotis, C. A., Hua, S., Chu, G. C., Fletcher-Sananikone, E., Locasale, J. W., Son, J., Zhang, H., Coloff, J. L., Yan, H., Wang, W., Chen, S.,

Viale, A., Zheng, H., Paik, J. H., Lim, C., Guimaraes, A. R., Martin, E. S., … Depinho, R. A. (2012). Oncogenic kras maintains pancreatic tumors through regulation of anabolic glucose metabolism. *Cell*. https://doi.org/10.1016/j.cell.2012.01.058

Yokoyama, U., Iwatsubo, K., Umemura, M., Fujita, T., & Ishikawa, Y. (2013). The prostanoid EP4 receptor and its signaling pathway. *Pharmacological Reviews*. https://doi.org/10.1124/pr.112.007195

Yu, G., Wang, L. G., Han, Y., & He, Q. Y. (2012). ClusterProfiler: An R package for comparing biological themes among gene clusters. *OMICS A Journal of Integrative Biology*. https://doi.org/10.1089/omi.2011.0118

Zasłona, Z., Pålsson-McDermott, E. M., Menon, D., Haneklaus, M., Flis, E., Prendeville, H., Corcoran, S. E., Peters-Golden, M., & O'Neill, L. A. J. (2017). The Induction of Pro–IL-1β by Lipopolysaccharide Requires Endogenous Prostaglandin E2 Production. *The Journal of Immunology*, *198*(9), 3558–3564. https://doi.org/10.4049/jimmunol.1602072

Zelenay, S., & Reis e Sousa, C. (2016). Reducing prostaglandin E2 production to raise cancer immunogenicity. *OncoImmunology*. https://doi.org/10.1080/2162402X.2015.1123370

Zelenay, S., Van Der Veen, A. G., Böttcher, J. P., Snelgrove, K. J., Rogers, N., Acton, S. E., Chakravarty, P., Girotti, M. R., Marais, R., Quezada, S. A., Sahai, E., & Reis E Sousa, C. (2015). Cyclooxygenase-Dependent Tumor Growth through Evasion of Immunity. *Cell*. https://doi.org/10.1016/j.cell.2015.08.015

Zhang, L., Li, Z., Skrzypczynska, K. M., Fang, Q., Zhang, W., O'Brien, S. A., He, Y., Wang, L., Zhang, Q., Kim, A., Gao, R., Orf, J., Wang, T., Sawant, D., Kang, J., Bhatt, D., Lu, D., Li, C. M., Rapaport, A. S., … Yu, X. (2020). Single-Cell Analyses Inform Mechanisms of Myeloid-Targeted Therapies in Colon Cancer. *Cell*. https://doi.org/10.1016/j.cell.2020.03.048

Zhang, Q. wen, Liu, L., Gong, C. yang, Shi, H. shan, Zeng, Y. hui, Wang, X. ze, Zhao, Y. wei, & Wei, Y. quan. (2012). Prognostic Significance of Tumor-Associated Macrophages in Solid Tumor: A Meta-Analysis of the Literature. *PLoS ONE*. https://doi.org/10.1371/journal.pone.0050946

Zhang, Y., Velez-Delgado, A., Mathew, E., Li, D., Mendez, F. M., Flannagan, K., Rhim,

A. D., Simeone, D. M., Beatty, G. L., & Di Magliano, M. P. (2017). Myeloid cells are required for PD-1/PD-L1 checkpoint activation and the establishment of an immunosuppressive environment in pancreatic cancer. *Gut*. https://doi.org/10.1136/gutjnl-2016-312078

Zhang, Y., Yan, W., Mathew, E., Bednar, F., Wan, S., Collins, M. A., Evans, R. A., Welling, T. H., Vonderheide, R. H., & Di Magliano, M. P. (2014). CD4+ T lymphocyte ablation prevents pancreatic carcinogenesis in mice. *Cancer Immunology Research*. https://doi.org/10.1158/2326-6066.CIR-14-0016-T

Zhen, D. B., Rabe, K. G., Gallinger, S., Syngal, S., Schwartz, A. G., Goggins, M. G., Hruban, R. H., Cote, M. L., McWilliams, R. R., Roberts, N. J., Cannon-Albright, L. A., Li, D., Moyes, K., Wenstrup, R. J., Hartman, A. R., Seminara, D., Klein, A. P., & Petersen, G. M. (2015). BRCA1, BRCA2, PALB2, and CDKN2A mutations in familial pancreatic cancer: A PACGENE study. *Genetics in Medicine*. https://doi.org/10.1038/gim.2014.153

Zheng, G. X. Y., Terry, J. M., Belgrader, P., Ryvkin, P., Bent, Z. W., Wilson, R., Ziraldo, S. B., Wheeler, T. D., McDermott, G. P., Zhu, J., Gregory, M. T., Shuga, J., Montesclaros, L., Underwood, J. G., Masquelier, D. A., Nishimura, S. Y., Schnall-Levin, M., Wyatt, P. W., Hindson, C. M., … Bielas, J. H. (2017). Massively parallel digital transcriptional profiling of single cells. *Nature Communications*. https://doi.org/10.1038/ncomms14049

Zhivaki, D., Borriello, F., Chow, O. A., Doran, B., Fleming, I., Theisen, D. J., Pallis, P., Shalek, A. K., Sokol, C. L., Zanoni, I., & Kagan, J. C. (2020). Inflammasomes within Hyperactive Murine Dendritic Cells Stimulate Long-Lived T Cell-Mediated Anti-tumor Immunity. *Cell Reports*. https://doi.org/10.1016/j.celrep.2020.108381

Zhivaki, D., & Kagan, J. C. (2021). NLRP3 inflammasomes that induce antitumor immunity. In *Trends in Immunology*. https://doi.org/10.1016/j.it.2021.05.001

Zhu, Y., Herndon, J. M., Sojka, D. K., Kim, K. W., Knolhoff, B. L., Zuo, C., Cullinan, D. R., Luo, J., Bearden, A. R., Lavine, K. J., Yokoyama, W. M., Hawkins, W. G., Fields, R. C., Randolph, G. J., & DeNardo, D. G. (2017). Tissue-Resident Macrophages in Pancreatic Ductal Adenocarcinoma Originate from Embryonic Hematopoiesis and Promote Tumor Progression. *Immunity*. https://doi.org/10.1016/j.immuni.2017.07.014

Zonari, E., Desantis, G., Petrillo, C., Boccalatte, F. E., Lidonnici, M. R., Kajaste-Rudnitski, A., Aiuti, A., Ferrari, G., Naldini, L., & Gentner, B. (2017). Efficient Ex Vivo Engineering and Expansion of Highly Purified Human Hematopoietic Stem and Progenitor Cell Populations for Gene Therapy. *Stem Cell Reports*. https://doi.org/10.1016/j.stemcr.2017.02.010

Zuo, C., Baer, J. M., Knolhoff, B. L., Belle, J. I., Liu, X., Alarcon De La Lastra, A., Fu, C., Hogg, G. D., Kingston, N. L., Breden, M. A., Dodhiawala, P. B., Zhou, D. C., Lander, V. E., James, C. A., Ding, L., Lim, K. H., Fields, R. C., Hawkins, W. G., Weber, J. D., … DeNardo, D. G. (2023). Stromal and therapy-induced macrophage proliferation promotes PDAC progression and susceptibility to innate immunotherapy. *The Journal of Experimental Medicine*. https://doi.org/10.1084/jem.20212062